Thermal and Mechanical Characterization of

Human Hair Fibres

THESIS

Submitted in partial fulfillment

of the requirements for the degree of

DOCTOR OF PHILOSOPHY

by

K CHANDRAKALA

ID. No. 2014PHXF0404H

Under the Supervision of

Prof. Ramesh Babu Adusumalli

&

Under the Co-Supervision of

Prof. Karthik Chethan Venkateshan

BITS Pilani

Pilani | Dubai | Goa | Hyderabad

BIRLA INSTITUTE OF TECHNOLOGY & SCIENCE, PILANI

Hyderabad Campus

2019

CERTIFICATE

This is to certify that the thesis entitled "**Thermal and Mechanical Characterization of Human Hair Fibres**" and submitted by **CHANDRAKALA KUNCHI**, ID. No. **2014PHXF0404H** for award of Ph.D. of the institute embodies original work done by her under my supervision.

Signature of the Supervisor:

Name in capital letters: **Prof. RAMESH BABU ADUSUMALLI**

Designation: Associate Professor
                                  .
Date:

Signature of the Co-Supervisor:

Name in capital letters: **Prof. KARTHIK CHETHAN VENKATESHAN**

Designation: Associate Professor

innovate   achieve   lead

"Where there's a will,

there's a way."

In loving memory of my dear husband, Mahesh T

Acknowledgements

support, discussions and friendship throughout this study. I am thankful to my ex-mentor Dr. RMVGK Rao for encouraging me to pursue this research work. I express my sincere thanks to Mr. Praveen Kumar and Mrs. BhagyaLaxmi, SRCD division for their cooperation during my Ph.D. work.

I extend my thanks to our lab technicians Mr. Appala Reddy, Mr. Somi Reddy, Mr. Bhaskara Raju, Mr.Khan and Mr. Raju for helping me in conducting experiments in Chemical Engineering Department. I would like to extend my thanks to under graduate students Mr. Shubham M, Ms. Sakshi K, Mr. Pushkar P, Mr. Bibhu Prasad T, Ms. Deeksha Reddy N and Mr. Lokesh A for their support and help towards my research work. I wish to extend my gratitude to Mr. Surya R Vadlamani and Mr. Arvind for proof reading of my thesis. I am extremely grateful to our Central Analytical Laboratory assistants Mr. Uppalaiah A, Mr. Mallesh G, Mr. Kumar K and B. Suryanarayana and Mr. B Laxman, from Mechanical Engineering Department for their cooperation during my Ph.D. work.

I owe thanks to a very special person, my husband, **T. Mahesh (Late)** for his continued and unfailing love, support and understanding during my pursuit of Ph.D degree that made me to complete this thesis even though he passed away in the midway of my Ph.D. work. He is always around at times I thought it is impossible to continue, but he helped me to keep things in perspective. I appreciate my son **T. Sai Sanjeev** for abiding my ignorance and the patience he showed during my thesis writing. Words would never say how thankful to my son. My heart felt regards goes to my father-in-law Mr. T. Anantha Rao and mother-in-law Mrs.T. Bujjaamma for their love and moral support especially during the sudden demise of my husband. At the end, but from my heart, I deeply appreciate my family members Mr. K Kannaiah (Father), Mrs. K Aruna Kumari (Mother), Mr. K Murali Mohan (Brother) for their faith in me and for continuous support. It was under their influence I gained so much drive and the ability to tackle challenges which were piling up on my head. I take this opportunity to extend my sincere gratitude and appreciation to all those who made this Ph.D thesis possible.

Last but not the least, for the immense shower of blessings for timely accomplishment of the work in a presentable manner to the level of my satisfaction I must thank the "Almighty", to whom I always surrender. To those I may have Wronged, I ask Forgiveness. To those I Neglected to help, I ask for Understanding. To those who helped me, I sincerely Thank you

Date: *Chandrakala K*

Abstract

Hair is a naturally occurring fibre that is very abundant in animals and human beings. It has a very complicated structure and has three visibly distinct regions namely cuticle, cortex and medulla. The outer region is called cuticle. Cortex is the largest region with a cross sectional diameter of 30 to 100 µm and it contains elongated cells of ~5 µm diameter which are called cortical cells. Medulla, the central region is discontinuous and has a diameter of 8 to 12 µm and its structure is not fully understood. Hair cortex region has keratin proteins and these proteins could be crystalline and amorphous and there would be lot of interfaces between crystalline and the amorphous regions. In the crystalline region it is understood that keratin is always in folded state i.e. it is in native state which is alpha helix state. Amorphous regions are random coils which are networks and these networks are dominated by physical entanglements as well as cystine bonds i.e. disulphide bonds. Hair structure resembles nanocomposite wherein amorphous keratin matrix and crystalline keratin intermediate filaments exists with high degree of intermingling. Lot of work has been conducted on human hair which includes independent studies on Single fibre mechanical properties and thermal characterization of human hair fibres. Few studies have also been conducted on the nanoindentation of fibres in lateral and longitudinal sections. Gaps in literature would be lack of integration and comprehensive study of human hair fibre both in terms of mechanical (nano, bulk) and thermal (bulk) properties. The objective of this thesis was to integrate the mechanical and thermal characterization both in terms of the nano scale as well as bulk scales. The key objectives are

1. To find a correlation of mechanical (nano and bulk) and thermal properties of hair with respect to age and gender.
2. To find the differences in the nanomechanical properties between cortex and medulla regions of hair.
3. To compare the tensile properties of hair with respect to scalp positions P1-P4 using statistical analysis.
4. To find a correlation between mechanical and thermal properties.

In order to achieve the above objectives, one surface test (nanoindentation) and two bulk tests (tensile and thermal) were conducted by taking the samples from 3 to 70 years old people

including male and female. Nanoindentation (load in mN and depth in nm) equipped with Berkovitch diamond tip was used to measure the nanomechanical properties by indenting the cross sections of single hair fibres. Tensile tests were done using 20 mm length single hair fibres and fractography was also carried out using SEM. Thermal tests were done using Differential Scanning Calorimetry (DSC).

The conclusion that was obtained from this thesis was that there was no major correlation of age and gender with both nanomechanical and bulk (tensile and thermal) properties. The medulla and cortex regions revealed hardness values of 70 - 170 MPa and 200 - 312 MPa respectively. Similarly lower values of indentation modulus were observed for medulla compared to cortex. Post-yield incremental modulus change at around 33 % strain was observed indicating the fourth region in the tensile stress–strain plot. Considering the composite nature of hair by taking amorphous and crystalline domains into consideration, modulus, yield stress, maximum stress and work of elongation were measured from tensile stress-strain plots and these were in the range of 2 - 6 GPa, 60 - 190 MPa, 130 - 340 MPa and 30 - 100 MJ/m^3 respectively. For these four tensile properties, statistical ratings were given separately for all four scalp positions P1 - P4 using Relative rating method and Grey relational analysis. In both methods, the overall rating with respect to scalp positions P1 - P4 did not show significant quantitative differences and from this observation it may be said that baldness pattern is not influenced by the quality of hair.

Typical values of melting enthalpy of α-keratin and peak temperatures were found to be 6.29 ± 0.20 J/g and 235 ± 0.6 $^{\circ}$C respectively. But the onset of melting temperatures was between 221 - 231°C. Melting enthalpy and yield stress values were compared and a good non-linear (sigmoidal) correlation was found which seems to provide an accurate representation of a composite keratin structure. A good correlation was also found between onset of melting temperature and indentation modulus.

CONTENTS

List of Figures

List of Tables

List of Abbreviations

ASTM	American Society for Testing and Materials
AFM	Atomic Force Microscopy
ANOVA	Analysis of Variance
A^o	Angstrom
α-keratin	Alpha keratin
BISFA	International Bureau for Standardisation of Man-Made Fibres
CLSM	Confocal laser scanning microscopy
°C/min	Degree centigrade per minute
DSC	Differential Scanning Calorimetry
ρ	Density
EDAX	Energy Dispersive X-ray analysis
GPa	Gigapascal
GRG	Grey Relational Grade
GRA	Grey Relational Analysis
E	Modulus (Tensile)
h_{max}	Depth at peak load (NI)
H	Hardness (NI)
HDPE	High Density Polyethylene
HV	Vickers Hardness
HS	High Sulfur
HGT	High glycine tyrosine
IF's	Intermediate Filaments
KAP	Keratin Associated Proteins
MPa	Megapascal
MS	Maximum Stress (Tensile)

mm	milliliters
µm	Micrometer
µl	Microliter
mN	Millinewton (NI)
18-MEA	Methyl eicosanoic acid
NI	Nanoindentation
nm	Nanometer
OM	Optical Microscopy
P_{max}	Peak load (NI)
PE	Polyethylene
PVC	Polyvinyl chloride
PTFE	Polytetrafluoroethylene
PP	Polypropylene
P1- P4	Position 1 (P1), Position 2 (P2), Position 3 (P3), Position 4 (P4) scalp positions
ν	Poisson's ratio
Er	Reduced elastic modulus (Indentation Modulus-IM)
RH	Relative Humidity
S/N	Signal to noise ratio
SEM	Scanning Electron Microscopy
TEM	Transmission Electron Microscopy
TGA	Thermogravimetric analysis
UHS	Ultra high sulfur
WE	Work of Elongation (Tensile)
XRD	X-ray diffraction
YS	Yield Stress (Tensile)

CHAPTER - 1

Introduction to Proteins and Hair

The current chapter describes gives an overview of keratin proteins, structure & properties of hair, available literature concerning the thermal and mechanical properties of hair. The chapter concludes with the limitations of existing research, objectives of the present research and overview of all chapters.

Proteins are the major constituents of hair and the most abundant protein in human hair is keratin, which is also a long polymer of repeating units called amino acids. Hair cross-section has three regions namely cuticle, cortex and medulla as shown in Figure 1.1(a). The cuticle is the outermost layer having a thickness of 2 - 5 microns. Cortex is the thickest (40 - 100 µm) and it is the visible part of the hair cross-section when observed under an optical microscope and it is composed of subunits called cortical cells. Medulla is the innermost part of the hair and it may be discontinuous in some sections of the hair sample. Medulla thickness varies between 8 - 12 µm and it also consists of cortical cells. Cortical cells are made of macrofibrils of 0.4 to 0.5 µm diameter which are glued together by a cell membrane complex. Each macrofibril can be considered as a composite which consists of microfibrils and amorphous keratin matrix rich in S-S linkages and is described in the later part of this chapter.

Figure 1.1:(a) Schematic diagram of human hair fiber structure [Bhushan 2010]
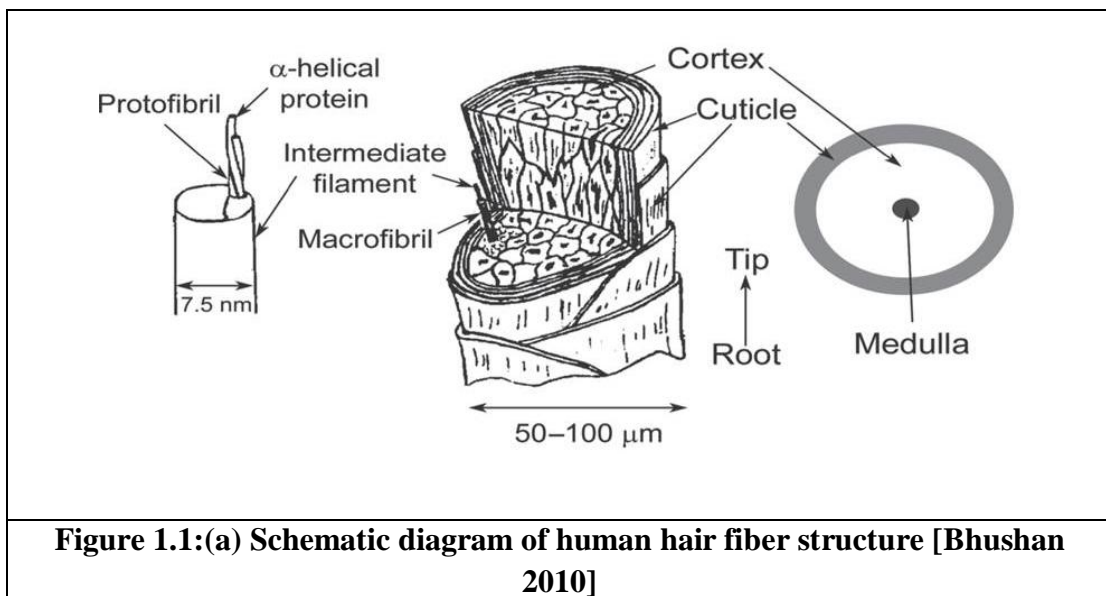
Proteins are essential for the functioning of all living cells. They are the structural components of muscles, tissues, and organs. Proteins are also present as enzymes and hormones and they are the most abundant nitrogen containing organic molecules present in plants and animals. Proteins are polymers of amino acids which are made up of carbon, oxygen, nitrogen, hydrogen, and sulfur. Every amino acid contains two functional groups - amino group (basic) and a carboxyl group (acidic) - along with side chain (R-group) (Figure 1.1(b)) specific to each amino acid and there are 21 different amino acids present in hair [Robbins 2002]. A peptide bond is a covalent bond linking two consecutive amino acids as monomers and it is present along the protein chain as shown in Figure 1.1(b).

Figure 1.1(b): Formation of peptide from two amino acids with amino (-H$_2$N) and carboxyl (-COOH) groups reacting to form peptide bond. R is the side group.
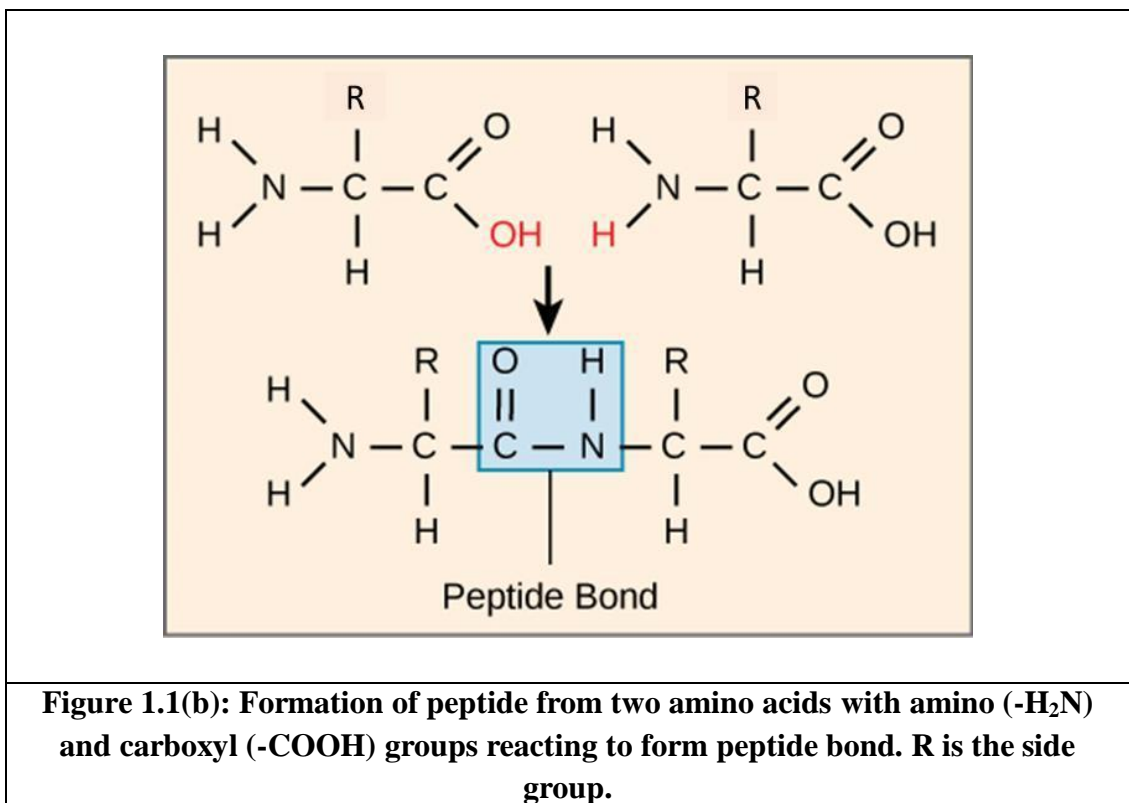
Proteins are very large molecules having different kinds of arrangement hence the structure of proteins has been divided into four levels as described below and also shown in Figure 1.2.

1. *Primary structure* is the linear sequence of amino acids forming the backbone of proteins.

2. *Secondary structure* is the spatial arrangement of amino acids by twisting of the polypeptide chain (backbone of the proteins). These polypeptide chains often fold into two types of secondary structures called as α helices and β sheets.

3. *Tertiary structure* is the overall structure of the polypeptide chains i.e., once the polypeptide chain forms α helix or β sheet, the entire structure curls into a shape as shown in Figure 1.2.

4. *Quaternary structure* is the final microscopic structure formed by the combinations of multiple units of β sheets or α helices. This is the first spatial structure visible when proteins are observed under atomic force microscopy.

From the above classification, the first observed structure is the quaternary structure and then the subunits (clusters) of the quaternary structure that are of the same three dimensional structures observed in the tertiary structure. The subunits that make up the tertiary structure are studied in the secondary structure and the chemical substructure of the secondary structure is studied in the primary structure. Figure 1.2 shows the schematic arrangement of all four structures.

Figure 1.2: Four levels of protein structures.
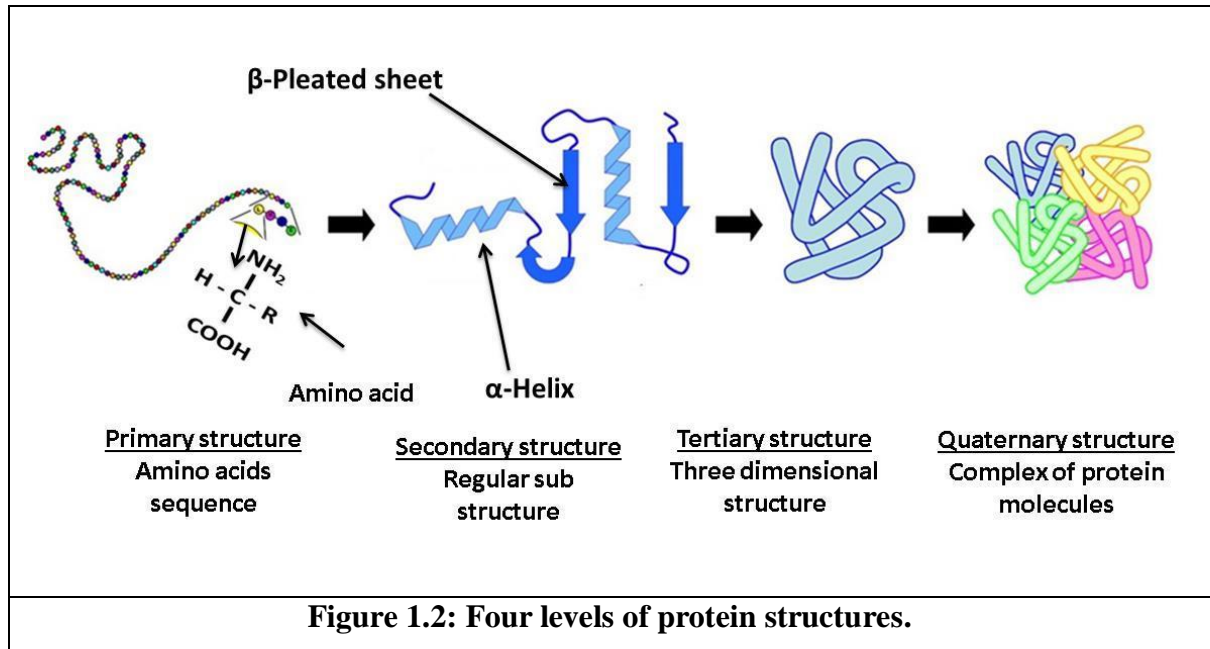
Protein structure is stabilized by covalent and non-covalent bonds. The covalent bonds that link amino acids are peptide (CO-NH) and disulfide bonds (S-S) between the side chain of cysteine amino acids and contribute to the structural conformation

and stability of proteins. The main non-covalent bonds are hydrogen bonds (Figure 1.3), electrostatic bonds and Van der Waals forces. Electrostatic bonds or salt bridges occur in a position parallel to the axis line of the rotation of the helix and also contribute to hair stress and elasticity. The secondary structure of α helix is a right handed coil stabilized by hydrogen bonds between the neighboring helix coils. The other secondary structure of proteins is the β sheets which is stabilized by the formation of hydrogen bonds between two or more adjacent strands.

Figure 1.3: Various types of side bonds in hair protein structure.
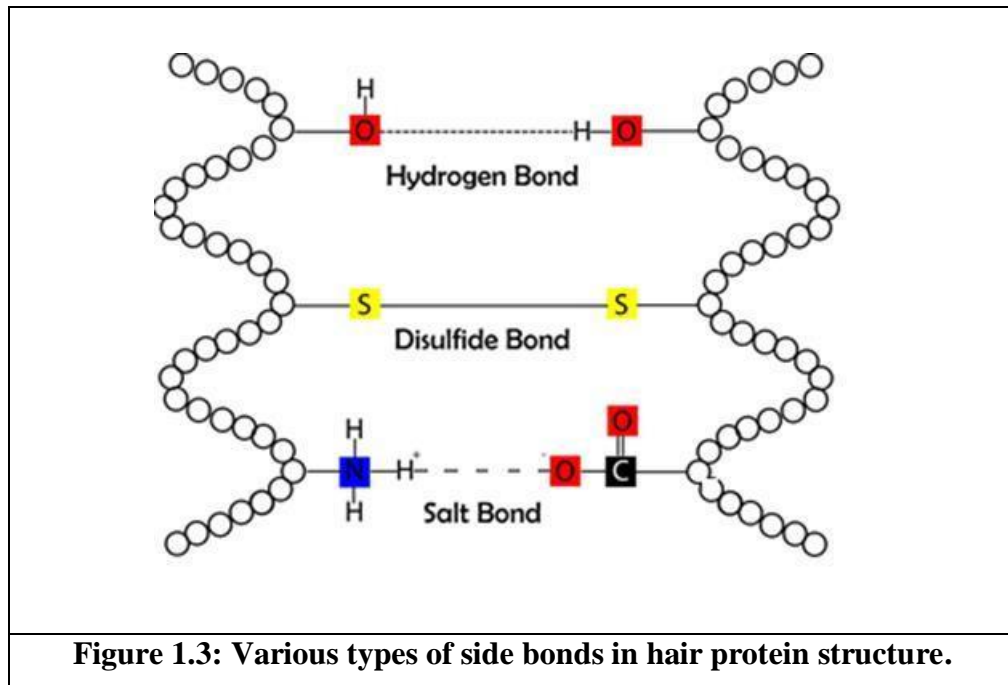
Proteins are considered as polymers of amino acids. Proteins can be classified into two main groups: Functional and Structural proteins. Functional proteins include enzymes, receptors, antibodies etc. and are globular in nature. These proteins are more complex in conformation than structural proteins, have a far greater variety of roles in metabolic reactions and are dynamic rather than static in their activities.

Structural proteins, on the other hand, are not globular but coiled and extended. These are insoluble in all common solvents such as water, dilute acids, alkalis, and salts and also in organic solvents. Keratin, Collagen, and Fibroin proteins are structural proteins as shown in Figure 1.4. These proteins are mainly from animal origin. Most of the structural proteins serve in a structural or as a protective role and they can stretch upon loading and later recoil to their original length upon unloading. Hair fibre is a keratin protein as discussed earlier.
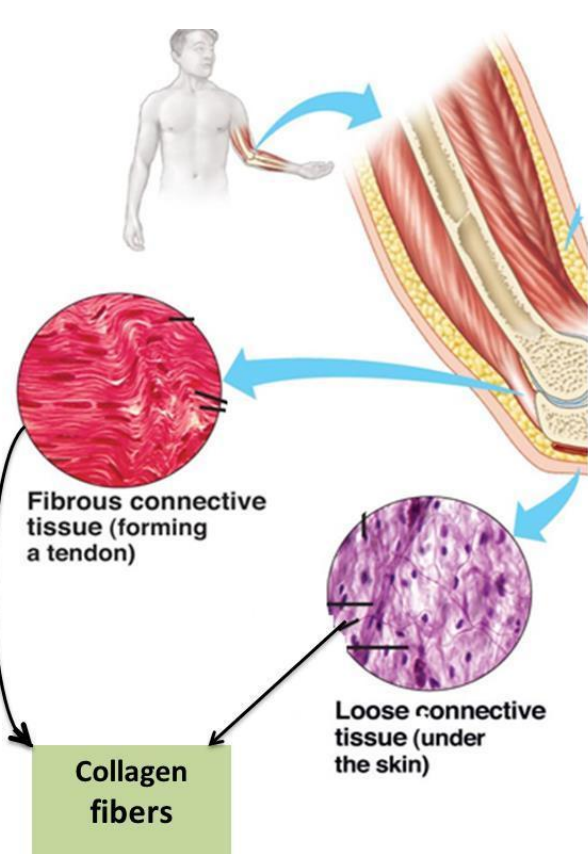
Keratin Protein

Hair, horns, wool, quills, feathers and beaks. Strain to failure of wool is above 30 % and its diameter is 20-50 μm.

These are tough, rigid and hard with α-helices (α keratin).

The covalent bonds that link amino acids are peptide and disulfide (S-S) bonds.

	Collagen Protein Skin, tendons (connect muscle to bone), cartilage, the organic part of bone and teeth, walls of blood vessels. These protein fibres have high tensile stress.
	Fibroin Protein Silk fibres with 1-3µm diameter and 20-30 % strain are known to have high elastic modulus (10 GPa) Microcomposite consists of a crystalline protein as fibres and cross-linked amorphous network (60 %) as matrix

Figure 1.4: Classification of Structural Proteins.

1.1. Overview of keratin proteins

Keratin is a structural protein which is present in the outer layer of human skin and as the primary protein in hair and nails. Keratin is also the main constituent in animal hairs, and its mineral and organic composition is similar in human and animal hairs. Human hair is a composite made of amorphous keratin matrix and crystalline keratin α helix coils which aggregate together by forming disulphide bonds. The spaces in between the α helix coils of keratin are again filled by the keratin matrix. This aggregation of the α helices of keratin proteins is called intermediate filaments. The matrix is rich in cystine content, which contains unique sulfur containing cysteine amino acid (crosslinks of disulfide bonds). The formation of disulfide bonds in cystine is by oxidation of two cysteine amino acids as shown in Figure 1.5 [Claude and John 2005].

Figure 1.5: Disulfide bond formation from two cysteine amino acids.
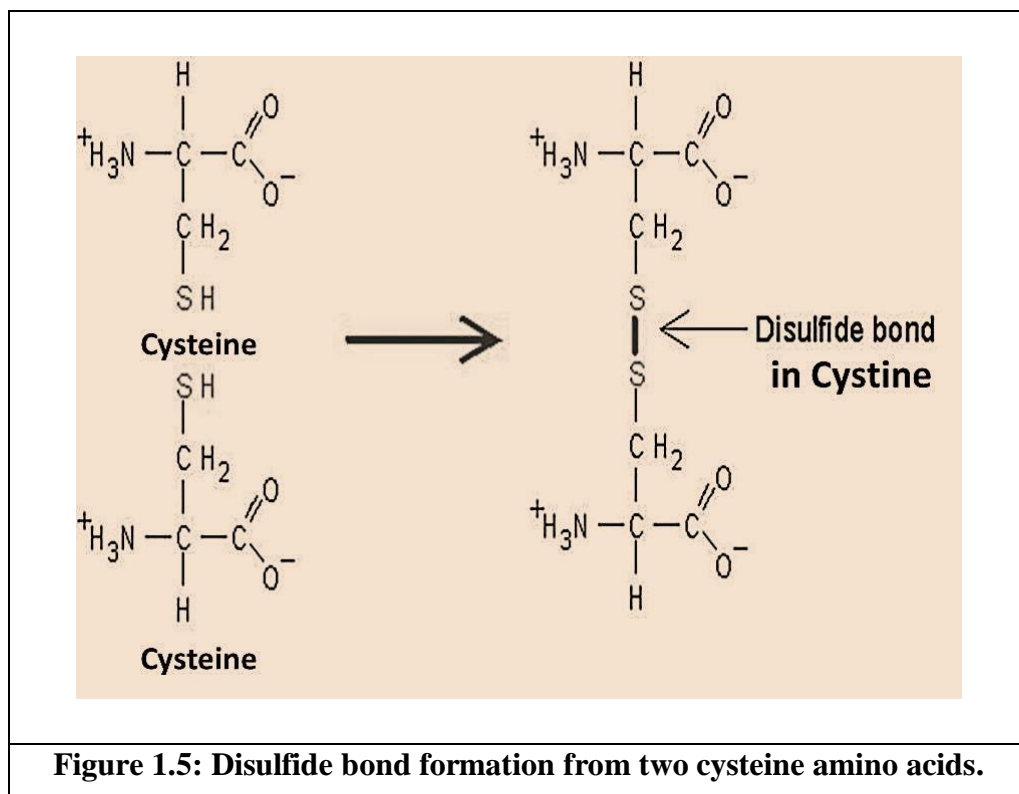
The hair shaft which is formed by keratinized cells contains highly organized structure with high resistance to various environmental conditions such as tension, friction, UV radiation and chemical attack. Hair and Nail are the important keratin proteins and their structure is described below.
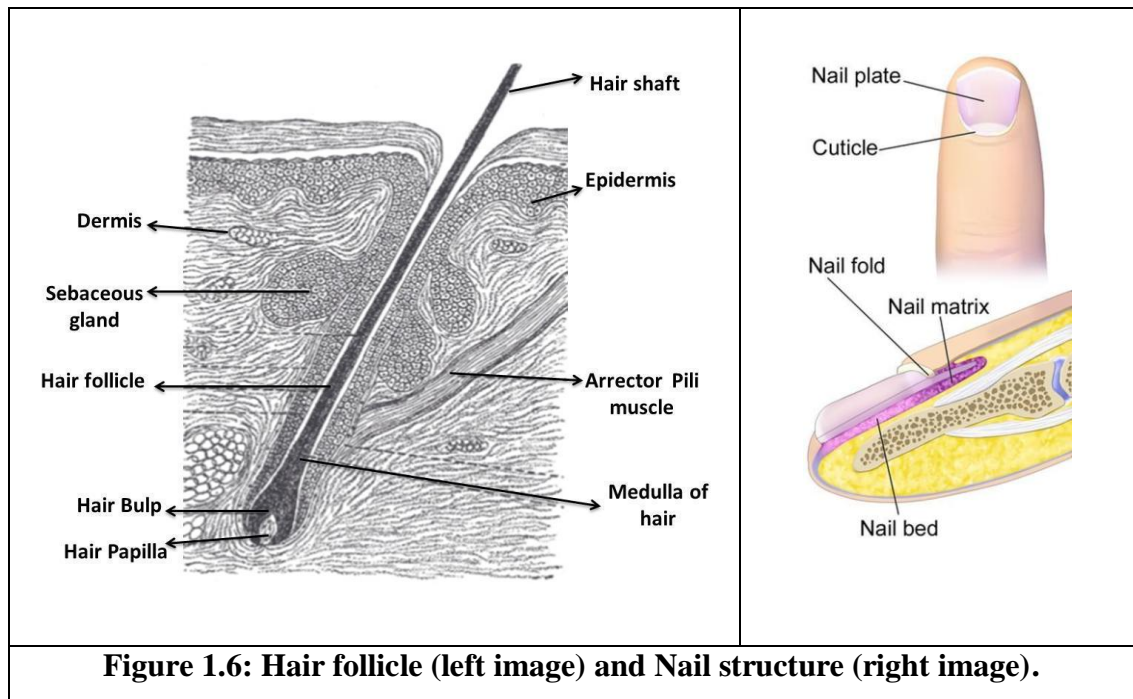
Figure 1.6: Hair follicle (left image) and Nail structure (right image).

Human hair is a biological tissue that is mainly composed of keratin protein and it grows out through the epidermis of mammals. Hair is composed of proteins between 65 % and 95 % by weight depending on moisture content which can be as high as 34 % by weight [Robbins 2002]. Hair is a keratin-containing appendage that grows from large cavities or sacs called follicles. Hair follicles extend from the surface of the skin through the epidermis into the dermis as shown in Figure 1.6. In nails, keratin is in the form of broad masses of short fibrils compared to hair having longer keratin fibrils. The mean water content for normal nails is around 11.90 % and for brittle nails it is 12.48 %. Hair and nails have a matrix that develops the keratinizing cells and the newly formed cells pushes the older cells in forward direction thus making hair and nails to grow longer. Shridhar Chillal from India had made it to the Guinness Book of World Records in 2016 for having the 'Longest Fingernails on a Single Hand Ever'. Nails are made of a tougher keratin protein. Structurally nails contain nail plate, matrix and nail bed. The matrix develops the cells thus the nail plate is formed progressively as shown in Figure. 1.6. The nail bed is the skin below the nail plate. It is made up of two types of tissues, dermis and epidermis just like in the skin. The dermis is the living tissue which includes capillaries and glands and the epidermis is the layer just beneath the nail plate. The keratin sheets in nail stack on top of each other, giving the nail enough thickness and stress [Forslind et al. 2004]. Onychosis is

a one type of nail disease reported in humans. Hardness of healthy nails is approx. 0.23 GPa and Young's modulus is around 4.62 GPa as derived by nanoindentation [Laura et al. 2009].

1.2. Structure and Chemical composition of hair

The hair shaft is 40 - 120 μm in diameter and consists of three separate regions: cuticle, cortex and medulla (Figure 1.7 and Figure 1.9). The cuticle is the outermost part, and it is a thin region with flat overlapping cells encircling cortex. The cortex is the thickest region and it contains well organized keratin fibre bundles characteristic of hair shaft. The innermost part of hair is the medulla which may be completely absent or present continuously or discontinuously along the length of the hair shaft. Cuticle, cortex and medulla are discussed in detail in the following paragraphs.

The natural color of the hair is rendered by the melanin pigments present in the cortex. There are two types of melanin pigments present in hair. First one is eumelanin which gives the shades from brown to black. Second one is pheomelanin which gives the orange and red colors to the hair. The hair colour depends not only on type of melanin pigment present but also on the quantity, spatial distribution of the pigment and the shape of the pigment granules [Claude and John 2005].

Hair grows around 1cm per month. The hair growth cycle is divided into three phases and they are anagen, catagen and telogen phases. At a given scalp location, different hair strands are going through different phases at any given time. Anagen is the active phase of the hair cycle. When the cells in the root of the hair divide at a rapid rate, the anagen phase can range between two and seven years. The catagen phase is the transitional stage and lasts for two to three weeks. The telogen is the ending phase which also lasts for few weeks. At this phase, growth is completely stopped and a new hair that begins to grow below the telogen follicle pushes the old telogen hair fibre out and it is eventually shed. This could be the reason why most of the people collect few hair follicles when combed and this should not be treated as a hair fall. There are three types of human hairs: lanugo (prenatal hairs), vellus (body hair) and terminal hairs. In humans, the first type of hair that grows usually in third or fourth month of fetal life is called lanugo hair. These lanugo hairs are lightly pigmented or sometimes not pigmented at all. Vellus hair is short and fine that covers body and its role is to protect

the skin and keep the body warm. The terminal hair is longer, thicker, pigmented and mature hair that grows on the scalp.

1.2.1. Cuticle

The cuticle has scale like cells that form layers (5 - 10) and these layers cover each other like roof tiles (Figure 1.8). The number of scale layers can also serve as evidence in identification of origin of hair follicles in forensic studies. Each cuticle cell is around 0.3 - 0.5 µm thickness and length of each cuticle cell is approximately 5 - 10 µm [Robbins 2002]. The cuticle contains smooth unbroken scale edges near the root side of hair shaft. However cuticle damage is observed near the tip of hair shaft in the form of broken scale edges and lifting of scales due to weathering and mechanical damage from the effects of normal grooming actions, like combing, brushing, and shampooing. Sunlight could also aid in cuticle damage. The cuticle deteriorates and progressively thins until two or three superimposed cell layers remain leading to the phenomenon of split ends. The cuticle cell is covered with a very thin membrane, called as epicuticle and beneath this membrane the cell is composed of three layers: A-layer, exocuticle, and endocuticle [Claude and John 2005].

Figure 1.7: SEM image of fractured hair revealing cuticle, cortex and medulla in single hair shaft.
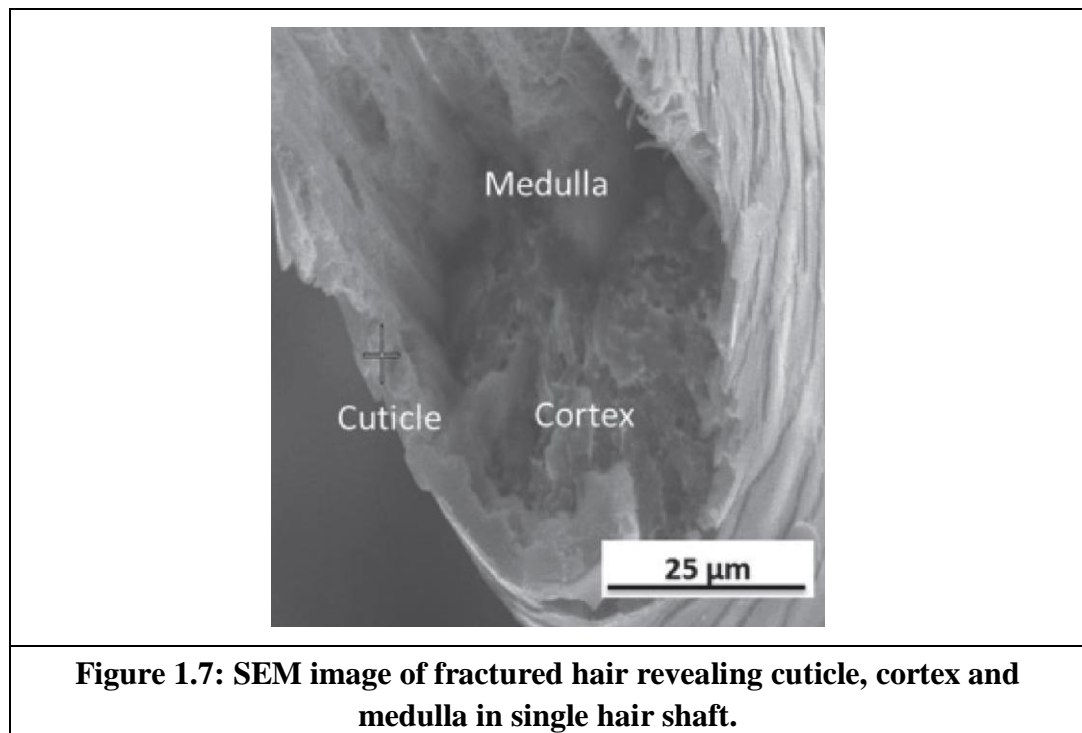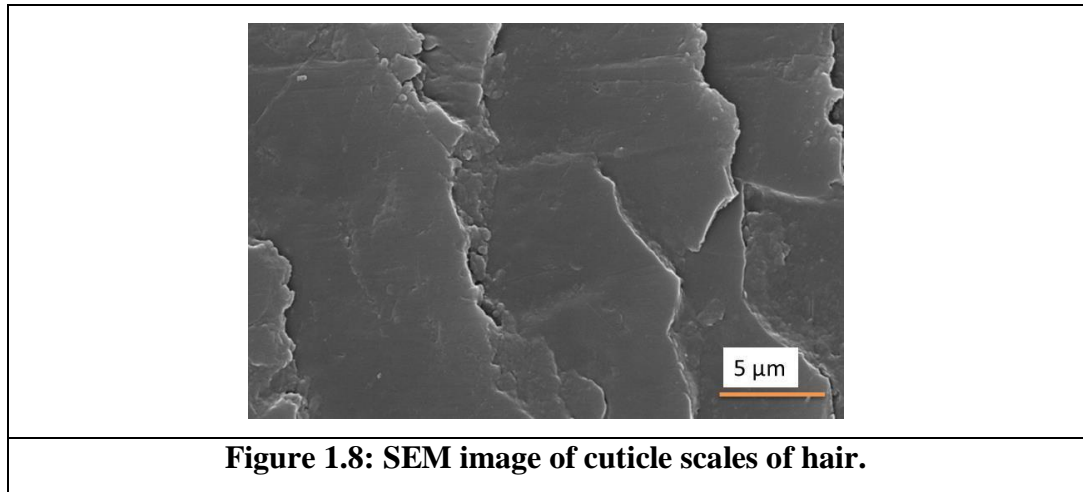
Figure 1.8: SEM image of cuticle scales of hair.

The epicuticle is about 5 - 7 nm thickness and acts as a semipermeable membrane. The epicuticle plays an important role in determining the surface properties of hair. It consists of a proteinaceous layer covered by a lipid layer (methyl eicosanoic acid 18-MEA being the main constituent). Beneath the epicuticle, the A-layer and exocuticle are regions composed of proteins with cystine content of around 30 % and 15 % respectively. The proteins in these regions of the cuticle cells are strongly crosslinked and belong to the high sulfur (HS) and ultra-high sulfur (UHS) groups of keratin associated proteins (KAP), which are similar to the proteins that make up the matrix in some parts of the cortex. The cuticle in this part is poorly soluble and resistant to chemicals but it shows a little swelling in water. The endocuticle consists of proteins of very low sulfur content. It is porous, soft and has a weekly cross linked structure accessible to water.

1.2.2. Cortex

It consists of high level of organized proteinaceous material which gives it unique mechanical properties. The cortical cells are of length around 100 μm and diameter of 2 - 5 μm. In case of wool, cortex contains three different cortical cells called ortho, para and mesocortical cells with varied percentage of protein composition. In human hair, the type of cortical cells is unclear, but ortho cortical cells observed in curly hairs [Claude and John 2005] and their proportion and distribution depends on degree of curliness. The cortical cells consists macrofibrils as shown in Figure 1.10 and Figure 1.11 [Claude and John 2005]. The macrofibrils are perfectly oriented along the axis of fibre. They are made up of organized structured proteins as reinforcements

called microfibrils or Intermediate Filaments (IF) which is embedded in amorphous keratin protein called as matrix (rich in S-S linkages).

1.2.2.1. Intermediate Filaments (IF's)

All hard keratin fibres irrespective of their biological origin (human hair, wool fibres or porcupine quills) have a common feature of X-Ray Diffraction patterns. It is due to the association of Type I and Type II keratin chains. Based on their sequence homology they form highly structured crystalline phases which are called intermediate filaments (IF's) and their formation is a four-step process as discussed below.

1. The organization of α-helices

2. The association of type I and type II keratin to form a dimer

3. The gathering of two dimers to form a tetramer

4. The organization of a pseudo-hexagonal structure (IF's structure) by the association of seven or eight tetramers

X-ray diffraction study shows that the α-structure of keratins and the formation of dimers happen in the process of keratinization at an early stage and the final step of maturation of hard α-keratin takes place at the upper end of the follicle. This helix consists of 3.7 amino-acid residues per turn and it is stabilized by the hydrogen bonds [Claude and John 2005].

1.2.2.2. Matrix

The intermediate filaments (IF) are embedded in the matrix made of proteins called Keratin Associated Proteins (KAP) which is different from type I and type II keratins of the IF and are considered as amorphous. The relative percentage of matrix (KAP) in the cortex is about 60% while it is only ~ 40 % in case of IF's. Despite having matrix with high cystine content, KAP's mechanical and physical behavior (particularly water swelling) of cortex region do not resemble like a highly cross linked polymer. The matrix plays crucial role in providing the hair structural stability by binding together with intermediate filaments. The intercellular spaces also called
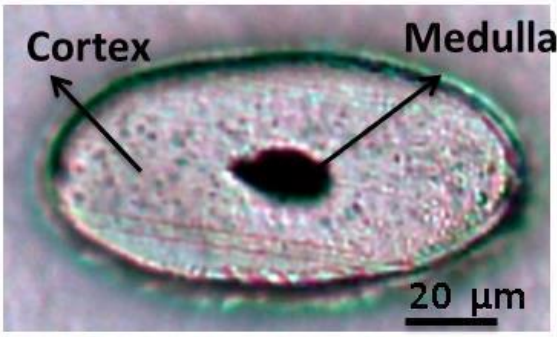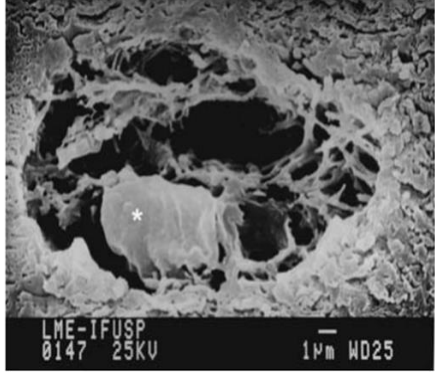
as cell membrane complex (cell membrane complex) play an important role in cell cohesion in both the cuticle and the cortex regions of hair [Claude and John 2005].

| Figure 1.9: Hair cross section revealing cortex and medulla regions. | Figure 1.10: SEM fractography of hair revealing macrofibrils. |

Figure 1.11: Schematic structure of human hair [Grace et al. 2016].
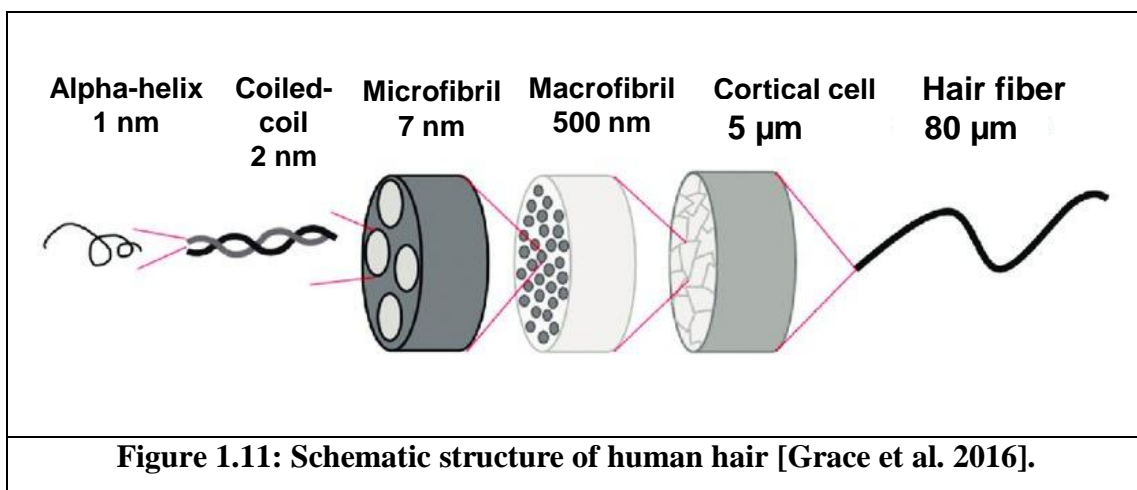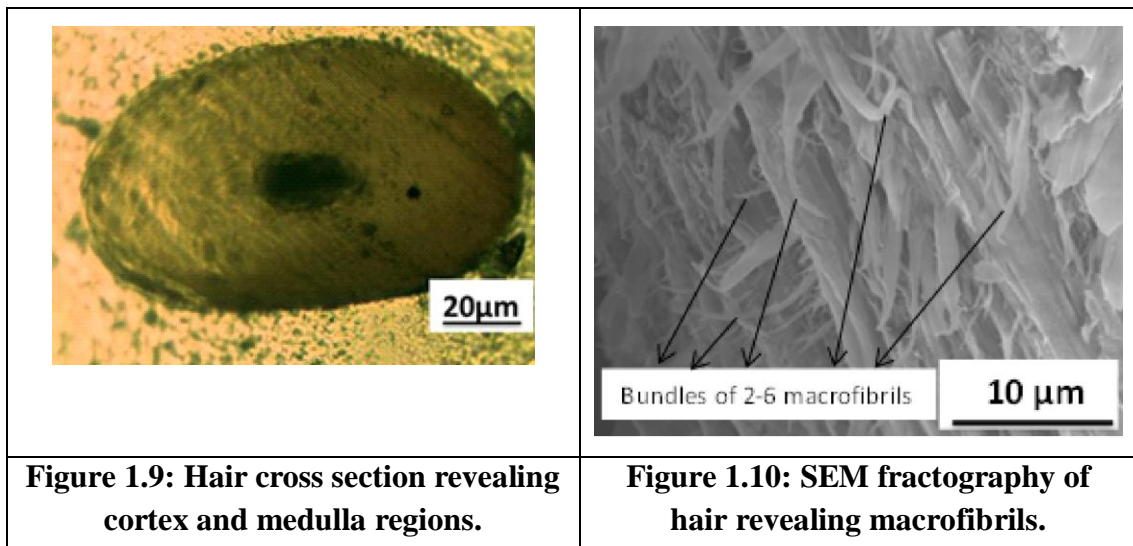
1.2.3. Medulla

The medulla is the major part of the fibre in the case of furs of many mammals as shown in Figure 1.9 and Figure 1.12. In human hair it may completely absent or present in fully or fragmented form. Clement et al. [1982] reported that the medulla of human hair also contains microfibrillar structure similar to that of cortex, but the orientations of microfibrils are not parallel with the hair axis as shown in Figure 1.13. From the SEM image of Medulla region, one can observe macro globular structure and also micro globules with air vesicles in between. It can be said that, medulla has loose packed structure with large empty spaces between them.

The proteins content in medulla is low compared to cortex. The medulla index (ratio of medulla diameter to hair diameter) is always less than 0.3 in human hairs. To distinguish between human hairs and animal hairs, it is essential to examine the medulla, but it cannot be used as a basis for individual identification of hairs. Wagner et al. [2007] observed thick and thin types of medulla in human hair and also studied the morphology of thick medulla using Transmission Electron Microscopy (TEM). They also found that medulla contains more globular structures with cavities and organization of the microfibrils increases from the medulla centre to medulla periphery.

Figure 1.12: Hair cross-section with visible medulla of 20 μm diameter.	Figure 1.13: SEM image of porous thin medulla of human hair [Wagner et al. 2007].

Hutchinson et al. [1999] found the effect of medullation on hair cycle by examining medulla size for anagen phase of terminal hairs. During stage of anagen phase, the size of medulla is thicker and at end of anagen phase it is virtually absent. If hair diameter is assumed as 100 %, then the medulla cross-sectional area, medulla major axis and medulla minor axis will be around 7 %, 23 % and 26 % respectively. The micro morphological parameters, hair index (ratio of the minimum hair shaft diameter to the maximum hair shaft diameter) and medulla index remains same for male and female of Thai origin [Srettabunjonga et al. 2016] with age group of 0 - 80 years. From the literature on human hair medulla, few studies are done and also assumed that that its contribution is negligible on various properties of fibres, but recently its

effect on optical properties is seems to be significant [Hutchinson et al. 1999, Wagner et al. 2007 and Tolgyesi et al. 1983].

1.2.4. Chemical Composition of Human Hair

Hair is mainly composed of keratin protein with high content of cystine amino acid (around 15 %). Lipids and water are also present depending on location in hair (cuticle, cortex and medulla). The lipid content of the hair is approx. 2 % and small quantities of carbohydrates and inorganic salts are also present in hair. The main chemical composition of hair is shown in Figure 1.14.

The main cuticle layers endo- and exocuticles have different chemical compositions. The endocuticle contains low content of cysteine (3 – 6 %), and more amount of hydrophilic amino acids whereas exocuticles are rich in cysteine (15 – 20 %). Medulla contained virtually no cystine but lower amount of hydroxy amino acids. The cortex of hair contains different keratin proteins based on the amount of specific amino acids [Claude and John 2005].

Keratin protein (Amino acids)	65–95% $\overset{\oplus}{N}H_3—CH—R$ (R: functional group), $CH—CO_2^{\ominus}$
Cystine	$\overset{\oplus}{N}H_3—CH—CH_2—S—S—CH_2—CH—\overset{\oplus}{N}H_3$, $CO_2^{\ominus}$, $CO_2^{\ominus}$
Lipids	Structural and free
18-methyl eicosanoic acid (18-MEA)	$H_3C—CH(CH_3)—(CH_2)_{16}—COOH$
Water	Up to 30%
Pigment and trace elements	Melanin

Figure 1.14: Chemical species present in human hair [Bhushan 2010].

In human hair, wool and other keratin fibres, the relative amounts of IF proteins and KAP's can be variable. IF keratins called "low sulfur keratins" (their cystine content is about 6 %) belong to a class of proteins in form of filamentous structures. IF proteins (similar in all types of hair) are present in the form crystalline fibrils and KAP are in the form of amorphous matrix similar to polymer composite structure wherein fibre reinforcement resembles IF's and polymer matrix resembles KAP's.

The KAP proteins are classified into three types based on specific amino acid amounts.

1. The High Sulfur (HS) proteins containing around 20 % cystine residues.

2. The Ultra High Sulfur (UHS) proteins which contain higher content of cystine (30 – 40 %).

3. The High Glycine Tyrosine (HGT) proteins have large amounts of glycine and tyrosine amino acids.

The nature of KAP's will determine the spatial arrangement of IF. The presence of UHS based KAP's results a pseudohexagonal arrangement of the IF. Hair also contains variable amounts of inorganic elements (lower than 1 %) and they are alkaline metals (K, Na), alkaline earth metal (Mg, Ca, Sr), other metals (Zn, Fe, Mn, Hg, Cd, Pb, As, Se) and metalloids (Si, P). The aggregation of some metal can lead to systemic disorders in hair. For example the presence of heavy metals in tap water or air leads to an increase in heavy metals content in hair [Gibson et al. 1983].

Water is an essential component in proteins especially in the process of stabilization of protein structure. In hair or wool fibres, bound water and water absorbed by fibres affects all the physical properties and also reflects hair architecture [Claude and John 2005]. Thermal, spectroscopic and electrical studies shows that water is bound to proteins to a varying extent by hydrogen bonds either to the acidic or basic groups of the side chains or to the peptide bonds and also reported that water can condense on itself to form clusters. The most obvious expression of water absorption is hair swelling, but the swelling is highly anisotropic. The increase in hair length is only about 2 % but the diameter increase is around 15 % for the increase of relative humidity (RH) from 0 - 100 %. The reason is that water is basically absorbed by the hydrophilic matrix present in the cortical cells but does not penetrate into the crystalline regions of IF's or microfibrils. The water in hair has therefore little or no effect on the structure and dimensions of the microfibrils, as manifested by X-ray diffraction studies. Absorption of water molecules is assumed to take place at the boundary between microfibrils and the matrix. As a result, water is able to slightly distort the structure of microfibrils. Hence the microfibrils oppose the longitudinal swelling of the matrix but its volume is increased by diametric swelling of the hair. However, some observations suggest that some non-keratinous areas of hair like cell

membrane complex, the endocuticle and the intermacrofibrillar spaces might participate in hair swelling to a certain extent. Absorption of water also modifies the structure of the organized lipids. Water absorption and subsequent swelling depends mainly on pH level.

1.3. Properties of Human hair

The chemical and physical properties of the hair are influenced by age, gender, climate, surrounding environment and food habits. Although, chemical structure of hair is known, it is difficult to correlate this with the physical properties of the hair, since 21 different amino acids are found in human hair [Robbins 2002]. The properties affecting scalp hair are basically its mechanical properties. Among the mechanical properties of hair fibres, tensile and nanoindentation (localized compression) properties are discussed here. Among the physical properties of hair fibres, diameter and linear density are discussed. These are important properties in determining the quality of the fibre in terms of structural heterogeneity exists along the length and diameter of the hair shafts.

1.3.1. The physical properties of hair

The physical properties of hair depend on the organization of the various structural elements of the fibre (microfibrils, matrix, cell membrane complex, lipids). The amino acids, their individual composition variations in hair and their structural morphology determine the physical properties of hair. These properties are responsible for hair quality, appearance and their improvement is the main purpose of any hair treatment.

The diameter of human hair ranges between 40 - 100 µm and the length can vary from one mm to one meter. In several studies it is found that African hair is elliptic in cross-section and shows a large variation in diameter and has low tensile stress and strain as compared to Asian and Caucasian hair. It is reported that Asian hairs are circular in cross-section with diameter of 80 - 100 µm, but hair becomes gray and thin with aging, especially scalp hair. The hair diameter of Korean hair was [Jeong et al. 2011] found to increase for the first 20 - 30 years of age after that it began to decrease. In case of Japanese hair the maximum diameter is observed in the age group 40 - 49 years. The important factors considered for evaluating hair behavior in terms

of mechanical properties are cross-sectional area and it depends on age and degree of curl in hair [Sayathi et al. 2016]. The hair diameter and medulla index (ratio of medulla diameter to hair diameter) are measured using optical microscopy. Linear density is used in textile engineering and it is the amount of mass per unit length. This gives us an idea of the yarn size in synthetic fibres (Yarn is a continuous strand of fibres used in weaving and knitting to form fabric).The units used in linear density are g/cm, decitex (weight in grams of 10000 m of yarn), denier (weight in grams of a 9000m length of yarn) and tex (weight in grams of 1000 m of yarn). Denier is commonly used in the US and tex is commonly used in Europe. The higher the linear density (denier or tex), the heavier the yarn and linear density is used in evaluating the tensile properties of textile fibres in terms of cN/tex. In this thesis linear density of hair is found using mass (g) / unit length (cm).

The conversion factor for fibres from diameter to linear density is

$$d = 11.3 \sqrt{\frac{dtex}{\rho}}$$

Where d = diameter of fibre in μm ; ρ = density of fibre in g/cc; dtex = decitex

1.3.2. Mechanical properties of hair

The unique organization of structure of hair has remarkable effect on its mechanical properties. The slightest modification in the chemical composition or structure of hair may lead to a change in its nanomechanical properties. Mechanical properties may vary with respect to temperature, humidity, exposure to chemical and external environments. Mechanical properties of α keratin hair fibres are primarily dependent on the matrix, in which IF's are embedded [Feughelman 1982]. The four types of stresses generally considered are tension/compression (uniaxial mode), shearing, torsion and flexural and the stress can be applied in static or dynamic mode. In this thesis our focus is on tension and compression. Tensile tests were conducted to obtain bulk (microscale) mechanical properties and nanoindentation was carried out to get surface (nanoscale) mechanical properties. Tests were also conducted to observe the influence of medulla on nanomechanical properties.

1.3.2.1. Tensile properties of single fibres

The tensile properties of hair have been reported since long and are easy to perform due to the geometry of hair, but it is a tedious process to prepare samples because of the fineness of the fibres. The standard for specimen preparation for tensile testing of single fibres is ASTM-3379-75. The tabbing technique and direct gripping are used for tensile testing of single hair fibres as shown in Table 1.1. Since hair lengths are below 20 mm (few male donor hair samples) tabbing technique was adopted for all samples. There are certain critical requirements for testing fibres such as alignment of fibre and the fibres should not be damaged by the gripping mechanism. To avoid such premature failure, these grips are coated with rubber. The single fibre with 10 mm or 20 mm gauge length is adhesively bonded to a cardboard frame having a rectangular slot as shown in Figure 1.15. The cardboard, with the bonded fibre, is clamped to the grips of a tensile testing machine. After completing all the adjustments and alignment procedures, the cardboard frame is cut off on the two sides, so that the single fibre is ready to be tested. Load is applied in such a way that only the fibre experiences the load and not the paper frame. The specimen is pulled apart until failure and load (force) and apparent deformation (displacement) is recorded. The tensile maximum stress is the maximum load divided by the initial cross-sectional area of the fibre. Likewise yield stress, elastic modulus and strains are measured form the stress-strain plot.

Table 1.1 Two different methods used for single fibre tensile testing of fibres.

Parameter	Tabbing technique	Direct gripping
Test standard	ASTM D 3379-75[1] (or)Tabbing technique of ASTM D 3822-01	ASTM D 3822-01[2] (or) BISFA 2004[3]
Test speed	1 mm/min	2 mm/min (E-modulus) 10 mm/min (Strength and elongation)
Gauge length	16 mm	10 mm (E-modulus) 20 mm (Strength and elongation)
E-modulus	linear regression	between 0.2 to 0.5 % strain
Pre-tension weight	- variable -	60 mg/dtex
Climatic conditions	23 °C and 50 % RH	21°C and 65 % RH
Diameter	Light microscopy	Vibroscope 400
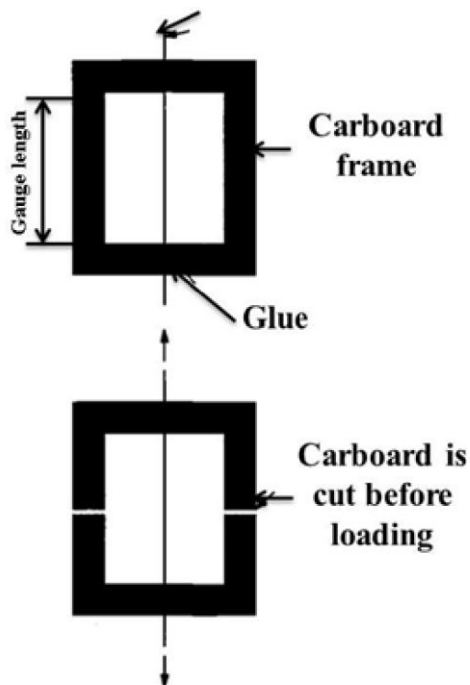
Figure 1.15: The cardboard frame (tabbing) technique to measure the tensile properties of a single hair fibre.

The tensile strain of hair is measured using extensometer or cross-head displacement. Force/displacement curve of single hair fibre is obtained from tensile test. Stress (force/cross-section area of fibre) and Strain (displacement/original length of fibre) are obtained using force-displacement data. The area under stress/strain curve of hair shown in Figure 1.16 can be divided into three regions for better understanding.

1. Between 0 to 2 - 3 % strain in which strain is proportional to stress applied and this region is called Hookean region, in which hair behaves like an elastic material.
2. Between 2 - 3 % to 25 – 30 % strain, strain increases rapidly without obtrusive change in stress and this region is called yield region.
3. After 30 % strain, stress is proportional to strain again, this is called as post yield region. In this region hair again behaves like an elastic material. The damage and fracture of hair fibre is observed in this region.

A lot of research was done on tensile properties of hair fibres and also on the three regions of stress/strain curves as a function of structural organization of keratin. Few studies on wool fibres under particular conditions observed transformation of α-keratin to β-keratin just beyond the Hookean region. From the yield region onwards, the percentage of β-keratin increases and at the end of this region around one-third of the keratin is in the form of β-structure under specific conditions. After 30 % of strain, the post-yield slope is independent of the hair region and the resistance to strain in this region is controlled by covalent bonds (specifically disulfide linkages). The hair in fact is never considered as a perfectly elastic material even in the Hookean region and return to the initial state of hair after releasing load takes place at a certain rate and hence the hair must be considered as a viscoelastic material. From the literature, hair fibres elastic modulus, maximum stress and maximum strain are 3.1 GPa, 201 MPa and 47 % respectively [Sayahi et al. 2016].

Tensile properties of twisted hair samples revealed that twisting followed by untwisting and giving 10 minutes time for relaxation has resulted the properties same as of virgin hairs [Dankovich et al. 2004]. But twisting alone reduced the properties of hair such as moduli, stress and strain values. Nikiforidis et al. [1992, 1993] studied hair tensile properties of two age groups considering a single position and also studied the properties of hair of people aged between 15 - 20 years considering two positions

(P1 - frontal and P4 - occipital). His group reported the need to consider the viscoelastic behaviour of hairs and the importance of linking the modulus ratio and energy ratio to the elastic and viscous behaviour of hair respectively.

The physical and tensile properties of pig hair with different breed and position (neck, back) are studied and found to be almost similar to other natural fibres like human hair and wool [Mohan et al. 2014] despite reporting a lower value of maximum strain (32 %). Slight variation in tensile properties with respect to breed and position on the body was also reported. Erik et al. [2008] reported that the tensile breaking force of hair has not shown any significant dependency on gender, age and presence of hair dyes. In another study [Kavitha et al. 2016] reported that no significant differences are observed when tensile properties of hair are compared between vegetarian and non-vegetarian samples, pigmented and non-pigmented samples but slight differences in elongation was observed when hair from young (<12 years) and old (>60 years) samples are compared. Insights on mechanical properties of hair fibres using simulations are provided by Antunes et al. 2016. They compared the mechanical property (Young's modulus) data with simulation data using steered molecular dynamics.

The hair fibre has high stress and toughness. Load required to obtain breakage of a natural healthy hair varies between 50 to 100 g. The average healthy scalp hair (around 120,000 hairs) may withstand 12 tons [Velasco et al. 2009] of load. African hair is fragile due to its highly twisted configuration. Asian hair is strong and the resistance to fracture is similar to that of Caucasian hair [Franbourg et al. 2003]. In grooming procedures, premature failure is increased by tensile and torsional fatigue [Kamath et al. 1982]. Three types of fracture are observed in the breakage of human hair under longitudinal extension using SEM and they are smooth fracture, step fracture, and fibrillated fracture. Relative Humidity (RH) and conditioning of the hair fibre play a major role in the type of fracture observed [Robbins 2002, Hearle 2000].

In tensile testing, sample is pulled in a direction perpendicular to the cross-section. A large volume of material is loaded which is equal to the product of the sample gauge length and cross-sectional area. Tensile test averages the mechanical response over the fibre length (ex. 20 mm of gauge length) whereas in contact mechanical testing or nanoindentation a probe with known or calibrated shape is brought down to a flat

surface of sample which measures local behavior over a contact diameter (ex. 10µm). Nanoindentation testing has become a popular for examining local variations in mechanical behavior of metals, wood, bone and fibres [Christopher 2006, Adusumalli et al. 2010, Ebenstein et al. 2006].

Figure 1.16: Tensile stress-strain curve of a single human hair fibre
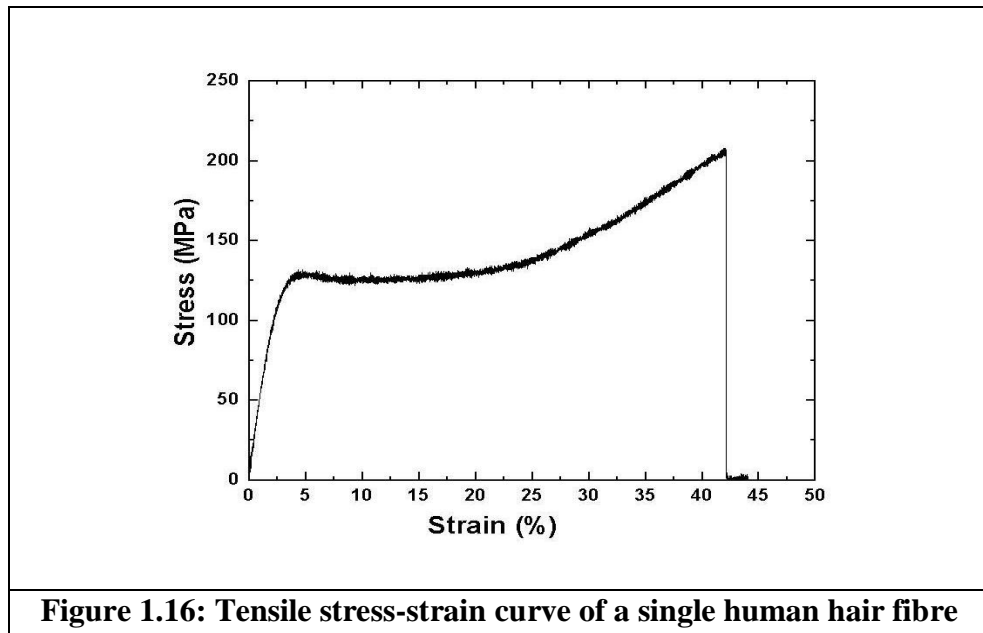
1.3.2.2. Nanoindentation of single fibre cross-sections

In a medical or a basic science context of use, research on natural materials is expanding with the application of modern materials characterization techniques with various length scales is shown in Figure 1.17. The introduction of these techniques in the study of biomechanics has also been associated with the application of materials science doctrine to biological problems i.e. focus has shifted subtly from purely mechanical explorations to investigations concerned with structure-property relationships.

Figure 1.17: Mechanical characterization diagram, explaining the relevant length scales involved in mechanical testing [Michelle 2011]
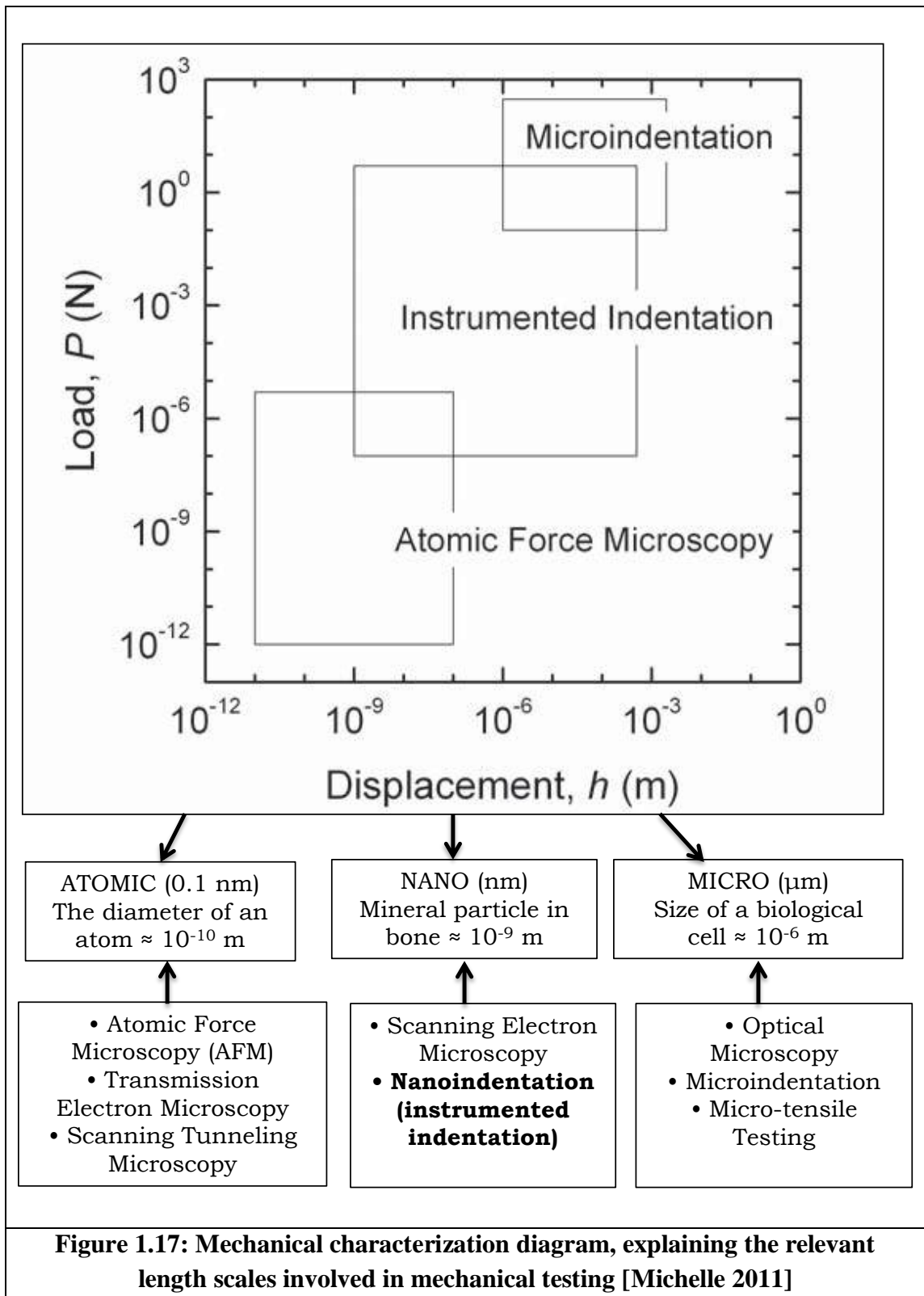
Indentation testing at very small length scales has been frequently referred to as nanoindentation although in reality it ranges from true nanoindentation to microindentation. Spherical, cube corner and Berkovich indenters are generally used in nanoindentation testing and tip diameter of these indenters are in nm.

Nanoindentation has emerged as a popular technique for characterizing the mechanical behavior of engineering materials as well as biological materials [Ebenstein et al. 2006]. Nanoindentation testing is used to measure the modulus (indentation modulus) and hardness of metals and biomaterials. From the literature, the first biological materials studied using nanoindentation is bone (modulus for bone is 20.1 ± 5.4 [Zysset et al. 1999]. Nanomechanical characterization of human hair fibres using nanoindentation provides valuable information about the hair constituents separately. That means cortex, medulla and cuticle properties can be determined quantitatively which is impossible in traditional tensile testing. It is also possible to determine the effect of cuticle damage, cortex damage and hair disorder treatments on mechanical properties especially modulus and hardness of the hair fibre. Nanoindentation is thus ideal for probing local heterogeneities in natural materials and may be applied to map out local heterogeneity in cortex zone of the hair shaft. [Michelle 2011]. The nanoindentation impressions on hair, bone and pulp fibres are shown in Figure 1.18.

Figure 1.18: Nanoindenatation indent impressions on (a) hair fibre cross-section [Samanta et al. 2016] (b) bone [Zysset et al. 1999] (c) pulp fibre [Adusumalli et al. 2010]
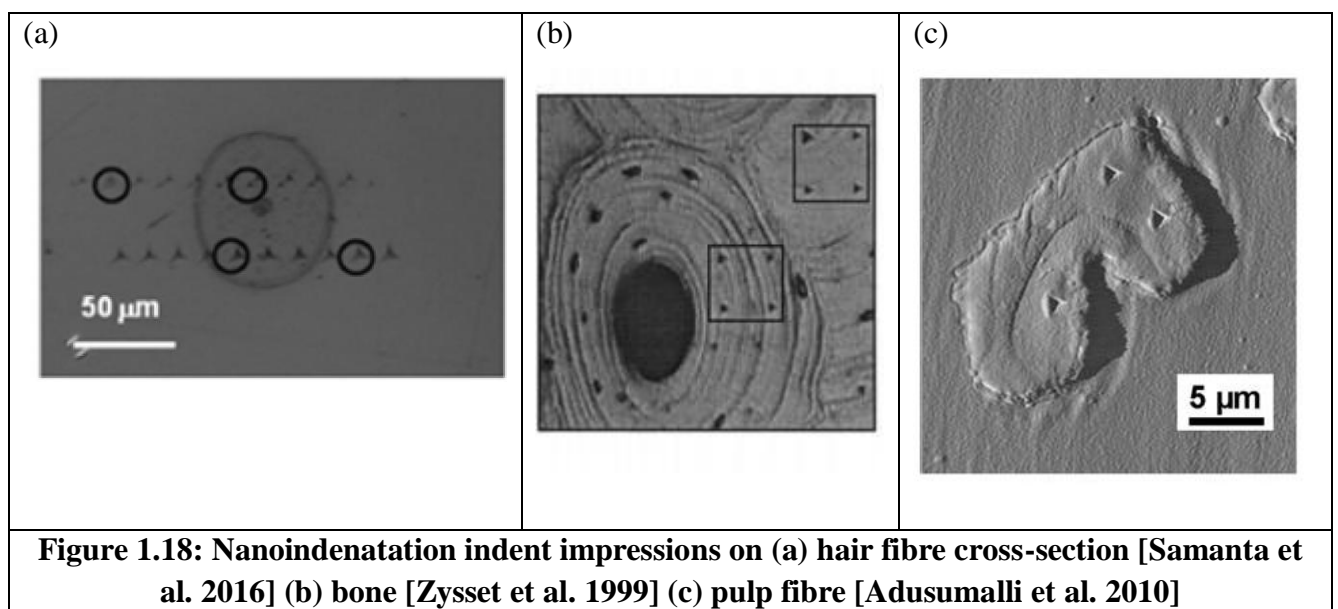
The conventional techniques used for measuring hardness of metals and thin films are Vickers Hardness (microindentation). In these methods, the residual impression on the sample is taken for calculating hardness value. In Vickers hardness test, area of residual impression (distance between the two diagonals of the indentation impression left on the surface of the material after removal of the load is measured and their

average calculated) is used as shown in Figure 1.19(a). In the nanoindentation technique hardness is measured from the maximum load like in Vickers test, but the modulus is obtained from the unloading portion of the load - displacement curve (Figure 1.19(b)). But the difference is in the measurement of area used to determine hardness. In Nanoindentation, projected area of contact with the known geometry of the indenter based on depth of penetration is used to determine hardness, similar to bloom stress of gels. In Nanoindentation impression dimensions after the test are not measured whereas in Vickers hardness test, impression dimensions are measured in both diagonals as described below.

Hardness in Vickers (HV) is calculated as

$HV = 0.1891*F/d^2$

Where F is the applied load and d is the average of the diagonal length [(d1+d2)/2] of indent impression in mm Hardness in MPa is calculated as follows:

$H = 0.1891*9.8*F/d^2$

Figure 1.19: (a) Impressions of Vickers indentation on aluminum with pyramidal diamond indenter (Adonias et al. 2004). (b) Load-depth curve for an elastic plastic solid from nanoindentation test [Fischer-Cripps 2011]
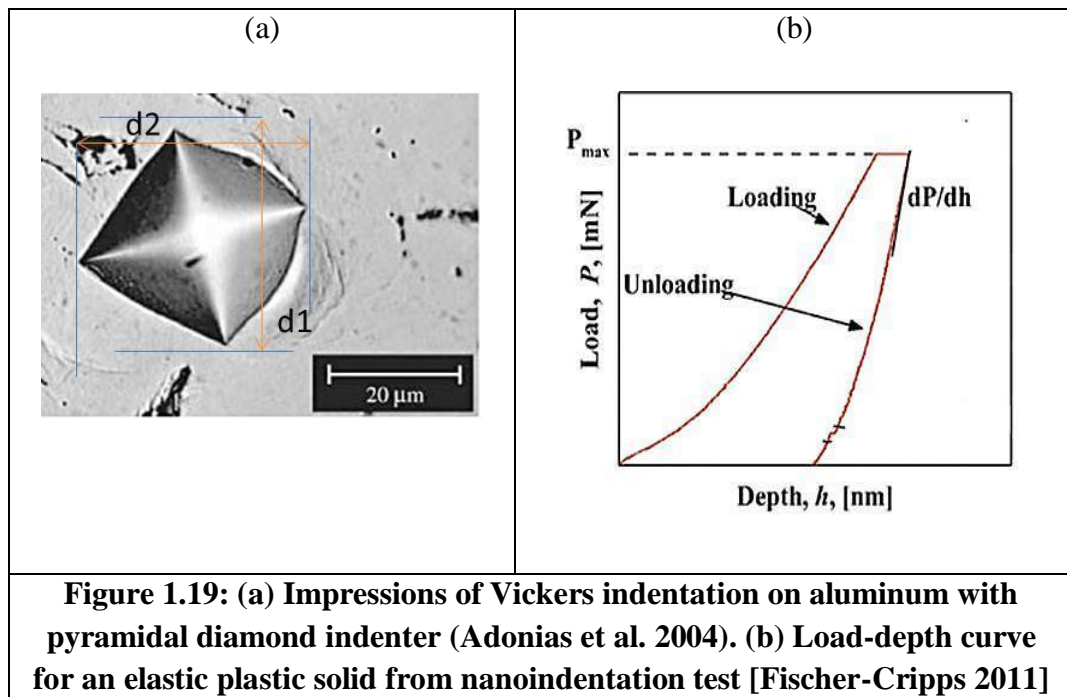
The Berkovich indenter is used for small scale indentation studies due to the fine edges of the pyramid which are more precisely constructed to meet at single point

rather than the inevitable line that occurs in Vickers Pyramid. The face angle of the Berkovich indenter is 65.27° which gives the same actual surface area to depth ratio as the Vickers indenter. The tip radius of a typical Berkovich indenter is 50 - 100 nm. The projected contact area (A) at peak load is usually determined from the contact depth of penetration (h_c) such that the projected area for Berkovich indenter is

$$A = 24.494 h_c^2$$

The load - displacement curves obtained from all experiments are evaluated according to Oliver-Pharr method [Oliver and Pharr 1992]. The parameters peak load (P_{max}), depth at peak load (h_{max}) and the initial slope of the unloading curve (S) are determined from the representative load-displacement curve recorded in nanoindentation experiment as shown in Figure 1.19 (b). Hardness H is measured as shown below.

$$H = \frac{P_{max}}{A} \dots\dots\dots\dots\dots\dots\dots\ (1)$$

The analysis of the load -depth curve proceeds with the determination of the reduced elastic modulus E_r (Equation 2).

$$E_r = \frac{1}{2} \sqrt{\Pi} \frac{S}{\sqrt{A}} \dots\dots\dots\dots\dots\dots\ (2)$$

E_r is termed reduced elastic modulus because it takes into account the compliance of the indenter tip by the relation

$$\frac{1}{E_r} = \frac{1-v^2}{E} + \frac{1-v_0^2}{E_0} \dots\dots\dots\dots\dots\dots\dots\ (3)$$

Where E and v and E_0 and v_0 are the elastic modulus and Poisson's ratio of the sample and indenter respectively. In comparably soft materials like hair fibres, where $E_0 >> E$, the difference between E_r and E is negligibly small and therefore no correction according to equation 3 is required (Fischer-Cripps 2011).

Measurement of hardness and modulus of latewood pulp fibres [Adusumalli et al. 2010] using nanoindenter equipped with Atomic Force Microscopy (AFM) revealed no variation in hardness between the softwood and hardwood, but bleaching treatment decreased the hardness for both the pulps due to the loss of lignin. Few studies [Wei et al. 2005] are reported on Caucasian, African and Asian hair (on surface and

cross-section) fibres and also effect of cosmetic treatment on nanoindentation modulus and hardness for limited samples. They also observed the effect of conditioner on hardness and elastic modulus of virgin hair. Bhushan et al. 2006 observed less modulus for damaged hair compared to virgin hair and modulus decrease with increase humidity. Samanta et al. 2016 characterized the hair samples (virgin, bleached and chemical treated hair samples) using optical microscopy, AFM, field emission SEM, energy dispersive X-ray spectroscopy, nanoindentation, tensile testing and X-ray diffraction techniques. They found treated hair samples are showing better nanomechanical and micromechanical properties compared to virgin and bleached hair samples.

1.3.3. Thermal properties of hair fibres

Thermal characterization of keratin fibres like human hair, wool, nail, feather etc., were reported using Differential Scanning Calorimetry (DSC) to know the melting behavior of α-form crystallites present in keratin [Wortmann et al.1993, 2012, Cao 1999, 2005]. When hair or wool fibres are heated from room temperature to 300°C, different events are observed by DSC [Cao 1999, 2005] as shown in Figure 1.20. Unlike synthetic fibres, thermal characterization of hair keratin is difficult due to the nanocomposite structure of proteins and also due to the hygroscopic nature of keratin. Here composite indicates unidirectional fibre reinforced matrix in which crystalline Intermediate Filaments (IF's) are considered as high modulus fibres arranged in helical fashion. Cao [1999] reported on thermal characterization of wool fibres and human hair by considering moisture influence on peak temperature and melting enthalpy and concluded that human hair and wool have similar thermal characteristics.

DSC has also been used to determine the water content in wool or hair [Cao 1999]. Two distinct peaks corresponding to endothermal transitions have been observed in hair, one at around 235 - 240°C, attributed to melting of the crystalline regions of microfibrils, the other at around 250°C, due to the degradation of amorphous matrix proteins. Water appears to play a part as a plasticizer of the keratin structure and it is reflected by the fall in the glass transition temperature with increased water content of the fibre.
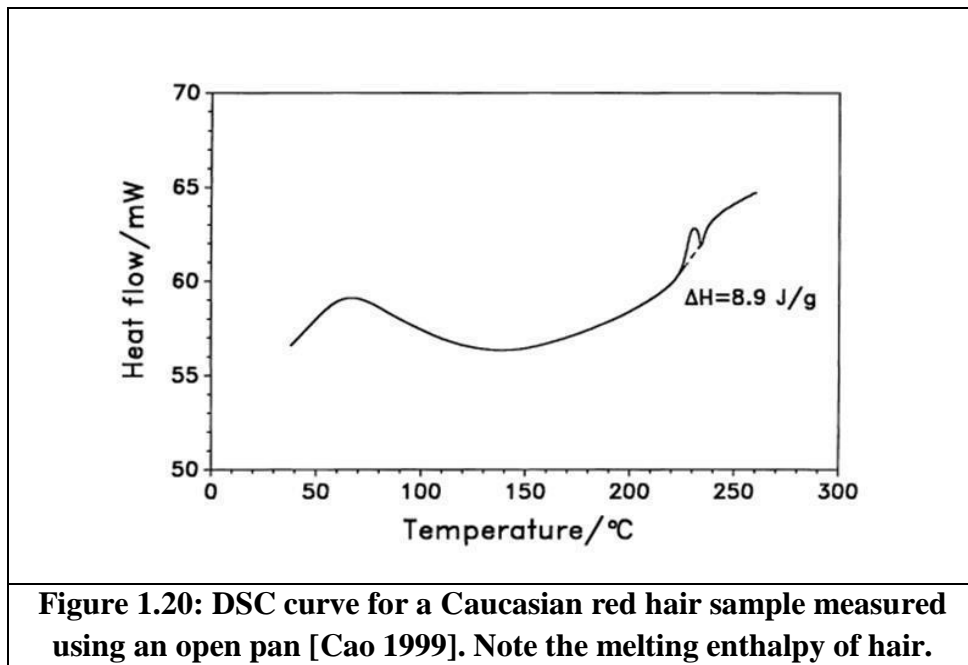
Figure 1.20: DSC curve for a Caucasian red hair sample measured using an open pan [Cao 1999]. Note the melting enthalpy of hair.

They also studied DSC with open pan and sealed pan (with o-ring) and found that open pan showed high peak temperature compared to sealed pan. The depression in peak temperature is explained using Flory's theory which suggests that water molecules interact with the polypeptide when the crystallites melt. From Flory - Huggins theory it is found that α - form crystallinity in human hair is around 22% which was also confirmed by XRD [Cao 2005]. Mohan et al. [2017] studied the thermal properties of pig hair fibre using DSC, TGA and concluded that they are similar to human hair fibres. In his review paper, Popescu et al. [2016] reported that hair fibre's DSC data using dry and wet DSC methods is not sufficient for claim substantiation and for better understanding of the hair damage. They concluded that DSC data should be supported by other techniques such as tensile test or XRD.

1.4. Research Gaps based on Literature Review

After the extensive literature review on human hair fibres, following gaps were found.

1. Mechanical properties of hair at micro (bulk) and nano-scale (surface) level using hair samples of different age and gender have not been studied thoroughly to understand the influence of local structural heterogeneities.

2. No studies were focused in estimating the difference in nanomechanical properties between cortex and medulla. It could be due to the low medulla diameter (<15 μm) or medulla is not present as a continuous structure in human hairs.

3. It is also observed from the literature that limited number of healthy samples from one or two scalp positions and one ethnicity or chemically treated hair samples and in few case only female hair samples were considered in determining the tensile properties of hair, but no comparison between scalp positions were reported taking hair as a composite structure wherein crystalline and amorphous domains are intertwined and intricate in nature.

4. Thermal characterization of hair using DSC has not been done to evaluate the effect of age on melting enthalpy and melting temperature.

5. Similarly, no correlations were reported between thermal and mechanical properties of hair even though hair has crystalline and amorphous regions.

Though lot of work has been done on animal hair fibres, to the best of my knowledge, no studies were reported for human scalp hair with a specific focus in understanding its intermingled morphology with coexistence of crystalline and amorphous domains, interfacial defects and % of crystallinity.

1.5. Objective of Present Research

In the present study a large number of hair samples from one ethnicity but different age groups (3-90 years), both genders and also from four different scalp positions are considered for thermal and mechanical testing. For the first time, an effort has been made to correlate the results of thermal data with that of mechanical (tensile test and nanoindentation) data. This thesis is also an attempt in deep understanding of the interfaces (within the cortex, between cortex and medulla) as well as how crystalline and amorphous domains are intermingled and defects are structured with respect to

crystalline and amorphous domains exist in human scalp hair. For detailed study of the interfaces and intermingled morphology of hair fibres, three techniques (one nano – "Nanoindentation" and two bulk- "Tensile" and "Thermal") were selected and hair fibre was considered as a composite during the interpretation of tensile, thermal and nanoindentation data. It should be noted that hair cortical cell structure resembles nanocomposite structure of wood cells wherein coexistence of crystalline, amorphous domains exists with high degree of intermingling. Graphical abstract of the thesis is shown in Figure 1.21.
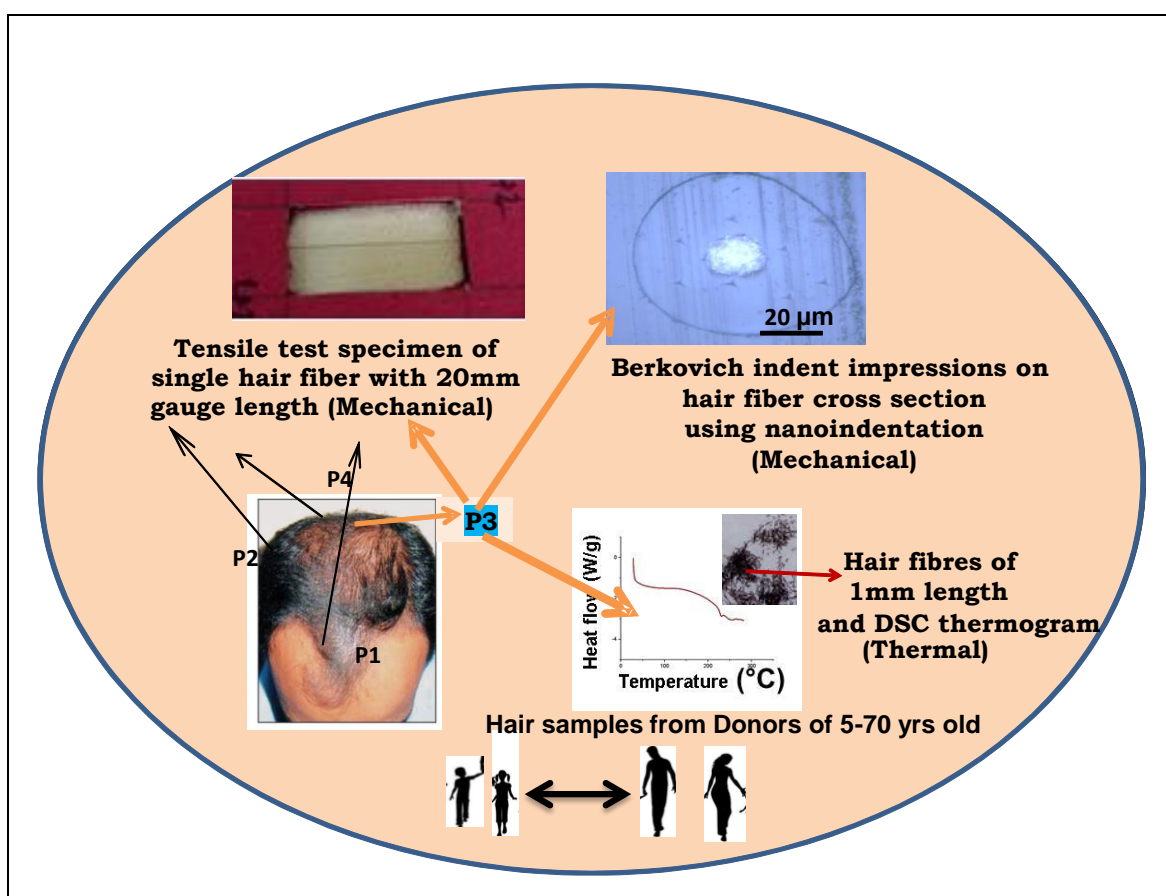
Figure 1.21: Graphical abstract of the Thesis. Tensile testing of hair collected from four scalp positions P1-P4, nanoindentation of cortex and medulla regions (indents on cortex region are shown) and thermal properties of hair (DSC thermogram). For both nanoindentation and DSC, samples from P3 position only considered. Mechanical and thermal properties are compared with respect to age and gender. Correlating the mechanical properties with thermal properties of hair is also the key objective of this thesis.

All the five objectives of this thesis are summarized below

1. To perform Nanoindentation of single hair fibre cross-sections and to compare the properties (hardness and indentation modulus) with respect to age and gender [surface test].
2. To compare the tensile (Single fibre Tensile test) and thermal (Differential Scanning Calorimetry) properties of hair with respect to age and gender [bulk tests].
3. To compare the quality of hair between cortex and medulla regions by performing Nanoindentations on cortex and medulla.
4. To measure the yield stress, modulus, maximum stress and work of elongation of all single fibres by considering the composite structure of hair and to compare these properties with respect to scalp positions P1-P4 using statistical analysis.
5. To find a correlation between thermal vs. tensile and thermal vs. nanoindentation properties by considering the heterogeneous and composite structure of hair.

The aim of this thesis is to understand the mechanical and thermal properties of healthy people's hair and to compare these properties with respect to person's age and gender. Two bulk techniques, tensile test and differential scanning calorimetry were carried out using 20 mm gauge length and 0.5 mm length fibres respectively where the response of all three regions (cuticle, cortex, medulla) were considered. This thesis is also about investigation of nanomechanical properties of cortex region and medulla region separately where local (surface) response of the amorphous and crystalline domains is measured in the form of hardness and indentation modulus respectively. Since the nanoindentation imprint width is around10 µm, 5 - 6 data points were collected from each fibre cross-section. For further understanding the composite nature of hair fibre by taking amorphous and crystalline domains into consideration, tensile yield stress, modulus, maximum stress and work of elongation were measured from tensile stress-strain plots. These four ensile properties were compared with respect to scalp positions because baldness (androgenic alopecia) severity follows the sequence of frontal-P1, parietal-P3, temporal-P2 and occipital-P4 using box-and-whisker plots. For detailed comparison with respect to scalp positions, two statistical analysis techniques namely Relative rating and Grey relational analysis were used. Finally, an attempt has been made to find a correlation between yield

stress (tensile) and melting enthalpy (thermal) and also between indentation modulus (nanoindentation) and onset of melting temperature (thermal).

1.6. Summary of the Thesis

The thesis is written in compilation format and includes seven chapters as outlined below and graphical abstract of the thesis is shown in Figure 1.21.

Chapter 1 provides a brief introduction to the proteins and hair fibres. The structure and chemical composition of human hair fibres are outlined. The physical, mechanical and thermal tests including new technique like nanoindentation which is important to determine the quality of hair (medulla and cortex) are described. This chapter also gives an overview of literature on human hair and summarizes the research gaps in the present literature. Nanoindentation (surface test), a novel technique that maps out local heterogeneity at nanoscale and traditional tensile test, thermal test at macro scale (bulk test) used to fulfill the objectives listed the current research work are described in detail.

Chapter 2 describes the detailed work involved in sample preparation for nanoindentation on hair cross-section and difficult aspects like embedding of hair, fibre alignment, surface smoothening, and measurement of medulla diameter using microscopy. It is also given nanoindentation hardness and modulus properties on medulla and cortex regions of hair. The hardness and modulus of hair comparison with respect to age and gender is included in this chapter.

Chapter 3 describes in detail about the collection of samples, physical properties of hair (diameter and linear density) and sample preparation for tensile testing of single hair fibres. Tensile testing and analysis of stress-strain curves using Origin software to find tensile yield stress, modulus, maximum stress and work of elongation of single hair fibres is outlined. Data is compared with respect to age, gender and position of hair. From the maximum stress of individual fibres, the weibull shape factor (β) has been calculated. Statistical methods like Relative rating, Grey relational analysis and ANOVA have been used to see if any tensile properties of hair samples vary with respect to position of the scalp. The fractography of the hair fibres has been studied using SEM. A comparison between nanoindentation modulus (surface) of hair cross-

section and tensile modulus (micro scale) of single hair fibres is shown. The hardness from nanoindentation and yield stress from tensile test (both are indicators of a material's resistance to plastic deformation) are also compared with respect to donor age.

Chapter 4 deals with thermal analysis of hair fibres (with and without conditioning at higher temperature) using Differential Scanning Calorimetry (DSC). Sample preparation, the onset of melting temperature, melting temperature and melting enthalpy of hair samples were measured from thermogram and compared with respect to age or gender.

Chapter 5 describes the correlations between thermal and tensile properties and thermal and nanoindentation properties of hair fibres. Yield stress from tensile data and melting enthalpy of hair fibres from thermal data is compared with respect to age of donor. Correlation between DSC studies (the onset of endothermic melting peak temperature of α-keratin) and nanoindentation (indentation modulus) studies are also shown. Also a correlation between hardness and slope of the heal flow curve between 120 - 210 ^{O}C is also described.

Finally, Chapter 6 and Chapter 7 highlight the overall conclusions, recommendations for future scope of research work respectively.

CHAPTER – 2

Nanoindentation of single fibre cross-sections

This chapter covers detailed information about the nanoindentation sample preparation which includes the selection of embedding medium for hair fibres, polishing techniques (microtome and diamond paste), nanoindentation parameters, measurement of hardness and indentation modulus from load-depth plots and comparison of nanoindentation data between cortex and medulla and also with respect to age and gender are described.

2.1. Introduction

Nanoindentation with load in μN and depth in nm is revolutionary technique in characterization of biological materials, composites and fibres [Das et al. 2009, Bhushan et al. 2006, Gindl et al. 2006, 2008] especially in determining the hardness of samples with area < 100 μm^2. The commonly used Vickers hardness test occupies > 1000 μm^2 area per indent which makes it unsuitable for hair fibres having medulla in central axis (Figure 2.1). Hardness of hair, especially cortex region needs to be determined as hair is a composite structure, and sulphur rich matrix portion of hair influences the hardness. Any external disease or cosmetic treatment causing reduction in hardness can be quantified using nanoindentation. Diseases such as AIDS and malnutrition cause reduction in mechanical properties, especially hardness and modulus. Studies on cuticle damage [Bhushan et al. 2008] and decrease of hair mechanical properties are of interest to dermatologists in treatment of hair disorders by chemical treatments are reported. Apart from tensile test, very few studies have been reported on hair mechanical properties, especially nanomechanical properties of cortical cells present in cortex and medulla. So far, much of the research has been focused on cuticle part of the hair; because this is the outer layer which gets affected by the hair conditioners [Bhushan et al. 2008]. Only two research papers [Bhushan et al. 2008, Samanta et al. 2016] focused on cortex region, the thickest part of the hair. This chapter aims at quantitative comparison of nanomechanical properties with respect to donor age by performing nanoindentation on fibre cross-sections i.e. on

cortex region. Mechanical properties with conventional indentation apparatus like Vickers hardness are also measured. It was observed that Vickers indentation is occupying more area. So measurement of hardness at particular location like medulla region in hair is not possible with Vickers indentation as compared to nanoindenation. This chapter will also discuss the specimen preparation for nanoindentation of single hair fibre cross-section which was a challenging task as hair, being a microfibre, misalignment and handling small lengths of the hair. This misalignment causes miscalculation of nanomechanical properties, so efforts have been made to minimize the misalignment to 3 - 5 °.

Figure 2.1: Vickers indentation on hair cross-section
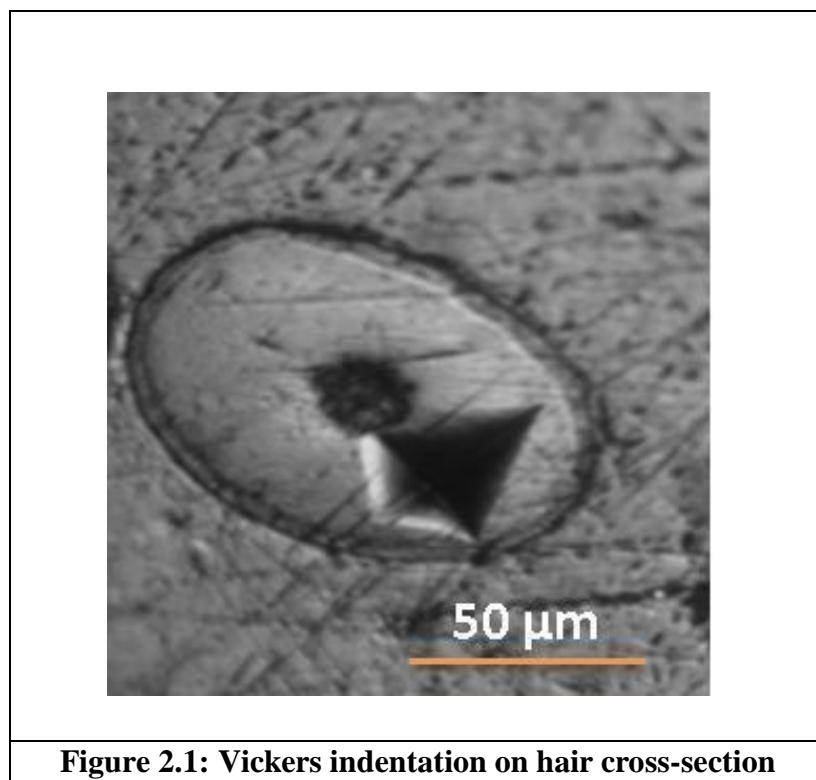
Inner diameter of hair shaft was considered as medulla region and it exists in hair shafts at the beginning of the anagen phase [Hutchinson et al. 1999]. Medulla is present in a discontinuous form as shown in Figure 2.2. Medulla's function is not yet completely understood since it is difficult to isolate it for further characterization. Recently, Wagner et al. (2007) studied the medulla region using SEM of cryofractured samples and observed three subunits of medulla (globular structures, unorganized microfibrils and smooth covering layer). From TEM it was found that thin medulla has a sharp interface with cortex whereas thick medulla shows gradual organization of the microfibrils from the medulla centre to medulla periphery i.e.

interface with cortex. But no study has been carried out to quantify the weak nanocomposite structure of medulla region because of their low diameters (2 - 15 µm). Wei et al. [2005] reported higher hardness and modulus for cortex compared to medulla, but the study was restricted to three hair samples (Caucasian, African and Asian hair) of unknown age. But Samanta et al. [2016] reported higher hardness, modulus and high surface roughness for medulla compared to cortex region. Both studies focused on effect of treatment of virgin hair samples on nanomechanical properties, but these studies did not take into account the differences that existed between medulla and cortex. In this chapter, an attempt has been made to study the nanomechanical properties of untreated human hair samples considering cortex and medulla regions separately. In cortex, fusi are small spaces that appear as tiny dark structures in the hair shaft; they may be filled with air or liquid as shown in Figure 2.2. Since fibres are embedded, measurement of hair cross-sectional diameter and medulla diameter was possible using microscopy. In forensic science, the knowledge of medulla diameter and medulla index is much appreciated because it differentiates the human hair from animal hair. This chapter will also address medulla index and its correlation with age.

Figure 2.2: Left image shows the schematic picture of a hair shaft [David 2005] and right image depicts all the three parts of hair fibre cross-section when viewed under SEM.
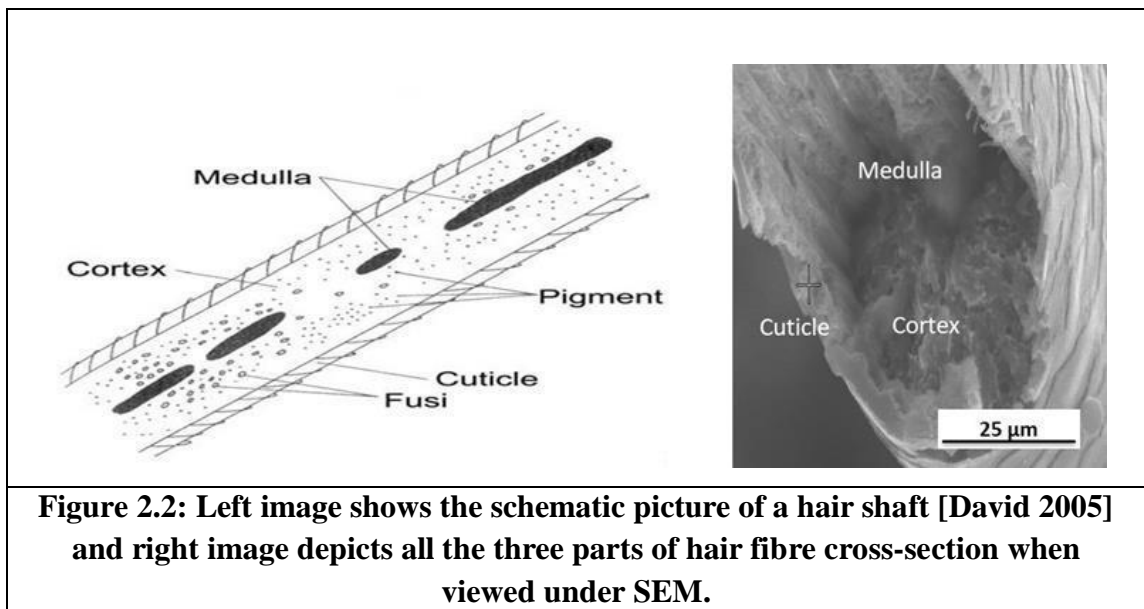
2.2. Materials and Methods

Hair samples were collected from scalp (vertex position) of 40 people of age ranging from 3 - 90 years old from Hyderabad, India, after getting approval from Ethics

Committee. All donors belong to Caucasian ethnicity. While collecting the donor's age, gender and health profile was documented anonymously. The hair was not plucked from the root, instead was cut near the scalp (approx. 20 mm) and marked the root side. Hair samples were washed with mild shampoo, rinsed in water, dried at room temperature and kept in ziplock covers. Video of sample preparation for nanoindentation test was provided in one of our papers [Mishra et al. 2016]. Cross-section analysis of hair is difficult process as single hair fibre sways, bends and buckles. Hence it should be embedded in a hard medium before analysis. Fong and Inami [1988] prescribed methods of rapid specimen preparation for cross-section analysis for forensic studies, but these methods cannot be utilised for performing experiments such as indentation because supporting medium has to remain stable. Nanoindentation is a sophisticated technique and it requires smooth cross-section of the specimen such that the indenter probe dents exactly perpendicular into the surface at the desired location. It is also important that embedding medium should not infiltrate into the sample interiors such as cortex or medulla. In this study, specimens were prepared for nanoindentation using cylindrical silicone mould filled with epoxy resin and suspending hair samples by attaching to a suspension pole [Wei et al. 2005].

2.2.1. Embedding of hair fibres in epoxy resin

Inner diameter of 6 mm and length of 30 mm translucent silicone pipes were used as moulds and sealed from one end using clay. Silicone pipes were sectioned from common laboratory silicon hose. Hair fibres of about 30mm were cut from the root side such that a minimum of 2 hair strand per specimen are available for embedding. Specimens were prepared for nanoindentation by placing hair strands in moulding clay (play-dough) which made into round clay ball and clay suspension pole as shown in Figure 2.3. First the cut section of hair samples suspended to clay ball and other side fixed to clay suspension pole exploiting the rigid structure of hair. This hair with an anchorage to stay aligned in the embedding medium is suspended in the silicone mould. Finally 2 - 3 hair fibres of about 30 mm length are placed in silicone pipe by filling with liquid epoxy resin (Agar 100-R1140A, Agar Scientific, UK) which proved to be good embedding medium for nanoindentation of cellulose fibres [Adusumalli et al. 2010]. Agar 100 premix kit is a three components mixture having epoxy resin, hardener (R1140B) and benzyl dimethyl amine (accelerator) and made it ready by

slowly mixing the constituents of small bottle into big bottle maintaining correct stoichiometry ratio. Epoxy embedding medium was cured at 60°C for 12 hrs.

Figure 2.3: Embedding of hair fibres into epoxy medium using modeling clay. A-sectioned silicone hose pipe acting as mould; B-fixing of hair fibres to round clay ball. C. Hair fibres attached to clay pole for better alignment. D. Silicone pipe filled with agar epoxy resin E. Aligned hair follicles in epoxy resin. F. Cured epoxy block having aligned fibres inside surrounded by silicone.

After curing the solid cast of hair-embedded-in-epoxy matrix (here after called as specimen blocks), was separated from the silicone mould for polishing as shown in Figure 2.4. First blocks carefully retrieved by cutting 1cm from top and bottom to remove the clay part. Later, blocks circumferentially separated from silicone mould as shown in the Figure 2.4. No mould releasing agents used because silicone does not stick to epoxy resin. It found that agar epoxy resin did not retain any air bubbles and no color imparted from the clay to the hardened resin. Hence a transparent resin block obtained which helpful in determining the degree of alignment of the hair fibres in epoxy block using stereomicroscopy. Samples were also made using a low viscosity epoxy resin DER 332 (Sigma-Aldrich) which made to harden using 99 % pure ethylene diamine (Acros Organics) in w/w ratio 10:1. The resin mixed homogenously for about 4 minutes by slow stirring to avoid formation of air bubbles in the solution

and then poured in the silicone mould with square blocks (Figure 2.5). Hair strands with load suspended inside the mould partially filled with epoxy resin before gelation begins with finer adjustments for alignment and cured for 24 hours at 60°C temperature in a dry non-circulating atmosphere. But the blocks non-transparent and fibres not in the middle of the block. For better transparency another embedding medium i.e. low viscosity epoxy resin (Spurr) cured for 8 hours at 70°C was used. It observed that transparency is not sufficient enough to make the nanoindentation sample. Hair samples embedded in agar epoxy which is also a low viscous embedding medium was found to be optimal for hair fibres and was used for all fibres.
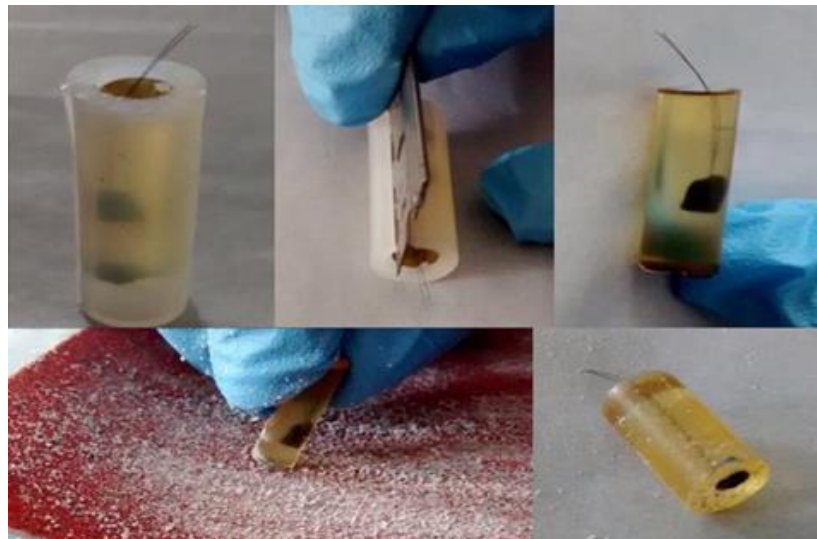
Figure 2.4: Removal of epoxy block from silicone pipe and polishing on both sides of epoxy block using emery paper (SiC) so that hair fibres are aligned in the middle of the cylindrical block.

Hair samples embedded into epoxy resin without clay (top image) made with hardener ethylenediamine with the ratio 100:11.4 (wt%) and (bottom image) with 8.7% (wt %) of ethylenediamine (non-stoichiometric ratio).	Hair fibres embedded in epoxy resin with clay using commercially available silicone mould from Sigm aldrich. Note the misalignment of the fibres.

Figure 2.5: Challenges in obtaining the parallel aligned fibres in the centre of epoxy block. Both embedding techniques using DER 332 epoxy were proved unsuccessful.
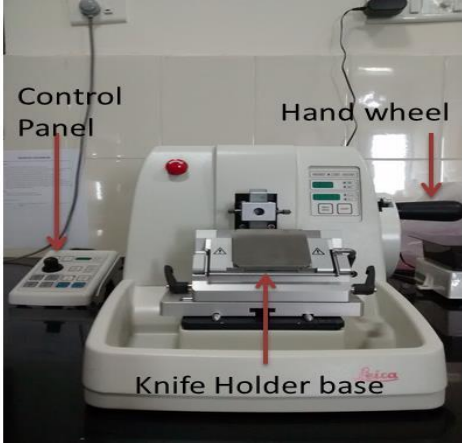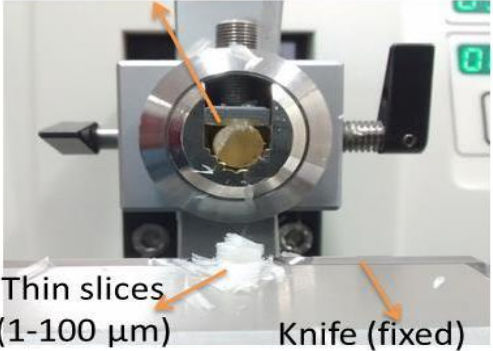
2.2.2. Surface smoothening of fibre cross-sections using microtome and diamond paste

Since the human hair fibres due to years of dressing, stress, shear and other genetic factors have a tendency to be curled or curved, so aligning these fibres in epoxy resin is one of the challenges in this thesis. Nanoindentation and microscopy of the hair samples require the samples to be aligned perfectly straight i.e. longitudinal about the axis of analysis because hair is an anisotropic fibre like wood and carbon fibres. Use of clips to hold them in place is also difficult as the embedding medium changes its phase from liquid to solid and clips of small size (< 5 µm) not available. This issue was partially tackled using the clay and epoxy resin as explained in preceding paragraph. More alignment of fibres was obtained during microtoming of blocks which are available as solid blocks after epoxy curing.
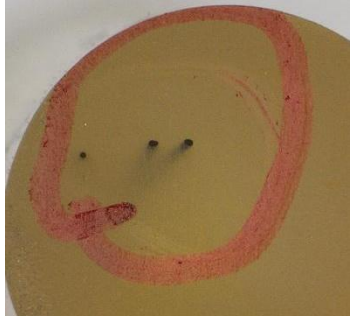
After separating resin blocks from the silicone mould, they are filed using SiC abrasive paper followed by microtoming with Rotary microtome - Leica RM2255 to view the fibre cross-section as shown in Figure 2.6. Based on fibre alignment, epoxy blocks were microtomed using tungsten carbide blade and sections of 10 µm were

removed initially followed by sections of 5, 2, 1 µm. Finally sections of 0.5 µm were removed using diamond knife (Histo Diatome) to get transparent smooth surface. The purpose of the diamond knife was to smoothen the surface by slicing 500 nm thin sections so that nanoindentation with low loads (< 1 mN) can be performed. Since tungsten carbide slicing showed unevenness (Ra value above 800 nm) as observed under microscopy we have used diamond knife for all our samples. Prior to usage of diamond knife, smooth surface was obtained on both sides for all samples using tungsten carbide blade and only one side was continued to microtome using diamond knife. All the samples were microtomed initially up to a sample height of 6 mm and further reduced to precisely 4.5 mm using a diamond knife. The embedded resin plays a key role because its transparency allows to check fibre alignment and its toughness avoids the cracks while fast smoothening using diamond blade. The microtome specimen holder and knife holder offers flexibility to change the direction of section and thus specimens which couldn't be aligned in molding are made ready for nanoindentation by aligning and cutting the blocks.

Rotary microtome is used to smoothen the surfaces of different materials i.e. polymers, composites, metals and fibres. This technique is an alternative to polishing with diamond paste. Microtoming the surface is faster and no localized imprints are formed, so any sample can be smoothened before viewing under optical microscopy and SEM. But it is common that knife markers may pass through the hair fibre cross-sections during microtoming, because hair is 40 - 100 µm diameter which is relatively higher compared to glass, aramid, viscose and wood pulp fibres. In few samples we observed knife markers on the cortex region which are not considered for nanoindentation. To avoid the influence of knife markers, polishing the surface with diamond paste or diamond suspension having diamond particles of 250 nm was carried out as shown in Figure 2.7. It is also possible to get a smooth and transparent surface using diamond polishing (Figure 2.7), but sometimes imprints of diamond particles can be seen. Metadi supreme polycrystalline diamond suspension is used for the final polishing of the samples. Samples having smooth surfaced fibre cross-section without any knife markers (Figure 2.8) on it are selected for nanoindentation.

Microtome used for cutting slices and to make the smooth surfaces. Control panel for automatic mode and hand wheel for manual mode.	Microtoming with Leica RM 2255 microtome showing slices of 1 - 100 microns, specimen cross-section and WC knife. During microtoming, slice thickness and total thickness removed are displayed.

Figure 2.6: Microtome used for making smooth surface of epoxy block. For nanoindentation smooth surface of the specimen is required because loads are in mN.

Diamond knife used for polishing	Grinding wheel used for polishing the samples using diamond paste	Diamond paste

Figure 2.7: Microtoming using diamond knife (slices thickness of minimum of 500 nm is removed) and diamond slurry of 250 nm used for polishing the fibre cross-section. Smooth surface required for nanoindentation is obtained in both cases.

Hair fibre cross-sections (3) after polishing with emery paper (SiC)	Hair fibre cross-sections (3) after polishing with emery paper (SiC) and diamond paste	Hair fibre cross-sections after polishing with emery paper (SiC) and diamond knife. A circle is drawn using marker for easy identification of fibres.

Figure 2.8: Hair fibre cross-sections after diamond polishing and microtoming with diamond knife.

2.2.3. Measurement of fibre diameter and medulla diameter using microscopy

Stereomicroscopy (5.6X) is used to find the diameter under longitudinal view. Optical microscopy (50X) in both transmission and reflection modes is used to find the single fibre cross-sectional diameter and medulla. Confocal laser scanning microscopy - CLSM (40X) in reflection mode is used to find the medulla and medulla index. Optical microscopy is sufficient for measurement of diameters because hair fibres are 2 - 5 times thicker than carbon, glass, aramid, wood and jute fibres. Stereomicroscopy is used to check the alignment (Figure 2.8) and optical microscopy is used to measure the whole fibre diameter, medulla diameter and also to check the roughness of the sample. Smoothness of samples after microtoming with diamond knife or diamond polishing was checked by determining the surface roughness (Ra) of few samples using optical profilometry (zygo). Ra values are found to be below 150 nm as shown in Figure 2.9. Optical profilometers utilize the wavelike properties of light while scanning the sample in the z-dimension to obtain 3D data through various techniques. All profilometers are interference microscopys and are used to measure height variations such as surface roughness on surfaces with great precision using the wavelength of light as the ruler. The fibre cross-sections having Ra value above 200 nm was not used to perform the indents.

Optical profilometry image on hair cross-section showing the implanted knife markers due to sectioning.	Surface profile of the cortex region (50 μm shown in left image) having the roughness value Ra of approx. 37 nm.

Figure 2.9: Optical profilometry image on hair cross-section after microtoming with diamond knife.
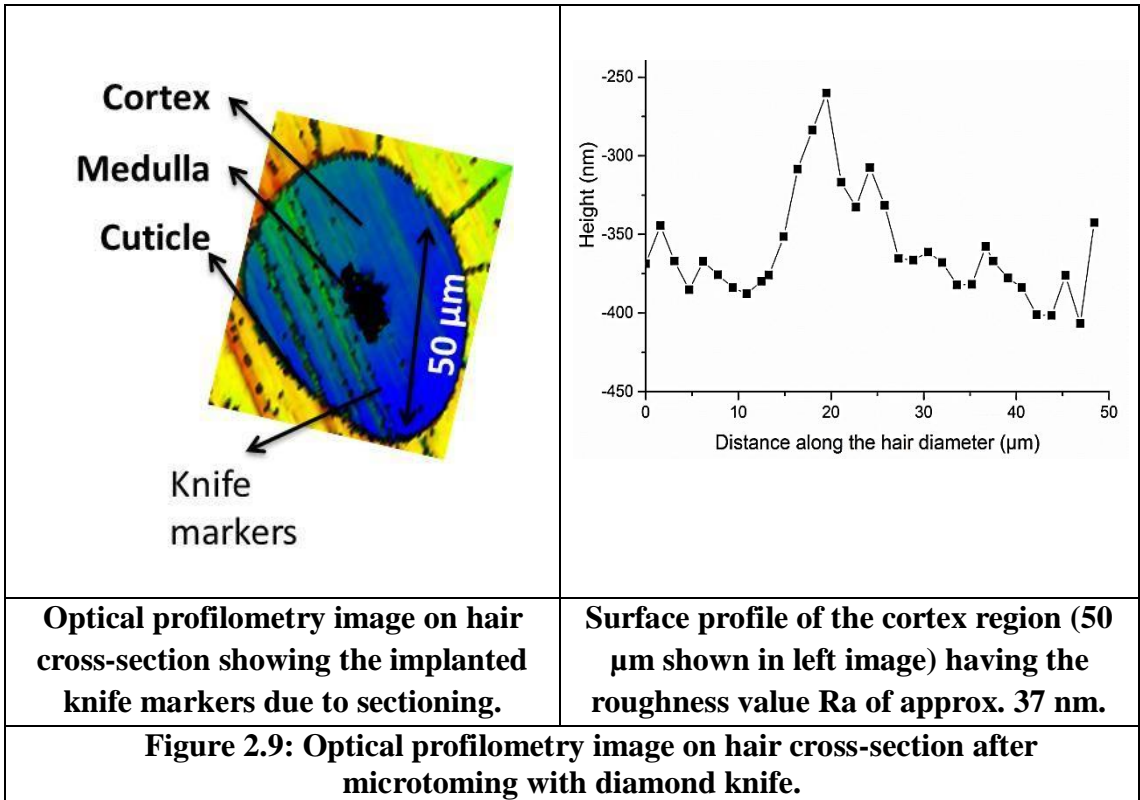
Stereomicroscopy (Olympus SZX7) was used for to check the alignment of fibres and to select the best fibre out of 3 fibres to perform the indents as shown in Figure 2.10. It is possible to check the alignment in both sides i.e., cross-section and longitudinal.

Figure 2.10: Two misaligned hair fibres not selected for tests whereas one aligned fibre selected for nanoindentation from the embedded hair samples.
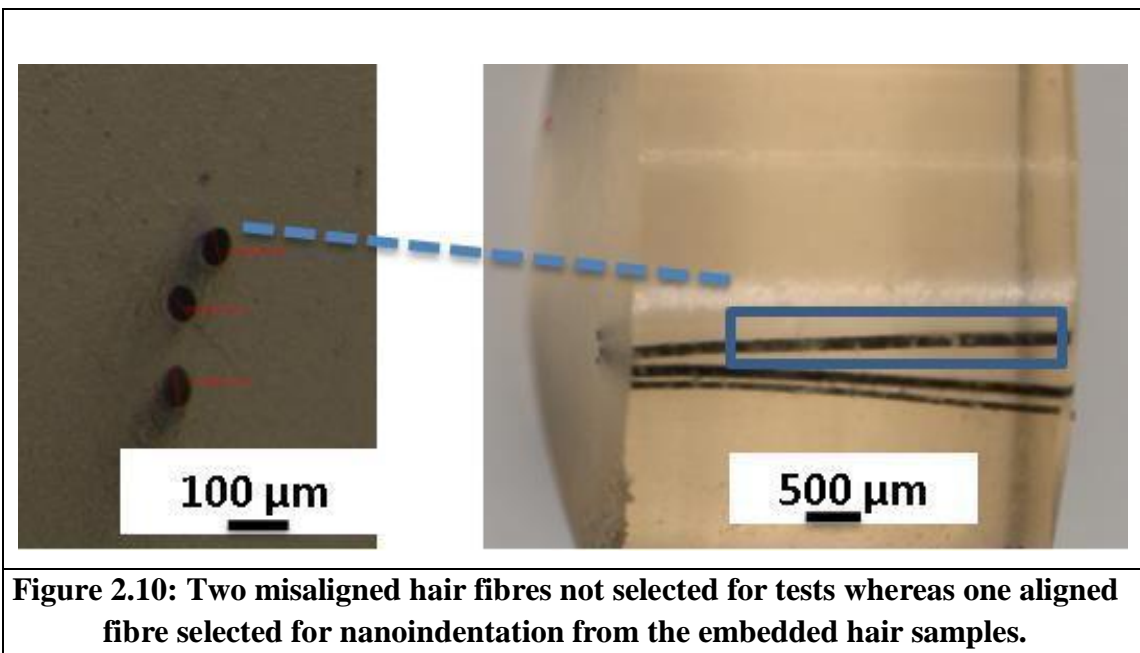
To measure the accurate fibre diameters, light microscopic images of samples having fibre cross-section were recorded using 4 mm height sample blocks. Misaligned fibres observed by noticing the shadow next to the fibre cross-section of optical microscopy images. Such fibres are omitted from diameter and nanoindentation measurements. Optical microscopy (Metavis U400) was used for measuring the diameter in both longitudinal view and cross-sectional view. It is common to report medulla index rather than medulla because increased medulla diameters is found to have increased fibre diameters. Medulla index is defined as the ratio of medulla diameter to hair shaft diameter and it is important in understanding the fracture patterns of hair samples.

$$\text{Medullary Index} = \frac{\text{Mean diameter of the Medulla}}{\text{Mean diameter of the whole hair shaft}}$$

Figure 2.11: a) Stereomicroscopy image of hair fibre b & c) Optical microscopy image of black hair and white hair cross-sections respectively d) Confocal laser scanning microscopy respectively of black hair. Note the presence of medulla in c and d.
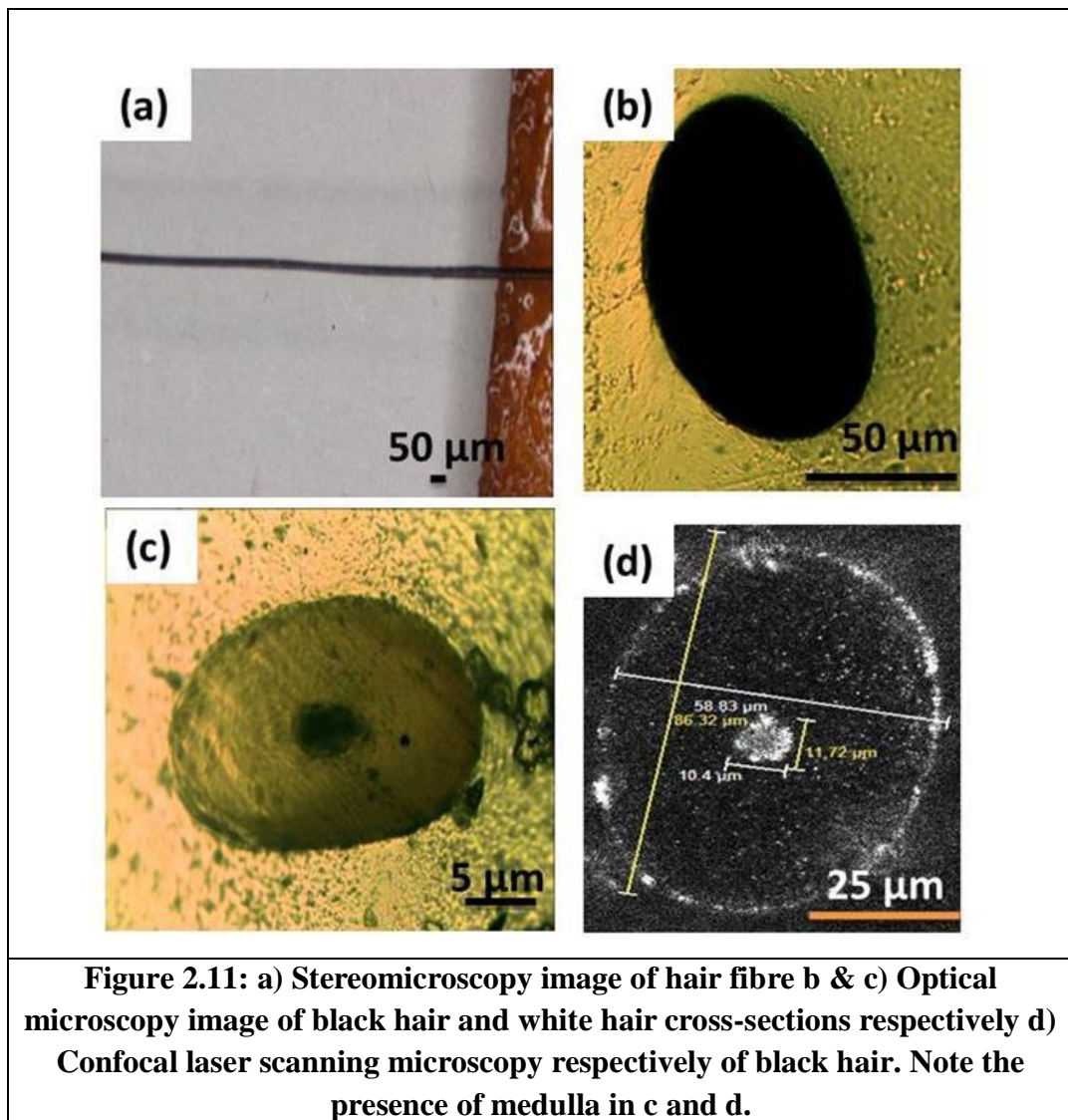
In contrast to optical microscopy, CLSM (Leica DMI8) is used for better imaging due to its ability to produce an image of the focal plane exclusively which is possible due to a pin-hole assembly. Here samples were viewed under reflection mode and medulla diameters were measured as shown in Figure 2.11. Human hair cross-section with medulla was compared with phant stem with pith as shown in Figure 2.12. To find the medulla in black hair samples, hifin aerosol (oil soluble) is used as lubricant in addition to silicone oil. The microscopic studies showed that CLSM is a superior technique in identifying medulla than a normal optical microscopy.

Figure 2.12: (a) Plant stem structure showing thin bark, wood and pith (core region with diameter of 2-4 mm) (b) Human hair cross section showing cuticle, cortex and medulla (core region with diameter of 8-12 μm).
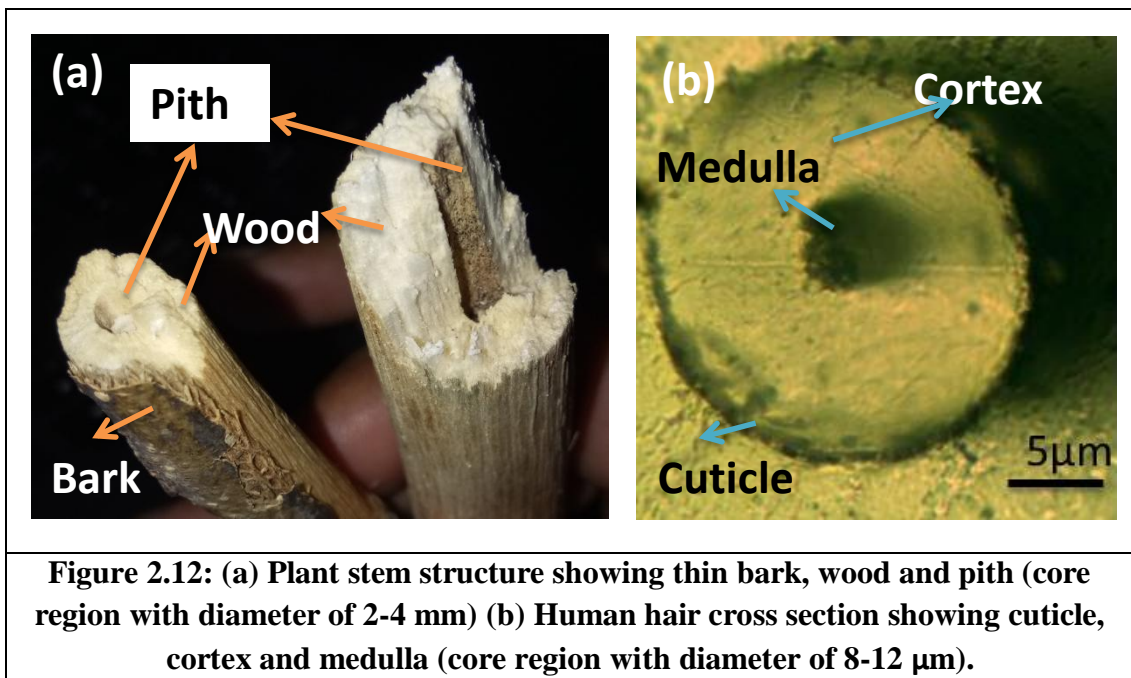
2.2.4. Nanoindentation of single fibres cross-section

After sectioning, the specimen blocks are fixed to aluminum disks vertically using cyanoacrylate adhesive and mounted on the sample holder of a nanoindenter and tests were performed using three different nanoindenters equipped with Berkovich diamond indenter (Figure 2.13). MTS Nanoindenter equipped with optical microscopy was used for first set of samples. Micro Materials Nanoindenter (NanoTest TM) known for its high loads and depths and it is equipped with an open platform and a powerful optical microscopy was used for second set of samples. Hysitron TriboIndenter is a popular nanomechanical testing instrument in the category of low loads and depths and it is equipped with optical microscopy as well as in-situ

scanning probe microscopy (SPM) for selection of precise test location was used as a reference. The in-situ SPM images were obtained by raster scanning the indenter probe over the sample surface to allow for pre- and post-test observation of the material surface. Post-test imaging is useful in protein and cellulose fibre testing which have medulla of 5 - 20 µm diameter and cortex of 30 - 45 µm thickness. In this study, 4 - 6 indents are placed on cortex region and one indent on medulla region. Instead of performing the array of indents, separate indents are placed on medulla to avoid the influence of interface effects. Indentation was performed at ambient temperature and relative humidity. Thick region of the hair fibres (cortex region) on the sample surface was located using the nanoindenter's optical microscopy and test was conducted with a lateral accuracy of $\pm$ 100 nm. Indentation was carried out with allowable drift rate 0.1nm/s, test speed of 10nm/s in load controlled mode, reaching peak load of 1.5 mN in 15 sec and the holding time at peak load was taken as 30s to monitor the visco-plastic creep. For other sets, Berkovich indenter was loaded to a peak load of 10 mN, held for 30s and unloaded at a speed of 0.66 mN/s A three sides (triangular based) pyramidal diamond Berkovich indenter tip (TB 14979) was used to perform the indents on hair cross-sections in circular pattern. A peak load of 1.5mN, 10mN and 20mN was applied to the hair cross-section based on the smoothness of sample, but care is taken not to overlap the indents. Figure 2.13 show the Berkovich indenter tip on hair embedded epoxy block and also its SEM image (Figure 2.13 – right image). Figure 2.14 depicts the schematic diagram of nanoindentation on hair cross-section.

Figure 2.13: Berkovitch diamond indenter on hair-embedded-epoxy block during nanoindentation test (left image), Berkovitch diamond indenter (middle-image) and SEM image of Berkovitch diamond indenter tip (Right image).
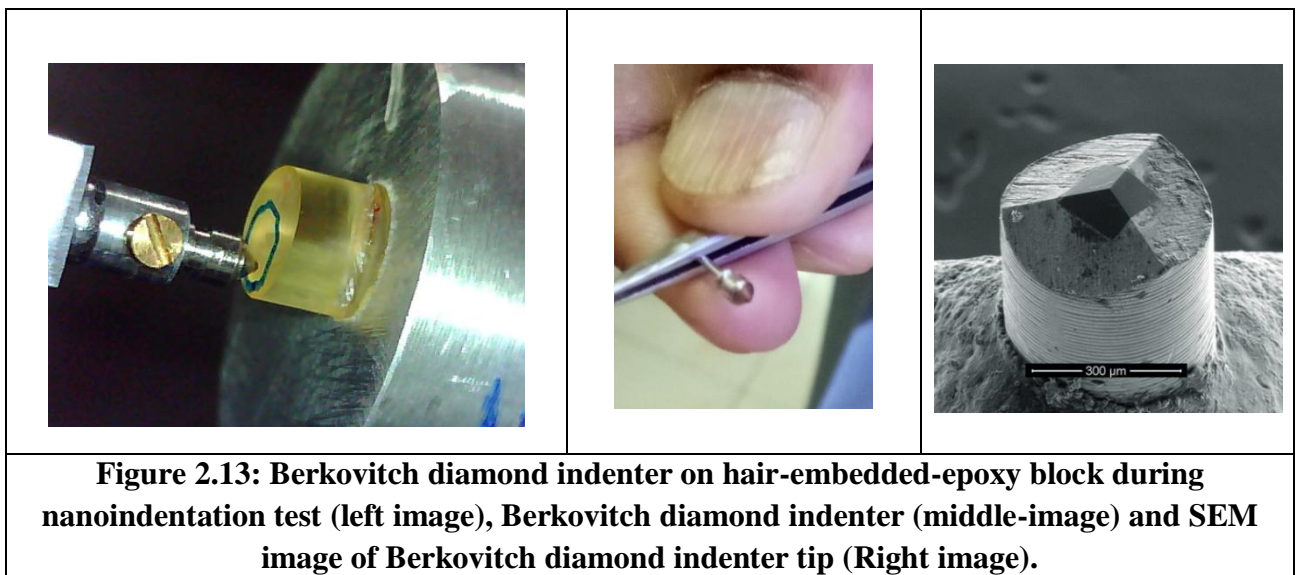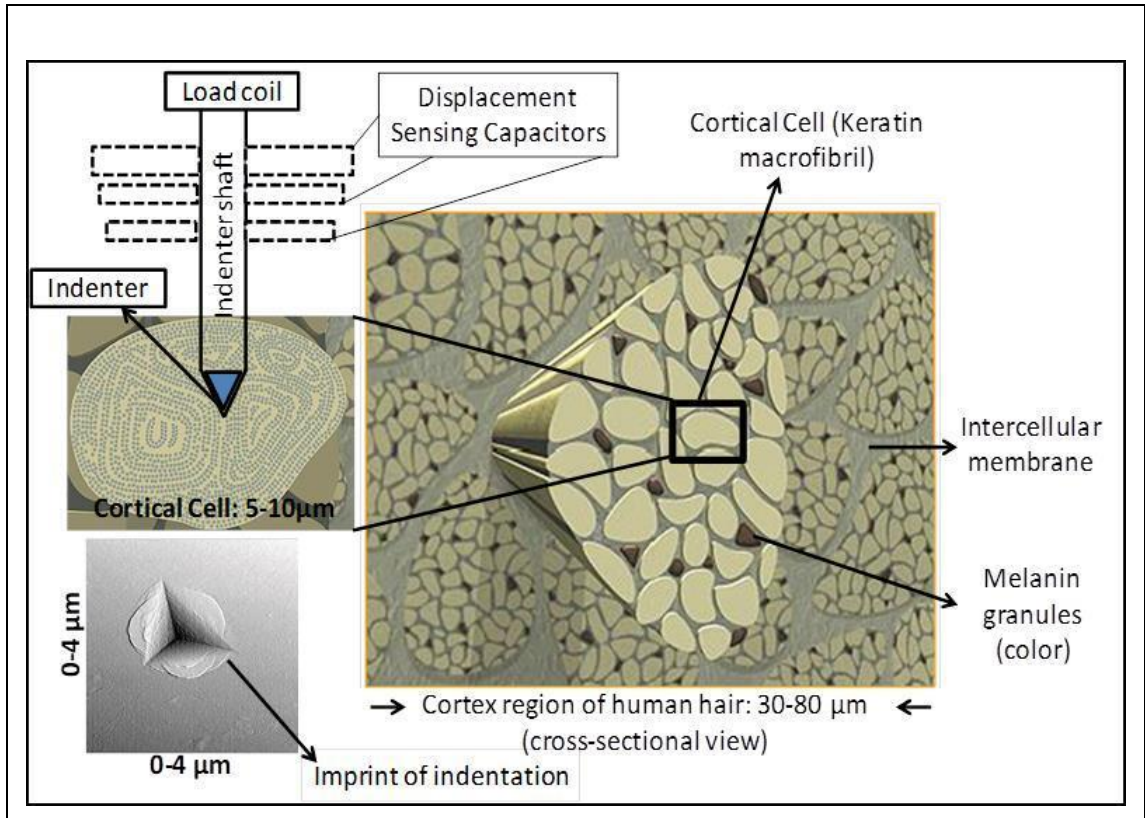
Figure 2.14: Schematic diagram depicts the cross-section of the cortex region and Nanoindentation on hair cross-section. Cortical cell is considered as unidirectional composite, in which fibres are macrofibrils (bundle of intermediate filaments, α keratin) and matrix is cystine rich protein [Mishra et al. 2016].

2.2.5. Measurement of Hardness and Indentation Modulus

The contact area (A) at peak load is usually determined from a measure of the contact depth of penetration (h_c) such that the projected area for Berkovitch indenter is given by

$$A = 24.494 \, h_c^2 \ .$$

The parameters peak load (P_{max}), depth at peak load (h_{max}) and the initial slope of the unloading curve (S) are determined as per literature [Oliver and Pharr 1992] from the representative load - displacement curves shown in Figure 2.15. The hardness is obtained by dividing P_{max} by projected area and the reduced elastic modulus E_r is obtained from equation shown in Figure 2.15.

Figure 2.15: Typical Load (P) vs Depth (h) curve from nanoindentation [Fischer-Cripps 2011] and measurement of modulus from unloading part of the curve.
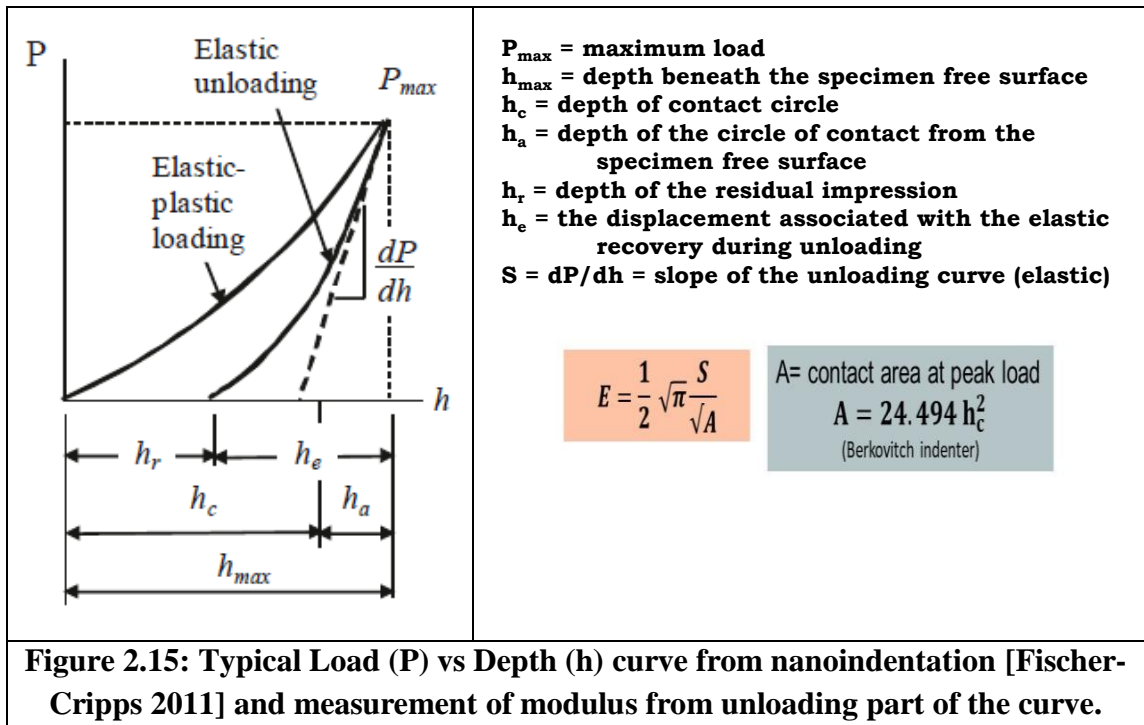
2.3. Results and discussions

2.3.1. Fibre cross-sectional diameter and medulla index with respect to age

As shown in Figure 2.16, hair cross-section is found to be elliptical but it is assumed circular and equivalent diameter is measured. From our studies it can be concluded that diameter was found to be between 69 to 100 µm in cross- sectional view and 59 to 96 µm in longitudinal view, which indicates that cross-sectional method consistently resulted in higher values with some exceptions due to misalignment of fibres during embedding. For all donors, hair cross-sectional diameters are in the range of 60 - 110 µm with coefficient of variation between 5 – 19 %. As reported in our previous publication [Mishra et al. 2016], donor age is not influencing the hair fibre longitudinal diameter and cross-sectional diameter though few reports [Jeong et al. 2011, Srettabunjong et al. 2016] discussed a correlation between age and diameter. It is known fact that cross-sectional area measurement is the correct way of measuring diameter, but the sample needs to be embedded, because hair fibres are flexible and curly. Since we can't embed all fibres, we optimized our method for longitudinal measurement as shown in Figure 2.16. Among donors from Figure 2.16, one of the 5 year old male donor has least diameter (69 µm) and 41 year old female donor has

highest diameter (101 μm).The average diameters of 12 samples measured in longitudinal and cross- sectional view as a function of age are compared and found that difference in both diameter values is between 5 to 15 %. So it can be concluded that longitudinal view measurement was acceptable and less tedious and it was used in our tensile measurements. Increase in diameter results in decrease of tensile stress and flexibility and it is significant for fibres having diameter between 6 - 40 μm (like aramid, glass) and not so significant for hair fibres.

Figure 2.16: (a) Comparison of diameter (b) Diameter measurement by cross-sectional method i.e. samples are embedded in epoxy and surface is smoothened using microtome followed by diameter measurement using microscopy (c) Diameter measurement by longitudinal method.
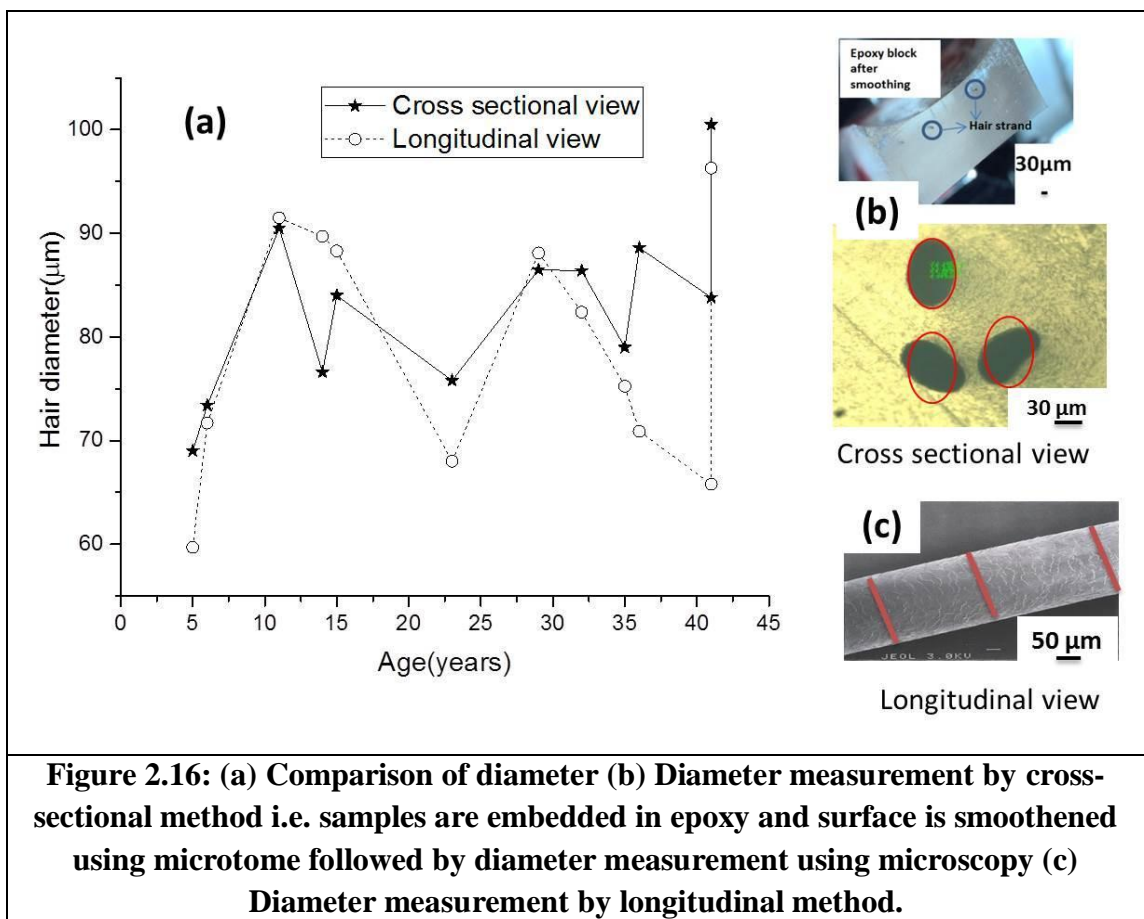
As shown in Figures 2.11 and 2.17, medulla diameter is measured and the shape of the medulla is found to be less elliptical than hair cross-section [Hutchinson et al. 1999]. From Figure 2.17 it can be noticed that from one donor's two hair samples have medulla and other hair sample has no medulla. Inner diameter of 8 - 15 μm of hair shaft is considered as medulla region and it is shown as white color whereas cortex region is shown as darker color. From the literature it is found that medulla region exists in hair shafts at the beginning of the anagen phase, so two hair samples

must have been from anagen phase. The other hair sample might have thin medulla and also due to the fact that medulla is softer and weaker compared to cortex, CLSM was not able to recognise thin medulla region. Medulla index for the all the hair shafts (having medulla) are measured as shown in Figure 2.18 and found that donor age has no correlation on medulla index [Srettabunjong et al. 2016]. Constant value of medulla index of 0.12 - 0.27 indicates that medulla diameter is not dependent on hair shaft diameter. From the data reported in Figure 2.18, it can be said that medulla is absent in ages between 48 - 80 yrs, so medulla index is zero.

Figure 2.17: Confocal laser scanning microscopy (CLSM) shows visible medulla (left, right) and absence of medulla (middle) in hair fibres.

Age (years)	Hair diameter (µm)	Medulla diameter (µm)	Medulla Index (MI)
5	109.5	18.5	0.17
11	108.3	23.6	0.22
11	108.5	20.5	0.19
14	103	12.6	0.12
23	94	20	0.21
29	96.5	13	0.13
32	114	20	0.18
32	97	26.3	0.27
35	80	13	0.16
41	107	16	0.15
41	106	27	0.25
64	87.5	14.5	0.17

Figure 2.18: Left: Medulla index measured from CLSM hair cross-section images. Comparison between medulla index (zero indicates absence of medulla) with donor age in right image.

2.3.2. Hardness and indentation modulus (IM) of hair fibres with respect to age and gender

It is observed from the Figure 2.19 that the depths are approx. 400 - 500 nm for hair cortex region and 600 nm for epoxy resin for load of 1.45 mN. For the same load daughter and son have less hardness compared to mother and father. The results of nanoindentation test with respect to donor age and gender for cortex region are shown in Table 2.1. From all tests, the measured indentation modulus was found to be in the range of 3.0 - 8.1 GPa and hardness in the range of 196 - 400 MPa. The coefficient of variation for hardness and indentation modulus is between 2 - 9 % indicating the significance of the nanoindentation test and this is primarily due to the small regions used for indentation tests. Indentation studies on the longitudinal section of human hair fibres have been reported earlier [Wei et al. 2005] with few insights into the micromechanics of hair. Indentation modulus of 6.7 GPa and hardness of 300 MPa was reported for Asian hair cross-section which matches quite well with the values presented in Table 2.1. In another investigation by AFM microscopy, it is reported that surface roughness of hair increases significantly with age [Jeong et al. 2011], indicating micro level differences within the cortex region.
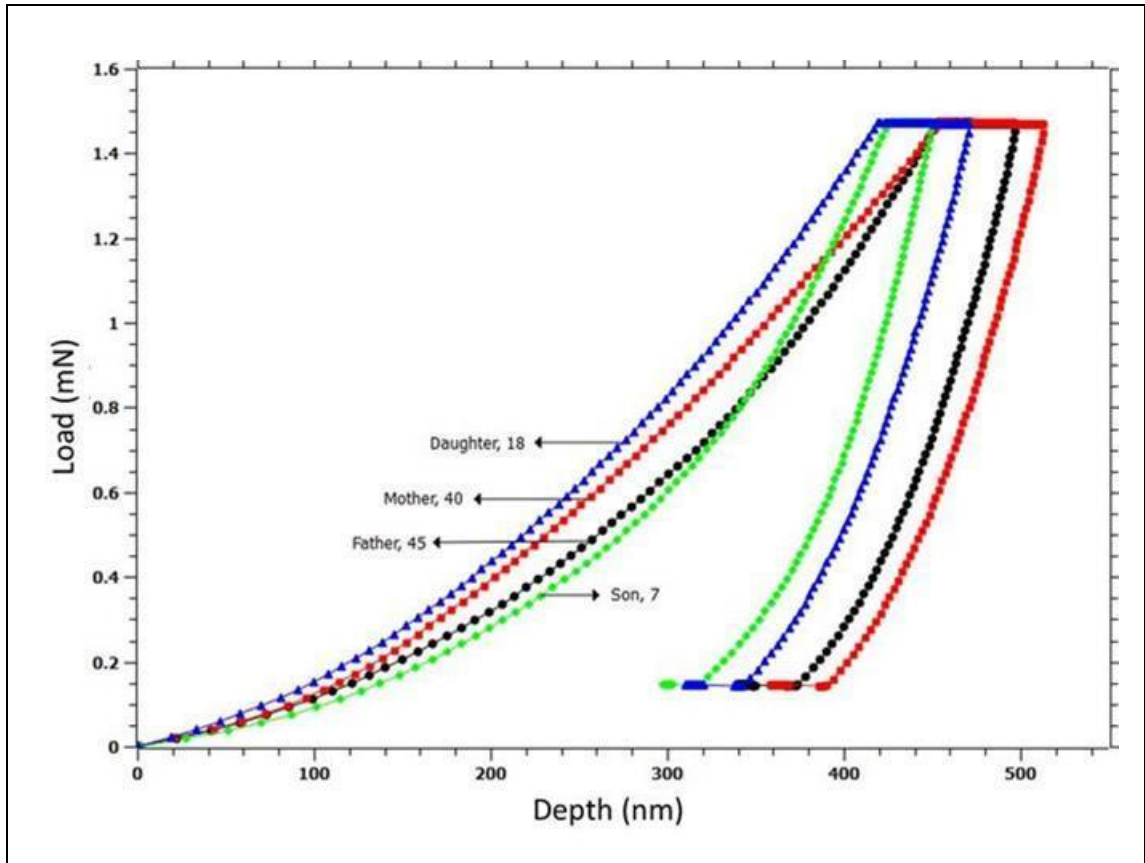
Figure 2.19: Load-depth plots of nanoindentation test performed on single hair fibre cross-sections. Note that mother is having slightly lower modulus and hardness and daughter is having slightly higher modulus and hardness within a four member family.

Sample (Age, Gender)	Indentation Modulus (GPa)	Hardness (MPa)
	Table 2.1: Indentation modulus and hardness of single hair fibre cross-sections	
3,M	6.23 ± 0.24	252 ±26
5,M	7.31 ±0.27	310 ±18
5,M	6 ±0.20	280 ±05
5,M	7 ±0.30	294 ±12
6,M	7.08 ±0.78	288 ±55
6,M	7 ±0.20	294 ±12
7,M	7.53 ±0.82	376 ±72
9,F	6.51 ±0.46	280 ±47
11,M	6 ±0.50	250 ±20
11,M	5 ±0.20	261 ±13
12,M	5.34 ±0.76	234 ±28
14,F	7 ±0.20	270 ±15
15,M	6 ±0.10	257 ±07
18,F	8.17 ±0.99	400 ±59
23,F	5 ±0.20	248 ±23
M,25	6.34 ±0.52	273 ±15
26,F	6.52 ±0.95	268 ±64
28,F	5.77 ±0.33	222 ±12
29,F	5 ±0.10	232 ±08
30,F	8.02 ±0.47	341 ±120
30,F	5.42 ±0.25	206 ±17
32,F	7 ±0.20	298 ±12
32,F	3 ±0.20	204 ±14
35,F	6 ±0.30	262 ±16
35,M	6.85 ±1.19	266 ±93
36,M	4 ±0.10	255 ±16
38,M	5.64 ±0.89	224 ±42
38,M	5.37 ±0.13	222 ±13
40,F	6.64 ±0.37	254 ±32
40,M	6.72 ±0.61	277 ±15
41,M	6 ±0.10	263 ±08
41,F	6 ±0.40	267 ±22
45,M	7.02 ±0.70	288 ±20
48,F	5.66 ±0.34	213 ±21
50,M	5.33 ±0.70	215 ±44
52,M	6.88 ±0.34	270 ±21
55,F	5.82 ±0.30	243 ±26
64,F	7 ±0.20	278 ±14
65,M	5.56 ±0.31	198 ±17
69,M	5.04 ±0.64	196 ±36
86,M	5.16 ±0.63	203 ±32
90,F	6 ±0.53	220 ±16
Epoxy	5.21 ±0.53	225 ±37
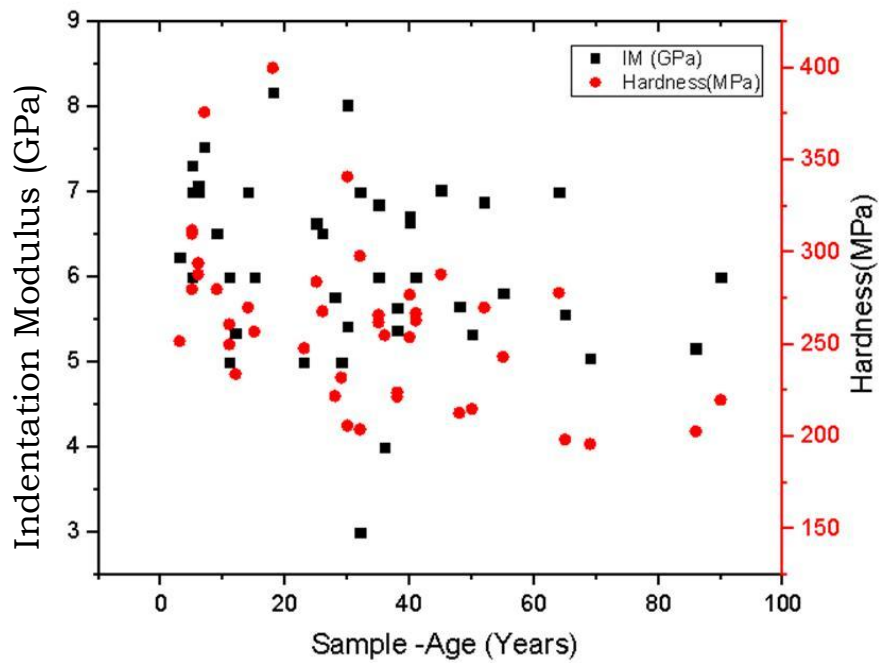
Figure 2.20: Nanoindentation test data plotted against donor age for cortex region. IM=Indentation modulus measured from unloading portion of the curve.
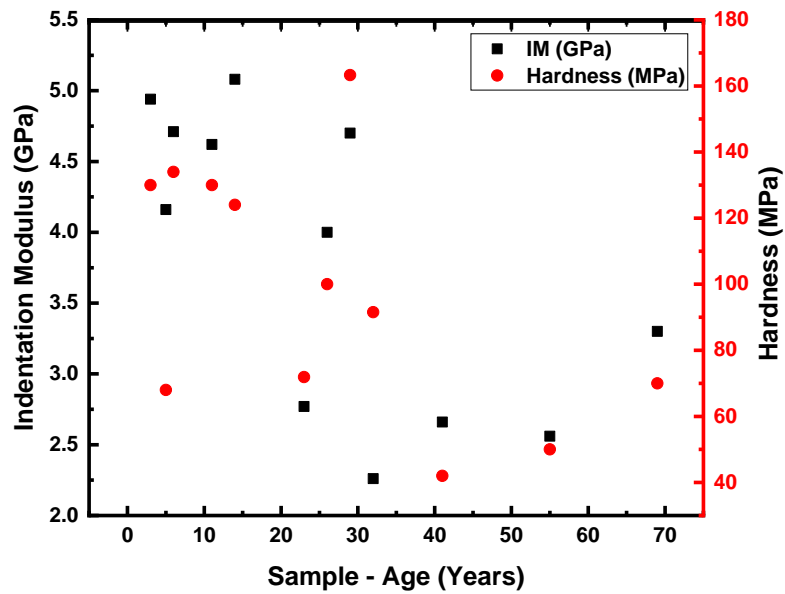
Figure 2.21: Nanoindentation test data plotted against donor age for medulla region.

Indentation modulus and hardness with respect to donor age and gender are displayed in Table 2.1 and Figures 2.20 - 2.22 for cortex region of all hair samples. It is observed that both hardness and modulus shows same trend confirming the nanocomposite structure of hair and overall packing and stability of helical intermediate filaments embedded in cystine rich matrix. Broadly speaking no significant variation in hardness and indentation modulus can be seen when data is compared with respect to donor age. However, one donor of same age and gender shows different modulus and hardness compared to other donor of same and gender (F32 - F32, F30 - F30) indicating nanostructural heterogeneities exists in hair cortex regions of those two donors as shown in Table 2.1. But this is not true in other donors of same age and gender (M5 - M5, M6 - M6, M11 - M11) in which no significant variation was found between two hair shafts when modulus and hardness are compared. Similar trend was followed when hair from donors of same age and different gender (M35 - F35, M41 - F41) are compared indicating strong and uniform structure of the nanocomposites exists in these hair cortex regions. It can be concluded that donor age has no significant influence on indentation modulus and hardness values despite slight negative correlation found between donor age and nanoindentation properties. This result was also reported in our earlier publication using different set of samples [Mishra et al. 2016].

Figure 2.22: Hardness (top image) and indentation modulus (bottom image) with respect to age and gender (data from cortex region only).
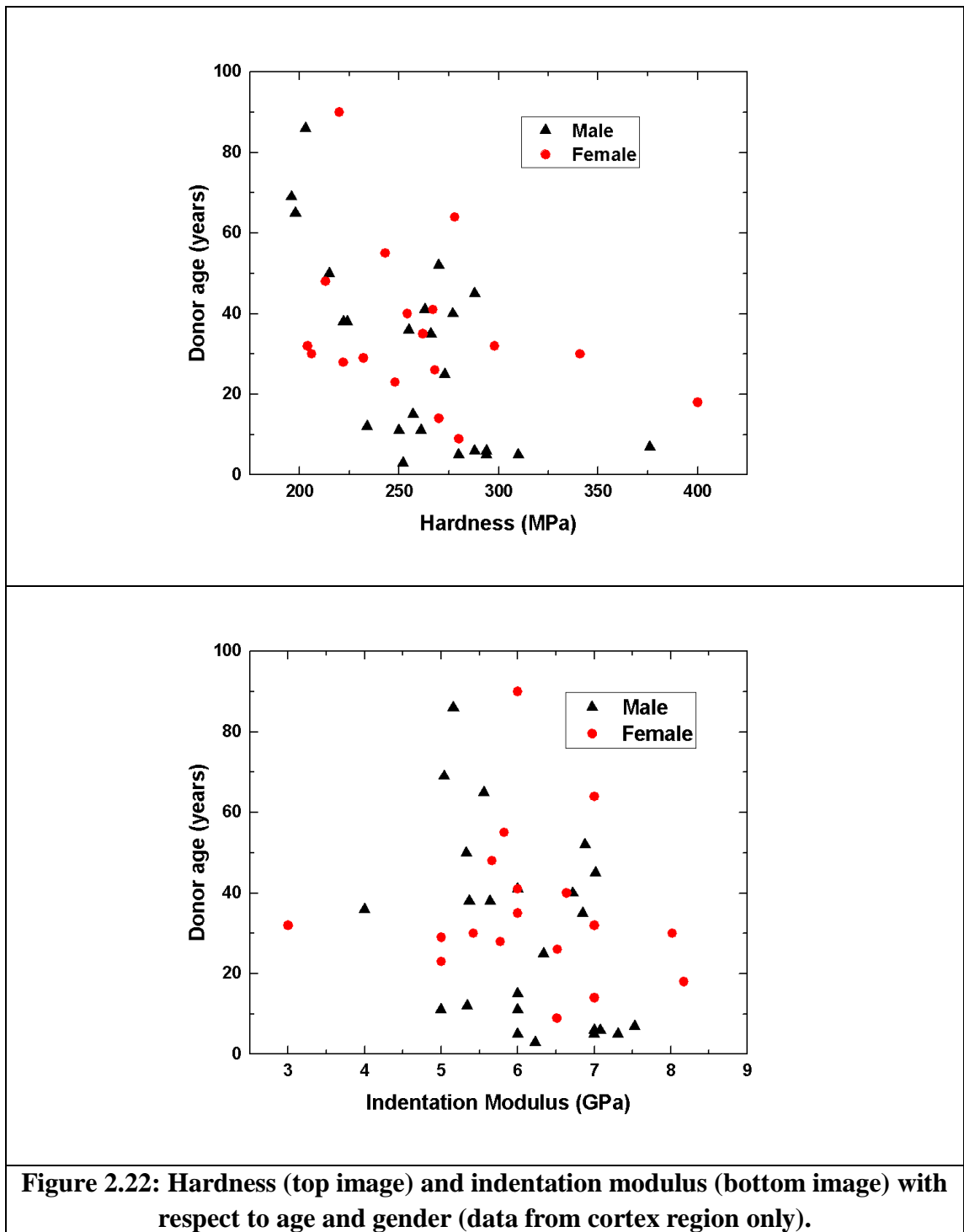
As shown in Figures 2.20 and 2.22, age and gender did not seem to have any influence on nanoindentation properties. The residual imprints (post indentation) of nanoindentation captured by SPM images on cortex region of hair with various scan sizes from 14 and 20 µm and depths of 0-771 nm are shown in Figure 2. 23.

Figure 2.23: Scanning Probe Microscope (SPM) images (Nanoindentation imprints) of Berkovich diamond indenter on hair cortex region.
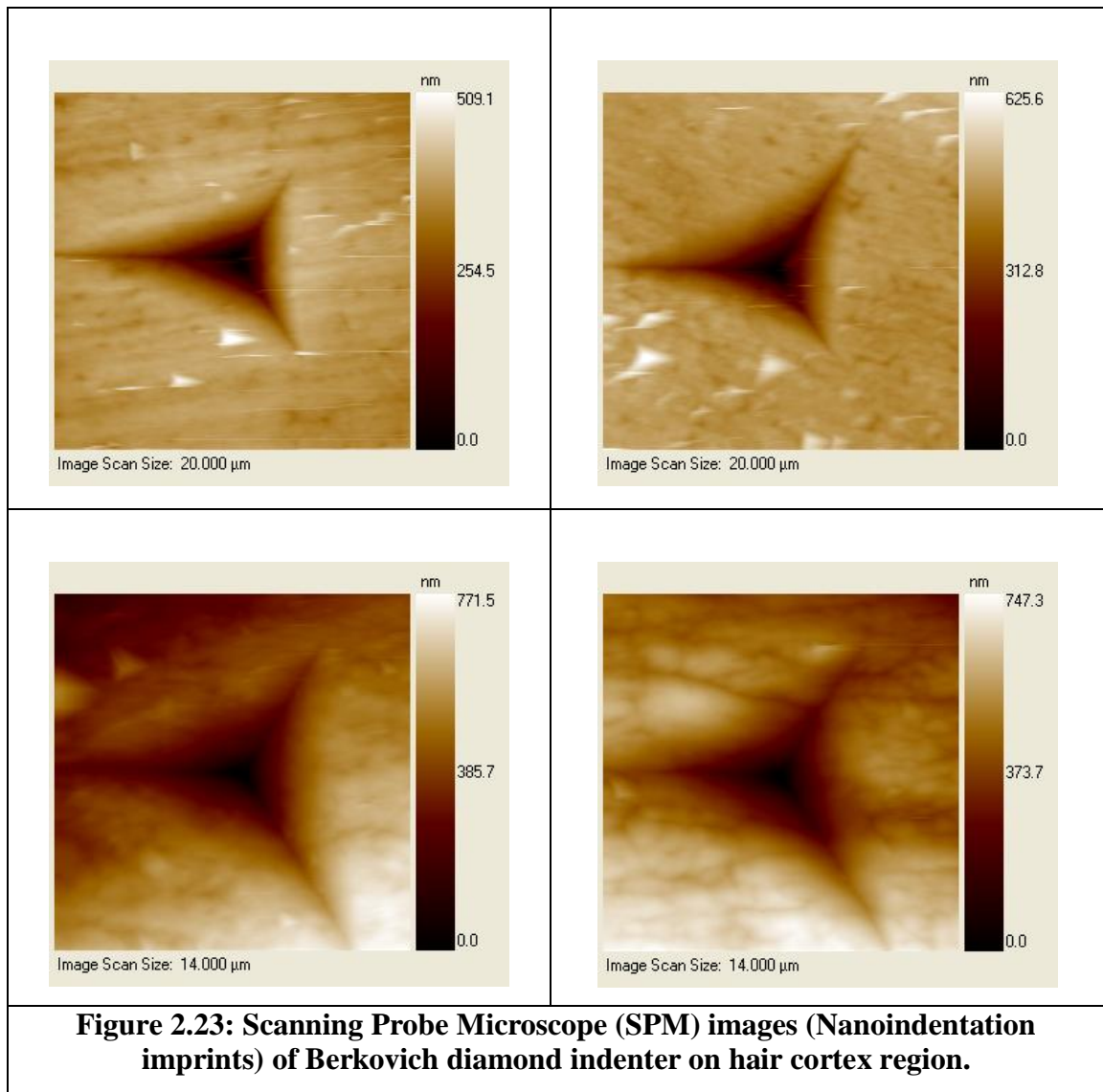
2.3.3. Hardness and indentation modulus of fibres with respect to cortex and medulla.

Representative load - displacement curves obtained from nanoindentation test are shown in Figure 2.24. It is observed from the Figure 2.24 that medulla is softer and weaker compared to cortex and epoxy resin. It is also clear that epoxy embedding medium did not infiltrate into the cortex and medulla regions. From the measured value it is found that medulla region of hair shows lower indentation modulus and hardness compared to cortex region of hair (Figure 2.24). However, absence of medulla resulted in equal or higher indentation modulus and hardness compared to cortex region. As shown in Table 2.1, embedding medium (epoxy) revealed the indentation modulus of 5.2 GPa and hardness of 225 MPa. From the 5 yrs male

sample, it is found that medulla revealed modulus of 2.2 GPa and hardness of 61 MPa in comparison to 7.3 GPa and 310 MPa respectively measured for the cortex region of the same fibre cross-section. Similar trend was observed for hair collected from 6 yrs male. This clearly indicates that medulla has the small percentage of the loosely packed mass and the epoxy did not infiltrate into the hair cross-section during embedding. For 40 yrs male hair, found that the central portion of the cortex (not the medulla) has higher modulus & hardness of 10.6 GPa & 472 MPa in comparison to periphery of the cortex region 6.7 GPa & 277 MPa respectively. It could be possible due to the phase compositions of α-keratin and cross-linked keratin of hair (formation of cystine) being not uniform across the diameter. The imprints of the indents are shown in Figure 2.23 and Figure 2.25 (for clarity 6 indents of 10 mN loads are shown, five on the cortex region and one on the medulla). Since indents are not viewed under microscopy, it can be assumed that indent was made on the interior of the cortex region. The residual imprints of nanoindentation captured by optical microscopy and scanning probe microscopy are shown in Figure 2.23 and Figure 2.25. To avoid the influence of specimen roughness and testing errors, two (Instrument-1 and nstrument-2) are used in this study. Both instruments resulted lower values of hardness and indentation modulus which are in the range of 40 - 170 MPa and 2.7 - 5.7 GPa respectively for medulla region. Slightly higher hardness (200 - 400 MPa) and indentation modulus are reported (3.4 - 8.8 GPa) for cortex region.
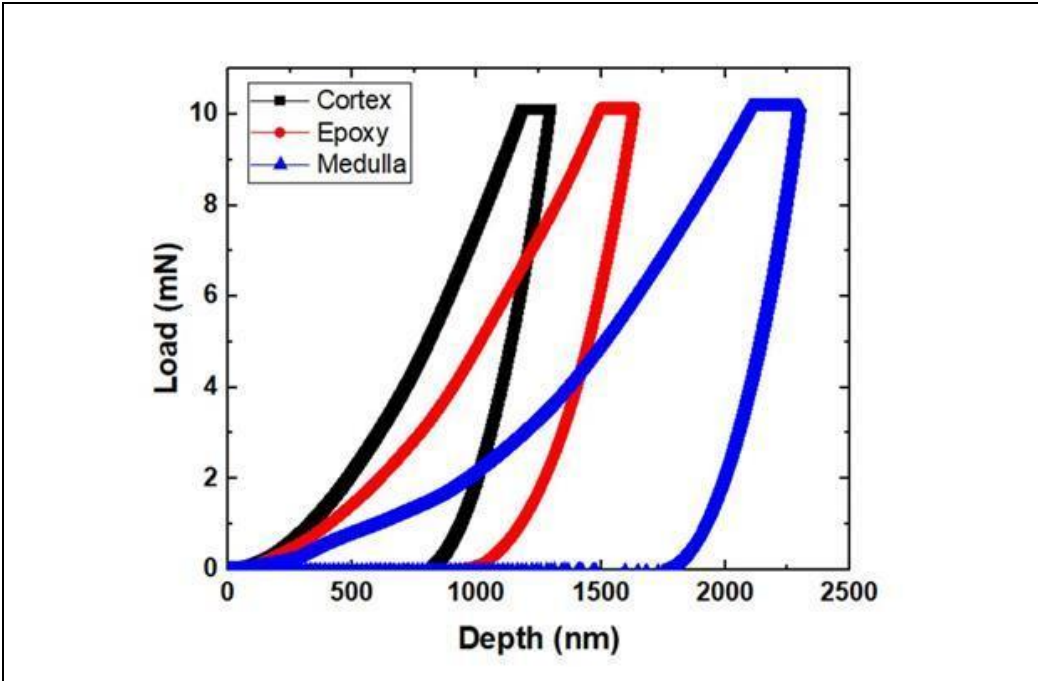
Figure 2.24: Typical load-depth graphs of nanoindentation test performed on hair fibre cortex and medulla regions. Indents are also placed on surrounding epoxy.
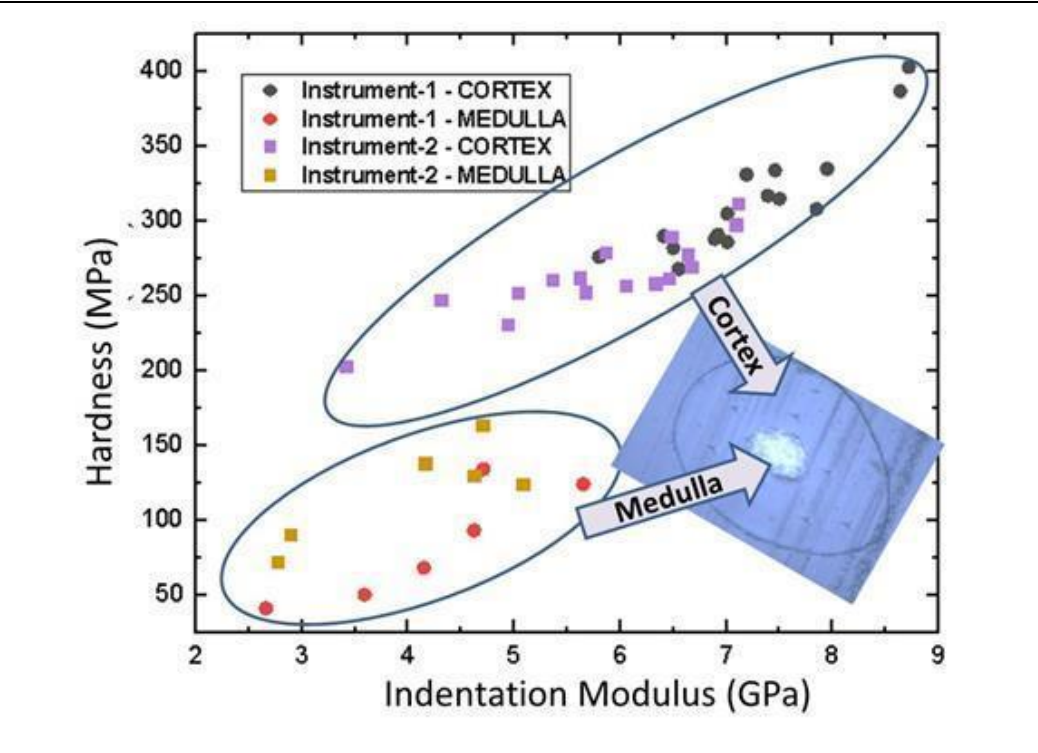
Figure 2.25: Variation of hardness and indentation modulus of hair samples with respect to cortex and medulla. Here nanoindentation on hair cross-sections was performed using two instruments (Instrument - 1 & Instrument - 2) to validate the results.

The lower values of hardness for medulla could be due to the weak nanocomposite structure of cortical cells especially weak amorphous matrix (low cystine content) surrounded by larger cavities [Wagner et al. 2007]. Similarly, lower values of modulus could be due to the less alignment of the microfibrils in medulla. Because it is reported [Mishra et al. 2016, Adusumalli et al. 2010, Gindl et al. 2006, 2008] that nanoindentation tool is successfully used to measure the response of the matrix in the form of hardness and response of the microfibrils in the forms indentation modulus in biocomposite fibres. Recently Bourmaud et al. [2012] also reported lower modulus values for xylem side of flax fibre stem and lumen side of flax fibre cross-section due to the late thickening of the cell walls. Here late thickening corresponds to less alignment of microfibrils resulting in lower values of indentation modulus.

Figure 2.26: Correlation between hardness and indentation modulus found for hair medulla region data indicating the variation in nanocomposite structure of macrofibrils especially orientation of helical intermediate filaments (microfibrils) in medulla.
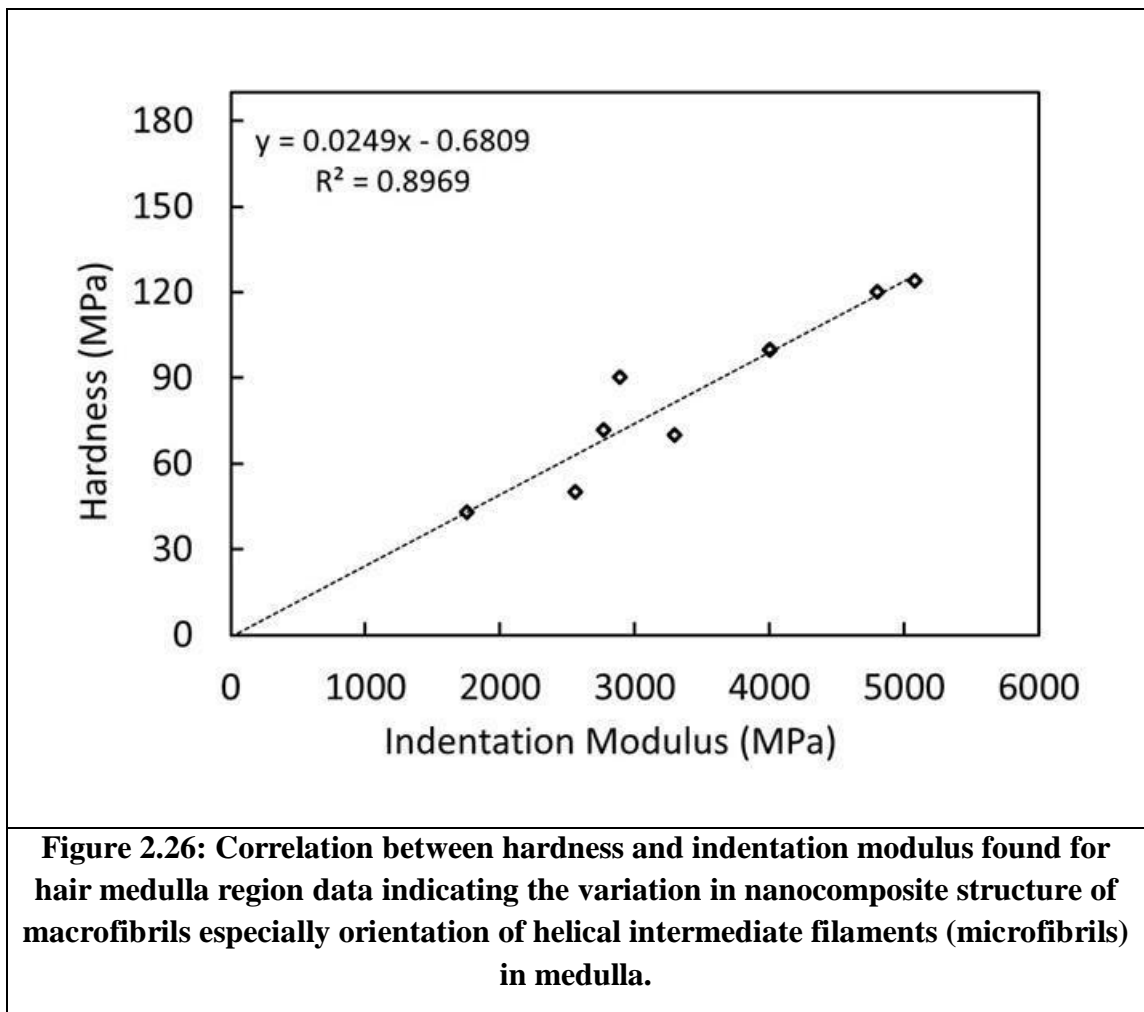
Wei et al. [2005] studied the nanomechanical properties of cuticle in lateral direction for Caucasian, Asian and African hairs and found higher hardness and modulus

compared to cortex and medulla (here indentation was done in longitudinal direction). Wei et al. [2005] also reported slightly higher hardness and indentation modulus for the hair cortex compared to hair medulla which is in full agreement with the results presented in this study. But Samanta et al. reported slightly higher hardness and modulus for medulla region compared to cortex region. In our analysis, few samples also revealed higher hardness and modulus when indents are performed on centre of the hair shaft assuming it is medulla, but medulla region was not observed when viewed under microscopy. From this study and Samanta et al. report, it can said that nanoindentation can be used as a tool to confirm the medulla absence in hair shafts which is of interest in forensic science [Srettabunjong et al. 2016] and in textiles for the estimation of dye uptake.

In order to get the deep insight of medulla's existence in hair shaft, more indentations are performed in medulla region of different donors. Hardness and indentation modulus were in the range of 40 - 170MPa and 2.25 - 5.25 GPa respectively with respect to donor age for medulla region. Figure 2.26 shows linear correlation between hardness and indentation modulus of medulla region of different hair samples with correlation factor (R^2) of 0.89. In fact such correlation between hardness and modulus also exist in cortex data (Figure 2.25) indicating the influence of macrofibril arrangement in nanomechanical properties. It should be stressed here that same macrofibrils are present in cortex and medulla regions, but they differ in macrofibril arrangement. No reports were found regarding variation of microfibril arrangement within the cortex region, but it was clearly reported by Wagner et al. [2007] that organization of microfibrils in medulla decreases from medulla border to center. Lower modulus values reported in the correlation could be due to the higher degree of anisotropy that exists in the centre of the medulla region. But the corresponding lower values of hardness could be due to the weaker amorphous network present in cortical cells of medulla and also due to the special arrangement of macrofibrils. It can be said from the correlation shown in Figure 2.26 that different levels of stressing of nanocomposite structure (i.e. arrangement of the macrofibrils with respect to fibre direction) occurred across the medulla regions of the hair shaft. Such correlation between two nanomechanical properties was not reported earlier though it may exist in wood and plant fibres. Gindl et al. [2006] reported higher hardness and low modulus for viscose fibres compared to lyocell fibres due to reduced lateral bonding

in lyocell. But lyocell and viscose fibres have only cellulose microfibrils arranged in fibre direction whereas in hair shaft, microfibrils embedded in cystine rich matrix are arranged in fibre direction.

This concludes that nanoindentation can be used as a tool in understanding the small structural defects that exist in cortex and medulla regions because hardness usually increases with increase in cross-linking of sulphur rich amorphous matrix and indentation modulus increases with better arrangement of microfibrils in cortical cells.

The results from nanoindentation of hair can be used in three fields.
- It can be used as a diagnostic tool in estimating structural differences in damaged hair caused by physical interventions such as combing, drying, curling and straightening. Since root side of the hair has good number of cuticles and tip side hair has damaged or less number of cuticles [Wei et al. 2005] there is high probability that dye uptake can cause damage to tip side cortical cells.
- It can be used in forensic science to identify and quantify the medulla in hair, wool and other animal fibres.
- This study can be extended to understand the core-skin structural differences that exist in other fibres such as Kevlar where core is less aligned than skin like medulla-cortex regions of hair shaft. Chegdani et al. [2017] and Bencomo-Cisneros et al. [2012] reported lower values of indentation modulus compared to tensile modulus for kevlar and flax fibres respectively due to the effect of increased orientation of the microfibrils during tensile stretching. But in hair, contradicting results are found that the tensile modulus and yield stress are slightly lower than indentation modulus and hardness respectively. Even though flax and hair are bio-nanocomposites, they differ not only in their chemical composition and also in their microfibril arrangement.

2.4. Conclusions

1. Nanoindentation tests are performed on cortex and medulla regions of hair shaft. Hardness and indentation modulus of cortex region are almost same for 15 donors indicating the age has negligible effect on nanomechanical properties.

2. From the nanoindentation test, it is found that medulla has less organised microfibrils and weak matrix resulting in lower values of modulus and hardness compared to the cortex region of the same hair shaft. For one male sample, it was found that medulla revealed modulus of 2.2 GPa and hardness of 61 MPa in comparison to 7.3 GPa and 310 MPa respectively measured for the cortex region of the same hair shaft. Hair samples without any visually discernible medulla showed no significant difference in properties between cortex and medulla regions.

3. The linear correlation between modulus and hardness data of medulla region indicates the different degree of microfibril orientation in cortical cells and also nano-structural heterogeneities that exist in hair composite.

4. Hair fibre cross-sectional diameter was found to between 70 - 100 µm. Medulla index (medulla to fibre diameter ratio) is found to be between 0.12 - 0.27 and it is not influenced by age.

5. The quantitative values of nanoindentation hardness and modulus of cortex and medulla regions of single hair shaft are of interest for dermatologists in treatment of hair disorders including the negative effects of hair dye penetration. Since the individual tests are performed on 100 μm^2 area, the observed differences between cortex and medulla will help in developing new insulation materials [Mohan et al. 2017] or textile dyes. These findings may also be of interest to forensic experts.

CHAPTER - 3

Tensile testing of single hair fibres

This chapter covers test results about the hair diameter measurements with optical microscopy, tensile specimen preparation and tensile testing of single hair fibres using Texture analyzer. The chapter also presents the optical microscopy and SEM fractography of tensile specimens. Statistical analysis of tensile properties using ANOVA, Relative Rating and Grey Relational Analysis was carried out to find any difference in tensile properties exists between scalp positions (P1-P4). Finally, comparison between nanoindentation properties and tensile properties were described

3.1. Introduction

The basic data on the mechanical properties of fibrous material can be obtained from tensile testing of single fibres. Generally fibres (viscose, pulp, flax, glass, aramid, wool, hair) are tested using paper frame technique instead of direct gripping. In this technique fibre is subjected to increasing axial load until it fractures. Tensile tests of human hair are carried out using single fibres and it has been found that only the cortex can influence the tensile properties and not the cuticle [Bhushan 2010]. The organisation of keratin within the cortex allows the hair to bear a load of up to a hundred grams. Cellulose, glass and carbon fibres generally yield prior to 5 % of strain but hair follows the Hooke's law up to 5 % strain and is almost perfectly elastic up to 45 % strain where it usually breaks. This is due to the helical structure of the keratin molecule. The percentage of elongation differs between ethnic groups (like Asian, Caucasian and African) with lowest being for African hair. Some studies have been conducted on Caucasian and Asian hair and how they are affected by cosmetic treatments, but very few samples were used in these studies. Beard hair has less modulus compared to scalp hair due to a lower percentage of disulfide bonds [Tolgyesi et al. 1983]. It is reported that thick hairs have low moduli and stress due to the presence of medulla [Nikiforidis et al. 1992]. None of the above studies focused on a mechanical characterization of hair from different positions of the human scalp, despite scalp positions are subjected to varying magnitudes of environmental,

physical and hormonal stimuli and correspondingly different hair balding patterns are observed [Menelaos 2014].

In this chapter single fibre tensile testing of hair collected from four different scalp regions of different donors is discussed and compared with respect to age and gender. Detailed study of tensile stress-strain plots and their corresponding SEM fractography are used to understand the structure-property correlation [Mishra et al. 2016]. The differences in tensile properties are quantified using statistical methods. Accurate measurement of hair diameter, linear density, detailed study of stress-strain plots and fractography post tensile tests along with structure-property correlations were also carried out to determine the differences among hair properties with respect to age, gender and scalp position.

3.2. Materials and Methods

Human hair samples from healthy people (donors) without any hair disorders with age ranging from 3 to 70 years were collected from the scalp. Hair samples were collected from both males and females living in Hyderabad, India (Caucasian origin) after getting approvals from Ethics Committee. Hair samples were collected from 4 positions of the scalp from different families and also from individual donors. The four positions are Frontal (front) - Position 1 or P1, Temporal (sides 5 cm from ear) - Position 2 or P2, Vertex (center) - Position 3 or P3 and Occipital (back) -Position 4 or P4 as shown in Figure 3.1. Hair at positions 1 and 3 are more exposed to sunlight and physical stress than those at positions 2 and 4. Moreover baldness patterns usually observed show lower hair density at certain positions (1 and 3) than others. This led to a need to take hair from four different positions to establish tensile property differences among them. In order to obtain samples with lower thickness heterogeneity, samples were cut 2 cm above the scalp and total length of hair being taken was around 5 - 8 cm. The hair samples were washed with mild shampoo, then with water and dried at room temperature. After drying, samples were kept in ziplock covers and were labeled. Before tensile testing of the hair samples, linear density in mg/cm is measured by taking a fixed number of samples (bundle of six hair fibres with length of 20 mm) and measuring their weight. The linear density value is calculated as:

Linear Density = Weight of the hair fibres (mg) / (no. of hair fibres * length of an individual hair)

Figure 3.1: The various positions of scalp are named with reference to the bone on human skull. Hair is collected from four different positions namely P1-P4. Note the high density of fibres in position 2 (P2).
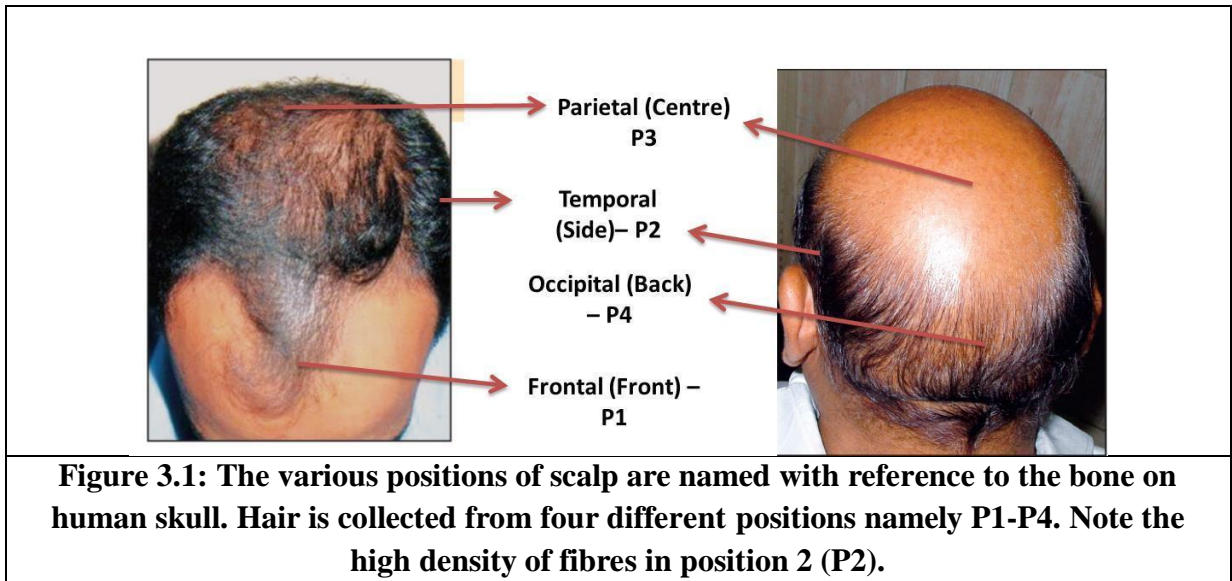
3.2.1. Sample preparation for tensile testing of single hair fibres

For tensile testing of single hair fibres, samples were prepared using paper frames as shown in Figure 3.2 and Figure 3.3. The paper frames (cardboard has high modulus) of dimension 30 mm X 20 mm with a rectangular hole of 20 mm X 10 mm were prepared to hold the samples at both ends, Araldite epoxy resin (as two components are carefully mixed in correct ratio) was used as glue. Cyanoacrylate was not used as glue due to its less stickiness with hair. After the resin gets hardened on both ends, the aligned hair samples are subjected to diameter (longitudinal view) measurement using microscopy. The diameter of hair is measured at three different positions along the hair fibre and average of three is considered for all samples as shown in Figure 3.4. The prepared samples are conditioned at 22° C and 55 % relative humidity (RH) in a humidity chamber for duration of 72 hours because % RH has the large influence on hair tensile properties. During sample preparation, care is taken to ensure that the hair is parallelly aligned to the loading axis and hair is in unstretched condition. Five tensile samples are prepared for each donor to obtain an average value of at least 3 measurements.
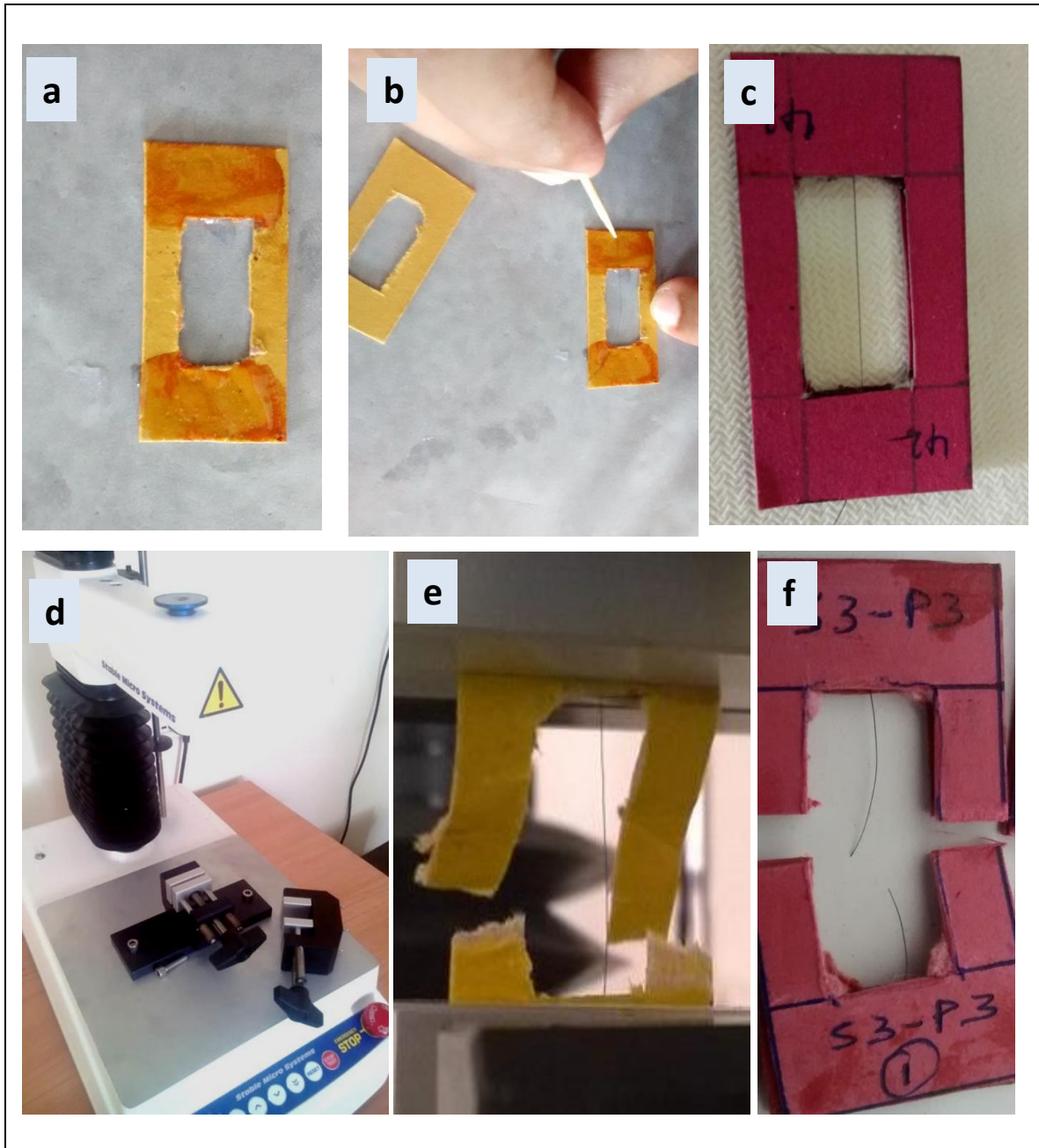
Figure 3.2: Single fibre tensile test of hair using rubber coated grips. (a) Glue is applied on both ends of the bottom frame, (b) Single hair is fixed to the bottom frame, (c) Specimen before tensile test, (d & e) Single fibre testing of hair fibres using 500 N load cell (mini Texture analyzer), hair is fixed between top and bottom frames after sides were cut (f) Specimen after tensile test.

3.2.2. Tensile testing of single hair fibres

The prepared samples are then subjected to tension using a Texture analyser from Stable micro systems, UK with 500 N load cell (located in room where temperature of 22 ± 2 °C and 50 ± 5 % relative humidity was maintained). Rubber coated tensile grips are used to avoid the slippage of the paper frame. The gauge length and test speed are 20mm and 20 mm/min (0.33 mm/sec) respectively as per ASTM D3379-75 standard. Before application of load, the paper frames are carefully cut at both sides such that the hair fibre can take the tensile load. The tension is applied by running a test in a displacement controlled mode using inbuilt software which gives the force in mN and displacement in mm. Typically the hair fibre takes the maximum load in the range of 700 - 1500 mN for the maximum displacement of 6 - 9 mm. When the post test samples are observed in the stereo microscopy, most of the hair breakages occurred in the middle or near an end of the sample frames and the rest showed jaw breaks (breaks within 1mm of an edge of a frame) and those are not taken into consideration for analysis.

3.2.3. Fractography of single hair fibres using optical microscopy and Scanning Electron Microscopy (SEM)

Samples prepared for the tensile test are subjected to longitudinal diameter measurements using optical microscopy equipped with a CCD camera and software (Olympus STM 6) in transmission mode. The fractured hair samples were also viewed under both optical microscopy and SEM to study the fractography and to understand the modes of failures. Optical microscopy was used to measure the fibre diameters of post tensile test samples as shown in Figure 3.3. From the Figure 3.3, it is observed that one end of tensile hair sample is curled after tensile test and also the end diameter of fractured sample decreased gradually. To check the fractography of hair fibres with SEM, one of the fractured ends of fibres was fixed to the stub using double-sided carbon tape, sputter coated and viewed from the top with different rotations to see the fractured modes especially step modes. From the SEM fractography images, macrofibril diameters were measured using Image J software.
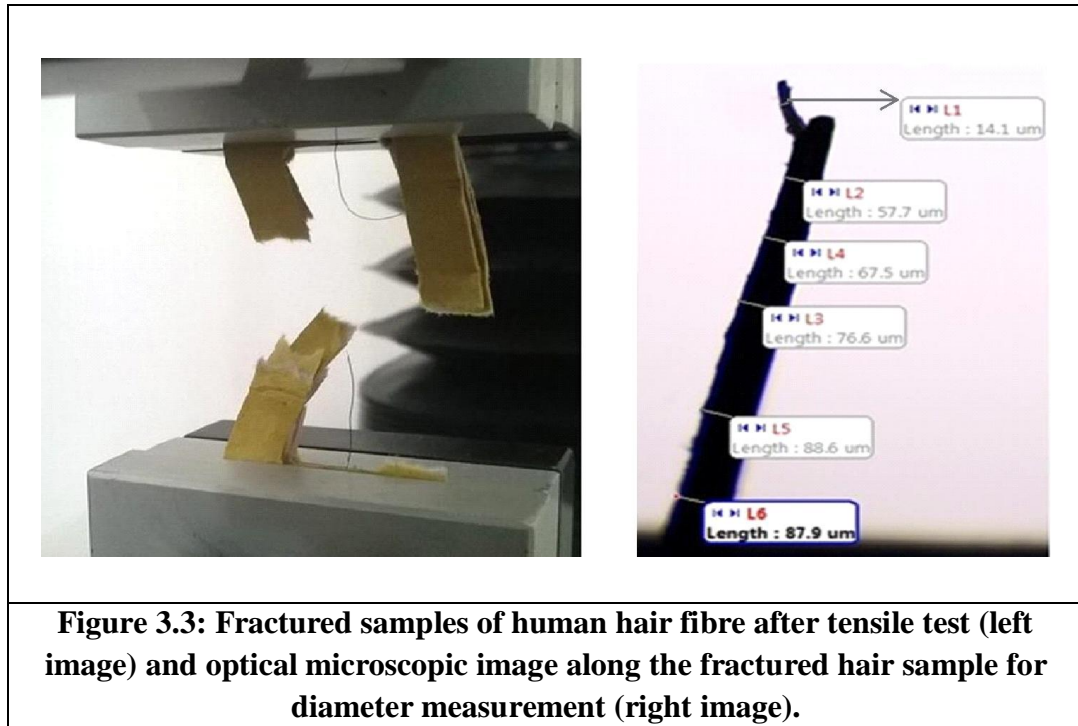
Figure 3.3: Fractured samples of human hair fibre after tensile test (left image) and optical microscopic image along the fractured hair sample for diameter measurement (right image).

3.3. Results and Discussions

3.3.1. Fibre diameter and linear density with respect to age and gender

The hair diameter with donor's age (family wise) is shown in Figure 3.4. It was found that positions P2 and P3 have relatively higher diameter and linear density compared to positions P1 and P4. From the Figure 3.5, maximum linear density is observed in female 41 years at positions (P1 - P4) and minimum linear density at P1, P3 and P4 positions are found for males between 36 - 38 years. Further, lowest values were observed for males between 5 - 7 years, least being for hair samples collected from 6 years old (0.013 mg/cm) for position P2 samples. Hair from positions P1 and P2 revealed relatively higher average linear density values compared to the hair from P3 and P4 positions. Similarly for the position P2, 41 yrs male had the lowest linear density (0.03 mg/cm) compared to other hair fibres. Overall linear density varied between 0.02 - 0.07 mg/cm except few outliers. Similarly hair fibre diameters are in the range of 40 - 100 μm as presented in Figure. 3.4. Amongst tested hair, from 12 yrs male had the highest diameter in all positions (P1 - P4) compared to hair from his parents and being highest at P2 (107 μm). It was found that the hair from 30 yrs female (45 μm) at P1 position and 45 yrs male at P4 position had the least diameter (42 μm). P3 position revealed highest diameter (91 μm) compared to other three

71

positions in case of 5 yrs male and it could be due to the presence of medulla (in case of 12 yrs male medulla is absent). Hair diameters of positions P1 to P4 were found to be in the range of 65 - 90 µm except few outliers.Diameters prior to testing are in the range of 65 - 104 µm, 62 - 92 µm, 60 - 96 µm and 63 - 91 µm for P1, P2, P3 and P4 positions respectively as shown in Tables 3.2-3.5.
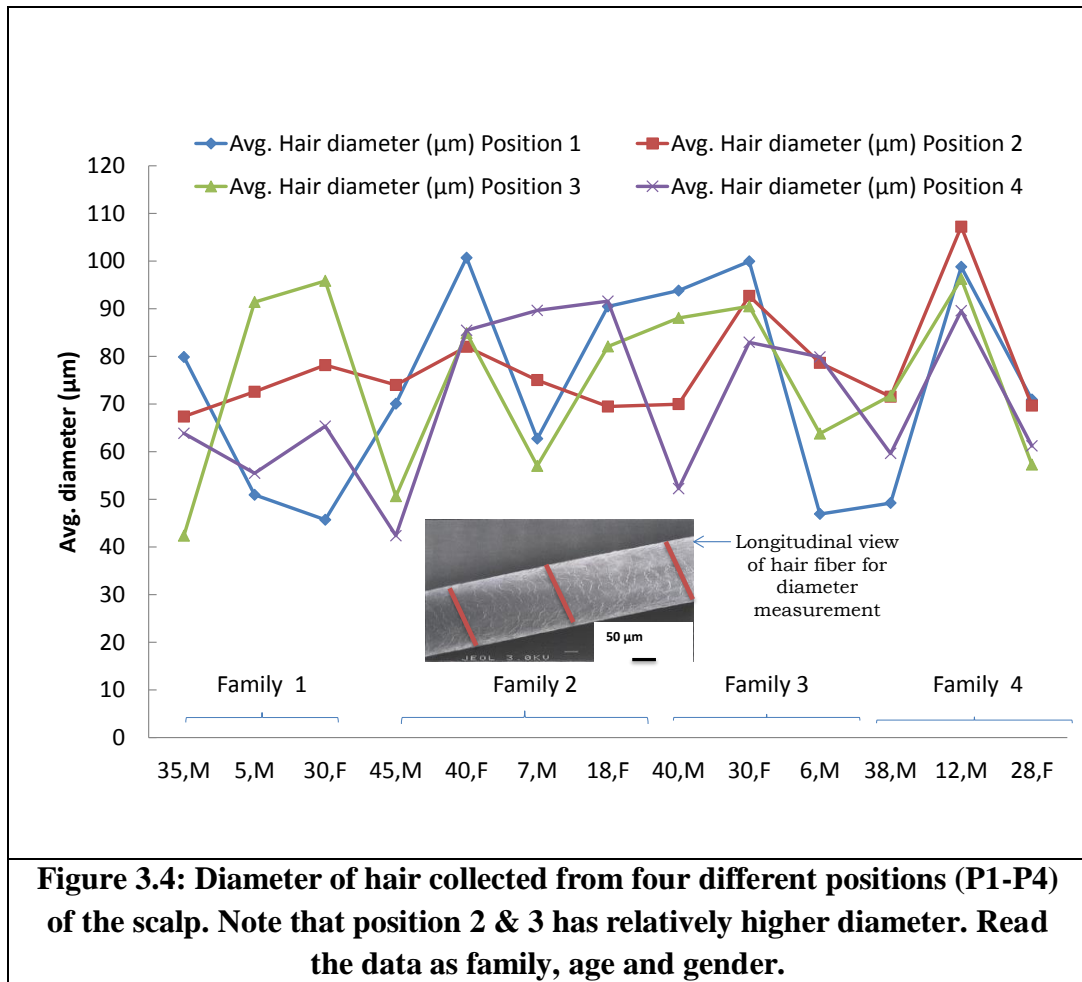
Figure 3.4: Diameter of hair collected from four different positions (P1-P4) of the scalp. Note that position 2 & 3 has relatively higher diameter. Read the data as family, age and gender.

It was reported that age has a negligible effect on diameter, but medulla can have a significant effect on diameter. However, another literature says ageing causes changes in the hair diameter mainly in the age group of 20 - 30 years and after which it begins to decrease. Difference of 10 - 20 µm in diameter is observed when individual hair diameters are compared between scalp positions (P1 - P4). But average values shown in Tables 3.2 - 3.5 revealed lowest diameter at P4 position (76 µm) and highest diameter at P1, P2 positions (81 µm). For a 41 years female, the highest average diameter is observed at the P1 position, then followed by P3 and P2 positions and all three positions revealed higher diameters compared to the hair diameters from the

same positions of 41 years male as shown in Tables 3.2 - 3.5. Hair from position P3 only considered for further studies because there is no significant trend in diameter or linear density with respect to position as shown in Figures 3.4 - 3.5.
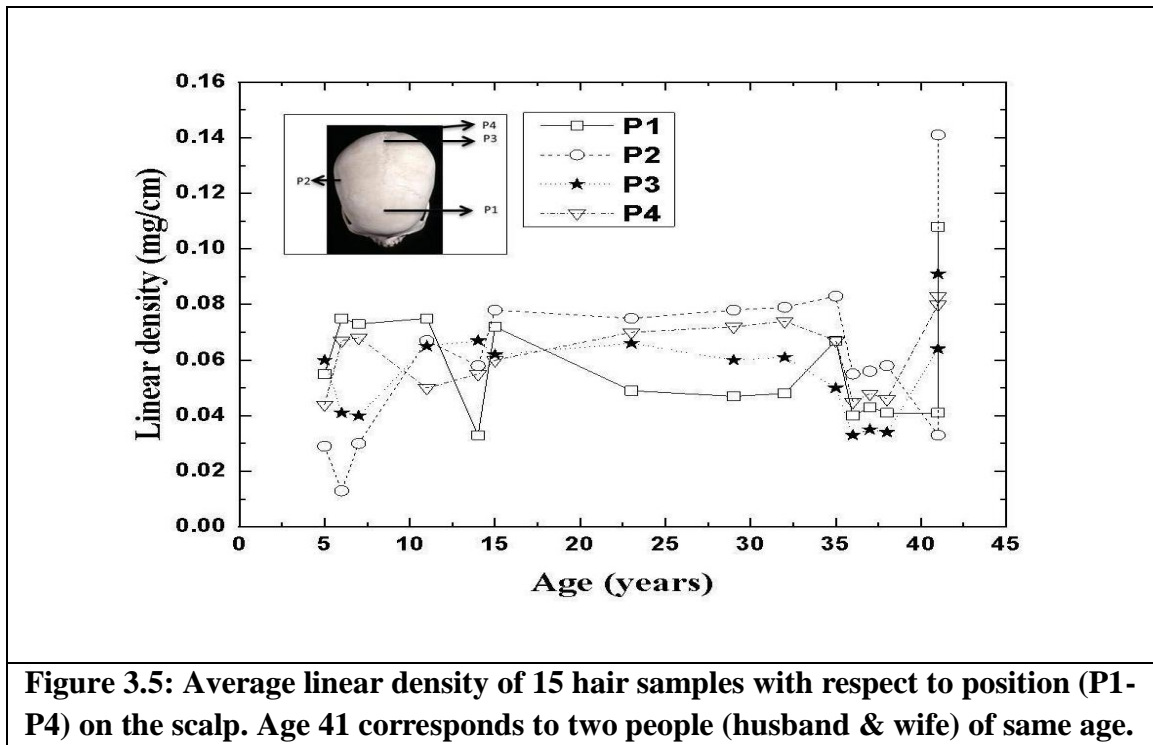
Figure 3.5: Average linear density of 15 hair samples with respect to position (P1-P4) on the scalp. Age 41 corresponds to two people (husband & wife) of same age.
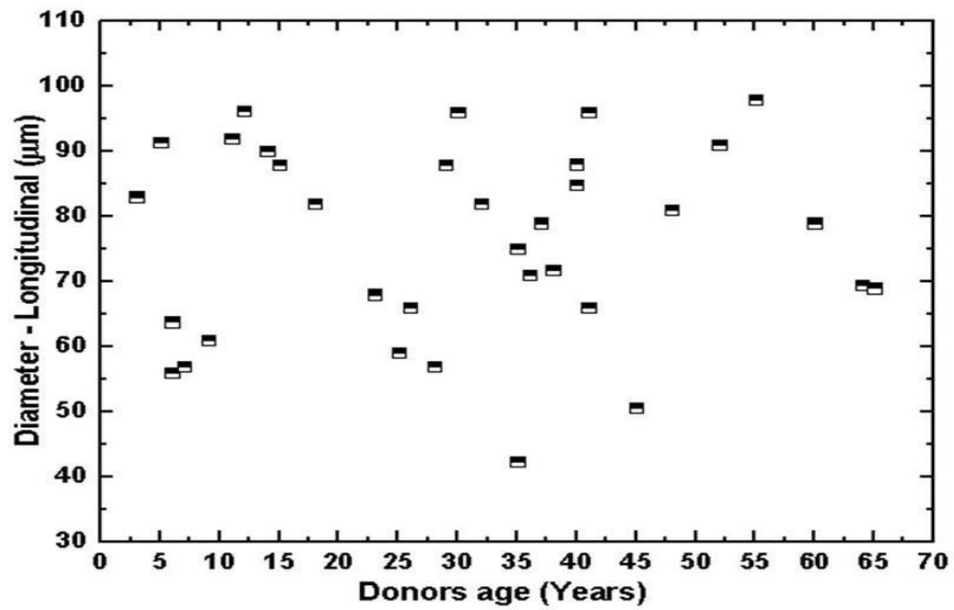
Figure 3.6: Diameter of hair fibres (position P3) as a function of donor age.
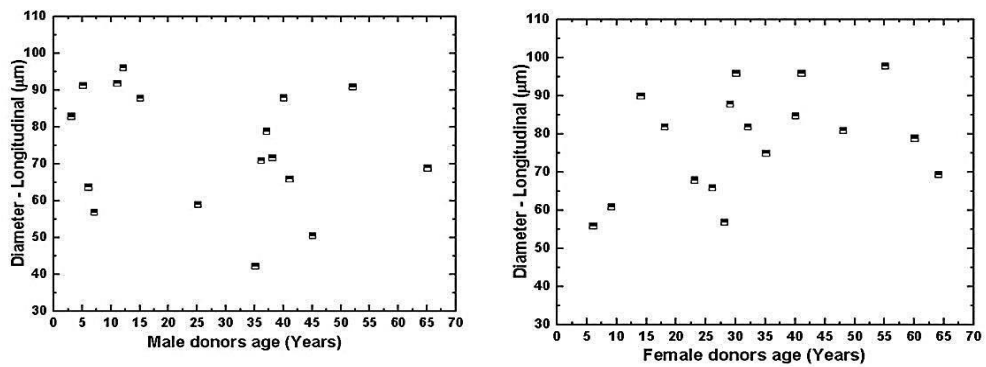
Figure 3.7: Diameter of hair fibres (position P3) as a function of male donor age (left image) and as a function of female donor age (right image).
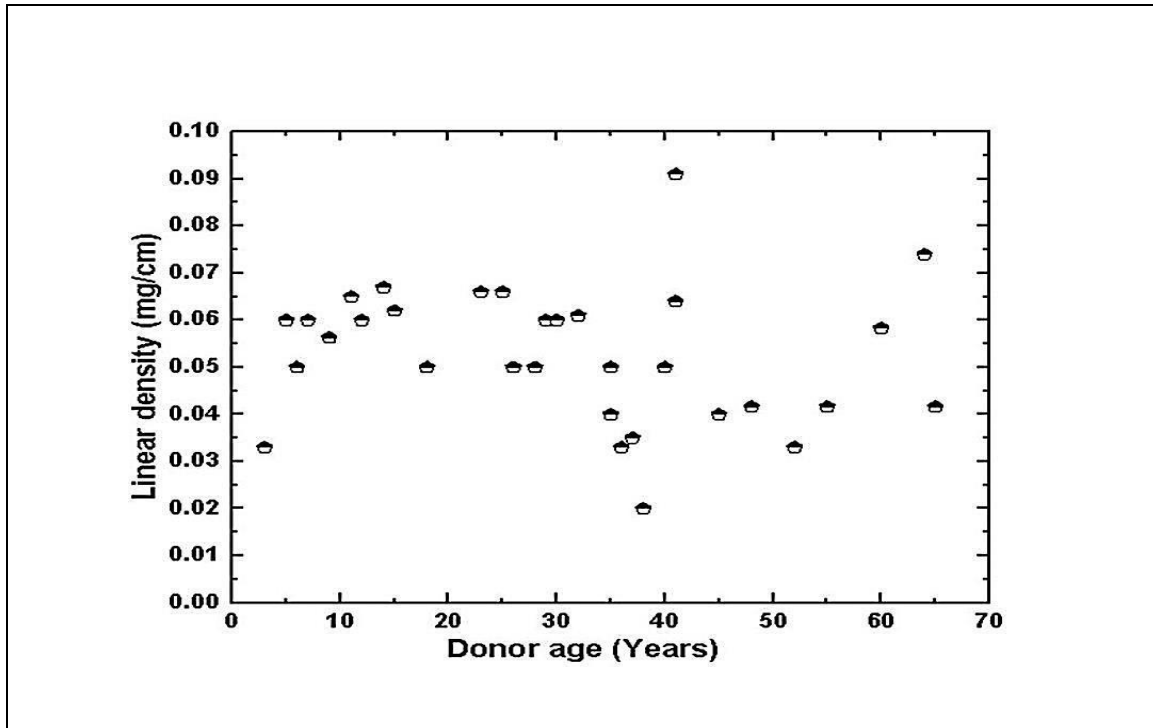
Figure 3.8: Linear density of hair fibres (position P3) as a function of donor age.
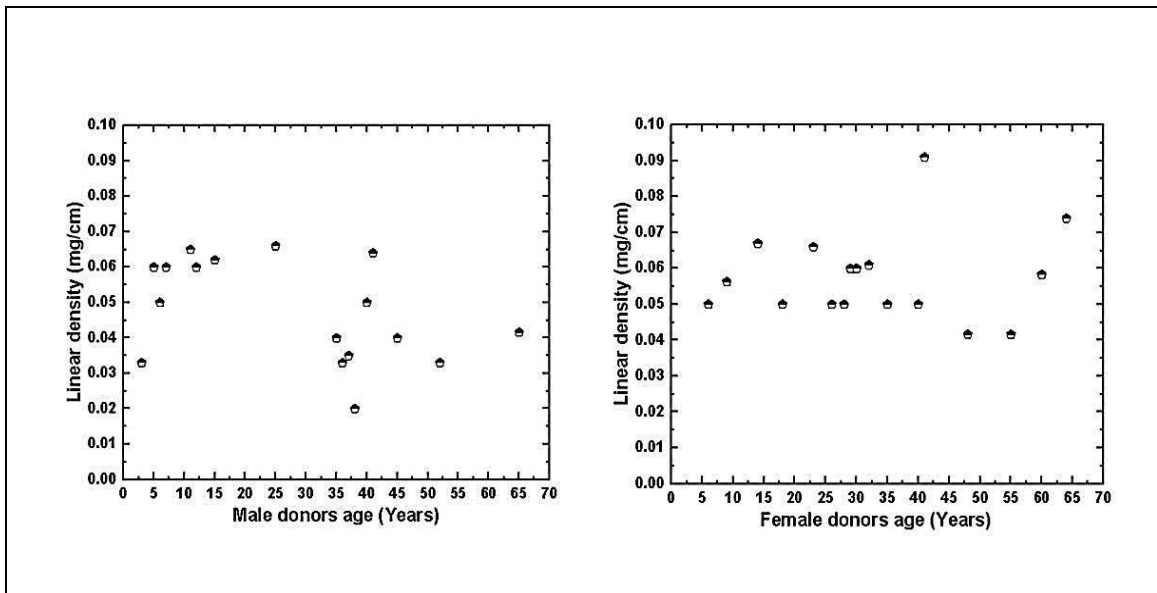
Figure 3.9: Linear density of hair fibres (position P3) as a function of male donor age (left image) and as a function of female donor age (right image).

Figure 3.6 and Figure 3.7 show the diameter measurements for all donors (for P3 position) with respect to age and gender respectively. No significant trend in diameter is seen and it can be concluded that diameter is not influenced by donor age and gender. Similar trend is observed in linear density with age and gender as shown in Figure 3.8 and Figure 3.9 respectively. Slight reduction in linear density was observed

75

with increase in age and this is more significant with respect to males. The diameter (longitudinal) and linear density of hair fibres were in range of 42 - 98 µm and 0.02 - 0.09 mg/cm respectively for all donors (P3 position). The diameter and linear density of hair fibres of all male donors were in the range of 42 - 96 µm and 0.02 - 0.07 mg/cm respectively and for all female donors the values are in the range of 56-98 µm and 0.04 - 0.09 mg/cm respectively. From Figures 3.4 - 3.9, it was observed that age, gender and scalp location have not shown any trend on diameter and linear density, because diameters vary from tip to root [Hutchinson et al. 1999] and person to person. Though samples were taken 2 cm above the scalp, it is not guaranteed that diameter is measured at selected heights from the scalp. From literature, the diameter of human hair fibre is in the range of 50 - 100 µm [Bhushan 2010].

3.3.2. Analysis of stress-strain curves of single hair fibres

The force - displacement data obtained from tensile test are re-plotted to stress-strain plot using origin software. The stress and strain values are calculated as shown below:

1. Stress = Force (mN) / Area (m^2) [MPa]
2. Stress= Force (mN) / (Linear density(mg/cm)*100) [mN/tex]
3. Strain = Elongation (displacement) / Initial length of the hair (gauge length)

Area is calculated from the diameter of hair assuming the hair's cross-section is circular. Usually human hair cross-section is found to be elliptical but due to minimal differences and calculation purposes, circular cross-section is assumed. The linear density with unit cN/tex is used traditionally in textile industry instead of cross-sectional area because textile fibres are small in diameter and are highly flexible.

Here yield stress is determined as onset of stress constancy and the end of linearity (Hookean region) whereas modulus is determined by fitting the linear line between 1-2 % strains of the stress-strain plot using origin software. Maximum stress and maximum strain are calculated from the respective maxima in the recorded stress-strain curve. The work of elongation is calculated as the area under the stress - strain curve.
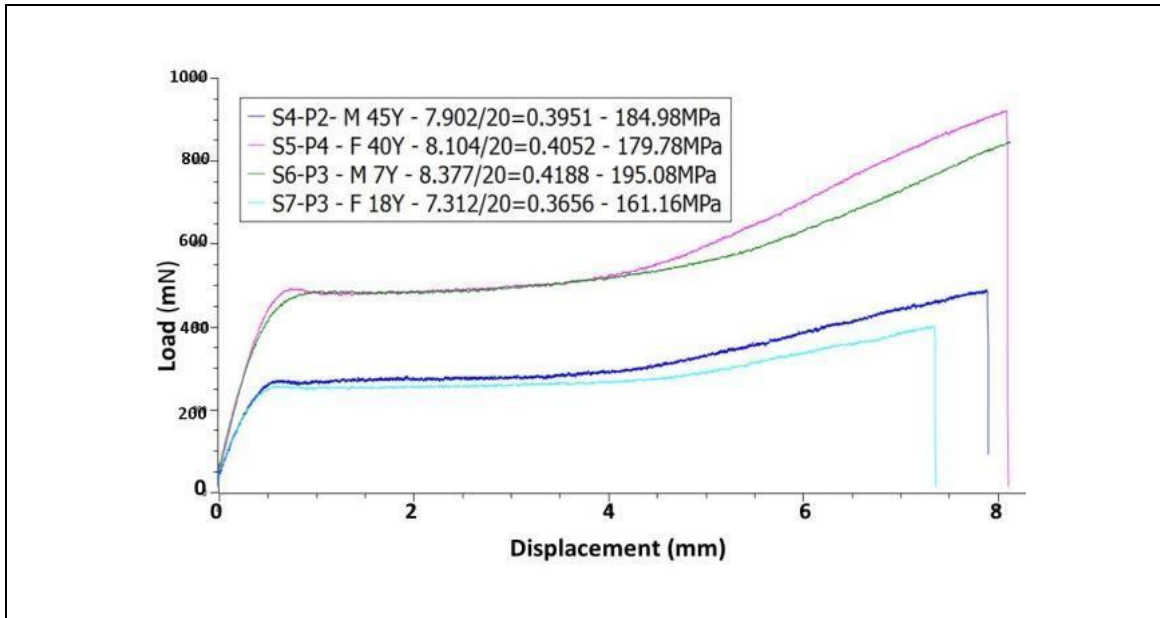
Figure 3.10: Typical load - displacement plots obtained from tensile testing of single hair fibre with gauge length of 20 mm.
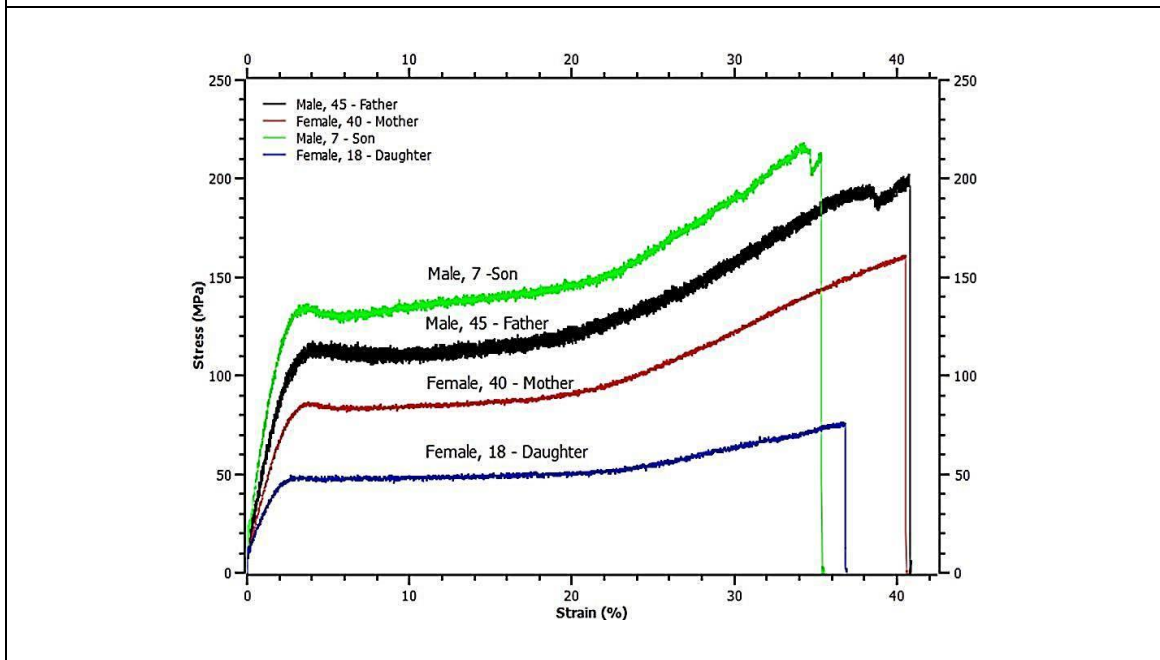
Figure 3.11: Typical Stress-Strain plots obtained from single fibre tensile testing of hair obtained from one family. Note that strain of 30-40% making hair different from other fibres such as cellulose.

The load - displacement plots of one family obtained from texture analyzer is shown in Figure 3.10 and their corresponding stress strain plots are shown in Figure 3.11. For one sample with 3 replicates, data is shown in Figure 3.12 wherein stress values are reported in mN\tex.
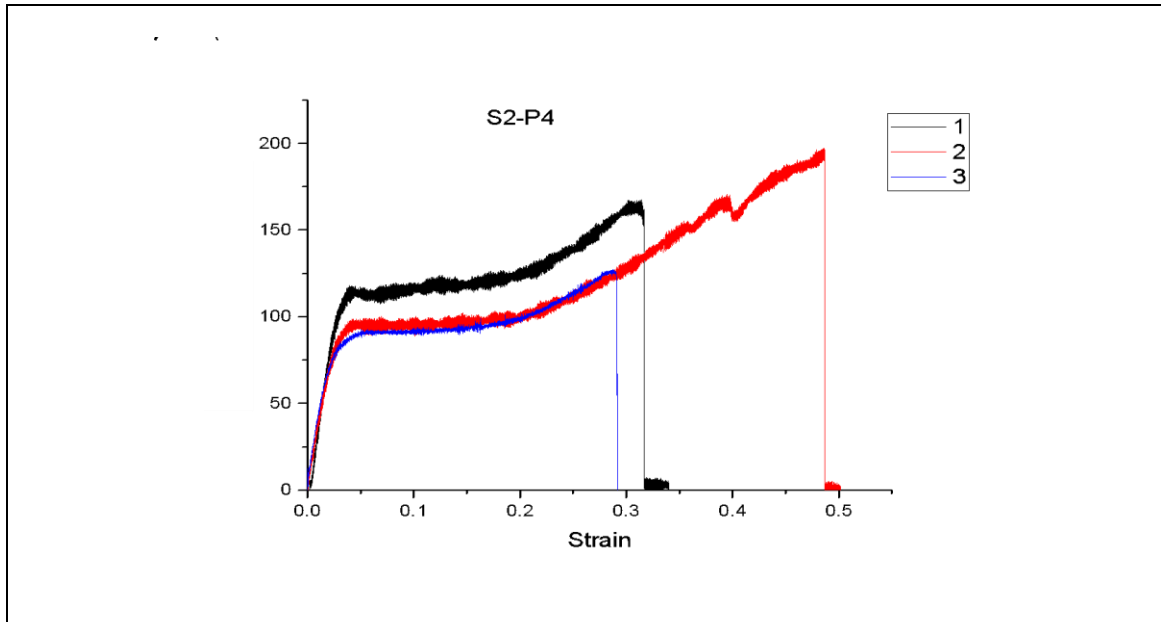
Figure 3.12: Typical stress-strain plots with replicates obtained from single fibre tensile testing of hair samples is shown and P4 indicates scalp position. Here stress is in mN\tex.
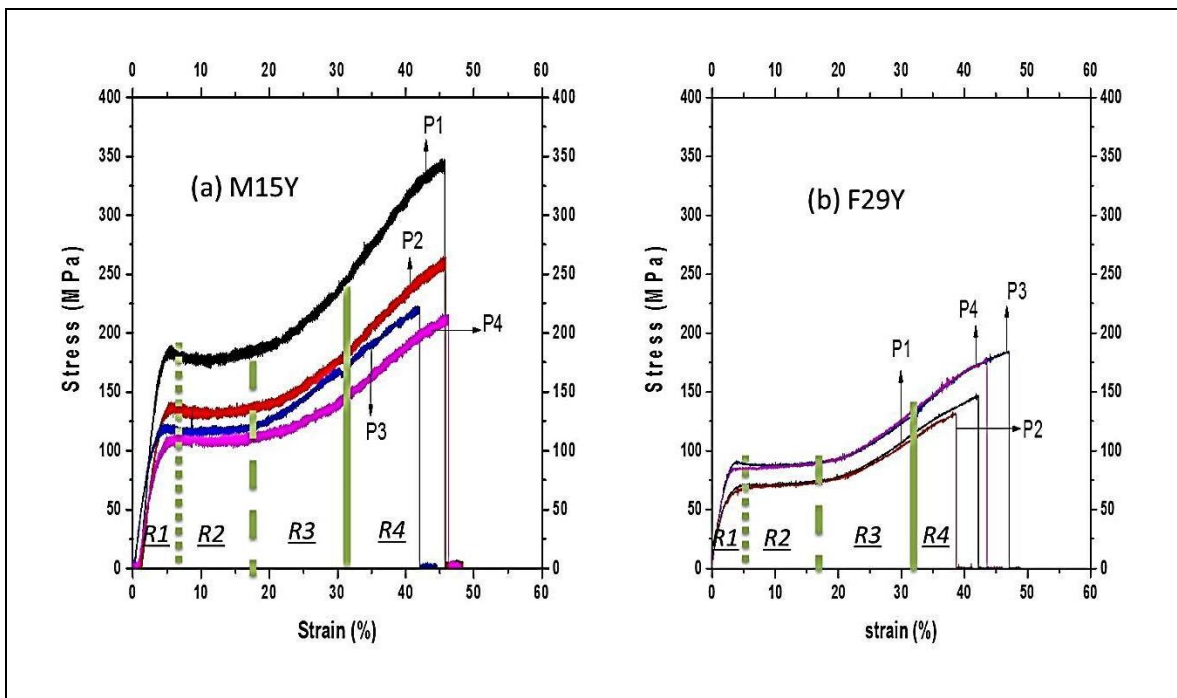
Figure 3.13: Typical stress-strain plots obtained from single fibre tensile testing of hair collected from four positions of the scalp. (a) Male 15 years (b) Female 29 years. In both cases, R1 is the hookean or pre-yield region, R2 indicates the start and end of the yield regions (plateau of constant stress) and R3 &R4 are post yield region-1 & 2. Note that yield doesn't correspond to the onset of plastic deformation.

Representative stress-strain plots are shown in Figure 3.13 with respect to positions P1 to P4 for two samples (Male 15yrs, Female 29 yrs). When subjected to a tensile

load, hair from all four positions showed elastic behaviour initially and further changed to viscoelastic behaviour, which is similar to other natural protein fibres like wool [Feughelman 2000, Hearle 2000]. From the tests it was found that hair is very elastic and can be stretched up to 50 % of the initial length. In most of the samples, hair curling is observed immediately after the fracture at one end of the fractured sample as shown in Figure 3.3. From the plots obtained, it can be said that stress-strain curves show four characteristic regions (R1 - R4) as shown in Figure 3.13 and are described below.

R1 - The first region is a Hookean region from 0 to ~3 % strain.

R2 - The second region is a plateau of constant stress (yield region) in which strain increases significantly without much increase in stress (between 4 - ~18% strain).

R3 - The third region is a post-yield region 1 in which strain increases with stress till about 33 % strain. In this region post-yield modulus (slope) increases gradually indicating the alignment of β-sheets embedded in amorphous matrix.

R4 - The fourth region also known as post-yield region 2 in which yielding and an ultimate failure occurs (between ~33 - 45 % strain).

Structure-property correlation

A detailed study of stress-strain plots has been carried out including slope change in post-yield region and corresponding structural analysis using SEM. Stress-strain plot of a human hair is normally split into three regions [Samanta et al. 2016, Kamath et al. 1982, Antunes et al. 2016] but for a comprehensive analysis of the curve, the plots are split into four regions (Figure 3.13) which includes post-yield features of modulus change and second yield [Feughelman 1982, Feughelman 2000, Miserez et al. 2009, Kreplak et al. 2004]. From the stress-strain plots (Figure 3.14b) it can be read as: a=elastic region, b=yield point, c=plateau region (constant stress), d=onset of change in post-yield modulus, e= change in post-yield modulus, f= second yield region due to yielding of the amorphous matrix (change in slope), g= failure point. Elastic region corresponds to the linear response region and slope of the linear region is the modulus of elasticity. The yield point is the limit of linearity, but not the onset of plastic deformation. Due to the entropy dominant response of amorphous matrix, strain

increases without any increase in stress and this plateau of constant stress continues until 10 - 15 % strain (1/3 of the entire fibre strain) and higher values of plateau strain correspond to a softer amorphous network. Since α to β keratin transition requires some stress change, the onset of transition with post-yield modulus change occurs post plateau of constant stress region. As long as the α to β transition continues and is followed by strain induced alignment of the β sheets, the modulus continuously increases until ~33 % strain and exhibits maximum slope in the range of 500 - 700 MPa. As soon as the slope i.e. modulus in the post-yield region starts to decrease (Figure 3.14), amorphous matrix starts to yield and continues until fracture. Though 290 - 420 MPa of post-yield modulus is reported for wool fibres [Feughelman 2000] the reduction of post-yield modulus (i.e., change of slope) at around 33 % strain is not discussed earlier. So a detailed structure-property correlation is provided immediately below considering cortical cell as a composite comprising of crystalline and amorphous domains [Feughelman 2000].The elastic modulus or the position of linearity qualitatively provides information regarding the packing, overall rigidity and stability of α-keratin crystals which are embedded in the crosslinked amorphous keratin matrix. The crystalline domain stability arises from the degree of elastic response due to its intra and inter packing and the stability of the interfaces between the crystalline and amorphous matrix. Analogously, in terms of thermal behaviour, the stability of crystalline α-keratin corresponds to the melting point temperature as observed in our previous work [Mishra et al. 2016].

1. The yield stress qualitatively provides information regarding the percentage of crystallinity. In combination with vibrational modes, the effective elastic stress transfer or resistance to yield occurs due to predominantly shear modes within α helix molecule which are elastic in nature. It has been reported in the literature [Miserez et al. 2009] that the onset of yield corresponds to significant conformational rearrangement wherein the helix molecules begin to unravel to form random coils. Hence the resistance to such conformational changes would relate to the amount and stability of the helices that form the crystalline domains indicating that the yield stress value corresponds to the percentage of crystallinity.

2. The percentage of strain in the plateau stress position qualitatively provides information regarding the degree and kinetics of conformational events. The conformational events correspond to predominantly segmental motions in the

amorphous network, which are entropic in nature [Hearle 2000, Miserez et al. 2009, Kreplak et al. 2004]. The higher the plateau stress position, it is an indication of higher degree of conformational motions in the soft and elastomeric amorphous matrix. However, if the plateau stress position existed beyond a strain value of 15 – 20 % based on relative humidity, it would correspond to additional contributions from α-helical keratin microfibrils being unravelled to form random coils [Miserez et al. 2009, Kreplak et al. 2004].

3. The incremental change in slope of the post-yield position qualitatively provides information regarding the degree of the continued unravelling of the α-keratin micro fibril followed by repacking of the random coils to form β sheets until which the random coils disappear completely to form recrystallized β sheet structure [Miserez et al. 2009, Kreplak et al. 2004]. Further, there is also an additional contribution arising from the strain induced alignment of the formed β sheets and its stability in the amorphous matrix. Correspondingly, this results in increased resistance to deformation until the β sheet macrofibril bundles are pulled out from the supporting amorphous keratin matrix of variable mechanical integrity. In case a highly networked, elastic and mechanically integrated amorphous matrix is present, it is primarily due to the formation of disulfide linkages as a result of cysteine-cysteine covalent interaction [Robbins 2002]. The second yield point (f) as shown in the stress-strain plot (Figure 3.14b) is an indication of the yield occurring in the amorphous matrix until some bonds are permanently broken. The failure point corresponds to the ultimate failure of the material at higher strain wherein the bonds of the amorphous matrix are permanently broken along with severe straining and pull-out of the crystalline β sheets.

4. The overall work of elongation of the material, qualitatively provides information in regards to all components of the hair sample and that includes crystalline α-keratin, amorphous keratin matrix, α to β transition phase and β keratin.

For specific structure-property description, the stress-strain curves of M15 and F29 are taken as representative plots (Figure 3.13) and the discussion is as follows. For M15, from the curve at the P1 position, it can be seen that the elastic modulus and yield stress values are the highest and this is an indication that the α keratin is relatively stable and is embedded well in the amorphous matrix. In addition, the curve

also indicates that the percentage of crystallinity is highest among the tested samples. For P1, the percentage of strain in the plateau stress region is the lowest and this is followed by a significant increase in the post-yield modulus (max. slope 800 MPa at around 32 % strain). This indicates that the degree of entropic response of the amorphous network is low and possibly the amorphous network is a hard elastomer. Post-yield, the increased resistance to deformation as observed by the post-yield modulus change for all positions (P1 - P4) is due to the unravelling of the α keratin to random coil followed by repacking to β sheet structure and the strain induced orientation of the same. Further, an additional contribution to resistance due to effective stress transfer between the stable α and β fibrils and the amorphous keratin matrix is possible. In the case of P4 position, the curve indicates lower stability of α keratin, a lower degree of crystallinity, a relatively soft amorphous network resulting in decreased post-yield properties (max. slope is 500 MPa at around 32 % strain). In contrast to M15, for F29 the curves for all four regions exhibit a very low stability of α keratin, a low degree of crystallinity, a very soft amorphous network resulting in highly reduced post-yield properties (max. slope <500 MPa at around 32 % strain for all four regions).
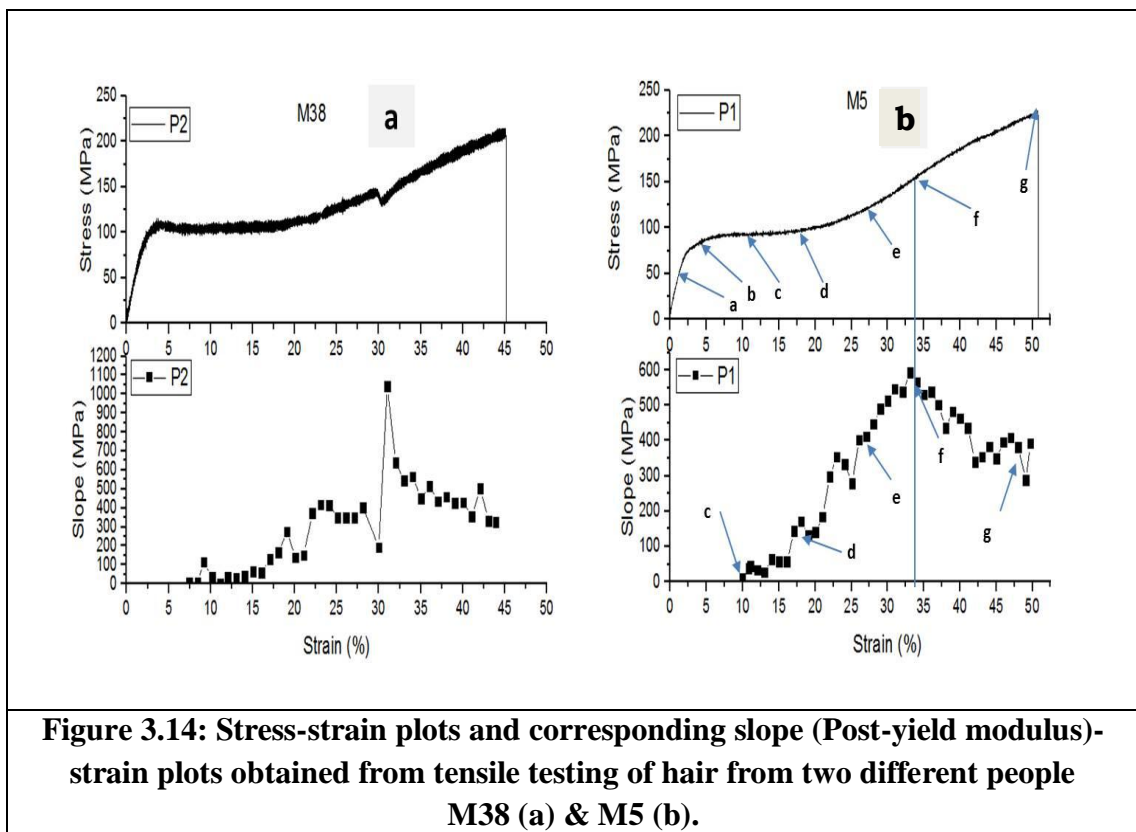
Figure 3.14: Stress-strain plots and corresponding slope (Post-yield modulus)-strain plots obtained from tensile testing of hair from two different people M38 (a) & M5 (b).

From the Figure 3.13, it is found that M15 hair has higher yield stress, maximum stress and work of elongation at the P1 position compared to P2, P3 and P4 positions (Figure 3.13a). As shown in Figure 3.13b, F29 hair yield stress for positions P3 and P4 is higher compared P1 and P2 positions and the maximum stress is 184 MPa for P3 position which is also higher compared to other three positions. The maximum strains are in the range of 39 - 47 % for both hair samples and for all positions. The individual stress-strain plots after stretching to different regions like pre-yield, yield, post-yield - 1 and post-yield - 2 (fracture regions) are shown respectively in Figure 3.15 to know the different stages of fibre deformation.

Figure 3.15: Typical stress-strain plots obtained from single fibre tensile testing of hair after stretching to different strain values.
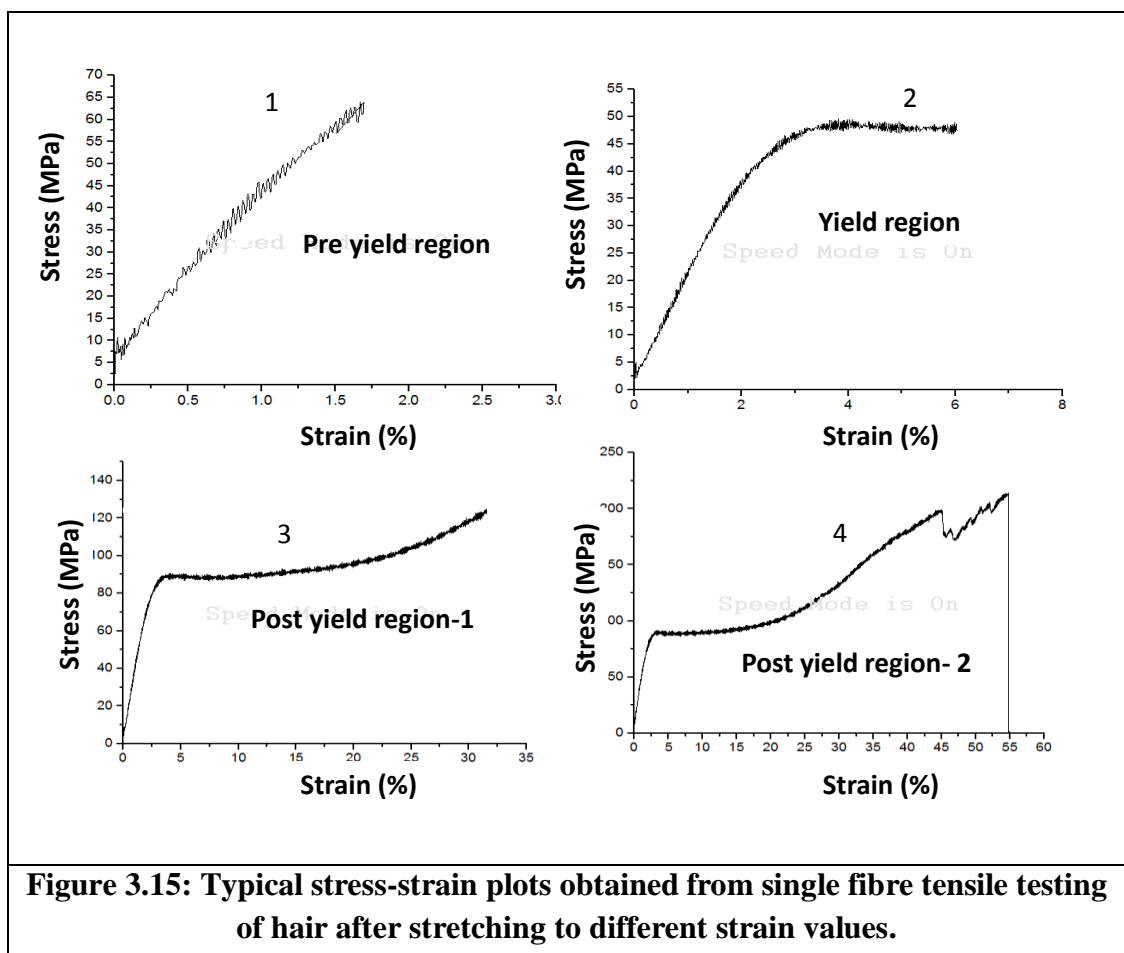
Stress-strain plots of flax, hair (natural fibres) and viscose (synthetic fibre) are shown in Figure 3.16. Flax fibres are found to have high tensile stress than viscose and hair. Hair is not a brittle fibre and its stress is one-third of the flax fibre but its strain to failure is 10 times the value of flax fibre. The reduction in hair stress and stiffness could be due to the fact that keratin microfibrils in hair are initially arranged in α helix

pattern and it converts into β pleated sheets while stretching. But in the flax fibre, cellulose microfibrils are covalently bonded with lignin (amorphous) matrix and bonds will break while tensile stretching. Arrangement of cellulose microfibrils with in flax fibre is very straight unlike helical arrangement of keratin microfibrils.
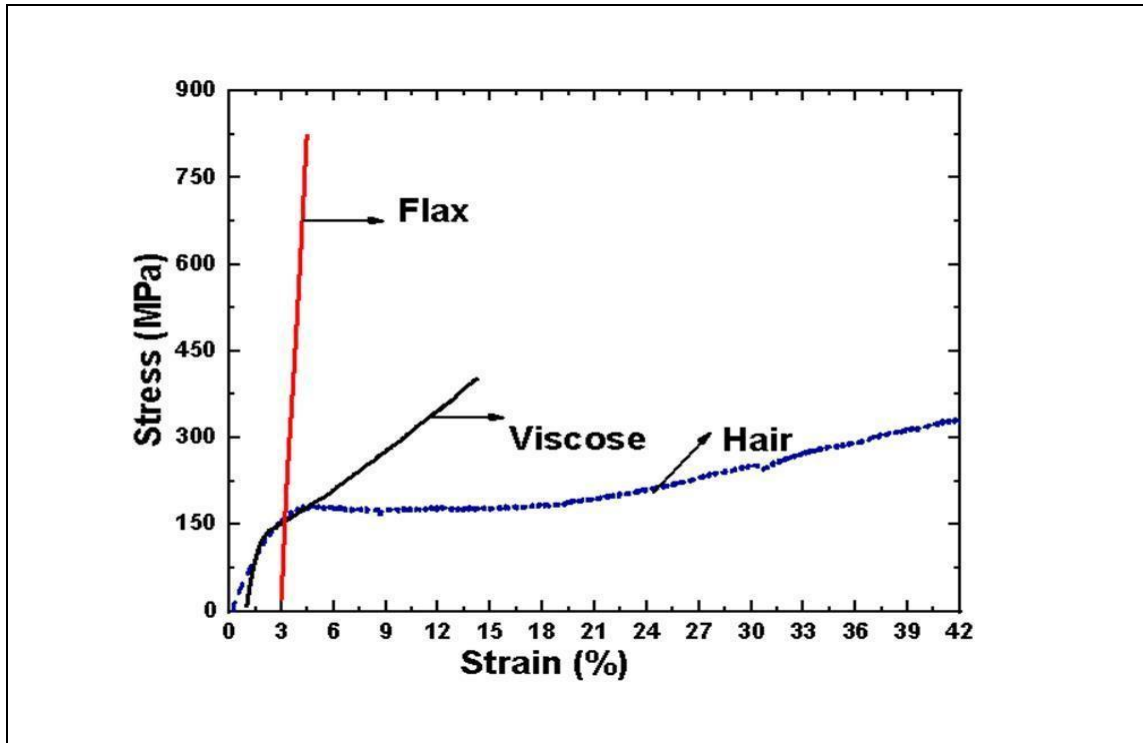
Figure 3.16: Typical stress-strain plots obtained from single fibre tensile testing of flax, viscose and hair fibres. Here flax is natural cellulose and viscose is a man-made cellulose fibre used widely in textiles. Strains are offset by 1% and 3% for viscose and flax respectively.

The maximum stress of individual fibres was recorded and probability of survival is plotted against this maximum strength in Figure 3.17 to find the weibull modulus β or weibull shape factor. β was found to be low for natural fibres (2.1 for flax and 3.4 for hair) compared to synthetic fibre (7 for viscose) as shown in Figure 3.17 [Revol et al. 2016, Chawla 1998]. For viscose fibres after removing matrix (less number of interfaces) only cellulose microfibrils are dissolved and rearranged into new cellulose microfibrils. It is clear that lower values of weibull modulus correspond to broader distribution. Since natural fibres have nano structural defects due to the existence of more interfaces (microfibrils-matrix) in the composite structure of their cells, their stress values gave a broader distribution. It is clear that wider distribution of tensile

data mostly results in lower values of weibull modulus which can be seen in Figure 3.17, where flax fibres and hair are compared.
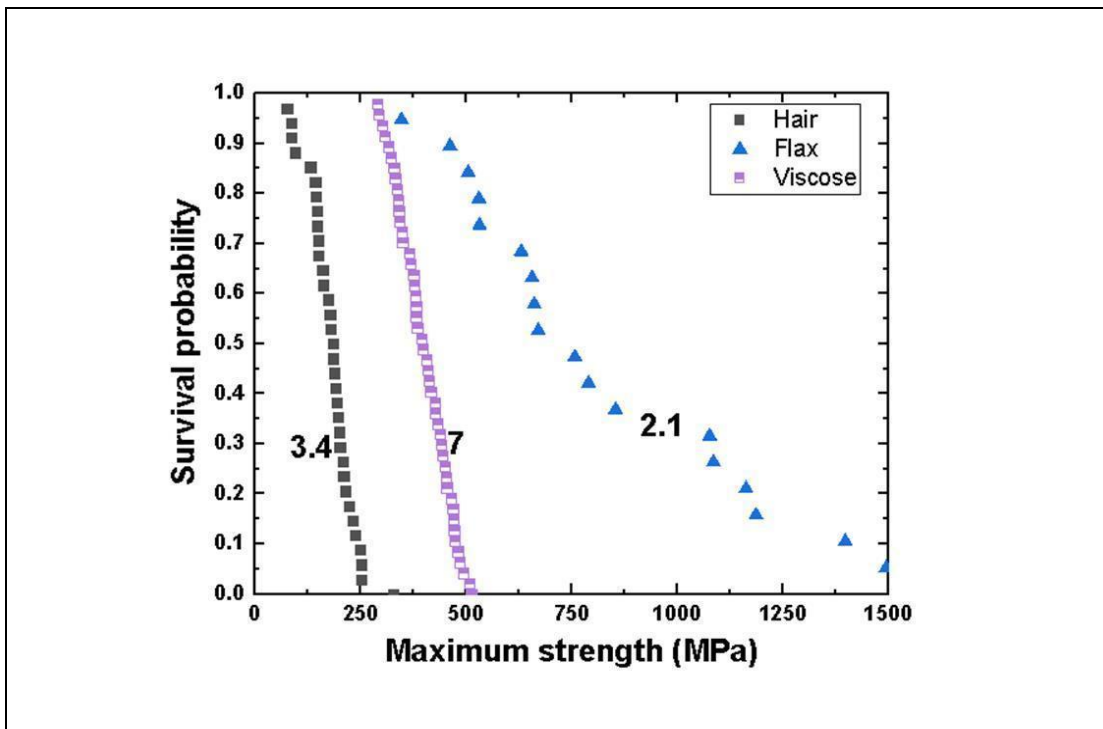
Figure 3.17: Weibull distribution of single fibre tensile stress values. Note the lowest values of Weibull modulus (β) for natural fibres such as flax (β=2.1) and hair (β=3.4) compared to synthetic fibre such as viscose (β=7). A lower value of β indicates broader distribution of stress values.

The tensile properties of 13 donors (elastic modulus, yield stress, yield strain, maximum stress and maximum strain) are shown in Table 3.1 and Figure 3.18. Here each data point is average of three values and intra-individual variation is provided as standard deviation. All the properties are measured by using origin software after converting load-displacement plots to stress-strain plots. It can be seen that yield stresses are in the range of 82 - 126 MPa and maximum stresses are in the range of 144 - 231 MPa. From Table 3.1, the elastic modulus is found to be in the range of 3.1 - 6.0 GPa. Yield strain of the hair fibres is found to be between 2.6 - 4.4 % (~10 % of the maximum strain) and this could be the reason why hair is not considered as choice of material in technical textiles or it may considered as a composite reinforcement because specific properties like E/ρ or σ/y may be high.

3.3.3. Tensile properties of hair fibres (position P3) with respect to age and gender

Gender (Age,Yrs)	Elastic Modulus [GPa]	Yield Stress [MPa]	Yield Strain [%]	Maximum Stress [MPa]	Maximum Strain [%]
M3	4.2±1.2	110±24	3.5±0.2	184±6	41±2
F6	4.4±0.5	98±6	3.6±0.3	187±19	42±1
F14	3.1±0.3	82±12	3.3±0.1	144±27	43±12
M15	4.8±1.6	125±39	3.7±0.2	231±86	42±5
M25	5.5±1.5	116±44	3.4±0.4	207±33	37±4
F26	4.5±0.6	95±18	2.6±0.3	201±15	41±1
F35	3.3±0.3	96±18	4.4±1.4	177±23	41±13
M38	3.8±1.3	101±25	4.0±0.7	163±38	49±8
M41	5.5±0.6	126±1	3.0±0.3	204±38	32±5
M52	5.2±1.4	114±31	3.1±0.2	200±64	37±1
F55	4.4±0.4	101±9	3.1±0.5	173±48	35±6
F64	6.0±0.3	117±29	3.3±0.2	194±38	44±7
M65	5.1±0.5	109±9	2.8±0.2	161±24	32±3

Table 3.1: Tensile properties of single hair fibres (position P3) of with respect to age and gender.

Figure 3.18: Maximum strain (top) and yield strain (bottom) as a function of age and gender for hair fibres (position P3). M3 indicates male 3 years old.
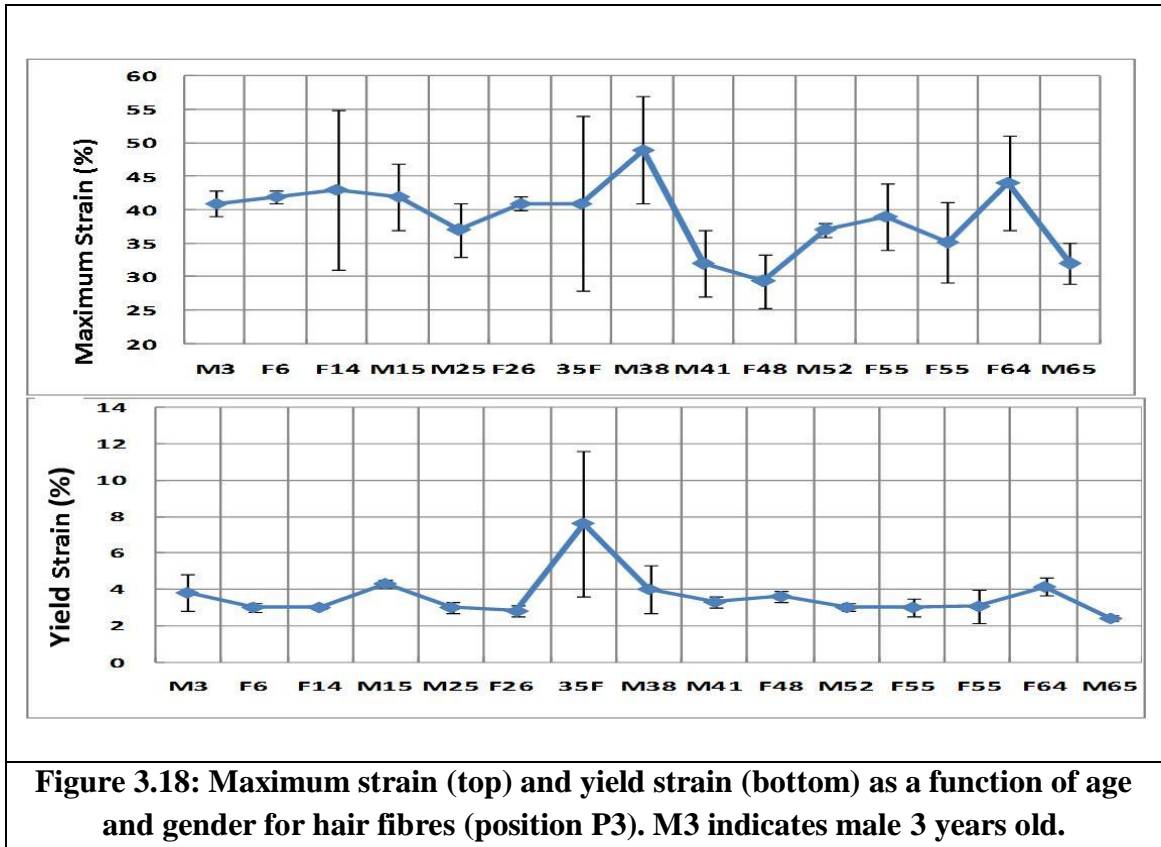
The yield stress and maximum stress shown in Table 3.1 shows no specific trend with donor's age and gender. Hair from F14 donor is found to have the lowest modulus (48 % lower than F64 donor), lowest yield stress (35 % lower than M41 donor), lowest maximum stress (38 % lower than M15 donor) and the highest elongation (34 % higher than M41 donor), indicating the weak structure of the hair composite.
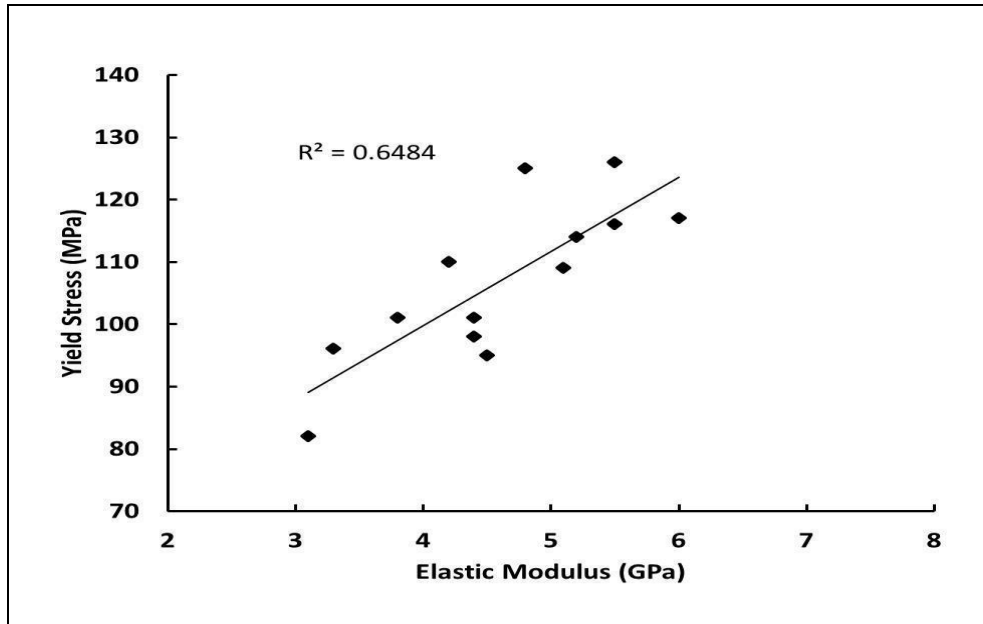
Figure 3.19: Comparison between yield stress and elastic modulus obtained from single fibre (position P3) tensile tests.

Since the fibre properties such as, elastic modulus and yield stress (onset of constancy of stress and the end of linearity) are considered to be within the elastic limits, a correlation between these properties is studied and shown in Figure 3.19. It can be seen that a positive trend with a moderate R^2 value of 0.7 is determined between yield stress (force at yield point /area) and elastic modulus (slope of the stress-strain curve before the yield point). It should be noted that, yield stress value primarily corresponds to the percentage of crystallinity and elastic modulus corresponds to the packing, overall rigidity and stability and quality of α-keratin crystals which are embedded in the amorphous keratin matrix. A highly crystalline material will exhibit a strong correlation with a higher regression value as observed for highly crystalline polymers In contrast, the composite nature of the hair fibres with a low percentage of crystallinity is expected to show a weaker correlation wherein the yield stress is dominated by the percentage of crystalline fractions and the elastic modulus is determined by the overall packing of the composite structure comprising of both crystalline and amorphous fractions.

Figure 3.20: Tensile properties (maximum stress, yield stress and modulus from top to bottom respectively) as a function of age for all hair fibres of position P3.
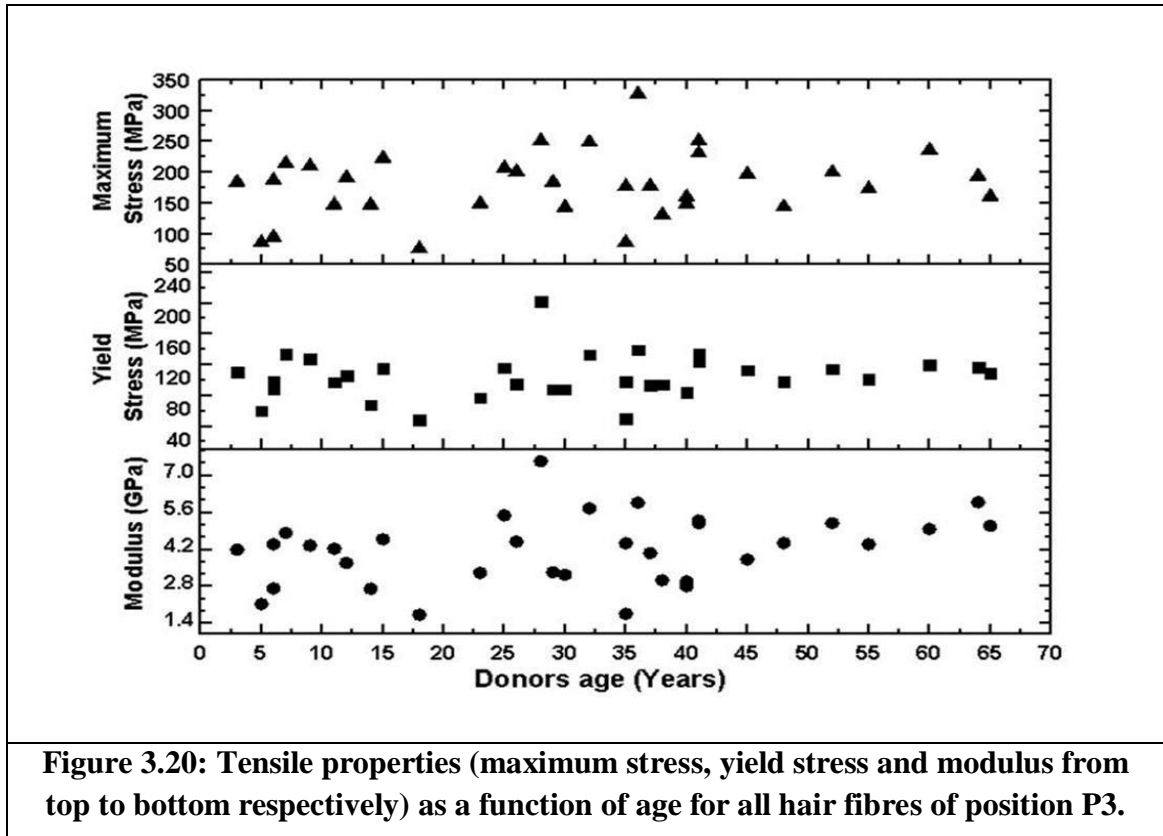
Tensile properties of single hair fibres of all donors with respect to age are shown in Figure 3.20 for position P3. In which modulus, yield stress and maximum stress are in the range of 1.73 - 7.55 GPa, 48 - 202 MPa and 76 - 327 MPa respectively. Similarly tensile properties of hair fibres of all male and female donors are shown in Figures 3.21 - 3.22 respectively. It is observed that modulus, yield stress and maximum stress are in the range of 1.77 - 5.97 GPa, 50 - 139 MPa and 86 - 327 MPa respectively for all male donors. In the case of all female donors modulus, yield stress and maximum stress are in the range of 1.73 - 7.55 GPa, 48 - 202 MPa and 76 - 251 MPa respectively. No significant trend in tensile properties can be seen when data is compared with respect to age and gender as shown in Figures 3.20 - 3.22. But the maximum stress, yield stress and modulus varies with age and gender but no trend was observed.
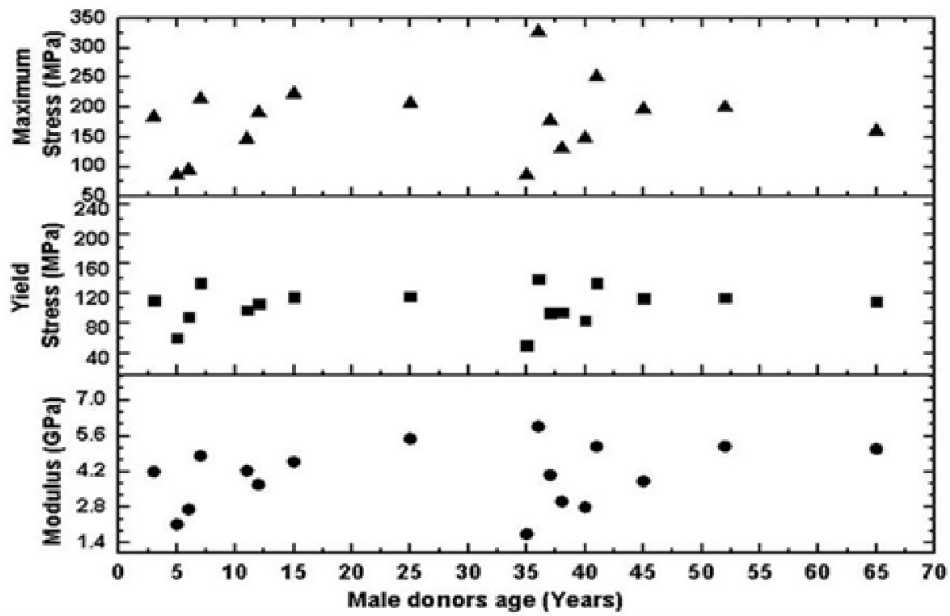
Figure 3.21: Tensile properties (Maximum stress, yield stress and Modulus from top to bottom respectively) as a function of male donor age for all hair fibres of position P3.
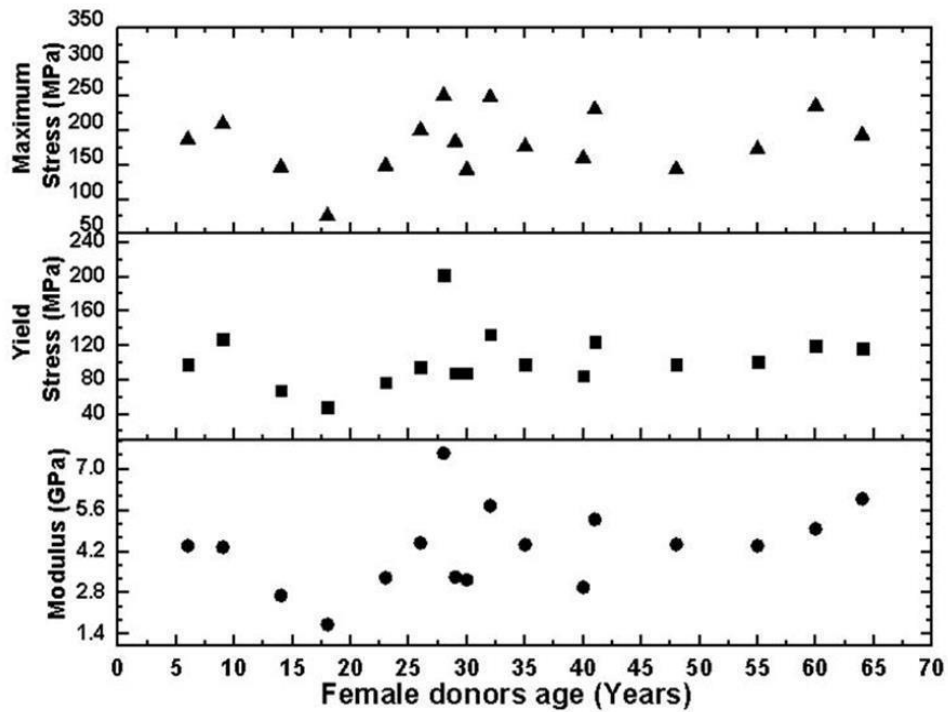
Figure 3.22: Tensile properties (Maximum stress, yield stress and Modulus from top to bottom respectively) as a function of female donor age for all hair fibres of position P3.

3.3.4. Tensile properties of hair fibres with respect to the scalp positions P1 - P4

Table 3.2: Tensile properties of single hair fibres of position 1 (P1)

Gender	Age (yrs)	Yield Stress (MPa)	Yield Strain (%)	Modulus-Hookean region (MPa)	Maximum Stress (MPa)	Maximum Strain (%)	Work of elongation (MJ/m^3)	Diameter (μm)
M	5	75±25	2.3±0.8	3435±818	228 ±17	51±2.3	67±12	72 ±5
M	6	136±21	3.8±0.4	3580±647	306±44	50±2.6	94±17	79 ±12
M	7	99±28	3.2±0.3	3635±899	192±30	41±2.8	50±7	73±4
M	11	118±18	3.7±0.2	4453±211	200±39	40±5.5	54±14	101 ±8
F	14	104±22	3.2±0.6	4253±619	179±31	33±1.9	41±7	85 ±9
M	15	178±16	4.5±0.8	6701±1070	348±24	46±10.6	99±27	73 ±7
F	23	62±29	2.3±0.5	2729±1129	165±15	42±6.1	45±7	76 ±12
F	29	66±03	3.2±1.7	2737±179	147±39	42±3.2	38±4	87 ±13
F	32	143±23	3.6±0.9	6195±1152	245±59	39±7.4	64±19	83 ±3
F	35	84±16	3.0±0.4	3913±378	189±18	54±5.1	65±6	80 ±7
M	36	98±35	3.1±0.8	4194±1633	194±52	39±1.5	47±18	65 ±2
M	37	85±03	4.4±0.9	2986±339	194±06	50±3.3	59±5	78 ±6
M	38	102±13	4.4±0.4	4363±044	174±62	45±4.1	53±12	82 ±22
M	41	79±34	2.7±1.3	3780±1131	158±39	37±1.5	39±15	74 ±13
F	41	191±10	3.7±0.3	8223±776	284±60	43±6.6	91±20	104 ±21
Avg	25	108	3.4	4345	214	43	60	81

Table 3.3: Tensile properties of single hair fibres of position 2 (P2)

Gender	Age (yrs)	Yield Stress (MPa)	Yield Strain (%)	Modulus-Hookean region (MPa)	Maximum Stress (MPa)	Maximum Strain(%)	Work of elongation (MJ/m^3)	Diameter (µm)
M	5	87± 114	1.4±0.2	6777±609	271±89	26±1.2	43±21	62±6
M	6	94±24	3.0±0.1	3299± 1117	215±43	51±1.7	68±12	77±8
M	7	83± 32	1.8±0.1	5411± 2149	196±74	26±0.6	31±12	80±5
M	11	71±19	2.8±1.3	3212±1003	149±17	37±3.7	36±05	82±14
F	14	100±14	4.0±0.8	4209±510	209±45	44±2.6	56±09	85±11
M	15	131±34	4.8±0.9	5317±218	265±68	46±2.8	73±17	77±8
F	23	87±71	3.2±0.7	3594±410	179±76	42±1.8	47±24	72±9
F	29	60±03	2.7±1.7	2770±095	132±1	39±0.3	32±03	86±13
F	32	85±26	3.3±19.7	3455±1168	168±37	45±3.7	48±11	90±10
F	35	104±13	3.1±0.8	4386±585	229±16	50±6.9	71±10	72±4
M	36	82±18	3.2±0.2	3461±693	187±65	49±2.9	55±15	86±8
M	37	92±48	3.3±0.1	3786±2380	222±79	50±1.9	68±27	89±9
M	38	106±44	3.3±0.9	4437±2896	214±90	45±3.2	59±32	72±8
M	41	145±23	3.4±0.5	6283±384	255±2	35±0.7	59±08	72±7
F	41	121±15	3.4±0.4	5095±571	230±21	48±1.7	71±08	92±7
Avg	25	97	3.1	4366	208	42	54	79

Table 3.4: Tensile properties of single hair fibres of position 3 (P3)

Gender	Age (yrs)	Yield Stress (MPa)	Yield Strain (%)	Modulus-Hookean region (MPa)	Maximum Stress (MPa)	Maximum Strain(%)	Work of elongation (MJ/m^3)	Diameter (µm)
M	5	89±3	2.8± 0	3696± 510	223±11	46±0.7	62±1	60±10
M	6	116±19	2.7±0.1	5289±558	268±1	48±2.7	78±10	72±10
M	7	65±6	1.7±0.3	4334±909	241±31	23±0	34±3	74±01
M	11	97±28	3.5±0.6	4230±887	147±64	36±8.2	40± 28	92±05
F	14	68±13	3.2±0.2	2716±1689	147±25	52±12.2	50±16	90±15
M	15	115±44	3.9±0.1	4591±1009	223±88	42±5.3	60±24	88±15
F	23	77±25	2.8±0.3	3318±1185	149±61	43±1.8	41±13	68±04
F	29	88±10	3.2±0.1	3340±149	184±19	47±1.9	54±7	88±08
F	32	133±18	4.7±0.9	5763±1567	249±22	43±2.3	68±7	82±13
F	35	98±13	3.2±0.6	4438±553	177±21	38±8.4	46±13	75±02
M	36	139±22	3±0.4	5977±711	327±41	46±12.5	96±20	71±13
M	37	93±11	3.1±0.4	4066±311	178±26	40±4.9	45±7	79±08
M	38	93±28	4.1±0.8	3142±1293	182±41	52±9.1	64±20	72±07
M	41	134±16	4.3±0.5	5194±162	251±37	37±9	60±23	66±03
F	41	124±16	3.6±0.7	5303±136	231±56	60±7.9	98±26	96±05
Avg	25	102	3.3	4360	212	43	60	78

Table 3.5: Tensile properties of single hair fibres of position 4 (P4)

Gender	Age (yrs)	Yield Stress (MPa)	Yield Strain (%)	Modulus-Hookean region (MPa)	Maximum Stress (MPa)	Maximum Strain(%)	Work of elongation (MJ/m^3)	Diameter (µm)
M	5	74±13	1.5±0.2	5121±757	233±51	27±0.9	37±7	71±12
M	6	80±17	3.1±0.5	2849±1400	215±47	50±2.3	66±17	75±08
M	7	115±37	1.8±0.1	6774±2803	260±46	27±5	42±10	72±04
M	11	98±25	3.6±1.3	3861±694	148±40	35±8.1	38±21	91±09
F	14	142± 61	2.8±1.8	6708±1581	249±97	36±12.8	62±21	73±08
M	15	104±9	4.9±0.2	4128±470	216±15	46±0.8	61±4	77±16
F	23	86±15	2.7±0.7	4040±518	164±36	43±10.2	48±19	83±07
F	29	83±6	3.3±0.1	3355±180	177±9	44±0.7	48±3	74±08
F	32	121±15	3.7±0.2	5500±688	192±18	33±2.5	43±2	80±12
F	35	93±17	4.8±1.1	3508±1339	170±31	53±9.5	64±13	70±08
M	36	86±18	3.2±0.2	3550±633	172±77	42±7.8	46±29	77±09
M	37	87±46	3.1±0.4	3576±1773	191±49	49±0.5	58±24	85±07
M	38	131±35	3.5±0.7	6341±1764	245±46	47±12.1	76±36	63±11
M	41	90±12	4.3±0.6	3138±661	188±36	50±1.1	58±11	74±07
F	41	99±6	3.3±0.5	4107±304	194±22	56±6.6	74±10	74±09
Avg	25	99.3	3.3	4437	201	42	55	76

The tensile properties of all 15 samples (yield stress, yield strain, modulus in Hookean region, maximum stress, maximum strain and work of elongation) with respect to positions P1 to P4 are shown in Tables 3.2 - 3.5 respectively. The yield stress of hair from P1 position revealed slightly higher mean value compared to the hair from P2, P3 and P4 (P1 108 MPa > P3 102 > P4 99 > P2 97 MPa) positions. The trend slightly differs when mean maximum stress values are considered between positions (P1 214 MPa > P3 212 > P2 208 > P4 201 MPa). When the work of elongation values are considered, both P1 and P3 hair revealed slightly higher mean values in comparison to P2 and P4 hair samples. The elastic modulus of the pre-yield region revealed almost similar mean values (~4.35 GPa) for hair from P1 - P4 positions.
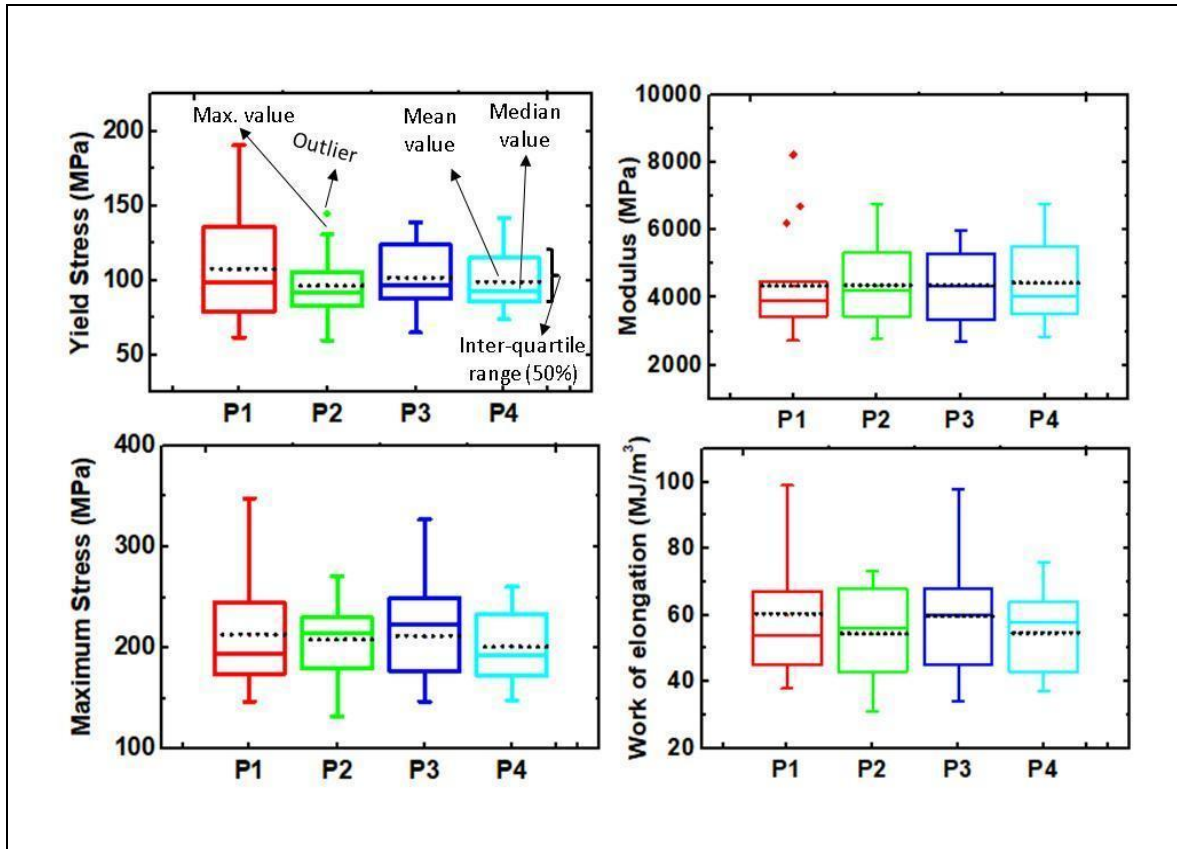
Figure 3.23: Box and whisker plot of tensile properties of 15 donors. Data is shown in Tables 3.2-3.5 and here it is shown with respect to the position on the scalp (P1-P4). Each plot represents 45 values (15 people with 3 replicates).

To compare the yield stress, maximum stress, modulus and work of elongation with respect to the scalp positions, box and whisker plots are constructed (Figure 3.23). The reason for choosing these four properties is that they represent the four regions of the stress-strain curves previously described. As shown in Figure 3.23, box and whisker plots shows no significant differences between positions when mean yield stress values are considered, though hair from P2 position revealed lowest yield stress. Mean values of the modulus are almost same for P1 - P4 positions, but the value of the P1 position is dominated by three samples (F41:8223; M15:6701; F32:6195 MPa). A similar trend is observed in the case of maximum stress and work of elongation. Though significant variations in overall range and the inter-quartile range are seen but the less difference in the mean values of the tensile properties are seen when compared with respect to four scalp positions, which leads to data optimization using different statistical methods as discussed below.

3.3.5. Statistical analysis of tensile properties of single hair fibres using ANOVA, Relative rating and Grey Relational Analysis (GRA) methods.

Table 3.6: ANOVA for Yield stress (YS), Modulus (M), Maximum stress (MS) and Work of elongation (WE) obtained from Single hair fibre tensile testing (P < 0.05 is significant).

Source of variation	Sum of squares	Degree of freedom	Variance	Test F (F factor)	P alue (level of significance)	Fα for P value of 5%	% of Contribution
YS							
Gender	692.7	1	692.7	0.91	0.352	4.45	4.63
Age	479.7	2	239.9	0.32	0.733	3.59	3.20
Position	890	3	296.7	0.39	0.761	3.2	5.95
Error	12885.5	17	758				86.20
Total	14948	23					100
M							
Gender	845626	1	845626	0.64	0.434	4.45	3.40
Age	702279	2	351140	0.27	0.769	3.59	2.82
Position	884948	3	294983	0.22	0.879	3.2	3.56
Error	22411455	17	1318321				90.20
Total	24844308	23					100
MS							
Gender	9315.5	1	9315.5	**5.11**	**0.037**	**4.45**	**22.22**
Age	122.3	2	61.13	0.03	0.967	3.59	0.29
Position	1448.6	3	482.87	0.26	0.85	3.2	3.45
Error	31018.8	17	1824.63				74.02
Total	41905.1	23					100
WE							
Gender	303.4	1	303.41	1.59	0.224	4.45	7.37
Age	448.7	2	224.33	1.18	0.331	3.59	10.90
Position	128.4	3	42.81	0.23	0.878	3.2	3.12
Error	3233.9	17	190.23				78.59
Total	4114.4	23					100

The results of the hair tensile properties with respect to position are presented in Tables 3.2 - 3.5. Three different statistical methods were used to conclude the influence of position on hair tensile properties. The first method is the commonly used statistical method ANOVA (Analysis of Variance) is used to evaluate the influence of age, gender and position on tensile properties of single hair fibres. One way ANOVA with significance level (P - value < 0.05) of 5% is used to determine the effect of position, gender, and age on yield stress, modulus, maximum stress and work of elongation as shown in Table 3.6. From one way ANOVA analysis, P value resulted 0.76, 0.87, 0.85 and 0.87 when scalp position is considered as source of variation for yield stress, modulus, maximum stress and work of elongation respectively. P value of 0.037 is obtained for maximum stress when gender is considered as source of

variation, which indicates maximum stress varies with gender, but without which gender. The other two statistical methods are Relative rating and Grey Relational Analysis (GRA). In relative rating, it is based on rating the four properties for one position individually (for 15 people) followed by cumulative rating, which involves summation of individual ratings of four properties. Finally "sum of the rating" is obtained for each position by summation of cumulative ratings (details for position 1 is described in Table 3.7 and for other positions P2 - P4 are in Tables 3.8 - 3.10). In individual rating, a scale of 1 - 5 was used with 1 and 5 being the lowest and highest set of values respectively.

Table 3.7: Relative rating method applied for the four tensile properties. Detailed procedure is given for position 1 (P1).

Gender	Age (yrs)	Yield Stress (MPa)	Yield Stress Rating (1-5)	Modulus (MPa)	Modulus Rating (1-5)	Maximum Stress (MPa)	Maximum Stress Rating (1-5)	Work of elongation (MJ/m³)	Work of elongation Rating (1-5)	Cumulative rating for Yield Stress, Modulus, Max.Stress & Work of elongation
M	5	75	1	3435	1	228	3	67	3	8
M	6	136	3	3580	1	306	5	94	5	14
M	7	99	2	3635	1	192	2	50	2	7
M	11	118	3	4453	2	200	2	54	2	9
F	14	104	2	4253	2	179	2	41	1	7
M	15	178	5	6701	4	348	5	99	5	19
F	23	62	1	2729	1	165	1	45	2	5
F	29	66	1	2737	1	147	1	38	1	4
F	32	143	4	6195	4	245	3	64	3	14
F	35	84	1	3913	2	189	2	65	3	8
M	36	98	2	4194	2	194	2	47	2	8
M	37	85	1	2986	1	194	2	59	3	7
M	38	102	2	4363	2	174	1	53	2	7
M	41	79	1	3780	1	158	1	39	1	4
F	41	191	5	8223	5	284	4	91	5	19
Max		191	34 (Sum)	8223	30 (Sum)	348	36 (Sum)	99	40 (Sum)	140 (Sum of the rating)
Min		62		2729		147		38		

Yiled stress	Rating	Modulus	Rating	Maximum stress	Rating	Work of elongation	Rating
60.0- 86.2	1	2716- 3817	1	132.0- 175.2	1	31.0- 44.6	1
86.2- 112.4	2	3817- 4919	2	175.2- 218.4	2	44.6- 58.2	2
112.4- 138.6	3	4919- 6020	3	218.4- 261.6	3	58.2- 71.8	3
138.6- 164.8	4	6020- 7122	4	261.6- 304.8	4	71.8- 85.4	4
164.8- 191.0	5	7122- 8223	5	304.8- 348.0	5	85.4- 99.0	5

NOTE: STEP 1= Note the maximum and minimum values for each property and for each position.

STE 2 = Divide the difference between maximum and minimum value by 5

STEP 3= Start the rating 1 for lower set of values and end the rating with 5 for higher set of values as shown in below table.

STEP 4 = Use the sum of the ratings (Column O) for comparison between positions

Table 3.8: Relative rating method applied for the four tensile properties. Detailed procedure is given for position 2 (P2).

Gender	Age (yrs)	Yield Stress (MPa)	Yield Stress Rating (1-5)	Modulus (MPa)	Modulus Rating (1-5)	Maximum stress (MPa)	Maximum stress Rating (1-5)	Work of elongation (MJ/m^3)	Work of elongation rating (1-5)	Sum of ratings of Yield stress, Modulus, Max.Stress & Work of elongation (4-20)
M	5	87	2	6777	4	271	4	43	1	11
M	6	94	2	3299	1	215	2	68	3	8
M	7	83	1	5411	3	196	2	31	1	7
M	11	71	1	3212	1	149	1	36	1	4
F	14	100	2	4209	2	209	2	56	2	8
M	15	131	3	5317	3	265	4	73	4	14
F	23	87	2	3594	1	179	2	47	2	7
F	29	60	1	2770	1	132	1	32	1	4
F	32	85	1	3455	1	168	1	48	2	5
F	35	104	2	4386	2	229	3	71	4	11
M	36	82	1	3461	1	187	2	55	2	6
M	37	92	2	3786	1	222	3	68	3	9
M	38	106	2	4437	2	214	2	59	3	9
M	41	145	4	6283	4	255	3	59	3	14
F	41	121	3	5095	3	230	3	71	3	12
Max		145	29	6777	30	271	35	73	35	129
Mini		60	(sum)	2770	(sum)	132	(sum)	31	(sum)	Sum of the rating

Table 3.9: Relative rating method applied for the four tensile properties. Detailed procedure is given for position 3 (P3).

Gender	Age (yrs)	Yield Stress (MPa)	Yield Stress Rating (1-5)	Modulus (MPa)	Modulus Rating (1-5)	Maximum Strength (MPa)	Maximum Strength Rating (1-5)	Work of elongation (MJ/m^3)	Work of elongation Rating (1-5)	Sum of ratings of Yield stress, Modulus, Max.Stress & Work of elongation (4-20)
M	5	89	2	3696	1	223	3	62	3	9
M	6	116	3	5289	3	268	4	78	4	14
M	7	65	1	4334	2	241	3	34	1	7
M	11	97	2	4230	2	147	1	40	1	6
F	14	68	1	2716	1	147	1	50	2	5
M	15	115	3	4591	2	223	3	60	3	11
F	23	77	1	3318	1	149	1	41	1	4
F	29	88	2	3340	1	184	2	54	2	7
F	32	133	3	5763	3	249	3	68	3	12
F	35	98	2	4438	2	177	2	46	2	8
M	36	139	4	5977	3	327	5	96	5	17
M	37	93	2	4066	2	178	2	45	2	8
M	38	93	2	3142	1	182	2	64	3	8
M	41	134	3	5194	3	251	3	60	3	12
F	41	124	3	5303	3	231	3	98	5	14
Max		139	34	5977	30	327	38	98	40	142
Min		65	(sum)	2716	(sum)	147	(sum)	34	(sum)	Sum of the rating

Table 3.10: Relative rating method applied for the four tensile properties. Detailed procedure is given for position 4 (P4).

Gender	Age (yrs)	Yield Stress (MPa)	Yield Stress Rating (1-5)	Modulus (MPa)	Modulus Rating (1-5)	Maximum Strength (MPa)	Maximum Strength Rating (1-5)	Work of elongation (MJ/m³)	Work of elongation Rating (1-5)	Sum of ratings of Yield stress, Modulus, Max.Stress & Work of elongation (4-20)
M	5	74	1	5121	3	233	3	37	1	8
M	6	80	1	2849	1	215	2	66	3	7
M	7	115	3	6774	4	260	3	42	1	11
M	11	98	2	3861	2	148	1	38	1	6
F	14	142	4	6708	4	249	3	62	3	14
M	15	104	2	4128	2	216	2	61	3	9
F	23	86	1	4040	2	164	1	48	2	6
F	29	83	1	3355	1	177	2	48	2	6
F	32	121	3	5500	3	192	2	43	1	9
F	35	93	2	3508	1	170	1	64	3	7
M	36	86	1	3550	1	172	1	46	2	5
M	37	87	2	3576	1	191	2	58	3	8
M	38	131	3	6341	4	245	3	76	4	14
M	41	90.1	2	3138	1	188	2	58	3	8
F	41	99	2	4107	2	194	2	74	4	10
Max		142	30	6774	32	260	30	76	36	128
Min		74	(sum)	2849	(sum)	148	(sum)	37	(sum)	16

The Grey Relational Analysis (GRA) described in Tables 3.11 - 3.13 used mainly in solving interrelationships among the multiple responses. As shown in Table 3.11a, gender, age and position are considered as factors (input parameters) with levels of 2, 3 and 4 respectively. Similarly, yield stress, modulus, maximum stress and work of elongation are considered as responses (output parameters). After determining the number of experiments with full factorial method (Table 3.11b), GRA was applied to find the optimum input parameters by measuring the grey relational grade (GRG) for all 24 combinations.

Since this work mainly focuses on finding the optimum parameter that is required to achieve the maximum value in responses, the quality characteristic namely "larger-the-better" is used. Similar to "sum of the rating", GRG is obtained in the GRA method using four step - procedure (Table 3.12 - 3.13). First step to find the S/N ratio for individual property as explained in Table 3.12. Second step is normalization of the S/N ratio data (range 0 - 1) and the third step is to find the grey relational coefficient for individual property (ranges between 0.33 - 1 since the distinguishing coefficient was taken as 0.5). The last and fourth step is to find the GRG by taking average of each property grey relational coefficient value (Table 3.13).

Figures 3.24a and 3.24b show the two statistical parameters namely "sum of the rating" and "grey relational grade" with respect to scalp positions P1 - P4. When the "sum of the rating" of the four positions are compared (Figure 3.24a), it resulted in slightly higher values for P1, P3 (140, 142) compared to P2, P4 (129, 128) positions. It is found that no significant difference exists between P1 - P4 positions, if the limits (60 - 300) of the "sum of the rating" are considered. Similarly, from the response graph (Figure 3.24b) and response table (Table 3.13) of the GRA method, it can be said that the position is not influencing any response property, because mean grey relational grade [Kurra et al. 2015, Krishnaiah et al. 2012] is almost same for all positions (P1: 0.5467; P2: 0.4947; P3: 0.4825; P4: 0.4857). From the Figure 3.24 it can be said that, the "sum of the rating" and "grey relational grade" are not approaching the half limit of their maximum values i.e. 180, 0.66 respectively. Lack of significant differences between the positions could be due to the negation of data because of heterogeneity among the samples considered. One study [Erik et al. 2008] also reported no difference in age and gender when single fibre tensile properties are considered. In other literature [Mohan et al. 2014] slight variation in tensile properties with respect to "position on pig body" is reported, but their study is not restricted to a single area of the body like scalp in humans. Since grey relational grade is considered as multi-objective performance index, mean grey relational grades are also compared for age and gender (Figure 3.24c). Again, no difference between the levels is observed, indicating that age and gender are not able to influence the tensile properties like position. As highlighted in Table 3.12, experiment number 12 showed the grey relational grade value of 1 indicating "Male-*position 1*-age group 15-29 yrs" as the best factor-level combination.

Table 3.11a: Factors and their assigned levels considered in GRA analysis.	Table 3.11b: Experimental layout following a full factorial design L_{24} that is gender with 2 levels, age with 3 levels and position with 4 levels (2*3*4) considered in GRA analysis (MINITAB software)

Control Factor	Level 1	Level 2	Level 3	Level 4
Gender	M-Male	F-Female		
Age (yrs)	L1 (0-14)	L2 (15-29)	L3 (30-44)	
Position on scalp	P1 (front)	P2 (side)	P3 (center)	P4 (back)

Expt. No	GENDER	AGE	POSITION
1	F	L1	P3
2	F	L1	P2
3	M	L3	P3
4	M	L2	P3
5	F	L2	P2
6	F	L1	P4
7	F	L3	P4
8	F	L3	P1
9	M	L1	P1
10	M	L1	P4
11	F	L2	P1
12	M	L2	P1
13	M	L3	P1
14	F	L2	P4
15	M	L2	P4
16	M	L3	P2
17	F	L1	P1
18	F	L3	P2
19	M	L2	P2
20	F	L2	P3
21	M	L1	P2
22	M	L3	P4
23	M	L1	P3
24	F	L3	P3

Table 3.12: Grey relational analysis for single fibre tensile properties of hair. Grey relational coefficient of each response (YS, M, MS, WE) and "Grey relational grade" calculated from them for each experimental run is shown in table. YS- Yield Stress; M- Modulus; MS- Maximum Stress; WE- Work of Elongation; S/N- Signal to Noise.

Exp. no	Experimental data (response)				S/N ratios for original response data				Grey Relation Coefficient (GRC)				Grey Relational Grade
	YS (MPa)	M (MPa)	MS (MPa)	WE (MJ/m³)	YS	M	MS	WE	YS	M	MS	WE	
1	68	2716	147	50	37.4273	69.1546	43.7009	34.3055	0.3713	0.3465	0.3397	0.4487	0.3765
2	100	4209	209	56	39.9152	72.4236	46.1137	34.8259	0.4731	0.5000	0.4715	0.4761	0.4802
3	115	4595	235	66	40.7226	72.4634	46.6266	35.5120	0.5193	0.5027	0.5140	0.5179	0.5135
4	115	4591	223	60	41.9691	73.6997	47.4270	36.5586	0.6115	0.6046	0.5978	0.5981	0.6030
5	74	3182	156	40	36.8836	69.8349	43.5359	31.4592	0.3546	0.3702	0.3333	0.3410	0.3498
6	142	6708	249	62	42.7164	74.7042	47.3661	35.5617	0.6844	0.7236	0.5905	0.5213	0.6299
7	104	4372	185	60	40.2083	72.3756	45.3116	34.9143	0.4889	0.4968	0.4177	0.4811	0.4711
8	139	6110	239	73	41.3859	74.5118	47.2084	36.9782	0.5646	0.6973	0.5723	0.6376	0.6180
9	107	3776	232	66	39.9386	71.4133	46.8802	35.6909	0.4743	0.4398	0.5379	0.5301	0.4955
10	92	4651	214	46	38.9130	72.0376	45.9989	32.5582	0.4260	0.4752	0.4630	0.3758	0.4350
11	64	2733	156	42	36.1109	68.7328	43.8191	32.2682	0.3333	0.3333	0.3444	0.3660	0.3443
12	**178**	**6701**	**348**	**99**	**44.6961**	**76.1136**	**49.3990**	**39.2783**	**1.0000**	**1.0000**	**1.0000**	**1.0000**	**1.0000**
13	91	3831	180	50	39.0406	71.3738	45.0091	33.5817	0.4315	0.4378	0.4004	0.4153	0.4212
14	85	3698	171	48	38.5330	71.2462	44.6155	33.6248	0.4106	0.4312	0.3800	0.4172	0.4097
15	104	4128	216	61	40.8050	71.9619	46.6874	35.6104	0.5245	0.4706	0.5195	0.5245	0.5098
16	106	4492	220	60	39.9629	72.4151	46.6705	35.5230	0.4756	0.4995	0.5179	0.5187	0.5029
17	104	4253	179	41	39.8955	71.7707	43.6947	31.1850	0.4721	0.4594	0.3395	0.3333	0.4011
18	103	4312	209	63	40.0121	72.3588	46.1140	35.5764	0.4782	0.4957	0.4716	0.5222	0.4919
19	131	5317	265	73	43.5741	73.5195	48.1757	38.2973	0.7928	0.5872	0.7056	0.8049	0.7226
20	83	3329	167	48	38.2711	70.4461	44.2841	33.2891	0.4005	0.3944	0.3643	0.4032	0.3906
21	84	4675	208	45	38.3207	72.1336	45.7543	31.9225	0.4024	0.4811	0.4458	0.3549	0.4210
22	99	4151	199	60	39.5003	71.4878	45.7607	35.0855	0.4524	0.4438	0.4462	0.4911	0.4584
23	92	4387	220	54	38.6684	72.6345	46.1294	33.1999	0.4159	0.5147	0.4727	0.3997	0.4508
24	118	5168	219	71	41.2361	74.1101	46.5242	35.7786	0.5537	0.6481	0.5049	0.5362	0.5607

Table 3.13: Grey Relational Grade (mean) of all factor-level combinations. Bold figures represent the higher value (optimal value). Gender, age and position has negligible influence on tensile properties because Grey Relational Grade of each level mean and total mean is almost same resulting smaller values of Δ.

Control Factor	Level 1	Level 2	Level 3	Level 4	Δ (Max – Min)
Gender	**0.5445**	0.4603	–	–	0.0842
Age (yrs)	0.4613	**0.5412**	0.5047	–	0.0800
Position on scalp	**0.5467**	0.4947	0.4825	0.4857	0.0642

102
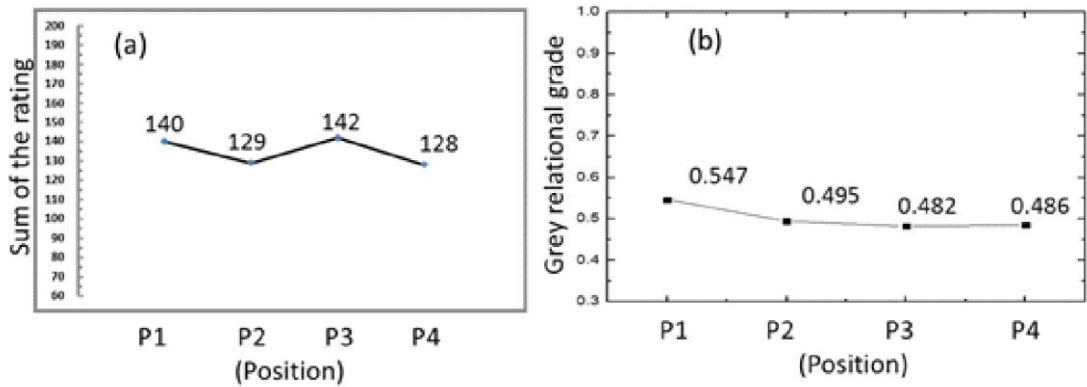
Figure 3.24: (a) & (b) Sum of the rating and grey relational grade with respect to scalp position respectively. Note that no significant difference exists between positions when tensile properties (yield stress, modulus, maximum stress and work of elongation) are compared.
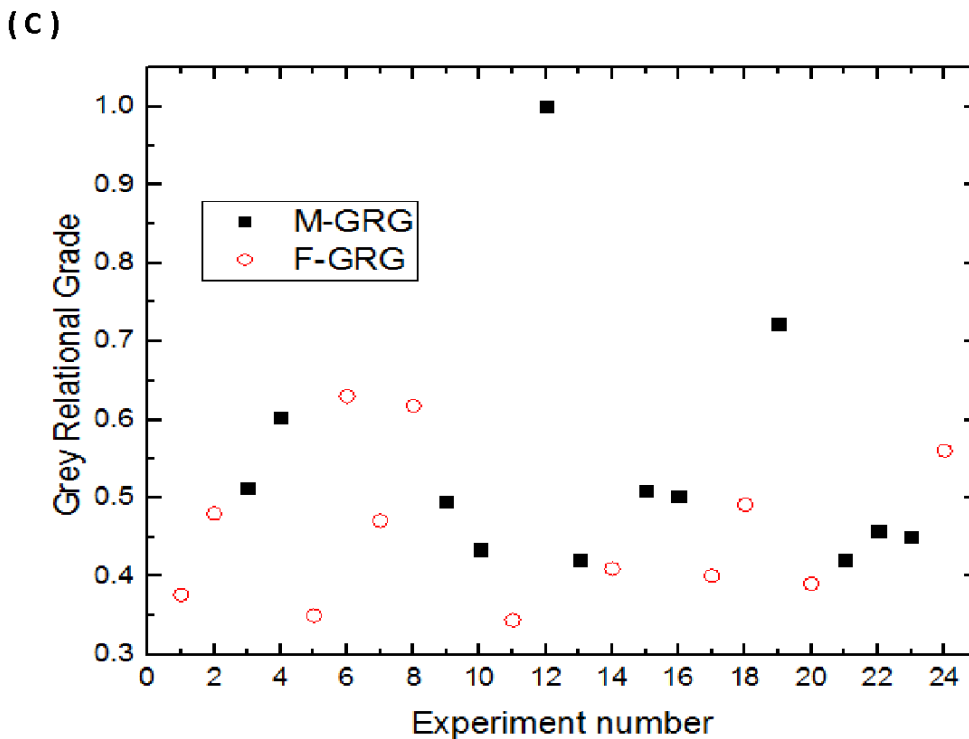
Figure 3.24: (c) GRG versus experiment number. Note that number 12 exhibits the highest GRG.

Based on tensile experiments and statistical observations, slightly higher mean values were observed for the P1 position (Figure 3.23 and Figure 3.24) despite having higher diameter for the P1 position compared to other three positions (Tables 3.2 - 3.5). It could be due to the strengthening of the hair composite structure with increase in whole fibre diameter and decrease in medulla diameter. But medulla diameter is not measured. Among the three factors considered, position is showing little influence on tensile properties followed by gender based on experimental and statistical observations. Among the positions, slightly higher mean value is observed for P1 position (Figures 3.23 - 3.24) based on relative rating, gray relational analysis and box-and-whisker plots. Among gender, male is slightly dominating compared to a female based on GRA results (Table 3.13 and Figure 3.24c) and it could be due to the hormonal effects. From the Figure 3.24c, it can be said that females generally have low GRG compared to males. As shown in Table 3.12, grey relational grade value of 1 was observed for "Male- *Position P1*- age group 15–29 years" indicating that hair collected from this combination can have better tensile properties compared to other combinations as shown in Table 3.11.The proposed relative rating and grey relational analysis of hair fibres seem to be in agreement with observational data (Figure 3.23) despite severe heterogeneity and variability due to age, ethnicity, diet and lifestyle, health and exposure.

3.3.6. Comparison between nanoindentation and tensile properties

Nanoindentation tests are commonly applied on small volumes like thin films, cell walls to obtain mechanical properties of materials. In tensile test the whole sample (gauge length) with constant cross-sectional area is considered to find mechanical response of material. In order to find a correlation between micro scale (bulk) properties from tensile test and nano scale (surface) properties from nanoindentation, the yield stress versus hardness and tensile modulus versus nanoindentation modulus are compared.

Comparison between nanoindentation hardness and tensile yield stress

Both hardness and yield stress are indicators of a material's resistance to plastic deformation. The indentation hardness and yield stress of hair with respect to donor age are shown in Figure 3.25. It is observed from the Figure 3.25 that a slight decrease in hardness is observed with increase in age but trend is not significant. It is

observed that, indentation hardness values are higher (more than double) than tensile yield stress values for all hair samples. In the case of nanoindentation, only the small region of the cortex (less defect free zone of < 100 μm^2) mainly consists of α-keratin (fibre) embedded in S-S rich amorphous matrix is subjected in compression mode whereas for tensile test, entire hair fibre including weak interfacial zone between α-keratin and amorphous matrix is considered. So the nanoindentation played a significant role in understanding the microstructure of true hair composite because higher hardness is due to the highly cross-linked S-S rich amorphous matrix.

Figure 3.25: Comparison between nanoindentation hardness and tensile yield stress of hair (position P3).
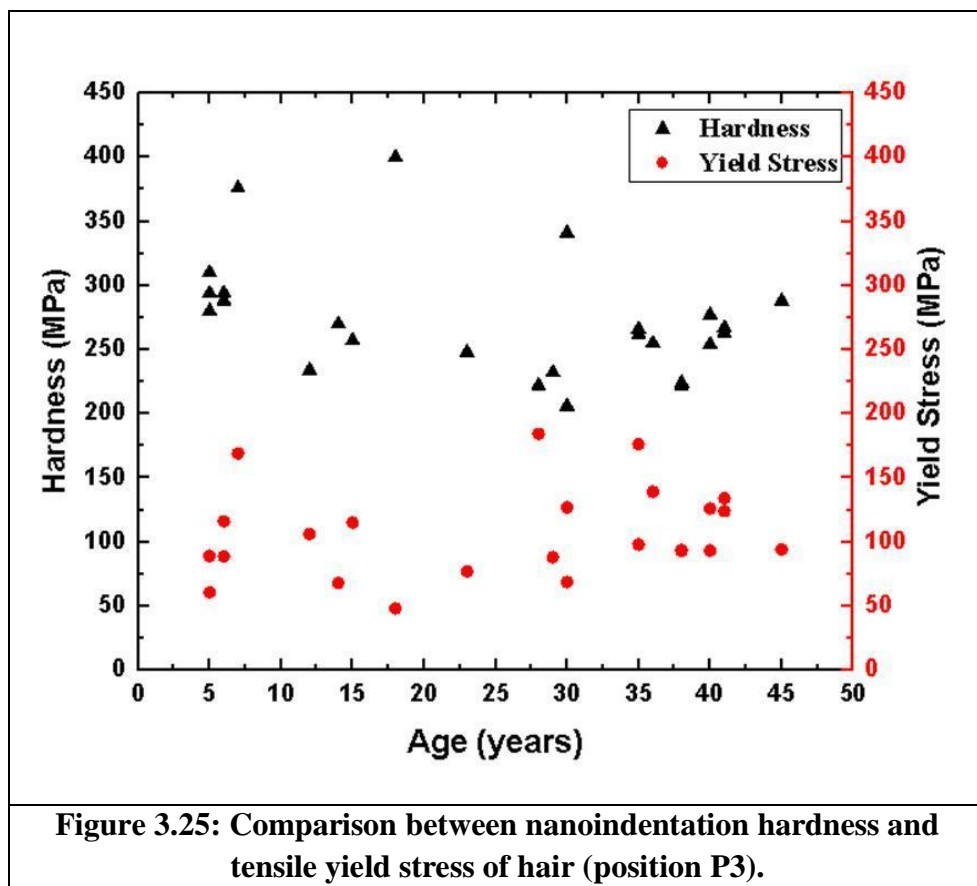
Comparison between nanoindentation modulus and tensile modulus

The slope of linear segment of stress-strain plot corresponds to modulus of elasticity (E). In polymer materials the elastic portion of the stress - strain curve are not linear (Figure 3.26). So for materials with nonlinear behavior of stress - strain curve, either tangent or secant modulus is normally used. Tangent modulus represents the slope of the stress-strain curve at some specified level of stress, while secant modulus is taken as the slope of a secant drawn from the origin to some given point of the stress-strain

curve as shown in Figure 3.26. The determination of these moduli is illustrated in Figure 3.26 [Callister 2007]. The elastic modulus measurement from tensile stress - strain curve and indentation modulus from initial portion of unloading from nanoindentation test are shown in Figure 3.27. Comparison of nanoindentation modulus and tensile modulus of hair samples with respect to donor age are shown in Figure 3.28. Though modulus measurements are obtained under different loads (tension and compression), increase in age showed no effect on modulus, but higher indentation modulus values (almost double compared to tensile modulus) are obtained as shown in Figure 3.28.

Figure 3.26: Schematic Stress-Strain curve showing non-linear elastic behavior and measurement of secant and tangent moduli [Callister 2007].

Figure 3.27: Elastic modulus measurement from stress - strain curve from tensile test (left image – using origin software) and indentation modulus measurement from (right image) load -displacement curve from nanoindentation test.

Figure 3.28: Comparison of indentation modulus and elastic modulus of hair (position P3) with respect to donor age.

From literature Chegdani et al. [2017] reported 1 GPa of indentation modulus for flax fibres (Berkovich indenter with tip radius of 40 nm) which is relatively low compared to its tensile modulus (40 - 70 GPa). Tests are repeated with MTS Nanoindenter

(Berkovich indenter with tip radius of 400 nm) found the indentation modulus of 20 GPa for the same flax fibre indicating the influence of tip radius and surface roughness on indentation modulus. Nanoindentation tests are also performed on vegetal fibres mainly on flax fibres to study the influence of maturity of fibres [Bourmaud et al. 2012]. They found that, modulus obtained by nanoindentation is lower than the tensile modulus due to the solicitation scale and geometry of the indenter for fibres in various parts of a stem. Since the fibres chosen have different packing geometry and crystallinity in different directions, indentation modulus revealed different value compared to tensile modulus. But glass fibre revealed 70 GPa of modulus in both tensile and nanoindentation tests, because it is a isotropic fibre.

As shown in Figure 3.28 indentation modulus is higher than tensile modulus for hair, this is because hair is a composite of crystalline α keratin coils embedded in amorphous keratin matrix. These helical coils can be elongated easily without using excessive force as the helical coils can extend greatly and become a random coil without losing their structural integrity when tensile stress is applied. But during the nanoindentation test, these helical coils require excessive force for compression as the spaces in between the helical coils are filled up with amorphous keratin matrix. There is no question of underestimation of fibre longitudinal indentation modulus due to the indenter tip geometry in nanoindentation testing of hair. Because in hair, microfibrils are made of helical intermediate filaments i.e. microfibrils are not really oriented in fibre direction if lower values of nanoindentation depths are considered (< 1500 nm).

3.3.7. Fractography of single hair fibres using optical microscopy and SEM

Optical microscopy was used to measure the diameters of pre and post tensile hair samples and SEM was used to know the fracture modes of fibres and corresponding structural analysis. From the diameter measurements (of pre and post tensile test) using optical microscopy as shown in Figure 3.29, Figure 3.30, Figure 3.31 and Figure 3.32 found that diameter is reduced by approx. 2 μm irrespective of the position as a result of tensile stretching and it could be due to high poisson's ratio ~0.38 as reported for keratin fibres [Zhenxing et al. 2009].
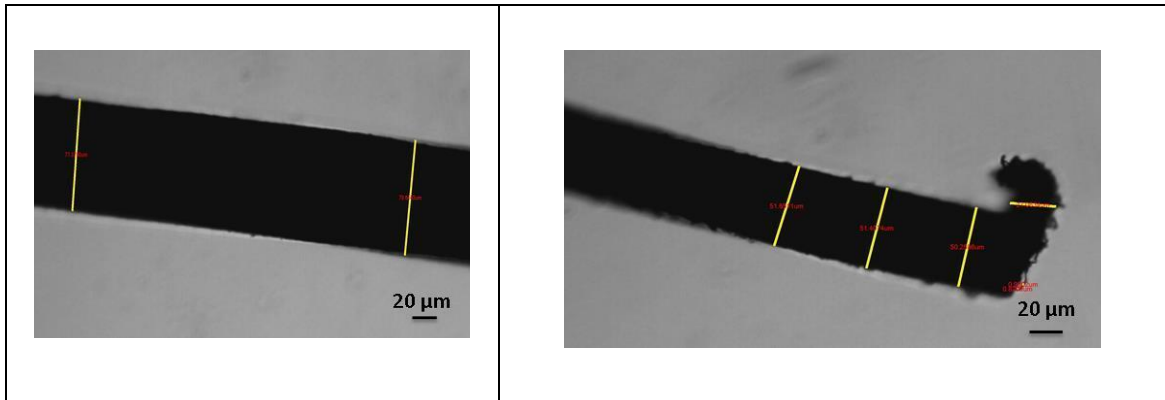
Figure 3.29: Optical microscopy images before (left) and after (right) tensile testing of single hair fibre.

Hair fractures are not always smooth and instead exhibit severe straining (post α to β transition) and this is evidenced by a change in diameter at the vicinity of the fractured ends. SEM fractography is conducted on M5, M6, M36, F23, F35, M38 and F41 samples for all four positions and found that fibres are fractured in different modes (smooth, step and split) though all hair samples are tested at same temperature and relative humidity.
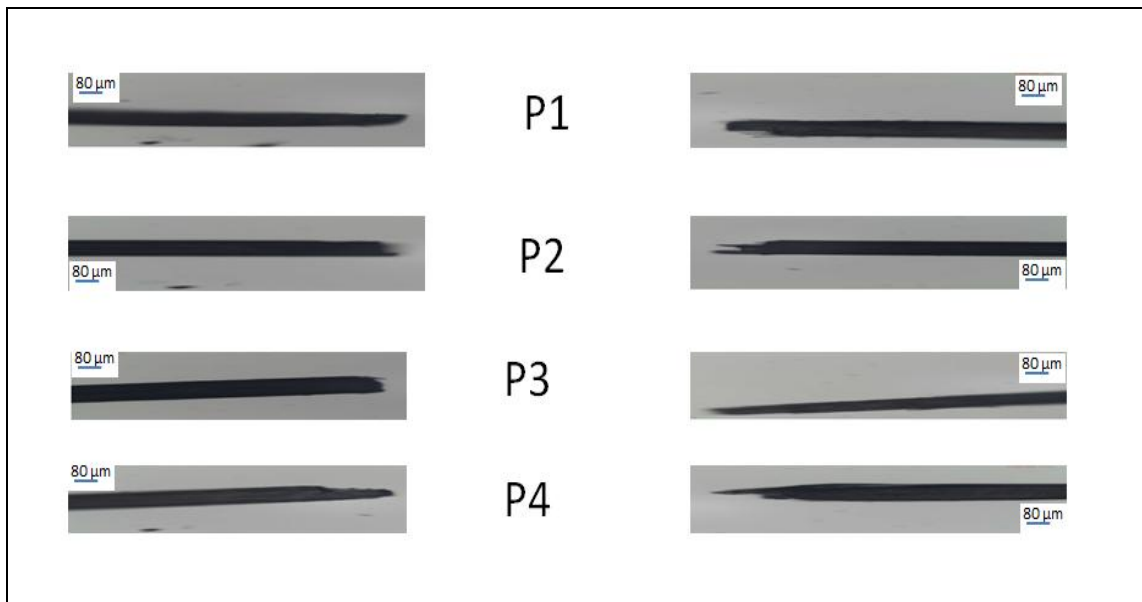
Figure 3.30: Tensile fractured images hair fibres of 15 yrs male sample (matching fracture faces shown with respect to position). Note the step (P1, P4) and split (P2 - P3) fracture modes.
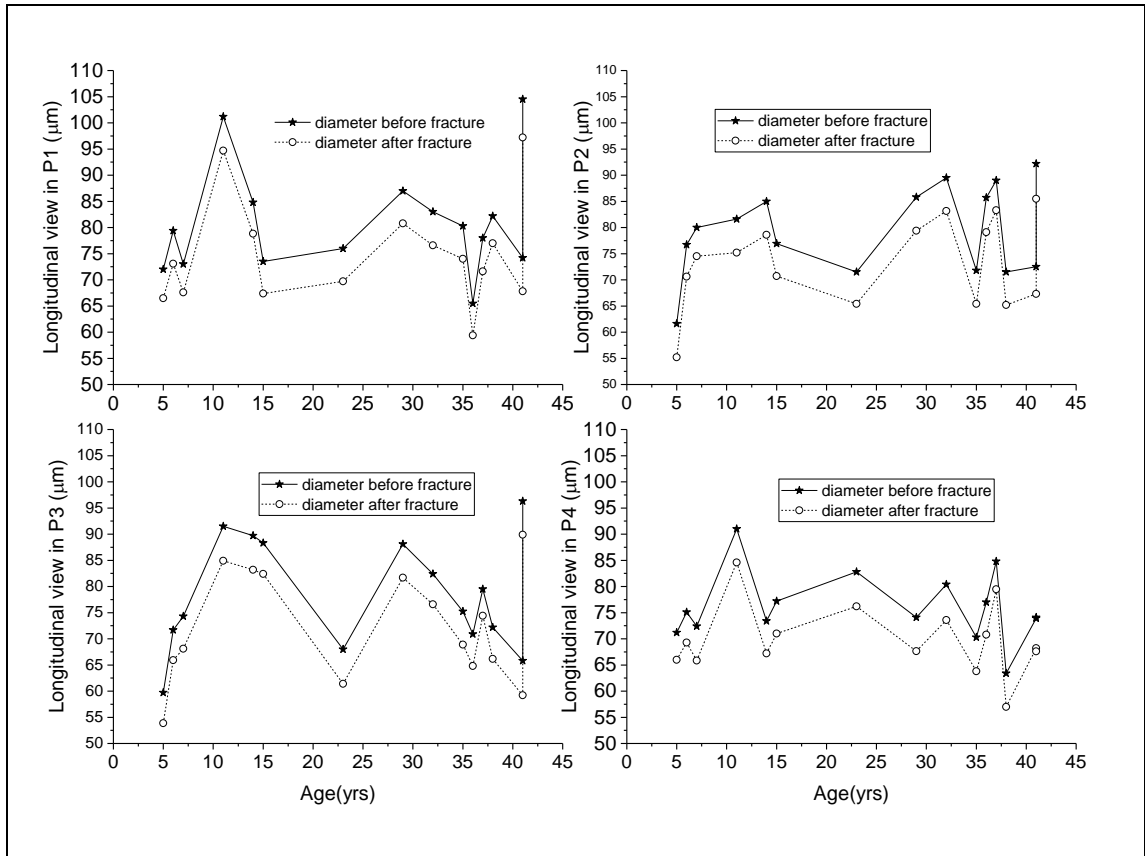
Figure 3.31: (a-d) Average diameter of 15 hair samples with respect to position (P1 - P4) on the scalp. Note the diameter reduction for fractured samples. Age 41 corresponds to two people (husband & wife) of same age and wife hair diameter is found to be higher than husband hair diameter except at P4 position.
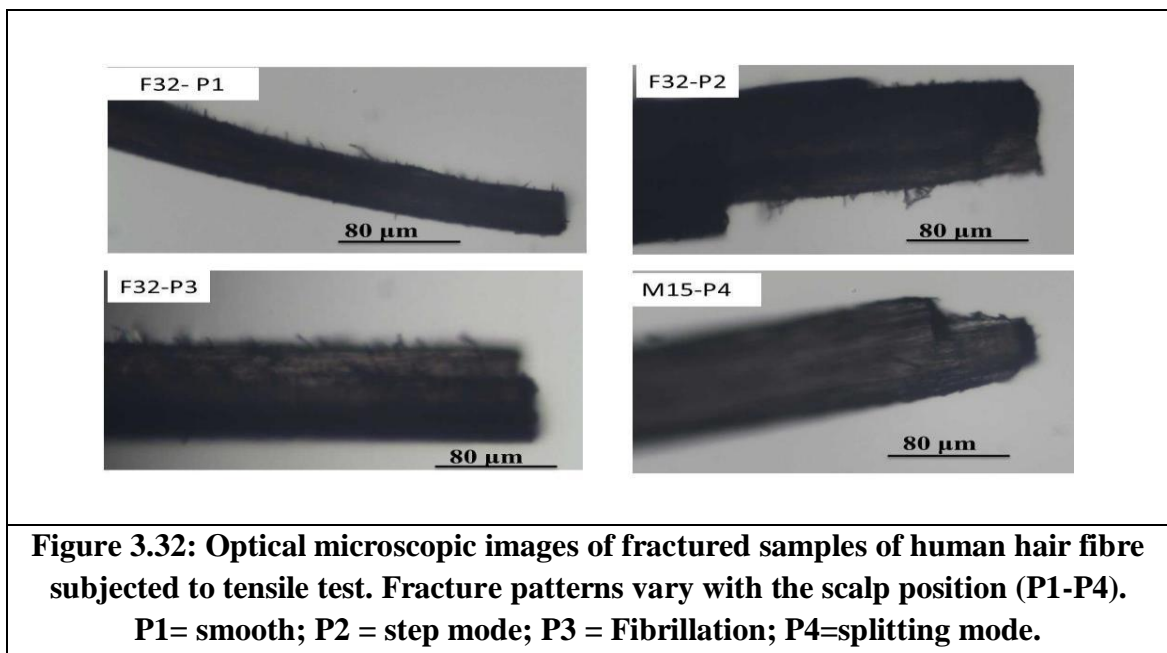
Figure 3.32: Optical microscopic images of fractured samples of human hair fibre subjected to tensile test. Fracture patterns vary with the scalp position (P1-P4). P1= smooth; P2 = step mode; P3 = Fibrillation; P4=splitting mode.
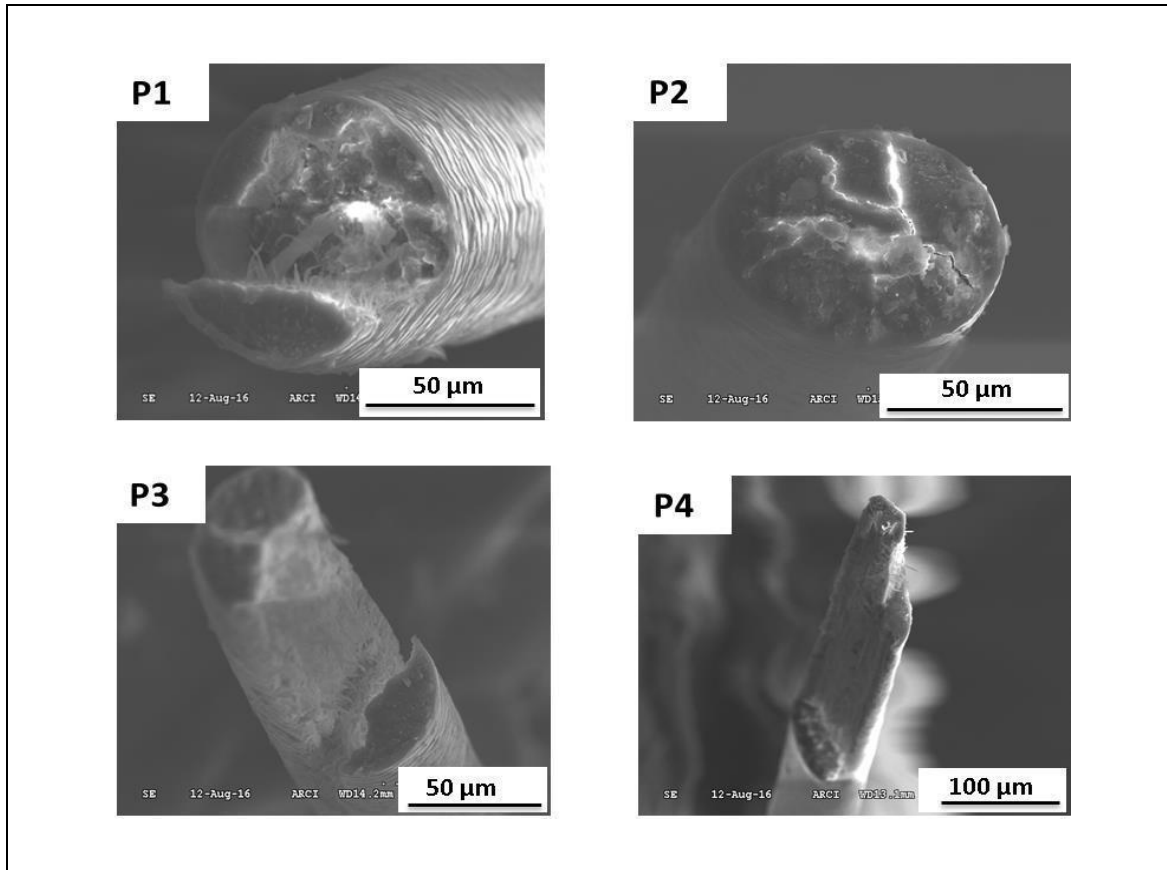
Figure 3.33: SEM fractographs of single hair fibres subjected to tensile testing. Data is shown for 6 yrs male sample with respect to scalp position (P1 - P4). Fracture pattern are splitting mode for P1, smooth fracture for P2 and step fracture for P3 and P4.

From the Figure 3.33, M6 fractured sample from SEM revealed different fracture modes for different positions (P1 - split; P2 - smooth; P3 & P4 - step). Hair from P2 - P4 positions indicate that cracks are initiated at medulla or at the vicinity of the medulla and propagated along the length side (step fracture; P3, P4) or propagated across the diameter (smooth fracture; P2). Whereas for P1 (split fracture), the crack initiation may have occurred at the interface between cuticle and cortex and propagated across the diameter (partially) resulting in severe damage to the cortical cells. Here 25 nm thick cell membrane complex layer [Forslind et al. 2004] which holds the cortical cells together might played a role in step mode with yielding and fibrillation.
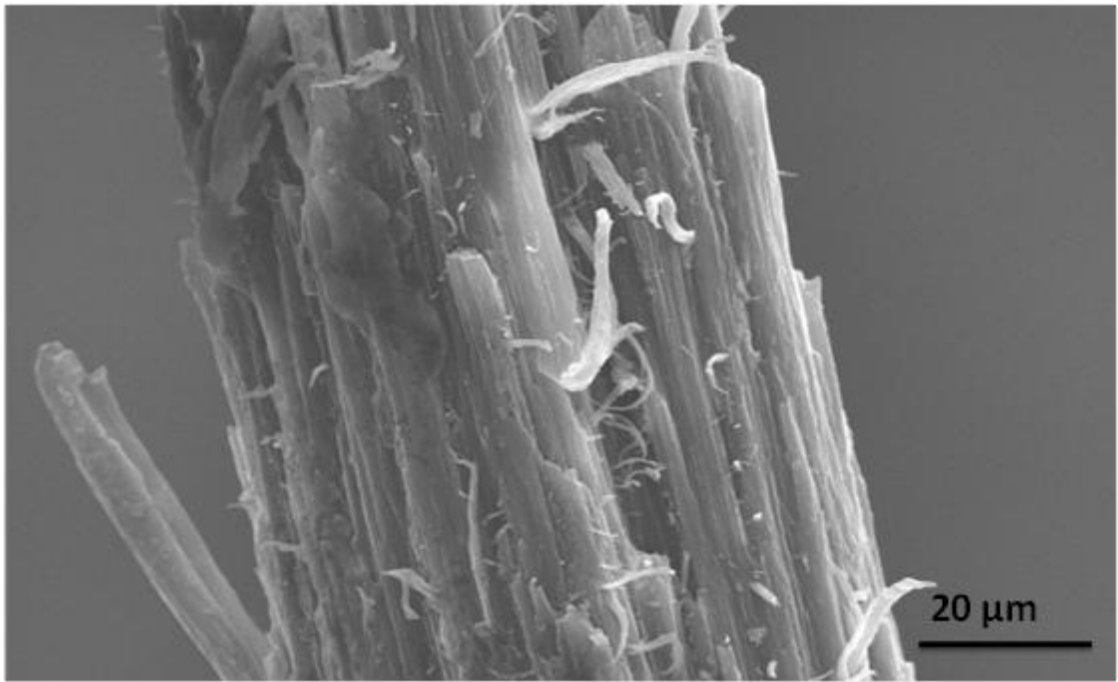
Figure 3.34: SEM fractograph of single hair fibre revealing split mode fracture and shows severe macrofibril pull-out and surface fibrillation.
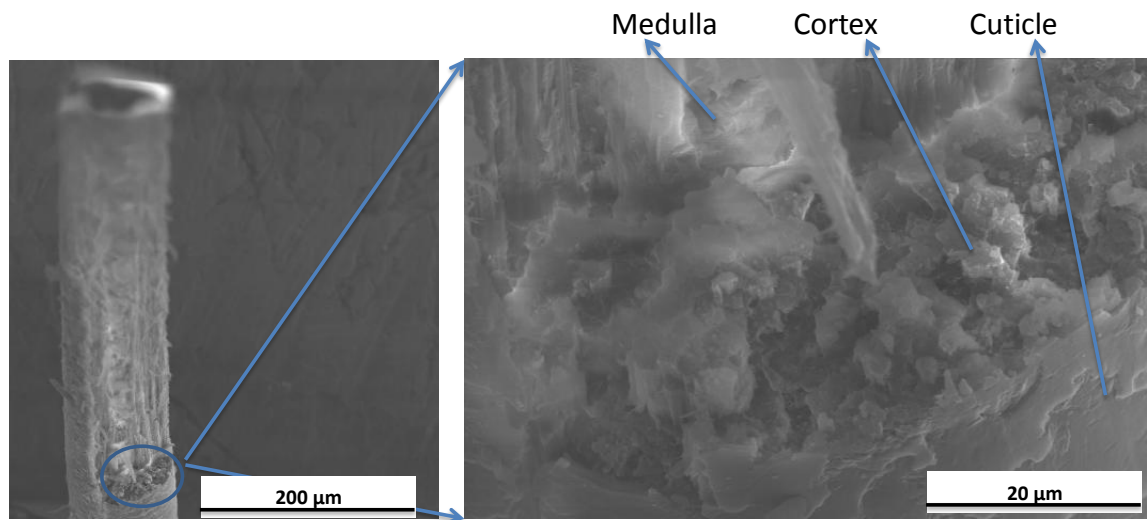
Figure 3.35: SEM fractographs of single hair fibres (6 yrs Male). From the images it can be seen that tensile fracture initiated from the medulla.

Individual macrofibrils (300-400 nm) or bundles of macrofibrils (400 nm - 2 µm) that have been pulled out as a result of split fracture mode are shown in Figure 3.34 and

lengths of these bundles are between 6-15 µm. Among all fracture modes, step fracture is dominant with > 600 MPa of post-yield modulus and may be influenced by the defects close to the medulla. It can be concluded that crack initiation and propagation happened along fibre direction, causing extensive shearing at the interface of cortical cells by damaging the continuous layer of cell membrane complex.

Figure 3.36: SEM fractographs of single hair fibres (family) after the tensile test. It can be seen that male hair underwent almost brittle fracture whereas female hair revealed ductile fracture.
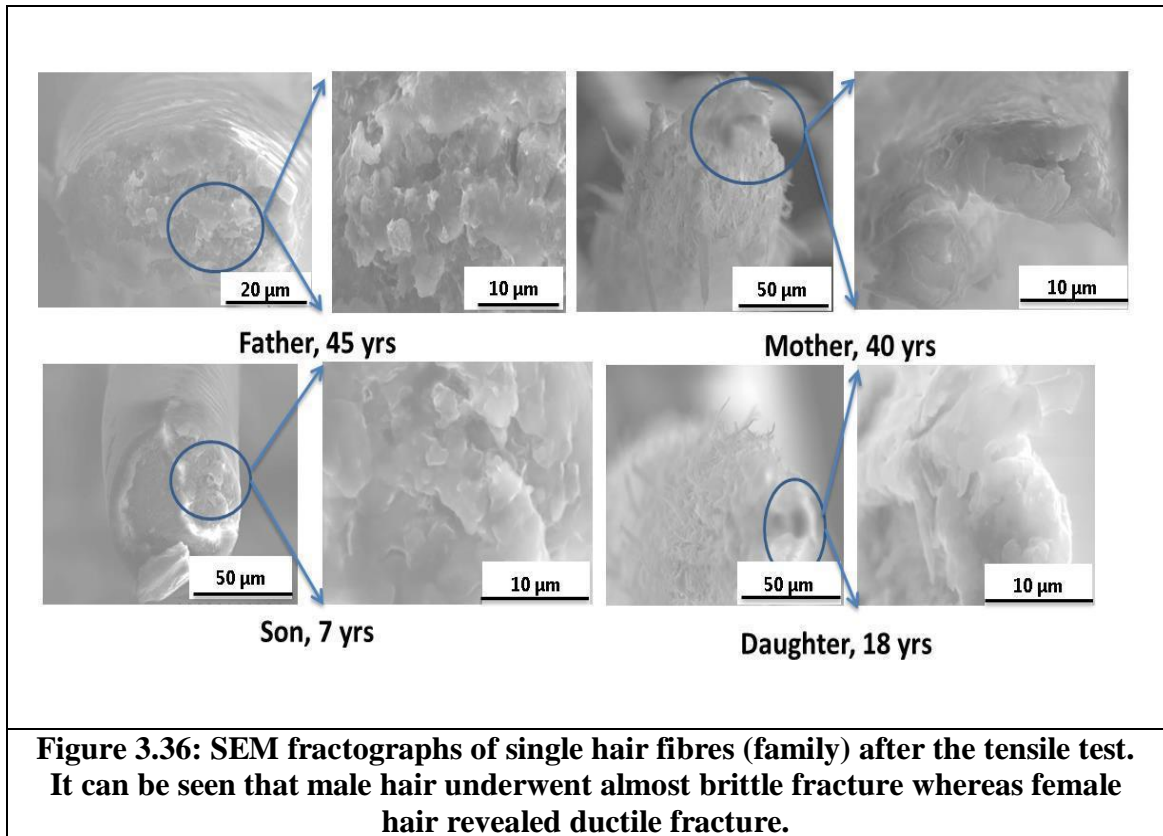
As per literature [Kamath et al. 1982], a smooth fracture at extreme relative humidity and step fracture at 45 - 65 % relative humidity is common. Even though samples considered in this study are tested at the same temperature (21 - 22°C) and relative humidity (50 – 55 %), no correlation is found between fracture mode and scalp position. In most of the tensile tests, the hair samples coiled back after large straining and fracture shows the elastic nature of hair. So, the fractured surface of hair after the tensile test is analysed using SEM and shown in Figure 3.36 for one family hair samples. The fracture surface is completely yielded with fibres protruding out in directions perpendicular to straining in case of the 40 yrs and 18 yrs old females. Whereas hair fracture surface of 45 yrs and 7 yrs old male's show a cleaner fracture

across the diameter with a longitudinal split, which could have attributed to the load drop as evidenced in stress-strain curve of the respective samples in Figure 3.11. The SEM images of the other samples also show the two fracture morphologies aforementioned with certain cases where the fracture is split along the longitudinal axis of the hair possibly influenced by the presence of the medulla. The SEM fractography of one such sample (Figure 3.35 confirms the presence of medulla) reveal fibrous network features with thicker fibre bundles along the longitudinal direction while thin and dispersed bundles spread in all directions including medulla. This serves as evidence to a fibre composite structure of hair fibre where smaller keratin fibrous structures are reinforcements in a matrix of non-oriented and randomly distributed S-S cross-linked proteins. It is a known fact that few hairs have the cortex and medulla (either continuous along the axis or discontinuous) and other fibres have cortex region only filled with perfect cross-linked structure.

Tensile testing of single hair fibres which are conditioned at 70°C for 12hr are compared with hair fibres conditioned at room temperature for 12hr. The corresponding force verses displacement curves are shown in Figure 3.37. It is observed that tensile properties of hair conditioned at 70°C is not showing any significant difference when compared to properties of hair samples conditioned at room temperature, so embedding of hair fibres and curing of epoxy resin at 70°C is acceptable.

Figure 3.37: Comparison of tensile properties of hair (room temperature vs at 70°C).
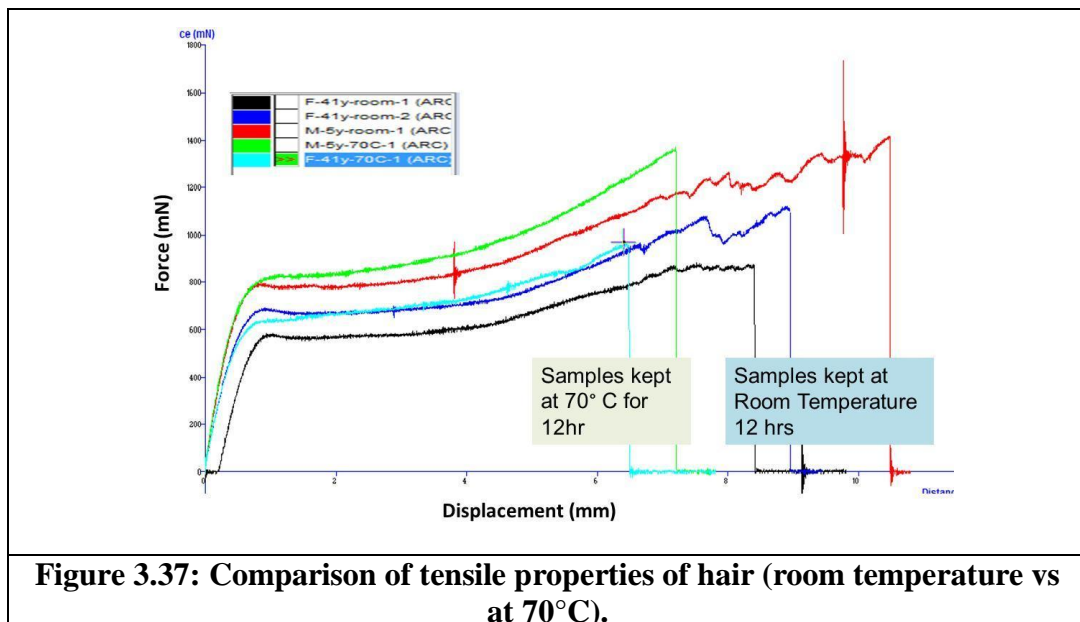
Figure 3.38 presents stress-strain behavior for three kinds of ethnic hair - Caucasian, Asian, and African as reported in literature [Bhushan 2010]. The stress-strain curve shows that Asian hair has highest ultimate stress and strain to break, followed by Caucasian hair. African hair shows very low mechanical properties in terms of young's modulus, yield point, and strain to break. The low mechanical properties of African hair are thought to arise from high stresses encountered during combing and tangling due to its curly structure [Bhushan 2010]. A typical stress strain curve obtained for wool fibres from literature [Linda et al. 1992] is shown in Figure 3.39.

Figure 3.38: Stress-strain curves of hair fibres [Bhushan 2010].

Figure 3.39: Stress-strain curve of a typical romney wool fibre [Linda et al. 1992].
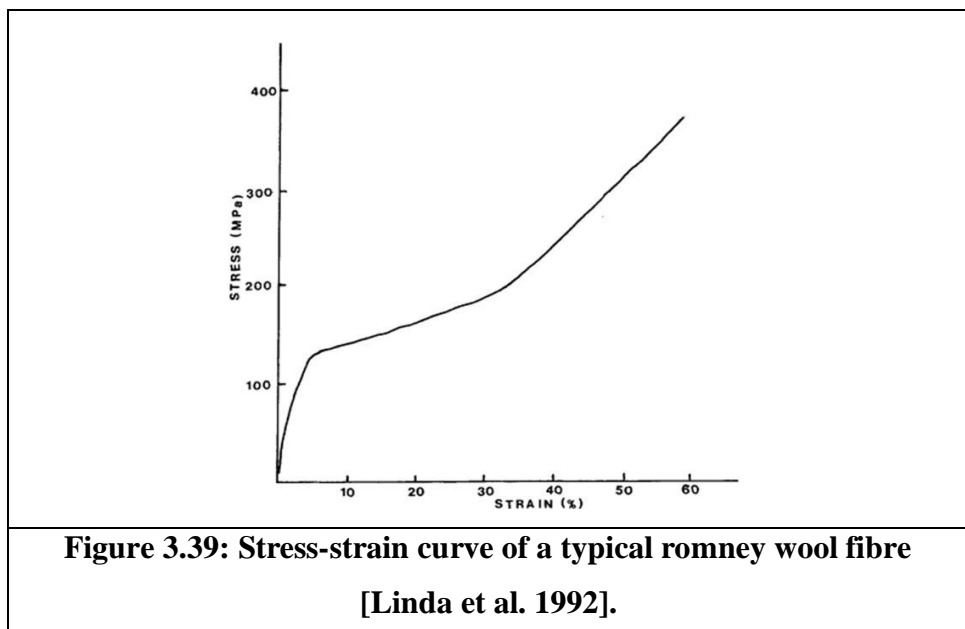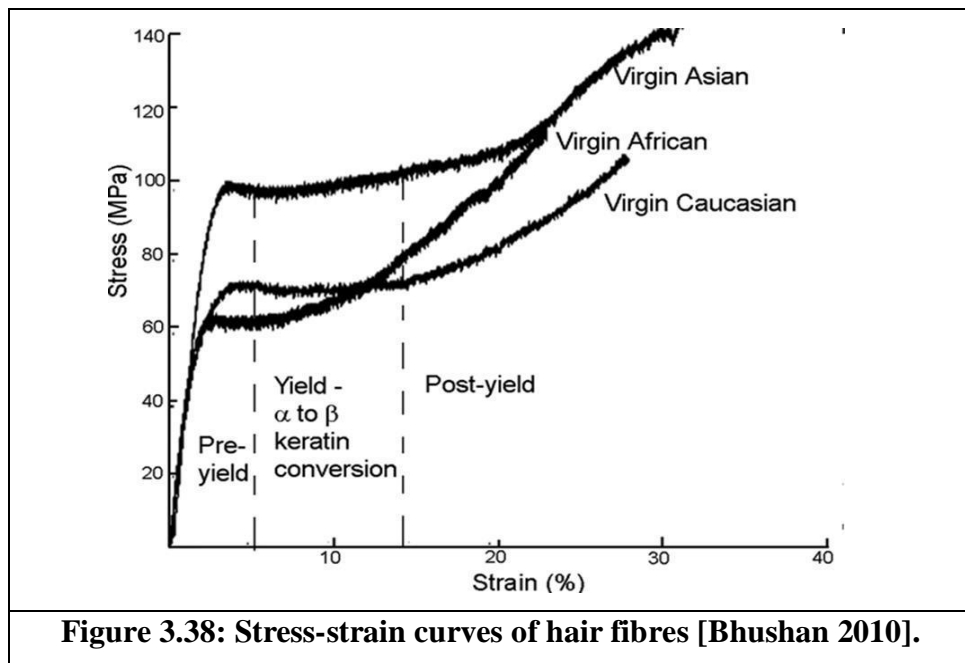
Chemical composition of hair using EDAX and XRF

Chemical composition (especially sulfur) of hair was measured using SEM-EDAX and XRF (X-ray fluorescence). The image taken from SEM - EDAX is shown in Figure 3.40. EDAX (Energy-dispersive X-ray spectroscopy) and it is an X-ray technique used to identify the elemental composition of materials.

Figure 3.40: SEM/EDAX (Scanning Electron Microscopy and Energy Dispersive Spectroscopy) analysis of single hair fibre cortex surface. Note the damaged cuticle.
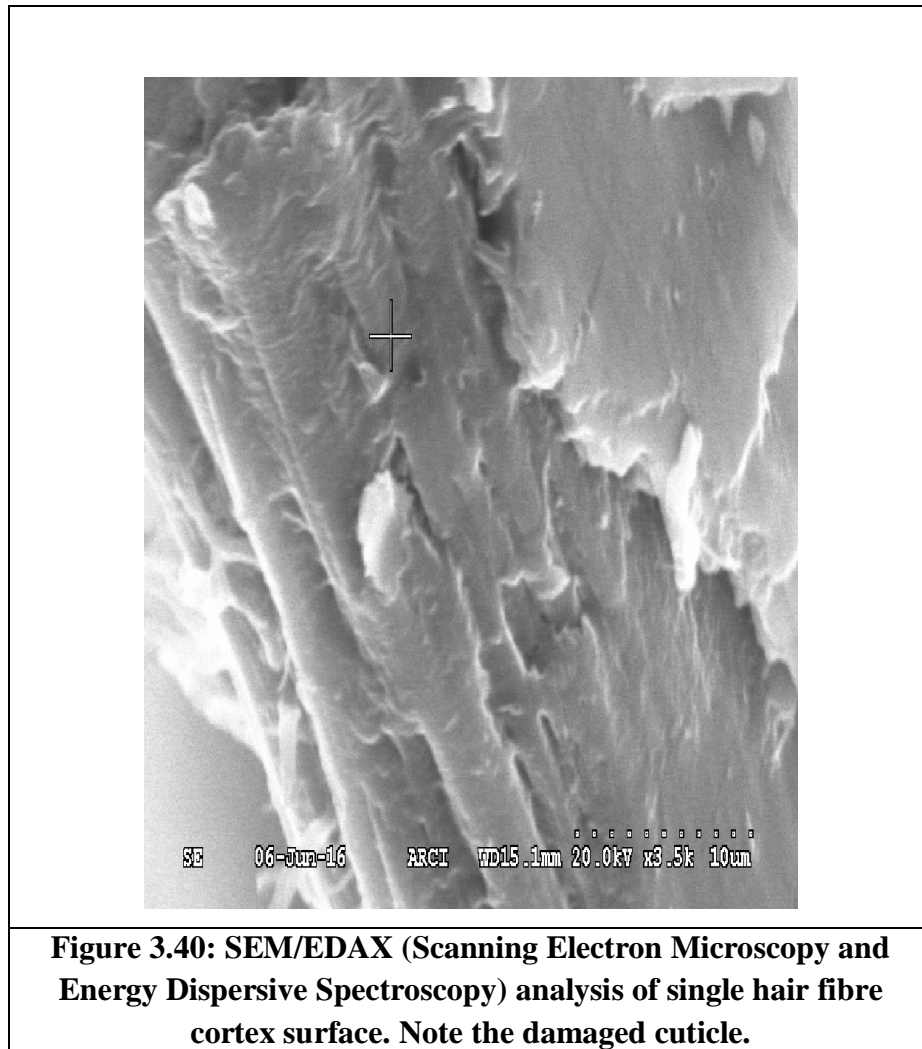
XRF (X-ray fluorescence) is a non-destructive analytical technique used to determine the elemental composition of materials. XRF determine the elemental composition of a sample by measuring the fluorescent (or secondary) X-ray emitted from a sample when it is excited by a primary X-ray source. Each of the elements present in a sample produces a set of characteristic fluorescent X-rays ("a fingerprint") that is unique for that specific element. Atomic number 11 (from sodium (Na) onwards can

be detected in this instrument. Sample container consists of a thin mylar film (diameter of 63.5 mm) at bottom as shown in Figure 3.41.

Figure 3.41: Top view (left image) and side view (right image) of XRF instrument sample container.
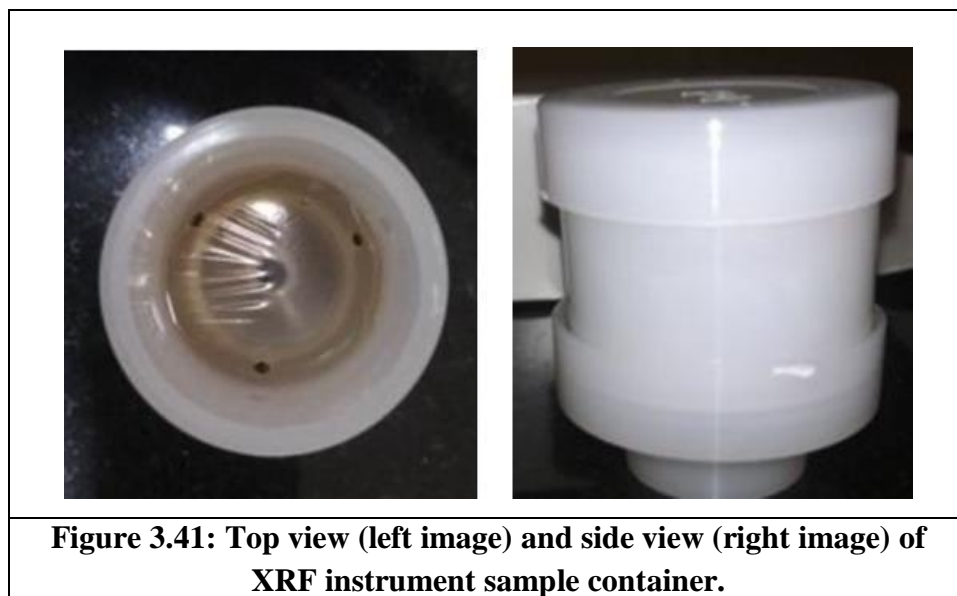
In EDAX, on specific location of the material is used to identify its elemental composition, but in XRF total material is considered for elemental composition.

Table 3.14: Composition of elements present in human hair (position P2) for age group of 5-41 years from XRF (Sulphur concentration: 7Y>6Y>14Y>15Y>11Y>5Y>41Y).

M-5Y		M-6Y		M-7Y		M-11Y		F-14Y		M-15Y		F-41Y	
Compound	Content (%)	Compound	Content (%)	Compound	Content (%)	Compound	Content (%)	Compound	Content (%)	Compound	Content (%)	Compound	Content (%)
Si	1.606	Si	0.443	Si	0.596	Si	0.696	Si	0.864	Si	0.466	Si	0.273
P	8.153	P	4.05	P	4.284	P	5.06	P	4.246	P	3.151	P	3.253
S	28.337	S	44.459	S	46.18	S	33.45	S	44.016	S	39.795	S	25.025
Cl	23.85	Cl	22.553	Cl	15.405	Cl	17.413	Cl	12.477	Cl	11.446	Cl	7.075
Ca	8.334	Ca	5.744	Ca	6.566	Ca	9.053	Ca	6.556	Ca	5.462	Ca	4.608
Ti	0.146	Cr	0.032	Fe	0.116	Ti	0.104	Ti	0.082	Fe	0.131	Ti	0.388
Fe	0.122	Br	0.151	CHO	26.663	Fe	0.121	Fe	0.132	CHO	39.419	CHO	59.275
Zn	0.157	CHO	22.435			CHO	34.031	Zn	0.106				
CHO	29.2							CHO	31.51				

Hair is cut in to small fragments around 1mm length and around 9.5 mg of hair is placed in the sample holder (Figure 3.41) of the XRF machine to find elemental

composition. From XRF data of human scalp hair shown in Table 3.14, the sulphur content of human hair is varying with age.

3.4. Conclusions

Single hair fibre diameters (longitudinal view) are in the range of 30 - 104 µm and linear densities of hair fibres are between 0.02 - 0.09 mg/cm and it follows the same trend as the fibre diameter. Hair diameters and linear density with respect to age, gender and also position are compared, but no significant trend was found between them.

First time, tensile testing of single hair fibre from four different positions (P1 - P4) of the scalp is carried out because scalp is divided into four parts i.e. frontal - P1, temporal - P2, parietal - P3, and occipital - P4. From the experimental and statistical analysis (Relative rating and Grey relational analysis), it is found that there is no significant difference in terms of mechanical properties of hair samples from different scalp positions (P1 - P4). This may be attributed to the presence of microscopic and nanoscopic structural heterogeneities. From grey relational analysis, it is observed that for 'Male- Position P1 with age group 15 - 29 years' has better tensile properties.

The tensile properties of single hair fibres are compared with respect to age, gender and position using statistical methods. It is observed that modulus, yield stress, maximum stress and work of elongation are in the range of 2 - 6 GPa, 60 - 190 MPa, 130 - 340 MPa and 30 - 100 MJ/m^3 respectively. SEM fractography revealed step, split and smooth fractures.

From the tensile stress - strain curves, four characteristic regions are identified and the fourth region is identified first time as part of this thesis work. The fourth region is observed by measuring a change in post-yield incremental modulus at around ~33 % strain in which yielding and an ultimate failure occurs. Fourth region is called post-yield region 2 and it can be seen in all the stress-strain plots between ~33 - 45 % strains. The post-yield incremental modulus change correlated well with fracture features wherein significant macrofibril (diameters of 400 - 2000 nm) pull-out is observed.

Nanoindentation and tensile properties of hair are carried out to obtain a correlation between hardness versus yield stress and also between nanoindentation modulus

versus tensile modulus with respect to donor age. Though there was no significant trend with age, indentation modulus and hardness values are almost twice the value of tensile modulus and yield stress respectively confirming the fact that hair structure at nano-level resembles a stiff composite material. This could be due to the helical arrangement of intermediate filaments embedded in amorphous matrix (microfibrils) which are difficult to compress (nanoindentation) and but are easy to extend (tensile stretching). This concludes that nanoindentation played a significant role in understanding the microstructure of true hair biocomposite structure because higher hardness is due to the highly cross-linked S-S rich amorphous matrix and higher indentation modulus is due to the stronger α-keratin microfibrils (fibre). The thermal properties of hair fibre with Differential Scanning Calorimetry (DSC) and experimental correlation between thermal and nanoindentation and also thermal and tensile and properties were presented in chapter 4 and chapter 5 respectively.

CHAPTER – 4

Thermal characterization of hair fibres

This chapter covers the results from thermal testing of hair like onset of melting temperature, melting temperature and melting enthalpy of hair fibres. These results were compared with respect to donor age and gender.

4.1. Introduction

Hair contributes in thermal regulations like other epidermal appendages specific to all mammals. It protects body against environmental factors (heat, cold, sunlight, dryness etc.), injuries and impacts. The central part of hair shaft called medulla acts as thermal insulator exclusively in animals. Beard hair has thicker medulla compared scalp hair and it acts as insulation against outside temperature by keeping face and neck at constant temperatures. The effect of cosmetic treatments like hair straightener (Figure 4.1) which exposes the hair to temperatures of approx. 120 - 200°C is very different from the range of temperatures experienced in hair dryer (approx. 60 - 90°C). The amplitude of induced alterations is not fully estimated, but increases as a function of exposure time to high temperature. Regarding mechanical properties, it is shown that repeated thermal treatments in curling in certain conditions leads to an increase in post-yield modulus and also it improves fatigue resistance. It might be related to structural modifications with increased cross-linking due to thermally induced dehydration.

Figure 4.1: Hair straightener with temperature between 60 – 220 °C (used in hair cosmetics).

Differential Scanning Calorimetry (DSC) is an accurate way to assess thermal changes in the structure of materials. It is used to determine the water content and state of water in wool or hair [Cao 1999, 2005, Milczarek et al. 1992, Wortmann et al. 1993, 2012]. When hair fibres are heated from room temperature to 300°C different thermal events are successively observed by DSC. At temperature lower than or equal to 100°C, free or weekly bound water evaporates. Irreversible endothermal transitions occur at a temperature between 230 and 250°C. At a temperature higher than 350°C, thermogravimetry analyzer (TGA) shows a rapid loss of mass related to the breaking and decomposition of keratin protein.

4.2. Materials and Methods

Human hair samples are collected from people of Hyderabad, India (Caucasian origin) after getting approvals from Ethics Committee as described in the chapter 3. The hair samples with age ranging from 3 to 70 years are collected from the scalp (vertex region -P3 as shown in chapter 3). The hair samples are washed with mild shampoo, then with water and dried at room temperature. After drying samples are kept in zip lock covers and are labeled. A total of 17 donor samples are used in determination of melting enthalpy and peak temperatures.

4.2.1. Differential Scanning Calorimetry (DSC) testing of hair fibres

DSC is the most frequently used technique in thermal analysis of fibres. It is used to study the behavior of materials as a function of temperature or time. From DSC, the heat flow rate difference between sample and a reference is measured as a function of temperature or time while the sample and reference are subjected to a controlled temperature. The major applications of the DSC technique are in the fields of polymer and pharmaceuticals like for measuring melting temperature, crystallization behavior, glass transition temperature, heat of reactions and kinetics, etc.

Hair samples are cut to fine fragments of less than 0.5 mm length using sharp scissors in an air conditioned room maintained at 20°C. The fragmented samples are dried at 120°C for 4 hours in an oven to remove the moisture (~11.3 %) present in hair samples. A set of four samples from one family are taken without drying for thermal analysis to check the influence of pre-drying. Not much difference in peak temperature was observed as a result of drying. The conditioned hair samples of

around 2 - 3 mg are packed into a 50μl aluminum DSC pan. SHIMADZU DSC 60 is used for hair characterization. The DSC instrument is calibrated with Indium sample of 2 - 3 mg in Al pan. Temperature scans are run from 30°C to 280°C at a heating rate of 10 °C/min and at 30 ml/min flow rate of nitrogen. More than 40 scans are run and origin software is used for data interpretation especially in determination of melting enthalpy and onset of melting temperatures.
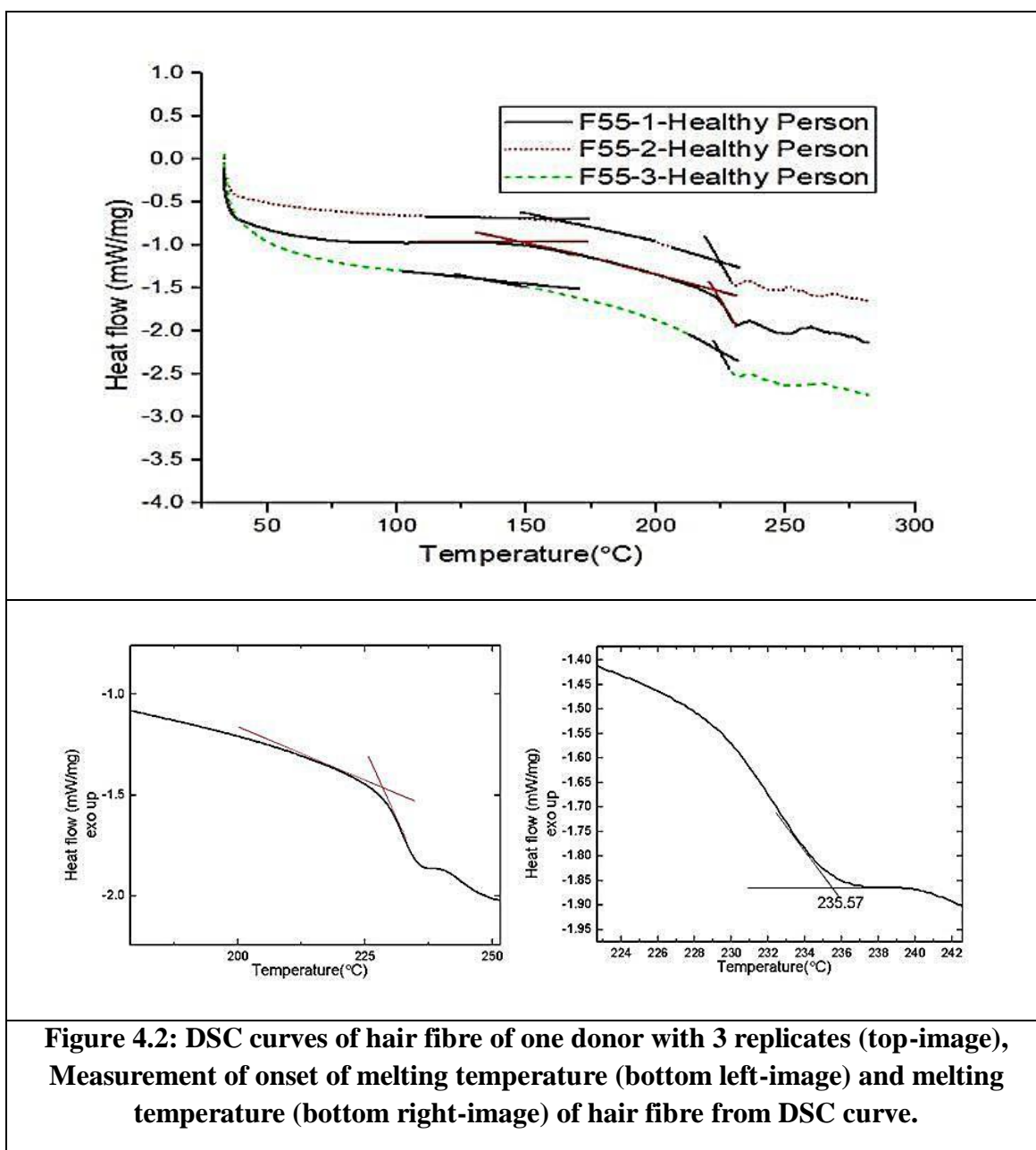
Figure 4.2: DSC curves of hair fibre of one donor with 3 replicates (top-image), Measurement of onset of melting temperature (bottom left-image) and melting temperature (bottom right-image) of hair fibre from DSC curve.

4.2.2. Measurement of temperatures (onset of melting and melting) and melting enthalpy

As shown in Figure 4.2, the onset of melting temperature is measured from the intersection of the tangents. The melting temperature (corresponds to complete melting of crystals present in material) is also measured from the intersection of tangents because peaks are not sharp as shown in Figure 4.2. In metals the melting peak is very sharp, but in semi crystalline polymers (PP, HDPE) or biocomposites such as hair melting peaks are very broader. The melting enthalpy is measured by creating a sigmoidal (extended s-shape) baseline because curves do not return to the base line after the first endotherm as shown in Figure 4.3.

Figure 4.3: Measurement of melting enthalpy (area under the peak) by creating a sigmoidal (extended S shape) baseline because curves do not return to the base line after the first endotherm.
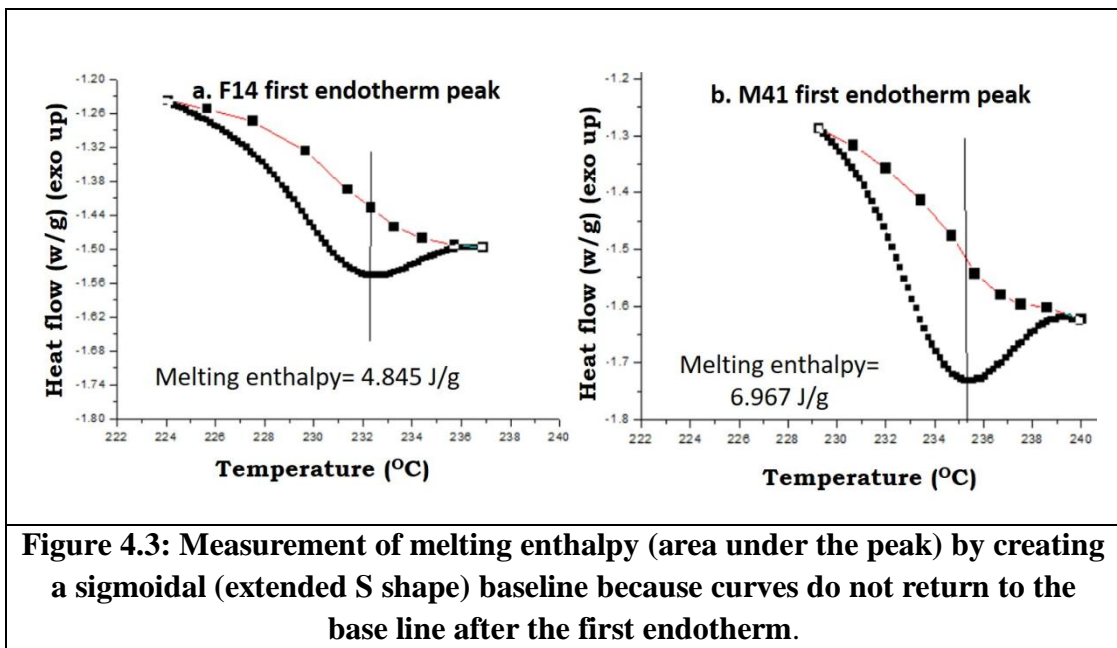
4.3. Results and Discussions

Representative DSC curves of hair fibres of four donors are shown in Figure 4.4 (without drying at 120°C) and Figure 4.5 (with drying at 120°C). Typical DSC thermogram of human hair shows the following effects of physical/chemical transformations while heating the specimen:

a) A broad endothermic peak in the temperature range of 40 to 120°C indicating removal of moisture is normally seen. In this study, it is found to be mostly

absent due to pre-drying of the hair samples at 120°C because presence of moisture complicates the DSC data interpretation.

b) A constant slope heat flow signal between 140 to 210°C indicating glass transition region of amorphous phase (matrix) of keratin i.e. rich in cysteine content. High slope indicates poor quality of the matrix.

c) An endothermic doublet peak in the range of 210 to 260°C indicating melting of ordered α helices with two distinctive regions of intra and inter regions of α-helices. Some studies describe the first peak as microfibrillar peak (helical IF's) and second peak as matrix peak (contains high sulphur keratin). In this study, the intensity of second endothermic peak is less or absent in few samples and in other samples peak is very broad.

d) No third endothermic peak was observed below 260 °C.

e) Above 260 °C onset of an exothermic event or an onset of an endothermic event indicating keratin decomposition by-products reaction (ex: amide crosslinking).
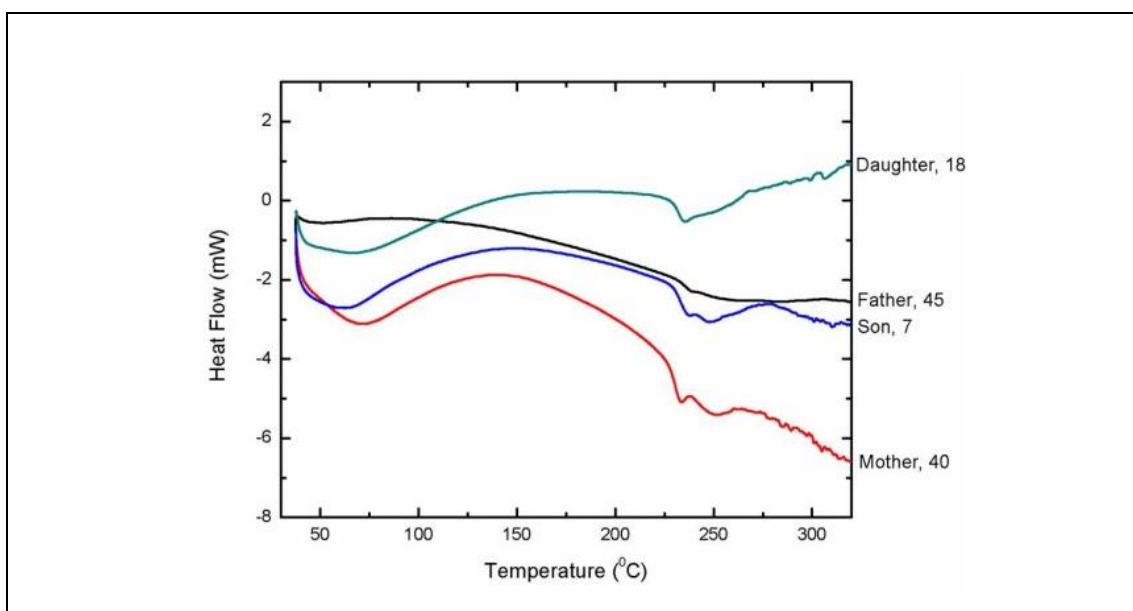
Figure 4.4: Differential scanning calorimetry curves of hair. The endothermic event between 40 - 120°C corresponds to water elimination from capillary tissue. The endothermic peak at approx. 230°C is attributed to the melting of the α-keratin.
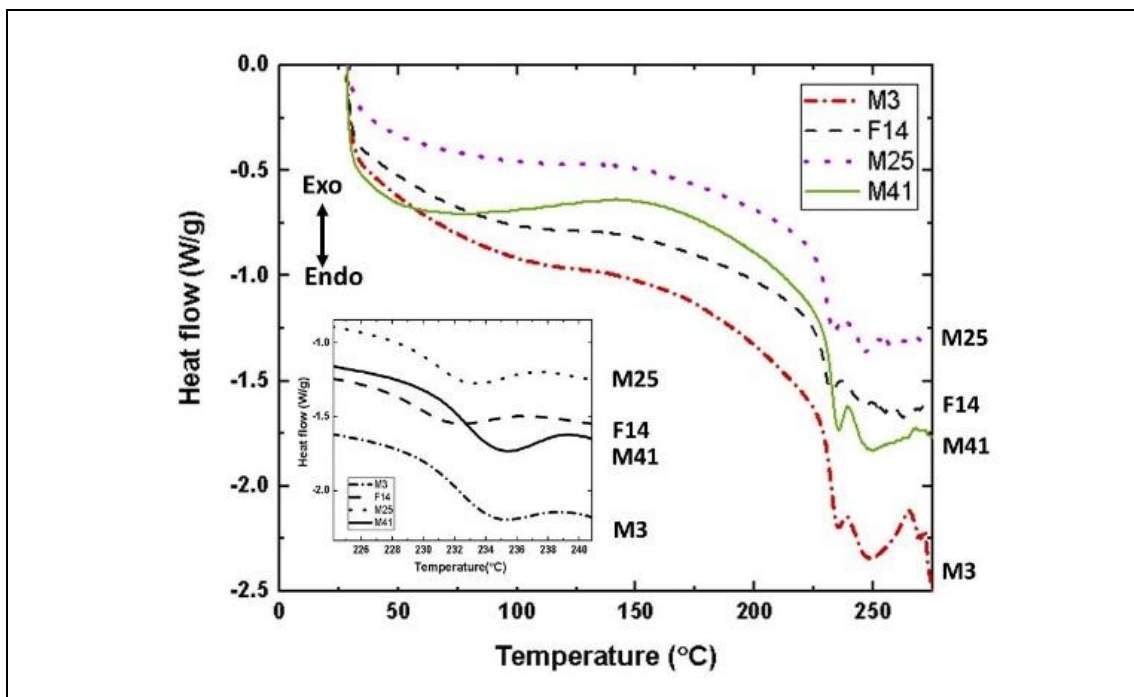
Figure 4.5: DSC curves of human hair samples of around 3 mg are heated with 10°C/min under nitrogen draft of 30 ml/min. M25 indicates male 25 years.

All the DSC curves are similar in terms of curve shape, for samples with drying (Figure 4.5) and without drying (Figure 4.4). However curves differ in the region of constant slope heat flow signal and endothermic peaks corresponding to their temperature representing crystalline phases of keratin. Above 275°C, DSC curves are not shown due to other thermal events mentioned above. In this study, first endothermic peaks corresponding to the melting of α- keratin crystallites (IF's are 50 % helical and have low sulphur content) is considered. Second endothermic peak (matrix having high sulphur content) is ignored because it is less reproducible and also showed difference in its intensity due to photochemical degradation effects.

Table 4.1: Melting temperature and melting enthalpy (based on dry weight) of human hair determined from DSC thermograms. M3 indicates male 3 years old and F6 indicates Female 6 years old.

Gender (Age,Yrs)	Onset Temperature (°C)	Melting Temperature (°C)	Melting Enthalpy (J/g)
M3	229	235.4	6.196
F6	231	237.6	5.379
F14	228	232.5	4.845
M15	228	234	6.525
M25	225	233	6.224
F26	232	240	5.667
F35	230	238	5.465
M38	227	235	5.824
M41	230	235	6.967
48F	227	233	7.462
50F	228	235	5.57
M52	229	235	6.289
F55	224	228	5.71
F56	231	238	5.42
F64	230	235	6.504
M65	228	237	6.267
F66	231	239	5.87
Avg	228.71	235.32	6.01

4.3.1. Onset of melting and melting temperature of hair with respect to age and gender

The thermal properties from DSC plots such as onset of melting temperature, melting temperature (first peak) and area under the first endothermic peak (melting enthalpy) of all samples are shown in Table 4.1. All the properties were measured using origin software and each data point is average of three values. The DSC curves shown in Figure 4.4 and Figure 4.5 confirms to the general DSC pattern reported for keratin, wool and human hair fibres. The first endothermic peak ($235 \pm 3°C$) due to melting of α-keratin is observed for all hair samples as shown in inset picture of Figure 4.5. Onset of melting and melting temperature of hair with age as shown in Figure 4.6 and are in the range of 224 – 232 °C and 228 – 240 °C respectively. It is observed from

the Figure 4.6 and Figure 4.7 that no significant trend with respect to age and gender. The samples F6, F26, F35, M41, F56, F64 and F66 have higher melting temperatures.
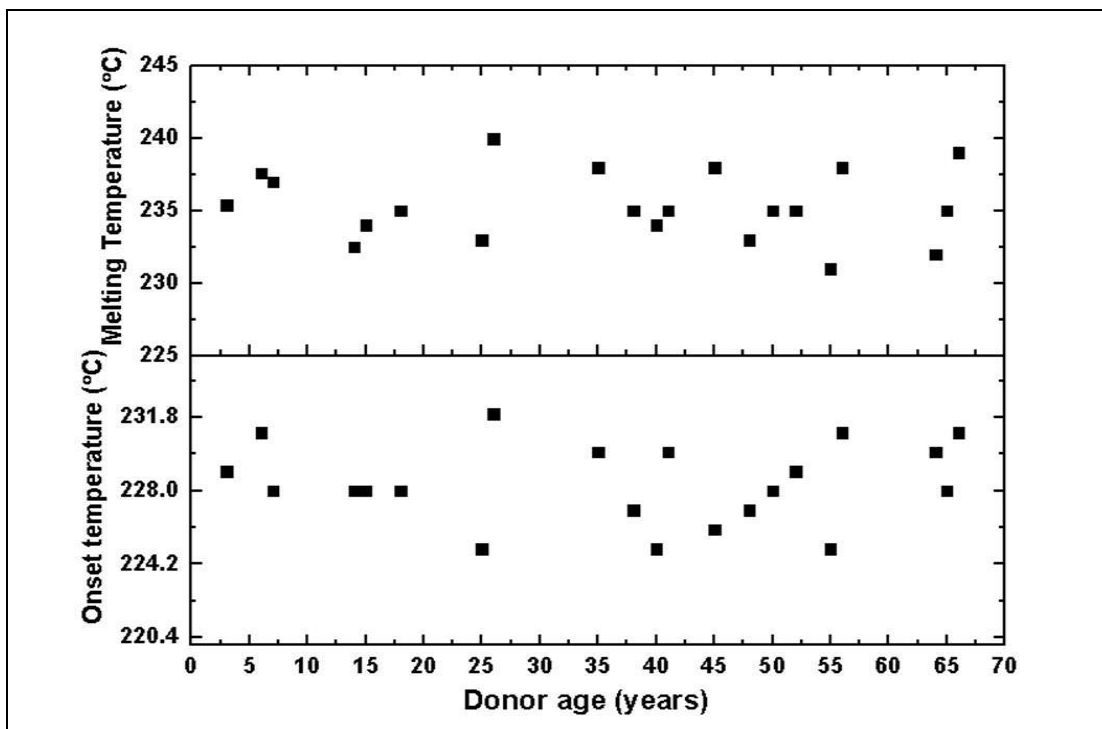
Figure 4.6: Thermal properties (melting temperature - top image and onset temperature - bottom image) of all hair fibres as a function of donor age.
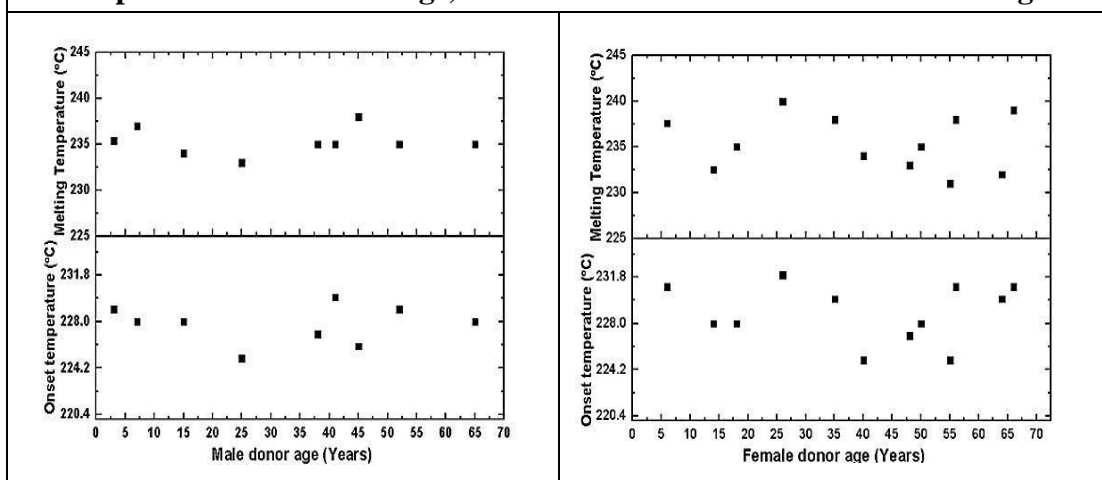
Figure 4.7: Thermal properties (melting temperature and onset temperature) of hair fibres as a function of male donor age (left image) and female donor age (right image).

4.3.2. Melting enthalpy of hair fibres with respect to age

Melting enthalpies are in the range of 4.845 - 7.462 J/g. The lowest enthalpy is observed for F14 (4.84 J/g) followed by F6 and F35 samples having 5.38 J/g and

5.46 J/g respectively. In contrast to this, F48, F64, M15 and M41 have higher melting enthalpy values of 7.46, 6.5, 6.52 and 6.97 J/g respectively. F55 sample has lowest onset temperature and lowest peak temperature among the 17 samples considered. In this study only the first endothermic peak for determination of melting enthalpy of α-keratin (Figure 4.5) is considered. The endothermic peaks that are obtained varied from *deep and narrow* to *shallow and broad*. The observed broader peaks and low melting enthalpy values could be attributed to structural defects in hair composite at interfaces or boundaries, orientational in homogeneities and heterogeneous crystal size distribution. It is observed that no specific trend between melting enthalpy with respect to age as shown in Figure 4.8.

Figure 4.8: Melting enthalpy as a function of donor age of all hair fibres.
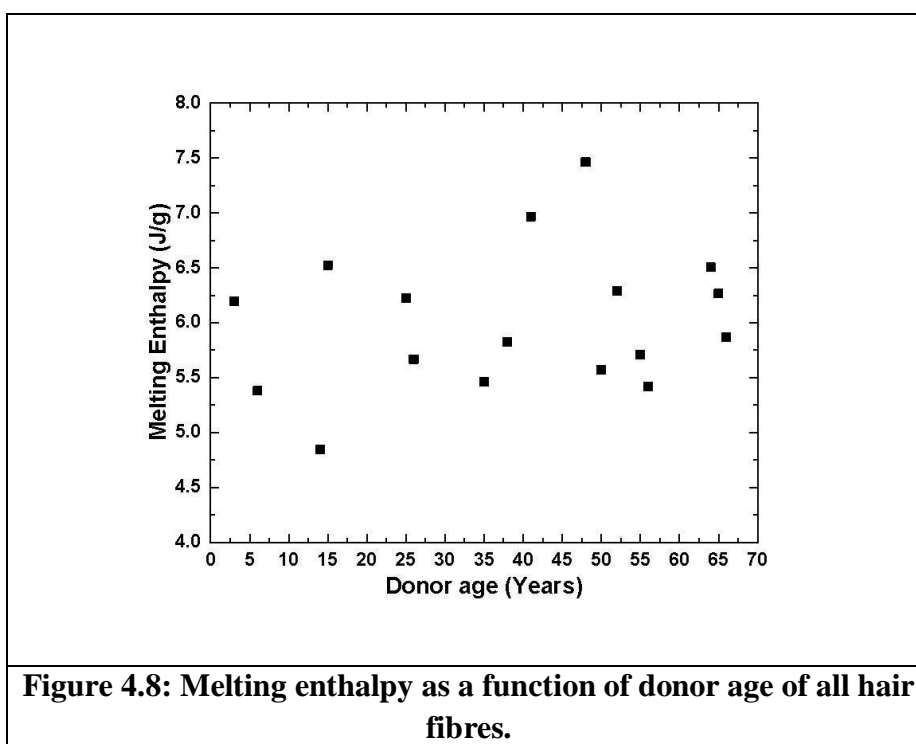
Statistical analysis of thermal properties of hair fibres.

The statistical method ANOVA was used to find the influence of age and gender on hair thermal properties. One way ANOVA with significance level (P - value < 0.05) of 5 % used to determine the effect of gender and age on melting enthalpy. From one way ANOVA analysis, P value resulted 0.64 and 0.99 when gender and age are considered as source of variation for melting enthalpy for male and female donors respectively. So, P >0.05 indicating no difference in melting enthalpy among the donors considered.

4.4. Conclusions

First time melting enthalpy is measured by creating a sigmoidal (extended s-shape) baseline because curves are deep and broad rather than sharp peaks observed in DSC testing of metals. Melting or first peak temperatures of all hair samples are in the range 228 – 240 °C. The average melting enthalpy of hair samples from all donors is around 6 J/g and it is closely matching with literature value of 7.2 J/g [Cao 1999] reported for Caucasian red hair samples. The onset of melting temperature, melting temperature and enthalpy of melting of α-keratin of 17 donor's hair samples are found no significant trend with respect to age or gender.

CHAPTER – 5

Correlation between Thermal vs Tensile and Thermal vs Nanoindentation properties

5.1. Introduction

Hair is normally subjected to thermal and mechanical treatments simultaneously such as hair straightening (hot flat iron) and curling. These treatments have adverse impacts in the quality of the hair such as S-S bond breakage, cuticle damage, loss of free and bound moisture and increase in cross-linking of amorphous matrix (end of the treatment). The quality of the hair fibres damaged by thermal treatments can be studied by Differential Scanning Calorimetry (DSC). For hair fibres, melting temperature of ~235°C is commonly reported [Mohan et al. 2017] and also measured in this study (see the previous chapter). Similarly fibre deformation and fractures induced by mechanical stimuli are studied by tensile test by applying loads upto 1000 mN and also by nanoindentation test with loads upto 10 mN. Both thermal and tensile tests measure the bulk properties of the hair fibres which includes cortex and medulla regions. As described previously, nanoindentation measures the surface properties of single fibre cross-sections in compression mode and depths of these indentations are approximately 800 - 1200 nm. Only 10 μm length or width is used for nanoindentation, which allows tests to be carried out separately on cortex and medulla regions. A correlation among the thermomechanical properties of hair fibres is discussed below because hair fibres consists of crystalline intermediate filaments (or microfibrils) and amorphous matrix enriched with S-S linkages. In healthy hair sample, both crystalline and amorphous regions are packed together in the form of a nanocomposite which is also known as macrofibrils. From the different correlations studied following two correlations were found when the data of three tests were compared. First correlation is between yield stress vs melting enthalpy and second correlation is between hardness vs slope of the heat flow curves between 120 - 210 °C. The yield stress determined from single fibre tests correspond to bulk response of hair which may be influenced by structural defects and inhomogeneties in α-keratin

whereas the hardness determined from nanoindentation correspond to local (surface) response of hair which is influenced by degree of cross-linking of matrix.

5.2. Correlation between Thermal and Tensile properties

Here the objective is to study the correlation between melting enthalpy (thermal) and yield stress (tensile). Since yield stress denotes the value wherein the stress - strain diagram deviates from linearity, the major contribution up to yield stress (linear region) will be derived from an ordered, elastic, rigid crystalline phase. Hence the percentage of the rigid crystalline phase will determine the magnitude of yield stress. Further, as described previously, the enthalpy of melting which also corresponds to the percentage of crystalline phase may exhibit a correlation with yield stress. In the review by Popescu et al. [2016], it is reported that hair fibres DSC data should be supported by other techniques such as tensile test or XRD in order to confirm the intensity of damage. But doing more than one test is cumbersome if correlations exist between two tests. In this study a correlation between thermal and mechanical properties are determined, so that one test will suffice to check the quality especially crystallinity portion of the hair protein.

In DSC thermogram, only the first endothermic peak is considered for determination of melting enthalpy of α-keratin present in hair keratin structure. Melting enthalpy and yield stress are measured using origin software as shown in Figure 5.1 (actually melting enthalpy was measured by considering sigmoidal base line as shown in Figure 4.3). Further, as commonly reported for semi-crystalline polymers [Menyhard et al. 2015, Batista et al. 2016] the melting enthalpy corresponds to the percentage of crystallinity of the α-keratin phase and that a strong correlation between the melting enthalpy and yield stress exists. In summary, the melting enthalpy obtained from the endothermic peak provides a relative quantification of the percentage of crystalline phase in hair samples. To study the correlation between melting enthalpy and yield stress for hair in a similar manner as reported for a semi-crystalline polymer like polypropylene [Menyhard et al. 2015], more than fifteen donor hair samples were compared.
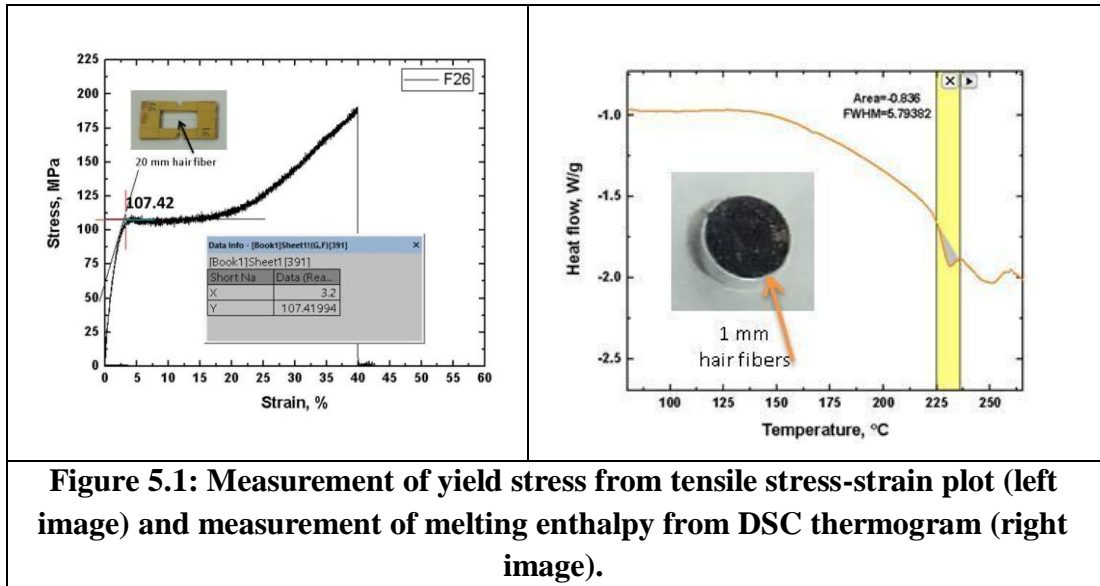
Figure 5.1: Measurement of yield stress from tensile stress-strain plot (left image) and measurement of melting enthalpy from DSC thermogram (right image).

$$y = \frac{A_1 - A_2}{1 + e^{(x-x_o)/dx}} + A_2$$
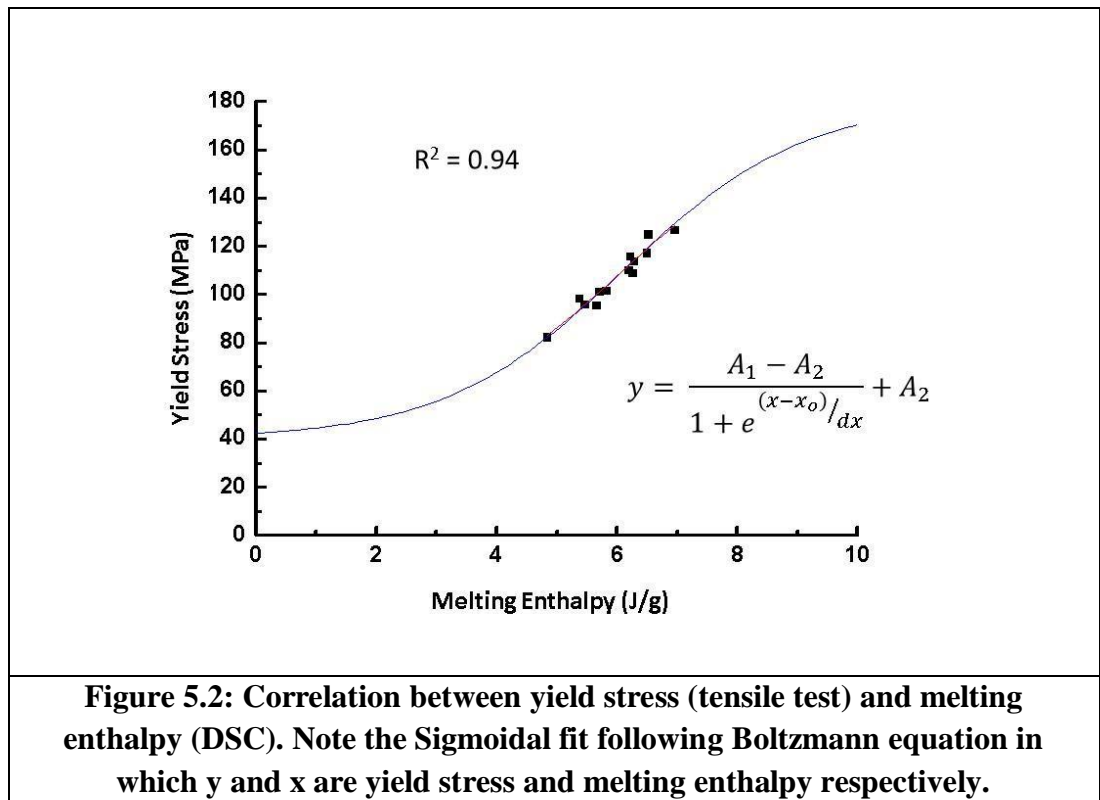
Figure 5.2: Correlation between yield stress (tensile test) and melting enthalpy (DSC). Note the Sigmoidal fit following Boltzmann equation in which y and x are yield stress and melting enthalpy respectively.

Figure 5.2 indicates a plot between melting enthalpy (area under peak in J/g) from DSC and yield stress from tensile test. The correlation is studied by simulating a non-linear least square curve fit with sigmoidal function (the Boltzmann equation, with a regression value of 0.94) as described below:

$$y = \frac{A_1 - A_2}{1 + e^{\frac{(x - x_0)}{dx}}} + A_2 \ldots\ldots\ldots\ldots\ldots\ldots(1)$$

As shown in Figure 5.2, y and x are yield stress and melting enthalpy. A1 and A2 are lowest yield stress (40 MPa) and highest yield stress values (180 MPa) respectively. Simulated x_0 is the melting enthalpy at y=110 MPa ((A1+A2)/2) where in maximum slope is observed (in our simulation the x_0 value is 6.1 J/g). ((A2-A1)/4dx) describes the slope at the point x_0 and indicates the steepness of the curve. Here dx is a shape or slope constant [Resendiz-Munoz et al. 2017] (in our simulation the dx value is 1.5524). If dx is small, the steepness of the curve will be very high and vice versa. Hence, dx can be considered as a thermomechanical heterogeneity factor to describe the heterogeneity of the properties obtained from hair samples.

The sigmoid correlation between the properties describes evolution from a set of properties for zero percentage crystallinity (completely amorphous plateau) to 100 percentage crystallinity (completely crystalline plateau). This is in contrast to simplified linear (rule of mixture) correlation wherein the crystalline and amorphous fractions are non-interacting. Hence it is concluded that a non-linear sigmoid correlation seems to provide an accurate representation of a composite keratin structure wherein the % crystallinity exhibits a range and crystalline and amorphous regions are intertwined and intricate in nature. Further, the correlation also indicates that the tensile and thermal properties in discussion correspond to a common structural aspect. In this case, the range of tensile and thermal properties corresponds to percentage crystallinity range of the 17 people.

Finally, the usefulness of the correlation can be envisioned in conducting DSC scans on hair samples in order to provide both thermal and tensile property evaluation quantitatively. As a note of caution for future investigations, the correlation plots that can be used for diagnosing /characterizing hair samples based on different ethnicities, age range, gender and lifestyle must contain a large sampling in terms of quantity and a substantial range of properties i.e. thermomechanical heterogeneity for them to be accurate and valid.

5.3. Correlation between Thermal and Nanoindentation properties

Here the objective is to find a correlation between slope of the heat flow curve (thermal) in the range of 120 - 210 °C and hardness (nanoindentation). The lower is the onset of melting temperature, (as show in Figure 4.3) the broader the melting peak and it is an indication of structural defects in protein due to the presence of more interfaces or boundaries, inhomogeneities and larger distribution of crystal sizes. Further, the lower onset of melting peak and more crystal defects should correlate with lower hardness measured from nanoindentation, but no such correlation was observed. Instead, a correlation between slope of the heat flow curve in the range of 120 - 210 °C and hardness was found. Similarly a correlation between onset temperature 1 (glass transition temperature -Figure 5.3) and hardness was also found. Hair is a hierarchical composite in which α-keratin fibrils are considered as reinforcement and cystine rich (S-S) highly cross-linked amorphous protein is considered as matrix. Normally response of the matrix in the forms of hardness and response of fibres (fibrils) in the forms indentation modulus in the cortex zone of < 100 μm^2 is observed for unidirectional fibre reinforced composites such as hair. Since the load applied is less than 10mN (depth of 1000 nm), hardness is related to interfacial defects exists between matrix and fibrils and structural heterogeneities exist in the entire cortex region. Melting temperature corresponds to temperature required to melt α-keratin crystallites. But the onset of melting temperature indicates end of the amorphous matrix softening, interface becomes weak and beginning of the α-keratin crystallites melting. Figure 5.3 shows linear relation between hardness and onset of temperature 1 with regression value of 0.87. Insight picture shows the measurement of onset temperature 1 using origin software and also hardness measurement from maximum load (nanoindentation). Figure 5.4 also shows linear relation with negative slope between hardness and slope of the heat flow curve between 120 - 210 °C (amorphous region of the DSC plot) with regression value of 0.64. It is clear from Figure 5.3 and Figure 5.4 that interface between amorphous matrix and crystalline intermediate filaments and amorphous matrix itself played an important role before melting of crystallites. From the DSC thermograms it is evident that higher the slope of the heat flow curve between 120 - 210 °C (amorphous region), lower the onset of melting.
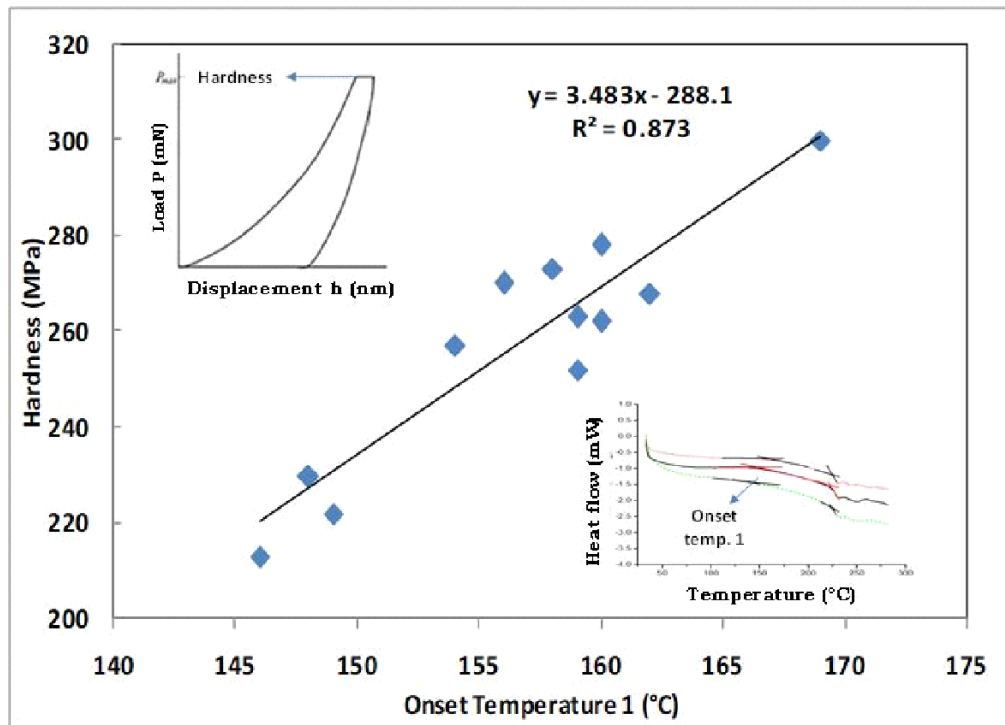
Figure 5.3: Correlation between hardness (Nanoindentation test) and onset temperature 1 or glass transition temperature (DSC thermogram) of hair fibres.
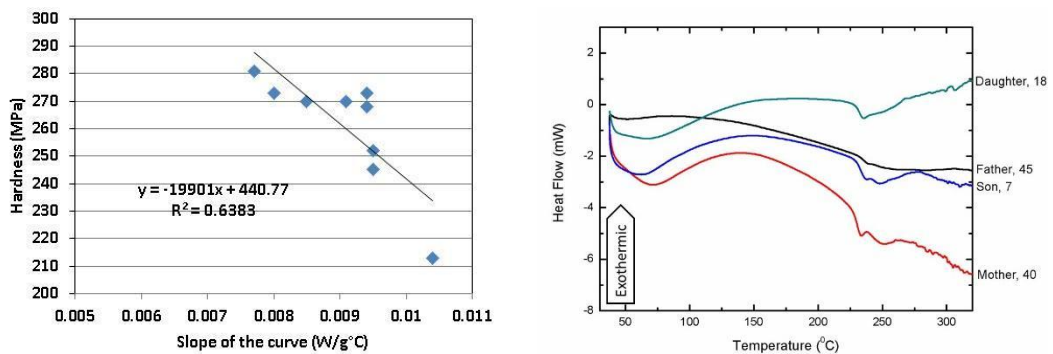
Figure 5.4: Correlation between hardness (Nanoindentation) and slope of the heat flow curve in the range of 120 - 210 °C (DSC) of hair samples(left image). DSC curves showing different slope of heat flow curves (right image).

Take the example of 18 yrs female (Figure 5.4 - right image) which shows high hardness (not shown) and constant lower slope of heat flow curve (120 - 210 °C) indicating higher degree of cross-linked amorphous matrix. The values of hardness obtained from nanoindentation correspond to the stability of α-keratin crystalline phase which is embedded within the amorphous phase of varying degrees of cross-

135

linking. Higher the slope of the heat flow curves, lesser the hardness value and it corresponds to the keratin proteins wherein degree of cross-linking of amorphous matrix exhibits a range.

Figure 5.5 shows linear relation between indentation modulus and onset of melting temperature with regression value of 0.91. Inset picture shows the measurement of indentation modulus measurement from slope of unloading curve of load vs depth (nanoindentation) and also onset melting temperature using origin software.

Though nanoindentation hardness was measured from the regions of 2 to 10 µm width and 0.4 to 1.0 µm depths, it correlated well with DSC slope of the heat flow curves between 120 – 210 °C wherein 1 mm length samples are considered for testing.
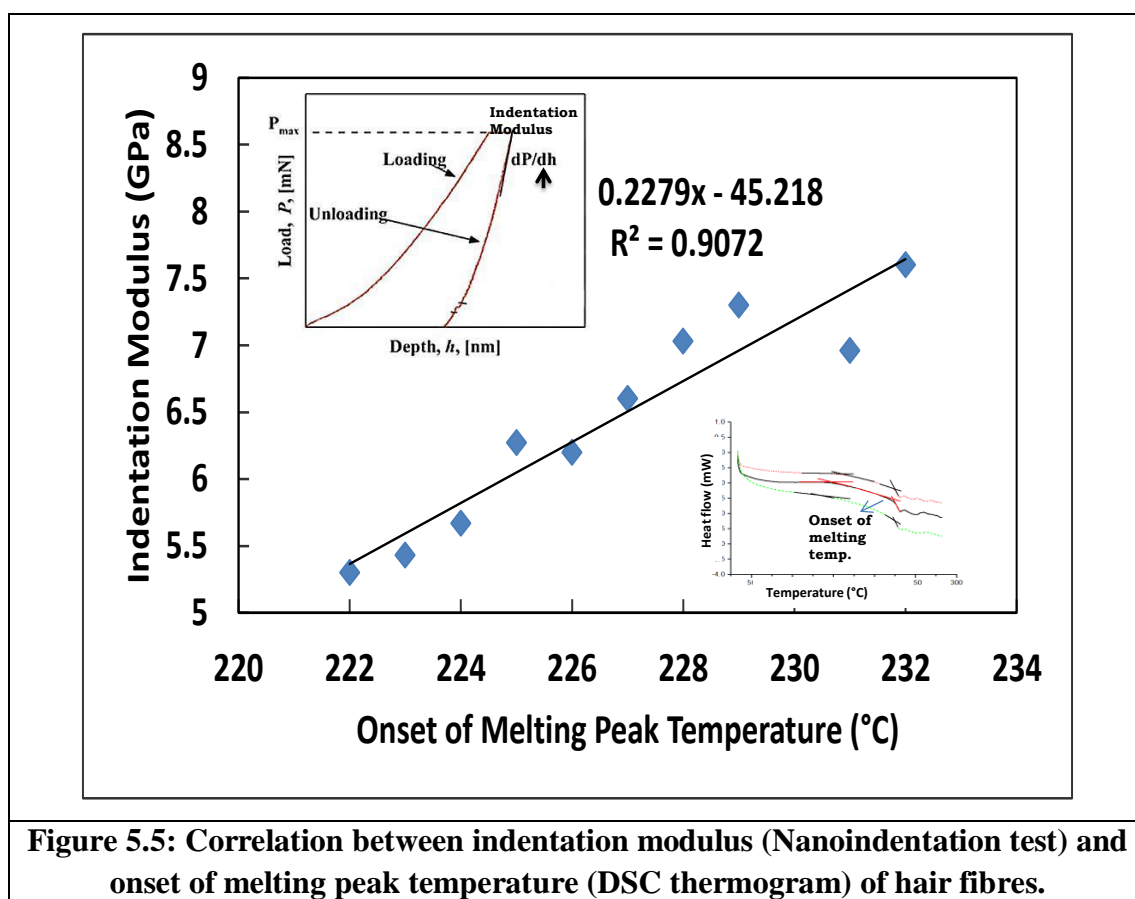
Figure 5.5: Correlation between indentation modulus (Nanoindentation test) and onset of melting peak temperature (DSC thermogram) of hair fibres.

5.4. Conclusions

Tensile yield stress and melting enthalpy are compared and it is found that a good non-linear (sigmoidal) correlation exists. The non-linear correlation for the 17 donors seems to provide an accurate representation of a composite keratin structure wherein the percentage of crystallinity exhibits a range and crystalline and amorphous regions are intertwined and intricate in nature. From the DSC curves and nanoindentation data, it has been concluded that higher the nanoindentation hardness, lower the slope of the heat flow curves in the range of 120 - 210°C of the DSC, which corresponds to stiffer keratin proteins making up the hair composites with higher degree of cross-linking of amorphous matrix.

CHAPTER – 6

Conclusions

1. It is found that hair diameter, nanoindentation (cortex region) hardness, modulus; hair tensile strength, modulus and melting enthalpy, onset of melting temperature are not influenced by donor age and gender because hair structure resembles nanocomposite wherein amorphous keratin matrix and crystalline keratin intermediate filaments exists with high degree of intermingling.

2. Nanoindentation hardness, modulus of medulla region revealed lower values compared to the cortex region of same hair fibre cross section because medulla has poorer orientation of microfibrils.

3. From the experimental and statistical (Relative rating and Grey relational analysis) data of tensile properties of single hair fibres, no significant trend was observed, when data was compared with respect to scalp positions (P1-P4).

4. A correlation was found between yield stress from tensile data and melting enthalpy from thermal data.

Single hair fibre diameters were found to be in the range of 40 - 110 μm. Medulla index defined as ratio of medulla diameter to hair fibre diameter was found to be between 0.10 - 0.25 and it is not influenced by age. Linear densities of hair fibres are in the range of 0.02 - 0.08 mg/cm and it is also not influenced by the donor age.

Sample preparation method for nanoindentation of hair fibres was successfully developed using agar epoxy resin system which is transparent and tough enough to avoid the cracks while smoothening. Indentation moduli were in the range of 3.4 - 7.1 GPa and hardness values were in the range of 203 - 350 MPa for the cortex region and also found that donor age and gender has no influence on these properties. It was found that an indentation modulus of 2.2 - 5 GPa and hardness of 70 - 170 MPa for medulla region, which indicates that medulla has weak composite structure in comparison to the cortex and first time this difference has been quantified. This could be due to the fact that organization of the microfibrils increases from the medulla

centre to medulla periphery, whereas in cortex, microfibrils are oriented almost parallel to the fibre axis.

From the tensile stress - strain curves, four characteristic regions are identified and the fourth region is identified for the first time by measuring a change in post-yield incremental modulus at around ~33 % strain in which yielding and an ultimate failure occurs. Considering the composite nature of the hair, four properties namely tensile modulus, yield stress, maximum stress and work of elongation were measured and typical values were found to be 5.1 ± 0.5 GPa, 109 ± 14 MPa, 208 ± 24 MPa and 60 ± 12 MJ/m^3 respectively. From the experimental and statistical (ANOVA, Relative rating and Grey relational analysis) data of tensile properties of single hair fibres, no significant trend can be seen when data was compared with respect to age, gender and position of the scalp (P1-P4). Slightly better tensile properties were observed for hair samples collected from frontal position (P1) of male donors. SEM fractography revealed step, split and smooth fractures.

Single fibre tensile test (bulk) data is compared with nanoindentation (surface) data and found that nanoindentation hardness and modulus revealed a higher value compared to tensile yield stress and modulus respectively indicating the effects of structural variations in hair. This may also be attributed to the α helical arrangement of microfibrils in hair.

From DSC studies it was found that the values of melting enthalpy and melting peak temperature were 6.29 ± 0.20 J/g and 235 ± 0.6 °C respectively. No trend was observed when melting peak temperatures were compared with respect to age and gender. Tensile yield stress and melting enthalpy are compared and found a good non-linear fit with sigmoidal function. This nonlinear sigmoid correlation seems to provide an accurate representation of a composite keratin structure wherein the % crystallinity exhibits a range. Correlation between thermal data (the onset of endothermic melting peak temperature of α-keratin) and nanoindentation data (indentation modulus) was also found indicating one test suffices to measure the intricate nature of the hair properties.

CHAPTER – 7

Future Studies

Samples affected by urban pollution and hair dying showed slightly lower values of stress and modulus. It is recommended that further research can be focused on hairs treated with different types of dyes and also on hairs that have been curled or straightened to know the effect of dyeing and thermal straightening/curling on mechanical properties of hair.

Few hair samples from cancer patients before undergoing chemotherapy were also tested and found no difference in their tensile and thermal properties which clearly indicates that keratin protein is not affected by cancer disease. But studies should be focused on properties of hair grown on scalp after chemotherapy or radiation treatment.

Nanoindentation technology can be used for other micron sized fibres to know the structure-property correlation and also to estimate the anisotropy of the fibre. It can also be used to estimate the level of heterogeneity existing in biocomposite structures such as hair, wool and silk fibres. In this thesis, studies are restricted to one particular cross-section (2 cm above the root side/scalp) and this can be extended to determine the hardness and indentation modulus of hair fibre cross-sections from root to tip regions to study the heterogeneity of the hair composite structure along the length direction.

By investigation of the correlation between thermal and mechanical properties for other materials, is to try and establish whether by conducting DSC scans (thermal tests), prediction of mechanical or any other properties can be made, both qualitatively and quantitatively.

References

Adusumalli RB, Mook W, Passas R, Schwaller P, Michler J. Nanoindentation of single pulp fibre cell walls. Journal of Material Science. 45, 2010:2558-2563.

Adonias Ribeiro Franco Jr, Giuseppe Pintaúde, Amilton Sinatora, Carlos Eduardo Pinedo, André Paulo Tschiptschin. The Use of a Vickers Indenter in Depth Sensing Indentation for Measuring Elastic Modulus and Vickers Hardness. Materials Research, 7(3), 2004: 483-491.

Fischer-Cripps Anthony C. Nanoindentation. 3rd Ed., Springer, New York. 2011.

Antunes E, Cruz CF, Azoia NG, Cavaco-Paulo A. Insights on the mechanical behavior of keratin fibrils. International Journal of Biological Macromolecules. 89, 2016: 477-483.

Batista Natassia Lona, Philippe Olivier, Gerard Bernhart, Mirabel Cerqueira Rezende, Edson Cocchieri Botelho. Correlation between degree of crystallinity, morphology and mechanical properties of PPS/carbon fibre laminates. Materials Research. 19(1), 2016:195-201.

Bhushan B, Chen N. AFM studies of environmental effects on nanomechanical properties and cellular structure of human hair. Ultramicroscopy. 106, 2006:755-764.

Bhushan B. Nanoscale characterization of human hair and hair conditioners. Progress in Material Science. 53, 2008:585-710.

Bhushan B. Biophysics of human hair: structural, nanomechanical, and nanotribological studies. 1st edn. Springer, Heidelberg, 2010.

Bencomo-Cisneros JA, Tajeda-Ochoa A, Garcia-Estrada JA, Herrera-Ramirez CA, Hurtado-Macias A, Martinez-Sanchez R, Herrera-Ramirez JM. Characterization of Kevlar-29 fibres by tensile tests and nanoindentation. Journal Alloy and Compounds. 536, 2012:S456-S459.

Bourmaud A, Baley C. Nanoindentation contribution to mechanical characterization of vegetal fibres. Composites Part B: Engineering. 43(7), 2012:2861-2866.

Christopher A Schuh. Nanoindentation Studies of Materials. Materials Today. 9(5), 2006:32-40.

Claude Bouillon, John Wilkinson. The Science of Hair Care. 2nd Ed., CRC Press, New York, 2005.

Cao J. Depression of the melting temperature by moisture for α-form crystallites in human hair keratin. Biopolymers. 77, 2005:38-43.

Cao J. Melting study of the α-form crystallites in human hair keratin by DSC. Thermochimica Acta. 335, 1999:5-9.

Clement JL, Pareux A LE, Ceccaldi PF The Specificity of the Ultrastructure of Human Hair Medulla. Journal of the Forensic Science Society. 22, 1982:396-398.

Callister William D. Materials Science and Engineering an Introduction, John Wiley & Sons New York, 2007.

Chegdani F, El Mansori M, Mezghani S, Montagne A. Scale effect on tribo-mechanical behavior of vegetal fibres in reinforced bio-composite materials. Composite Science and Technology. 150, 2017:87-94.

Chawla KK. Fibrous Materials. Cambridge University Press, New York, pp. 256. 1998.

Das B, Prasad KE, Ramamurty U, Rao CNR. Nanoindentation studies on polymer matrix composites reinforced by few-layer grapheme. Nanotechnology. 20(125), 2009:705-710.

David A. Katz. Hair Analysis. 2005. (http://www.mist.com/HAIR%20ANALYSIS.pdf)

Dankovich TA, Kamath YK, Ruetsch S. Tensile properties of twisted hair fibres. Journal of Cosmet Science. 55, 2004:879-890.

Ebenstein Donna M, Lisa A. Pruitt. Nanoindentation of biological materials. Nanotoday. 1(3), 2006:26-33.

Erik B, Havitcioglu H, Aktan S and Karakus N. Biomechanical properties of human hair with different parameters. Skin Research and Technology. 14, 2008:147-151.

Feughelman M. The physical properties of alpha-keratin fibres. Journal of the Society of Cosmetic Chemists. 33, 1982:385-406.

Feughelman M. Natural protein fibres. Journal of Applied Polymer Science. 83, 2002: 489-507.

Forslind B, Lindberg M. Skin, hair, and nails - structure and function. 1st Ed. Marcel Dekker Inc., New York. 2004.

Franbourg A, Hallegot P, Baltenneck F, Toutain C, Leroy F. Current research on ethnic hair. Journal of the American Academy of Dermatology. 48(6), 2003:S115-S119.

Fong W, Inami SH. Simple rapid and unique hand techniques for cross-sectioning fibres and hair. Journal Forensic Science. 33(2), 1988: 305-309.

Gindl W, Konnerth J, Scho¨berl T. Nanoindentation of regenerated cellulose fibres. Cellulose. 13, 2006: 1-7.

Gindl W, Reifferscheid M, Adusumalli RB, Roeder T, Weber H, Sixta H, Schöberl T. Anisotropy of the modulus of elasticity in regenerated cellulose fibres related to molecular orientation. Polymer. 49, 2008:792-799.

Gibson RS, Anderson BM, Scythes CA. Regional differences in hair zinc concentrations: a possible effect of water hardness. American J Clinical Nutrition. 37, 1983:37-42.

Grace X Gu, Isabelle Su, Shruti Sharma, Jamie L Voros, Zhao Qin, Markus J Buehler. Three-Dimensional-Printing of Bio-Inspired Composites. Journal of Biomechanical Engineering. 138, 2016: 021006-1-17. DOI: 10.1115/1.4032423

Hearle JWS. A critical review of the structural mechanics of wool and hair fibres. International Journal Biological Macromolecules. 27, 2000:123-138.

Hutchinson PE, Thompson JR. The size and form of the medulla of human scalp hair is regulated by the hair cycle and cross-sectional size of the hair shaft. British Journal of Dermatology. 140, 1999:438-445.

Jeong KH, Kim KS, Lee GJ, Choi SJ, Jeong TJ, Shin MK, Park HK, Sim WY, Lee MH. Investigation of aging effects in human hair using atomic force microscopy. Skin Research and Technology. 17, 2011:63-68.

Kamath YK, Weigmann HD. Fractography of human hair. Journal of Applied Polymer Science. 27, 1982:3809-3833.

Kreplak L, Doucet J, Dumas P and Briki F. New aspects of the alpha-helix to β-sheet transition in stretched hard alpha-keratin fibres. Biophysical Journal. 87, 2004:640-647.

Krishnaiah K, Shahabudeen P. Applied Design of Experiments and Taguchi methods. New Delhi, India: PHI Learning Private Limited. 2012.

Kurra S, Regalla SP. Multi-objective optimisation of single point incremental sheet forming using Taguchi-based grey relational analysis. International Journal of Materials Engineering Innovation. 6, 2015:74-90.

Kavitha S, Natarajan K, Thilagavathi G, Srinivas CR. Effect of oil application, age, diet, and pigmentation on the tensile strength and breaking point of hair. International Journal of Trichology. 8, 2016:155-159.

Laura Farran, Roland Ennos, Stephen J Eichhorna. Microindentation and nanoindentation of human fingernails at varying relative humidity. Journal of Materials Research. 24(3), 2009:980-984.

Linda A Dunn, Ian L Weatherall. Longitudinal variation in the stress-strain properties of wool fibres. Journal of Applied Polymer Science. 44, 1992:1275-1279.

Menyhard A, Suba P, Laszlo ZS, Fekete HM, Mester AO, Horvath ZS, Voros GY, Varga J, Moczo J. Direct correlation between modulus and the crystalline structure in isotactic polypropylene. EXPRESS Polymer Letters. 9(3), 2015:308-320.

Menelaos L Batrinos. The endocrinology of baldness. Hormones (Athens). 13, 2014:197-212.

Michelle L Oyen. Handbook of Nanoindentation with Biological Applications. Pan Stanford Publishing, Singapore. 2011.

Mohan NH, Debnath S, Mahapatra RK, Nayak LK, Baruah S, Das A, Banik S, Tamuli MK. Tensile properties of hair fibres obtained from different breeds of pigs. Biosystems Engineering. 119, 2014:35-43.

Mohan NH, Ammayappan L, Sarma DK, Debnath S, Tamuli MK. Characterization of thermal properties of pig hair fibre. J Nat Fibres. 14, 2017:459‑465.

Milczarek P, Zielinski M, Garcia ML. The mechanism and stability of thermal transitions in hair keratin. Colloid and Polymer Science. 270(11), 1992:1106-1115.

Miserez A, Wasko SS, Carpenter CF and Waite JH. Non-entropic and reversible long-range deformation of an encapsulating bioelastomer. Nature Materials. 8, 2009:910-916.

Mishra S, Kunchi C, Venkateshan KC, Gundakaram RC, Adusumalli RB. Nanoindentation and tensile testing of human hair fibres, Journal of Materials Science. 51(22), 2016:10191-10204.

Nikiforidis G, Balas C, Tsambaos D. Mechanical parameters of human hair: Possible applications in the diagnosis and follow-up of hair disorders. Clinical Physics and Physiological Measurements. 13(3), 1992:281-290.

Nikiforidis G, Tsambaos D, Balas C and Bezerianos A. A method for the determination of viscoelastic parameters of human hair in relation to its Structure. Skin Pharmacology. 6, 1993:32-37.

Oliver WC and Pharr GM. An improved technique for determining hardness and elastic modulus using load and displacement sensing indentation experiments. Journal Material Research. 7, 1992:1564-1583.

Popescu C and Gummer C. DSC of human hair: a tool for claim support or incorrect data analysis?. International Journal of Cosmetic Science. 38, 2016:433-439.

Robbins CR, Chemical and Physical Behavior of Human Hair 4th Ed. Springer, New York. 2002.

Resendiz-Munoz J, Corona-Rivera MA, Fernandez-Munoz JL, Zapata-Torres M, Marquez-Herrera A, Ovando-Medina VM. Mathematical model of Boltzmann's sigmoidal equation applicable to the set-up of the RF-magnetron co-sputtering in thin films deposition of BaXSr1-xTiO3. Bulletin of Materials Science. 40(5), 2017:1043-47.

Revol BP, Thomassey M, Ruch F, Nardin M. Influence of the sample number for the prediction of the tensile strength of high tenacity viscose fibres using a two parameters Weibull distribution. Cellulose. 23, 2016:2701-2713

Samanta A, M Bhattacharya, S Dalui, M Acharya, PS Das, DK Chanda, SD Acharya, SK Sivaraman, S Nath, AK Mandal, J Ghosh, AK Mukhopadhyay. Nanomechanical responses of human hair. Journal Mechanical Behavior of Biomedical Materials. 56, 2016:229-248.

Srettabunjonga S, Patompakdeesakula P and Limawongpraneeb S. Relative studies between hair index, hair area, and medullary index with age and sex in Thai scalp hair. Forensic Science International. 267, 2016:196-203.

Sayahi E, Harizi T, Msahli S and Sakli F. Physical and mechanical properties of Tunisian women hair. Int. Journal of Cosmetic Science. 2016:1-6.

Tolgyesi E, Coble DW, Fang FS and Kairinen EO. A comparative study of beard and scalp hair. Journal of the Society of Cosmetic Chemists. 34, 1983:361-382.

Wagner Rita De Cassia Comis, Pedro Kunihiko Kiyohara Marina, Marina Arina Silveira and In´es Joekes. Electron microscopic observations of human hair medulla. Journal of Microscopy. 226, 2007:54-63.

Wei G, Bhushan B and Torgerson M. Nanomechanical characterization of human hair using nanoindentation and SEM. Ultramicroscopy. 105(1), 2005:248-266.

Wortmann FJ, Wortmann G, Marsh J, Meinert K. Thermal denaturation and structural changes of α-helical proteins in keratins. Journal of Structural Biology. 177, 2012:553-560.

Wortmann FJ, Deutz H. Characterizing keratins using high pressure differential scanning calorimetry (HPDSC). Journal of Applied Polymer Science. 48, 1993:137-150.

Velasco Maria Vale´ria Robles, Dias Tania Cristina de Sá, Anderson Zanardi de Freitas, Vieira Nilson Dias Júnior, Pinto Claudinéia Aparecida Sales de Oliveira, Kaneko Telma Mary, Baby André Rolim. Hair fibre characteristics and methods to evaluate hair physical and mechanical properties. Brazilian Journal of Pharmaceutical Sciences. 45(1), 2009: 153-162.

Zhenxing Hu, Gaosheng Li, Huimin Xie, Tao Hua, Pengwan Chen, Fenglei Huang. Measurement of Young's modulus and Poisson's ratio of Human Hair using Optical techniques. Proc. of SPIE. 2009, Vol. 7522 75222Q-1.

Zysset PK, Guo XE, Hoffler CE, Moore KE, Goldstein SA. Elastic modulus and hardness of cortical and trabecular bone lamellae measured by nanoindentation in the human femur. J. Biomech. 32, 1999: 1005-1012.

List of Publications

International Journals

1. Shubham Mishra, **Chandrakala Kunchi**, Karthik Chethan Venkateshan, Ravi Chandra Gundakaram, Ramesh Babu Adusumalli. Nanoindentation and Tensile testing of Human Hair Fibres. **Journal of Materials Science** 2016, 51(22):10191-10204 (Scopus Indexed).

2. **Chandrakala Kunchi**, Karthik Chethan Venkateshan, Ramesh Babu Adusumalli. Effect of Scalp Position on Tensile Properties of Single Hair Fibres. **International Journal of Trichology**, 2018, 10:218-228 (Scopus Indexed, Pubmed Indexed).

3. **Chandrakala Kunchi**, Karthik Chethan Venkateshan, N.V.N. Deeksha Reddy, Ramesh Babu Adusumalli. Correlation between mechanical and thermal properties of human hair. **International Journal of Trichology**, 2018, 10:204-210 (Scopus Indexed, Pubmed Indexed).

4. **Chandrakala Kunchi**, Karthik Chethan Venkateshan, Ramesh Babu Adusumalli. Nanoindentation on hair cortex and medulla regions. Manuscript submitted to Fibres and Polymers (Scopus Indexed Journal). 2019 **(Accepted)**

5. Ramesh Babu Adusumalli, Karthik Chethan Venkateshan, **Chandrakala Kunchi**, Surya R. Vadlamani. Tensile testing of single fibres. **Structural Integrity Procedia** 2019 **(Accepted)**

Publications in International and National conference proceedings

1. **Chandrakala Kunchi**, Karthik Venkateshan, Ramesh Babu Adusumalli. Thermal Analysis of Human Hair. National Conference on Recent Advances in Challengers in Chemical Engineering and Applied Chemistry, ANURAG Group of Institutions, Hyderabad, March 16th - 17th 2018.

2. Ramesh Babu Adusumalli, **Chandrakala Kunchi**, Karthik Venkateshan. Hardness and modulus measurement of single scalp hair fibres. 10th World Congress for Hair Research, Kyoto 6060001, Japan, October 31st - November 3rd, 2017.

3. Karthik Venkateshan, **Chandrakala Kunchi**, Ramesh Babu Adusumalli. Thermal and Mechanical behaviour of Human Hair fibres. 10th World Congress for Hair Research, Kyoto 6060001, Japan, October 31st - November 3rd, 2017

4. **Chandrakala K,** Lokesh Anaparthi and Ramesh Babu Adusumalli**.** Application of Optical, SEM and Confocal Laser Scanning Microscopy in Hair Research. Electron Microscopy Society of India (EMSI) Conference 2017, Chennai, July 17th - 19th, 2017, P_P: 386-388 (ISBN: 978-81-933428-1-7)

5. **Chandrakala.K**, Deeksha N, Karthik V, Sanakar Ganesh P, Suresh Babu P and R.B. Adusumalli. Sample preparation for Nanoindentation of Hair Fibres. IIT Madras, CHEMCON 2016, 2016

6. **Chandrakala.K**, Shubham.M, Sakshi.K, Pushkar.P, Karthik Chethan. V, R.B. Adusumalli. Nanoindentation Studies on Human Hair Fibres. ChEmference 2015, Sixth National Level Annual Research Symposium of Chemical engineering Research Scholars, IIT Hyderabad, Hyderabad, December 5th-6th, 2015.

7. **Chandrakala K**, Bibhu Prasad T, Karthik Chethan V, R.B. Adusumalli**.** Tensile stress of Human Hair Fibre. TSCST- API, Centre for Chemical Sciences & Technology, JNTU Hyderabad, 2015 (ISBN: 978-83-82829-48-5).

BIOGRAPHY OF THE CANDIDATE

Name of the candidate	**CHANDRAKALA KUNCHI**
ID. No.	2014PHXF0404H
Academic credentials	2014 - 2018: Ph.D. - BITS-Pilani, Hyderabad Campus, Hyderabad, Telangana 2007 - 2009: M.Sc.(Engg.) - Chemical Engineering (VTU, Belgaum, Karnataka) 1994 - 1998: B.Tech. - Chemical Engineering (SVU, Tirupathi, Andhra Pradesh)
Work experience	1998 - 2009: Worked as a Project fellow at National Aerospace Laboratories (NAL), FRP Division, Bangalore, Karnataka. 2011 - 2012: Worked as an Environmental engineer at EPTRI, Hyderabad, Telangana.
Contact details	Telephone Number: +91-8096071259 Email: chandrakalakunchi@gmail.com

BIOGRAPHY OF THE SUPERVISOR

Name of the Supervisor	**Prof. RAMESH BABU ADUSUMALLI**
Designation and address	Associate Professor, Department of Chemical Engineering, BITS, Pilani, Hyderabad Campus
Education (Ph .D.)	University of Natural Resources and Applied Life Sciences (BOKU), Vienna, Austria (completed in 2008) Ph.D. in Cellulose Fibre Reinforced Composites.
Experience (years)	12
Number of publications	Journals -20
	International and National Conferences - 19
	Book Chapters - 2
Sponsored Projects	Title: Comparison of phenolic resin from two sources for their properties. Principal Investigator: Dr. Karthik Chethan Co-Investigators: Dr. Ramesh Adusumalli Funding Agency: Advanced Systems Laboratory (ASL) Amount Sanctioned: Rs. 9.81 lakhs Date of Commencement & Duration: March 2018 (12 months)
	Title: Characterization of Fibre / Matrix interface in Advanced Composites Principal Investigator: Dr. Ramesh Adusumalli Co-Investigators: Dr. Karthik Chethan, Dr. N. Jalaiah Funding Agency: Defence Research and Development Organization (DRDO) Amount Sanctioned: Rs. 9.96 lakhs Date of Commencement & Duration: Aug 2015 (15 months)
	Title: Nano-scale characterization of human hair fibres by using indentation technique Principal Investigator: Dr. Ramesh Babu Adusumalli Funding Agency: Dept. of Science and Technology (DST) Amount sanctioned: Rs 29.89 Lakhs Date of commencement & Duration: Aug 2014 (36 months)
No. of Ph.D. students guided (in progress)	3
Contact details: E-mail: ramesh.babu@hyderabad.bits-pilani.ac.in Weblink: http://universe.bits-pilani.ac.in/Hyderabad/rameshbabu/Profile	

BIOGRAPHY OF THE CO-SUPERVISOR

Name of the Supervisor	**Prof. Karthik Chethan Venkateshan**
Designation and address	Associate Professor, Department of Chemical Engineering, BITS, Pilani, Hyderabad Campus
Education (Ph.D.)	McMaster University, Canada (completed in 2006). Ph.D. in Materials Science and Engineering.
Experience (years)	19
Number of publications	Journals - 12
	International and National Conferences - 10
	Book Chapters - 2
	Patents - 1 Chewing Gum Elastomers from Soy Protein Fractions-US Patent filed in 2012, Application No: 13420751, published online.
Sponsored Projects	PI: Comparison of phenolic resin obtained from two sources for their properties. The project is funded by Advanced Systems Laboratory (ASL, DRDO), Hyderabad (ongoing project, Rs. 9.81 lakhs).
	PI: Development of bio-based formulations for 3-D printing applications. The formulations are based on a variety of biomaterials and biopolymers. The project is funded by Biotechnology Industry Research Assistance Council (BIRAC) as part of their Biotechnology Ignition Grant (BIG) scheme (ongoing project, Rs. 36.00 lakhs).
	Co-PI: Characterization of Fibre / Matrix interface in Advanced Composites. Sponsor: Advanced Systems Laboratory (ASL, DRDO), Hyderabad (Completed in 2016, Rs. 9.96 lakhs)
	Co-PI: Development of Zein Protein based systems for Bioplastics Applications. Co-PI's: MGPI, Inc; Sponsor: MGPI, Inc, Kansas, USA (Completed in 2011, USD 30,000).
	Co-PI: Development of Soy protein Polymers for Chewing Gum Application. Co-PI's: Dr. Xiuzhi Susan Sun and Wrigley; Sponsor: Wrigley, Illinois, USA (Completed in 2009, USD 95,000).
	Co-PI: Development of Carbon dioxide Cured and Protein based Binder Formulation and Preparation for Foundry Applications. Co-PI's: Dr. Xiuzhi Susan Sun, Dr. Donghai Wang and Foseco, Inc; Sponsor: Foseco, Inc, Netherlands (Completed in 2008, USD 130,000).
No. of Ph.D. students guided (in progress)	1
Contact details: E-mail: kvenk@hyderabad.bits-pilani.ac.in Weblink: http://universe.bits-pilani.ac.in/hyderabad/karthik/Profile	